



University of HUDDERSFIELD

University of Huddersfield Repository

Al-Jammal, Mohammad Khaled

Developing formulations designed to deliver antiseptic agents to target sites within the skin

Original Citation

Al-Jammal, Mohammad Khaled (2019) Developing formulations designed to deliver antiseptic agents to target sites within the skin. Doctoral thesis, University of Huddersfield.

This version is available at <http://eprints.hud.ac.uk/id/eprint/35319/>

The University Repository is a digital collection of the research output of the University, available on Open Access. Copyright and Moral Rights for the items on this site are retained by the individual author and/or other copyright owners. Users may access full items free of charge; copies of full text items generally can be reproduced, displayed or performed and given to third parties in any format or medium for personal research or study, educational or not-for-profit purposes without prior permission or charge, provided:

- The authors, title and full bibliographic details is credited in any copy;
- A hyperlink and/or URL is included for the original metadata page; and
- The content is not changed in any way.

For more information, including our policy and submission procedure, please contact the Repository Team at: E.mailbox@hud.ac.uk.

<http://eprints.hud.ac.uk/>

**Developing formulations designed to deliver
antiseptic agents to target sites within the
skin**

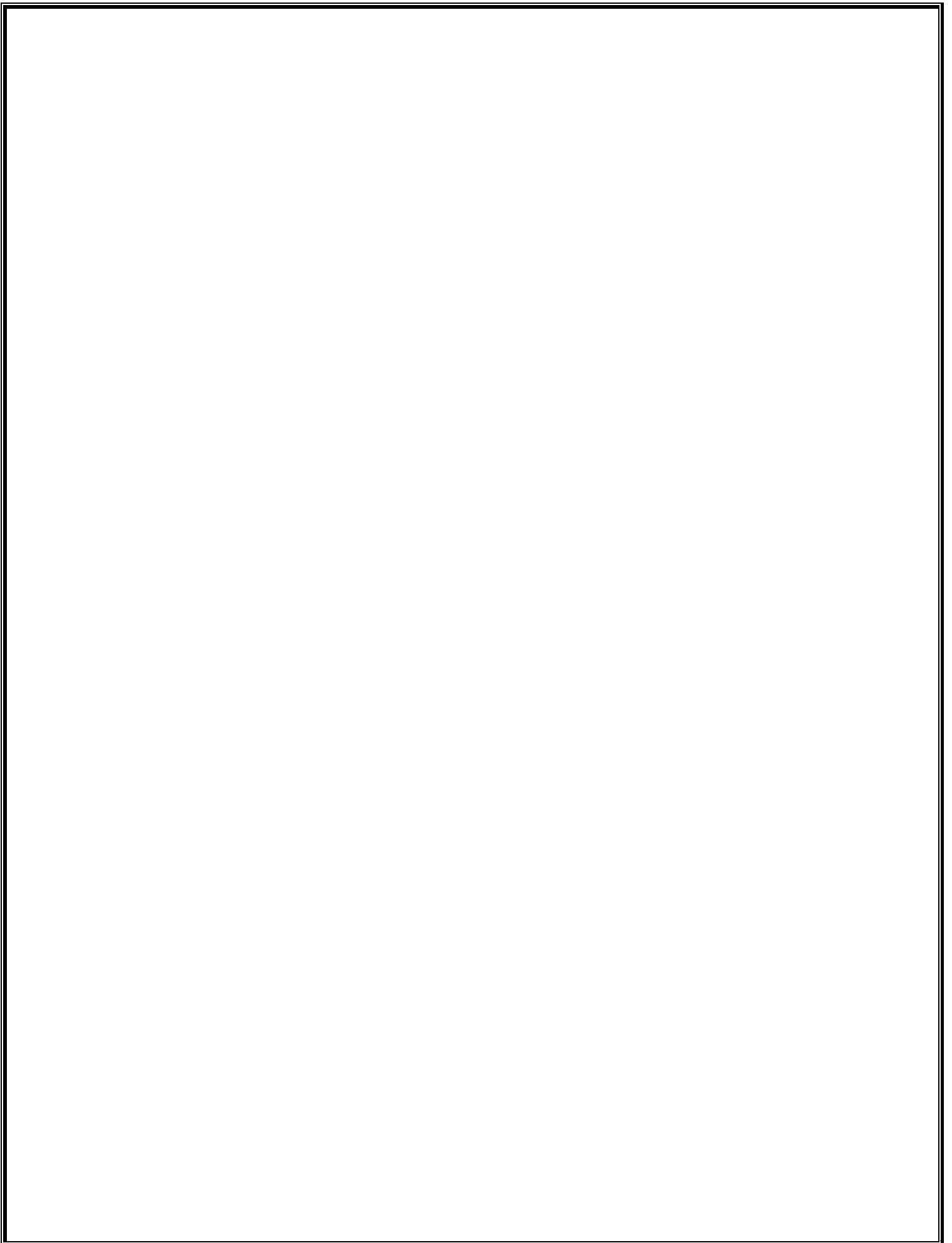
By
Mohammad Khaled AL-Jammal

Under supervision of
Prof. Barbara Conway

Thesis submitted in partial fulfilment of the
requirements for the degree of Doctor of Philosophy
In Pharmacy School
At

The University of Huddersfield
September 2019

University of
HUDDERSFIELD
Inspiring global professionals



Copyright statement

- i.** The author of this thesis (including any appendices and/ or schedules to this thesis) owns any copyright in it (the “Copyright”) and s/he has given The University of Huddersfield the right to use such Copyright for any administrative, promotional, educational and/or teaching purposes.

- ii.** Copies of this thesis, either in full or in extracts, may be made only in accordance with the regulations of the University Library. Details of these regulations may be obtained from the Librarian. Details of these regulations may be obtained from the Librarian. This page must form part of any such copies made.

- iii.** The ownership of any patents, designs, trademarks and any and all other intellectual property rights except for the Copyright (the “Intellectual Property Rights”) and any reproductions of copyright works, for example graphs and tables (“Reproductions”), which may be described in this thesis, may not be owned by the author and may be owned by third parties. Such Intellectual Property Rights and Reproductions cannot and must not be made available for use without permission of the owner(s) of the relevant Intellectual Property Rights and/or Reproductions

Abstract

Healthcare associated infections (HCAI) are a major concern due to their impact on morbidity and associated costs. To prevent subsequent infection, the use of an effective antiseptic agent is necessary before an incision is performed. However, there are two important issues that may restrict effective antiseptics; the first of these is that the penetration of most antimicrobial agents is very poor, and the antiseptic may not reach the deep layers of the skin; therefore microorganisms located in these layers are likely to survive. The second issue is the lack of miscibility between the antiseptic agent and the sebum which prevents the delivery to the target site within the hair follicle. Nanoemulsions are a promising drug delivery system which can potentially facilitate the penetration of an antiseptic agent to the deeper layers of the skin.

In this thesis, the capability of nanoemulsion formulations in the delivery of antiseptic agents to target sites within the skin was assessed. Triclosan nanoemulsions were prepared using two different techniques, a high-pressure homogenisation and high-shear homogenisation followed by ultrasonication. The parameters of the triclosan nanoemulsion were evaluated; these include various types and concentrations of surfactants (Tween/Span) and various oil concentrations (eucalyptus oil). The detection of the amount of triclosan retained within the skin was also investigated both quantitatively and qualitatively using tape-stripping technique followed by hplc and micro CT scanning respectively. The lowest concentration of the surfactant mixture (0.34%W/W) (Tween 80 / Span 80) produced the highest skin retention of the antiseptic agent, this was detected quantitatively in the tape-stripping method and confirmed qualitatively in the novel approach using micro CT scans.

Hansen solubility parameters (HSPs) were used to predict the miscibility of nano-formulations with artificial sebum, the HSP for artificial sebum was calculated using three different methods: contribution group method (Van Krevelen method), Y-MB method using HSPiP software and the third using the solubility and miscibility of known HSPs and regression statistics. HSPs were successfully used as a prediction tool in estimating the miscibility of nanoemulsion in artificial sebum using the three stated methods.

Keywords

Nanoemulsion, Triclosan, Hansen solubility parameters, Franz diffusion cell, eucalyptus oil, Healthcare associated infections.

Acknowledgement

All praise and gratitude to Allah, the most merciful and the most gracious, for providing me with the strength, the ability and the chance to complete this thesis.

I would like to dedicate this thesis to the courageous people of my homeland – Syria, to the martyrs, the injured and all those affected by the war. To you all I would like to say; justice shall be served one day.

Foremost, I would like to wholeheartedly thank my supervisor Prof. Barbara Conway, for her constant support, guidance and confidence in me throughout these years, I have been so fortunate to have an advisor with such patience and knowledge. Without her time and expertise, it would have been impossible to complete this thesis. I would also like to say a huge thank you to Dr. Mohammad Amin for his continuous help ,motivation, and guidance, his immense experience and knowledge were extremely useful and inspiring throughout this thesis.

I would especially like to thank my family. I also dedicate this thesis to my wonderful parents, your support, encouragement and unconditional love have always and will always be the source of my strength.

My darling, Asma has been extremely supportive of me throughout this entire process and has made countless sacrifices to help me get to this point. My lovely daughter, Layan, has continually provided the requisite breaks from philosophy and the motivation to finish my degree with expediency

Finally, many thanks to all the members of staff at the University of Huddersfield, whose advice and help significantly enriched this thesis. Without you all, I doubt that I would be in this place today. Thank you!

List of contents

Abstract	2
Acknowledgement	4
List of contents	5
List of Figures	10
List of Tables	14
List of Abbreviations	17
Chapter 1 - Introduction	1
1.1 Healthcare-associated infections (HCAI)	1
1.1.1 Factors contributing to HCAI	1
1.1.2 Types of HCAI	1
1.2 Skin structure	5
1.2.1 The subcutaneous layer	6
1.2.2 The dermis	6
1.2.3 The epidermis	7
1.2.4 The stratum corneum	8
1.2.5 Hair follicles	9
1.3 Wounds	11
1.3.1 Wounds definition and classification	11
1.3.2 Wound infection	14
1.3.3 Wound healing	15
1.3.4 Wound Dressings	17
1.4 Antiseptics	20
1.4.1 Alcohol	20
1.4.2 Biguanides	21
1.4.3 Iodine-releasing agents	22
1.4.4 Silver compounds	23

1.4.5	Phenols	23
1.4.6	Bis-phenols	24
1.4.7	Halophenols	25
1.5	Nanotechnology	25
1.5.1	Nanoemulsions	26
1.5.2	Production of nanoemulsions	30
1.5.3	Analysis methods for detection of retained drug in the skin	30
	Aims of the thesis	35
2	Chapter 2 -Methodology and Materials	36
2.1	Instruments and Apparatus	36
2.1.1	High-pressure homogeniser	36
2.1.2	High shear homogeniser	37
2.1.3	Ultrasound	37
2.1.4	Zetasizer	37
2.1.5	Franz diffusion cell	39
2.1.6	Inverse gas chromatography (IGC)	41
2.1.7	High-performance liquid Chromatography	42
2.1.8	UV Spectrometers	43
2.1.9	Micro CT scan	44
2.2	Materials	45
2.2.1	Analytes and general chemicals	45
2.3	Methodology	45
2.3.1	Preparation of nanoemulsions	45
2.3.2	Preparation of Artificial Sebum	46
2.3.3	Preparation the skin	46
3	Chapter 3 - Design and Development of Triclosan Nanoemulsion for Dermal Delivery	47
3.1	Introduction	47
3.1.1	Nanoemulsion and nanoemulsion formation	48

3.1.2	Hydrophile –Lipophile balance	50
3.1.3	Physicochemical characterisation of nanoemulsion formulations	50
3.1.4	Triclosan and mechanisms of action	54
3.1.5	Analysis and characterisation of nanoemulsions	55
3.1.6	Determination of triclosan in skin quantitatively and qualitatively	58
3.2	Aim and Objectives	60
3.3	Results and Discussion	62
3.3.1	Formulation study of triclosan nanoemulsion	62
3.3.2	Parameters used for High-Pressure Homogenisation	79
3.3.3	Parameters for High Shear Homogenisation followed by Ultrasound	81
3.3.4	Long-term stability of triclosan nanoemulsion	83
3.3.5	Development and validation method of HPLC determination of triclosan in nanoemulsion	86
3.3.6	<i>In vitro</i> skin permeation study	91
3.4	Conclusion	101
4	Chapter 4- Design and Development of Chloroxylenol Nanoemulsion for Dermal Delivery	103
4.1	Introduction	103
4.1.1	. Physicochemical characterisation of the nanoemulsion formations:	104
4.1.2	Chloroxylenol and mechanisms of action	105
4.1.3	Analysis and characterisation of PCMX nanoemulsions	106
4.1.4	Physicochemical characterisation of nanoemulsion formulations	106
4.1.5	Determination of PCMX in skin quantitatively and qualitatively	107
4.2	Aim and Objectives	108
4.3	Results and Discussion	109
4.3.1	Formulation study of PCMX nanoemulsion	109
4.3.2	Optimisation of homogenization and sonication parameters	117
4.3.3	Stability of PCMX nanoemulsion	119

4.3.4	Development and validation method of HPLC for the measurement of PCMX	127
4.3.5	<i>In vitro</i> skin permeation study	132
4.4	Conclusion	140
5	Chapter 5-Hansen solubility parameters (HSPs) as a tool to predict miscibility of nanoemulsion formulations with artificial sebum	142
5.1	Introduction	142
5.2	The composition of artificial sebum and similarity with human sebum	142
5.3	Overview of chemical bonds	143
5.3.1	Intra-molecular bonds	144
5.3.2	Inter-molecular bonds	144
5.4	Overview of Hansen Solubility Parameters (HSP) and miscibility theory	146
5.4.1	Theory and miscibility models	147
5.5	Methods to calculate Hansen solubility parameters (HSPs)	150
5.5.1	Theoretical methods in calculating HSPs	150
5.5.2	Experimental methods for calculating HSPs	153
5.6	Aim and objectives	156
5.7	Results and Discussion	157
5.7.1	Hansen Solubility Parameter calculations for antiseptic compounds and artificial sebum	157
5.7.2	Limitations in the calculation of HSPs for artificial sebum components	169
5.7.3	Hansen Solubility Parameters of artificial sebum	172
5.7.4	Miscibility of antiseptic with artificial sebum	173
5.8	Conclusion	176
6	Chapter 6- General Conclusion and Future Work	177
7	Chapter 7 – References	181
8	Chapter 8 – Publications	191

List of Figures

Figure 1.2 HLB scale for the classification of surfactant functions (Aulton and Taylor, 2013)	28
Figure 1.3 - Stages of micro CT principle	33
Figure 2.1 High-pressure homogeniser (Avestin, 2010)	36
Figure 2.2 Standard Franz cells (Sonam Vats &, Charu Saxena, TS Easwari, 2014)	40
Figure 3.1 Steps for the formation of a NE (Mason <i>et al.</i> , 2006)	49
Figure 3.2 Schematic diagram of high-pressure homogenization (Fontes <i>et al.</i> , 2015)	53
Figure 3.3 Schematic diagram of high-shear homogenization and ultrasounds technique	54
Figure 3.4 Chemical structure of triclosan (Ramos, 2009)	55
Figure 3.5 Proposed emulsions formulation using a wide range of HLB mixtures	64
Figure 3.6 Proposed NEs formulation using a narrow range of HLB mixtures	65
Figure 3.7 Size and PDI of NEs prepared with different oil concentrations	72
Figure 3.8 Size of NE with different emulsifiers at 3 cycles	76
Figure 3.9 Size of NE with different emulsifiers at 5 cycles	76
Figure 3.10 Size distribution of NE with different emulsifiers at 3 cycles	76
Figure 3.11 size distribution of NE with different emulsifiers at 5 cycles	76
Figure 3.12 size and PDI of NE prepared with different amounts of emulsifiers	78
Figure 3.13 Size and PDI of NE prepared with different types of emulsifiers	79
Figure 3.14 Effect of homogenization time on mean droplet size (A) and PDI (B)	81
Figure 3.15 Effect of Speed of mixer on mean droplets size (A) and PDI (B)	82
Figure 3.16 Effect of sonication time on mean droplets size (A) and PDI (B)	83

Figure 3.17 The effect of surfactant on triclosan NE during storage at 4 and 25°C for 3 months (A)effect of surfactant (T20/S20)at 5 cycles/4°C (B) effect of surfactant (T20/S20)at 5 cycles /25°C (C) effect of surfactant (T40/S40)at 5 cycles /4°C(D) effect of surfactant (T40/S40)at 5 cycles /25°C 84

Figure 3.18 The effect of surfactant on triclosan NE during storage at 4 and 25°C for 3 months (A)effect of surfactant (T60/S60)at 5 cycles/4°C (B) effect of surfactant (T60/S60)at 5 cycles /25°C (C) effect of surfactant (T80/S80)at 5 cycles /4°C(D) effect of surfactant (T80/S80)at 5 cycles /25°C 85

Figure 3.20 PDI result for the stability study of different type and amount of surfactant for triclosan NE storage at 4 and 25°C for 3 months 87

Figure 3.21 MDS result for stability study of different type and amount of surfactant for triclosan NE storage at 4 and 25°C for 3 months 88

Figure 3.22 UV spectrum for triclosan in methanol, showing the λ max at 287nm 86

Figure 3.23 Linearity curve of group A 87

Figure 3.24 Peak of triclosan at 6.737 min 89

Figure 3.25 Effect of the different amount of surfactant on skin permeation (mean \pm SD n=3) 92

Figure 3.26 Effect of the different type of surfactant on skin permeation (mean \pm SD n=3) 94

Figure 3.27 Effect of the different amount of oil on skin permeation (mean \pm SD n=3) 95

Figure 3.28(a) 3D image of the skin sample without formulation (b) screenshots from video every 10 seconds of skin sample without formulation (blue; skin, green; plate) 97

Figure 3.29 3D image of the skin sample with H1-P031 formulation (b) screenshots from video every 3 seconds of skin sample with H1-P031 formulation (blue; skin, red; triclosan, green; plate) 97

Figure 3.30 3D image of the skin sample with F3-P032 formulation (b) screenshots from video every 3 seconds of skin sample with F3-P032 formulation (blue; skin, red; triclosan, green; plate) 98

Figure 3.31 Comparison between two techniques (mean \pm SD n=3)	99
Figure 3.32 graph of all formulations (mean \pm SD n=3)	101
Figure 4.1 Chemical structure of PCMX	106
Figure 4.2 Effect of type of surfactant on mean droplets size (A) and PDI (B)	116
Figure 4.3 Effect of speed of mixer on mean droplets size (A) and PDI (B)	118
Figure 4.4 Effect of sonication on mean droplets size (A) and PDI (B)	119
Figure 4.5 NE formulations after heat-cooling cycle	121
Figure 4.6 NE formulations after the freeze-thaw cycle	122
Figure 4.7 The effect of surfactant on size of PCMX NE during storage at 4 and 25°C for 3 months (A)effect of surfactant concentration at 4°C (B) effect of surfactant concentration at 25°C (C) effect of type of surfactant at 4°C(D) effect of type of surfactant at 25°C	125
Figure 4.8 The effect of surfactant on PDI of PCMX NE during storage at 4 and 25°C for 3 months (A)effect of surfactant concentration at 4°C (B) effect of surfactant concentration at 25°C (C) effect of type of surfactant at 4°C(D) effect of type of surfactant at 25°C	126
Figure 4.9 UV spectrum for PCMX, showing the λ max at 288nm	127
Figure 4.10 Linearity curve of group A (one graph of the five graphs of linearity)	128
Figure 4.11 Selectivity test shows the resolution of the method - Peak of PCMX at 3.29 min	130
Figure 4.12 Effect of the different amount of surfactant on skin permeation (mean \pm SD n=3)	134
Figure 4.13 Effect of the different type of surfactant on skin permeation (mean \pm SD n=3)	135
Figure 4.14 screenshots from video every 3 seconds of skin sample with C1-P061 formulation (blue; skin, red; PCMX, green; plate)	136

Figure 4.15 screenshots from video every 3 seconds of skin sample with C2-P061 formulation (blue; skin, red; PCMX, green; plate)	137
Figure 4.16 Effect of the different type of Skin (human and porcine) on permeation (mean \pm SD n=3)	138
Figure 4.17 Graph of all PCMX formulations (mean \pm SD n=3)	140
Figure 5.1 The composition of artificial sebum (Valiveti, Wesley and Lu, 2008)	143
Figure 5.2 Molecules held together by dipoles (Manning, 2009)	145
Figure 5.3 Some group contributions as calculated by various researchers (Scott, 1992).	151
Figure 5.4 Solubility parameter component group contributions (method Hoftyzer–Van Krevelen) (Scott, 1992)	160
Figure 5.5 Chemical structure of triclosan	161

List of Tables

Table 2.1 List of test probes used in the determination of HSPs using IGC	42
Table 3.1 The HLB values of different percentages of emulsifier blend	63
Table 3.2 The HLB values of different percentages of emulsifier blend range 11-13	64
Table 3.3 The amount of triclosan in each vial	66
Table 3.4 The solubility of triclosan.	66
Table 3.5 Physicochemical characterisation of the NE formations for both technique HPH & HSH (n=3; mean±sd)	70
Table 3.6 Size and PDI of NEs prepared with different oil concentrations following 3 and 5 cycles	71
Table 3.7 Size and PDI of NEs prepared with different oil concentrations	72
Table 3.8 Ratio of blend emulsifier at HLB = 12.5	73
Table 3.9 Size and PDI of NEs prepared with different emulsifiers at 3 cycles	74
Table 3.10 Size and PDI of NE prepared with different emulsifiers at 5 cycles	74
Table 3.11 Size and PDI of NE prepared with different amounts of emulsifiers	77
Table 3.12 size and PDI of NE prepared with different types of emulsifiers	78
Table 3.13 The effect of the No of the cycle on size and PDI	80
Table 3.14 Standard deviation of intercept and slopes mean	88
Table 3.15 Range of accuracy for HPLC method for triclosan	90
Table 3.16 Range of RSD for both intra-day and inter-day precision	91
Table 3.17 parameters of different NE to study the effect of the amount of surfactant	92
Table 3.18 Parameters of different NE to study the effect of the type of surfactant	94
Table 3.19 Parameters of different NE to study the effect of the type of surfactant	95

Table 3.20 Parameters of different NE to compare between two techniques	99
Table 3.21 Variables Summary of all formulations used in skin	100
Table 4.1 The solubility of PCMX in eucalyptol, water, and PBS	109
Table 4.2 Physicochemical characterisation of the NE formations (n=3; mean±sd)	113
Table 4.3 Size and PDI of NEs prepared with different oil concentrations	114
Table 4.4 Ratio of blend emulsifier at HLB = 12.5	115
Table 4.5 Size and PDI of NEs prepared with different surfactant concentrations	116
Table 4.6 Effect of homogenization time on mean droplet size and PDI	117
Table 4.7 Effect of type and concentration of surfactant and oil in accelerated stability study for NE	123
Table 4.8 Standard deviation of intercept and slopes mean	129
Table 4.9 Range of accuracy for HPLC method for PCMX	131
Table 4.10 Precision test - Range of RSD for both intra-day and inter-day precision	132
Table 4.11 Parameters of different NE to study the effect of the amount of surfactant	133
Table 4.12 Parameters of different NE to study the effect of the type of surfactant	135
Table 4.13 Parameters of NE to study the effect of the type of Skin	138
Table 4.14 Formulations variables for PCMX	139
Table 5.1 The HSPs and solubility of different chemical structures in artificial sebum ; (Valiveti and Lu, 2007)	158
Table 5.2 Calculation of HSPs and molar volume for triclosan according to the Hoftyzer-van Krevelen methods)	161

Table 5.3 Calculated HSPs for PCMX and artificial sebum components according to Hoftyzer –Van Krevelen methods	162
Table 5.4 HSPs for Triclosan, PCMX and artificial sebum components according to Y-MB method.	164
Table 5.5 $\ln K_{sw}$ and $Vm * D\delta tD$ for different chemical compounds	166
Table 5.6 Output of Regression statistics	167
Table 5.7 The HSPs of paraffin wax and spermaceti wax by using IGC method	169
Table 5.8 HSPs of artificial sebum according to Hoftyzer –Van Krevelen method	172
Table 5.9 HSPs of artificial sebum according to Yamamoto-Molecular Break method	172
Table 5.10 the miscibility of triclosan and PCMX with artificial sebum considering two methodologies VK-H and Y-MB	173
Table 5.11 Two formulations of triclosan nanoemulsion used in miscibility studies	174
Table 5.12 The results of miscibility of two triclosan formulations with artificial sebum	174
Table 5.13 Two formulations of PCMX Nanoemulsion used in miscibility studies	175
Table 5.14 The results of miscibility of two PCMX formulations with artificial sebum	175

List of Abbreviations

Hansen Solubility Parameter	HSP
Micrometre	μm
Customer squared	cm
Centipoise	cP
Energy of vaporization	ΔE_v
Hydrophilic-lipophilic balance	HLB
High-pressure homogenizer	HPH
High-performance liquid chromatography	HPLC
High-shear homogenizer	HSH
Hansen Solubility Parameters in Practice	HSPiP
Inverse Gas chromatography	IGC
kilojoules	kJ
Limit of detection	LOD
Limit of quantification	LOQ
Mean droplet size	MDS
Mole	mol
Nanoemulsion	NE
Nanometer	nm
Oil in water	O/W
Phosphate buffer saline	PBS
Chloroxylenol	PCMX

Polydispersity Index	PDI
Revolutions per minute	rpm
Span 20	S20
Span 40	S40
Span 60	S60
Span 80	S80
Tween 20	T20
Tween 40	T40
Tween 60	T60
Tween 80	T80
Van Krevelen–Hoftyzer method	VK-H
Molar volume	V_m
Surface free energy	γ
Yamamoto-Molecular Break	Y-MB
Zeta potential	ZP
Solubility parameter	δ
Dispersion	δ_d
Hydrogen bonding	δ_h
Polar	δ_p
Total solubility parameter	δ_t

Chapter 1 - Introduction

1.1 Healthcare-associated infections (HCAI)

Healthcare-associated infections (HCAI) defined as infections which affect patients due to their medical treatment from healthcare providers. In UK affect around 300 thousand patients annually with a prevalence rate of 8.2%; these infections are a primary concern in National Health Service (NHS) hospitals, and HCAI is considered a major safety concern being associated with higher rates of morbidity and mortality, in addition, high healthcare costs of around £1 billion annually (Cole, 2011).

1.1.1 Factors contributing to HCAI

Various factors may be partially or fully responsible for the prevalence of HCAI including: *environmental factors* (in general)– such as air contamination due to air-conditioning systems and hospital beds being too close together, *patient-related factors* – such as severe hidden health conditions and lengthened stay in hospitals, and *healthcare-associated factors* – such as using invasive devices, selection pressure due to high use of antibiotics and surgical procedures. The interaction between the factors occurs in all healthcare systems and more than one factor combined may be the reason for the occurrence of infections such as high staff-to-patient ratios and the absence of adequate intervention programmes designed to minimise HCAI. (Al-Tawfiq and Tambyah, 2014)

1.1.2 Types of HCAI

Urinary Tract Infections (UTIs)

Catheter associated urinary tract infections are the most common type of infections that patients contract during their time under medical care and, more than 12% of reported infections are UTIs. Patients endogenous native microflora is what causes CAUTIs. When catheters are inserted, they act as a channel which allows the entry of bacteria.(Khan, Baig and Mehboob, 2017)

The occurrence of CAUTIs can lead to various complications in patients including meningitis and cystitis in addition to potential complications specific to male patients including; prostatitis, epididymitis and orchitis. (Khan, Baig and Mehboob, 2017)

Lower respiratory tract infections

These types of infections are accountable for approximately 20% of HCAI, and they are the infections which impact the respiratory routes, i.e., trachea, bronchi and the lungs and the most severe and fatal type of these infections is pneumonia which leads to mortality in almost 40% of cases. (Morse, 2009)

Gastrointestinal

Gastrointestinal infections account for around 22% of HCAI, they are mainly generated by *Clostridium difficile* (*C. difficile*) which is an organism that makes spores which are then released in faeces causing contamination to the environment. Spores can be transported to another patient by ingestion due to direct contact with an infected subject or through the environment. Another common organism that may lead to gastrointestinal infections is norovirus which is very contagious and leads to vomiting and diarrhoea. (Morse, 2009)

Bloodstream infections

Central line-associated bloodstream infections are a common type of infections contracted while under medical care, the mortality rate of these infections is 12%-25%. These can result from the prolonged use of catheters, which are inserted in the central line of patients to deliver fluids and drugs. This prolonged use and the infections that can be caused by this can have a determinantal effect on the health of patients and increase cost of care. An annual rate of around 30 thousand cases of CLABSI occur in the United States in facilities such as intensive care units. (Kooi *et al.*, 2017)

Skin and soft tissue infections

The severity of these type of infections is varied and usually controlled by the depth to which the skin or soft tissue is affected, with deeper infections requiring surgical intervention. These types of infections account for around 10% of HCAI.

1.1.2.1 Surgical site infections (SSIs)

Surgical site infections are the second most common type of infections affecting patients under medical care, they account for around 2%-5% of patients undergoing surgery. The main cause for SSIs is *Staphylococcus aureus* which can lead to a prolonged need of hospitalisation and a consequent risk of death to patients. Endogenous microflora lead to arising pathogens that subsequently lead to SSI in patients. The procedures taken and surveillance criteria for the surgery performed highly affects the incident rate of the SSIs occurring, which can be as high as 20% in some cases. (Khan, Baig and Mehboob, 2017)

1.1.2.1.1 Microorganisms

The patient's flora is the most common source for the microorganisms causing SSIs, the main bacteria found due to SSIs are: *Staphylococcus aureus*, *Escherichia coli* and *Enterococcus species* (Schaberg, 1994). The escalation in the number of SSIs is due to antibiotic-resistant pathogens which lead to higher amounts of patients which are severely ill which generate a demand to use a broader variety of antimicrobial agents. Antibiotic-resistant pathogens include *methicillin-resistant Staphylococcus aureus* (MRSA) or *Candida albicans*. (Schaberg, 1994) Other factors such as contamination in dressings, elastic bandages and hospital tap water may lead to less common

microorganisms which can subsequently cause unexpected outbreaks in infections; these microorganisms include *Clostridium perfringens*, *Rhodococcus bronchialis*, *Nocardia farcinica* and *Legionella pneumophila*. (Mangram *et al.*, 1999)

1.1.2.1.2 Current prevention strategies for SSIs

SSIs can be considered avoidable; guidelines were set and published by the National Institute for Health and Clinical Excellence (NICE) in 2008 to review management methods and strategies to prevent similar infections. these guidelines were published by and are currently adopted by health systems in the UK. These strategies are divided into three phases: the pre-operative phase, the intra-operative phase and the post-operative phase, where each phase has its specific set guidelines as follows:

The pre-operative phase: Hair-removal is not to be routinely used to minimise the threat of SSI. Antibiotic prophylaxis to be given to patients before clean surgery which involves prosthetic or implant insertion, clean surgery and contaminated surgery, potential adverse effects to be taken into consideration when deciding on antibiotic prophylaxis.

The intra-operative phase: Skin at the surgical site must be prepared using antiseptic instantly before the incision is made, and surgical incisions must be covered with relevant dressings when finishing the operation.

The post-operative phase: Advice is to be sought on the correct dressing for surgical wound management for healing wounds by secondary intention, this advice must be given by a member of staff with expertise on tissue viability (NICE Guidelines, 2008)

In the intra-operative phase, the use of skin antiseptics before the incision is made is mainly superficial, and the use of nanotechnology will improve the penetration of antiseptics in the layers of the skin.

1.2 Skin structure

Skin plays a number of important functions that help to maintain body homeostasis such as protection, temperature control, and sensation. It is considered as the first line of defence for the entire internal body from external threats such as sunlight, viruses, cold weather, dirt and dust, as well as playing a role in temperature regulation. For example, when the body is hot and needs to cool down, the blood vessels in skin swell and allow heat to be emitted; the sweat glands start secreting sweat and hairs lie flat to permit the heat to depart from the body. Also, the opposite is true in the case of the body needing to retain heat in cold conditions.

The skin is one of the more popular routes for drug application, either for local or systematic effects. The route has been used to deliver active ingredients to targeted sites within the skin to treat many skin disorders such as alopecia (Gelfuso *et al.*, 2013) or acne (Thiboutot, 2004) without exposing the whole body to the side effects of active pharmaceutical ingredients (APIs).

It consists of three distinguishable layers: the epidermis, the dermis, and the subcutaneous layer (Figure 1.1).

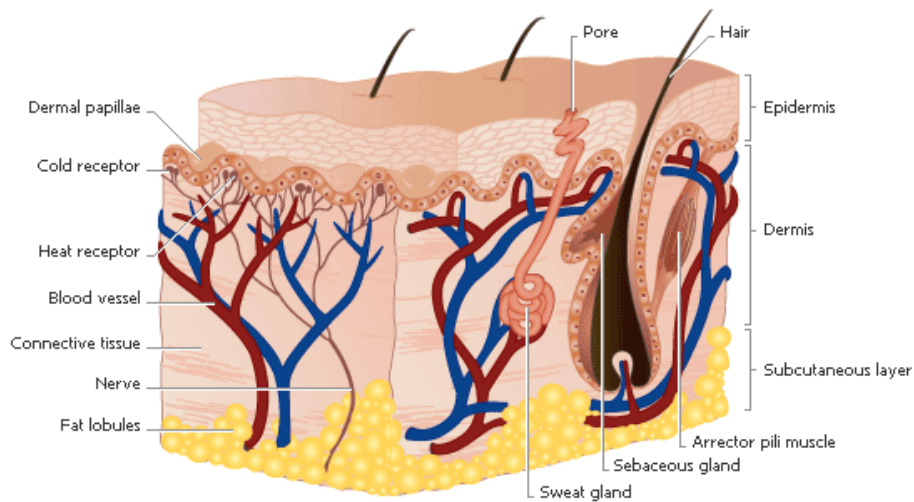


Figure 0.1 Structure of the skin (Uchechi, Ogbonna and Attama, 2014)

1.2.1 The subcutaneous layer

The subcutaneous layer is also called the hypodermis or superficial fascia; it is considered to anchor the skin to underlying structures. It mainly contains adipose tissue and blood vessels. The thickness of this layer is usually several millimetres except for some areas such as the eyelids where it is mostly absent. It also functions as storage for high-energy molecules and carries the principal blood vessels and nerves to the skin (Williams, 2007). The subcutaneous layer is not considered an important layer in the study of transdermal and topical drug delivery as it is rarely considered as a barrier.

1.2.2 The dermis

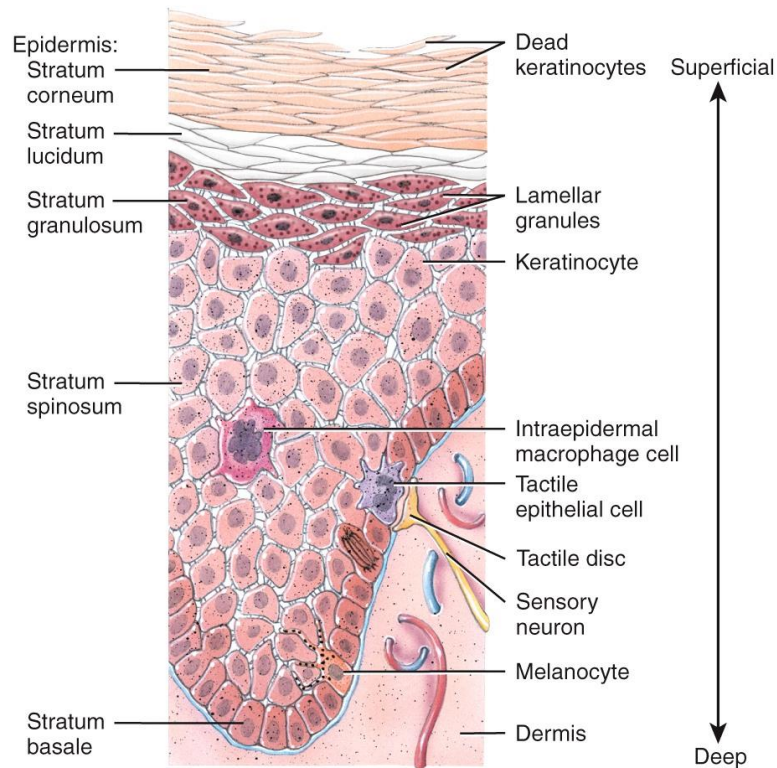
The dermis is a layer between the epidermis and subcutaneous tissue, it has a thickness of around 3-5 mm and contains connective tissue knitted with collagen, elastin and reticulin. The dermis plays an important role in transmitting nutrients, eliminating waste products, and control of pressure and temperature in the skin, consequently, it requires good blood circulation which it receives from the

arterial plexus that delivers blood to sweat glands, hair follicles, subcutaneous fat and the dermis itself (Williams, 2007).

1.2.3 The epidermis

The epidermis is the outermost layer of the skin, which overlies the dermis layer. It is composed of keratinised stratified squamous epithelium. Its most important functions are to control skin permeability, prevent the entry of biological pathogens, and synthesize vitamin D; the epidermis layer is also a self-regenerating layer.

The specific layers of the epidermis are the stratum basal which is a mitotic layer, continuously replacing epidermal cells, at a turnover rate of between 25 to 50 days. The stratum spinosum has cells that push upward and flatten out while the stratum granulosum cells contain granules of keratin. The stratum lucidum is observed only in non-hairy or thick skin and contains several layers of dead cells with indistinct boundaries. The stratum corneum is composed of 25 or more layers of dead squamous cells still joined together by desmosomes. Eventually, desmosomes break down, and cells flake off in a process called desquamation. Figure 1.2 shows the specific layers of the epidermis.



Location of four principal cell types in epidermis of thick skin

Figure 0.2 Structure of the epidermis (Tortora and Derrickson, 2014)

1.2.4 The stratum corneum

The major physical barrier of the skin is the stratum corneum (SC). Thus diffusion through the SC for a material permeating through the skin is often the rate-limiting step (Prow *et al.*, 2011). Additionally, it is the essential barrier to the diffusion of water out of the skin (Bennett, 1975). Cells are arranged in the SC as bilayers, which forms a 'bricks and mortar' arrangement. These cells are flattened, anuclear, protein-rich corneocytes tightly crowded together and exist amongst an extracellular lipid matrix (Prow *et al.*, 2011). The corneocytes are held together by corneodesmosomes, which help to form a tough outer layer by maintaining cellular shape and regular packing. Desquamation is the result of the break up the corneodesmosomes by proteolytic enzymes (Caubet *et al.*, 2004). Transport via the SC happens in three ways, transcellular, the intercellular and the appendageal routes. There is a thin (0.4 -10 μm),

irregular and discontinuous layer that covers the corneocytes on the SC surface; this layer is thought to have a negligible effect as a permeation barrier through the SC. The layer consists of bacteria, sweat and dead skin cells in addition to sebum which is secreted by the sebaceous glands (Tregear, 1966). Solutes were previously considered to take separate routes to permeate through the stratum corneum depending on whether they are polar or non-polar, as more lipophilic solutes go through the intercellular lipids and polar solutes take a transcellular route (Scheuplein, 1965). However, in most cases, this pathway has been marked unlikely due to the difficulty of repeated separation of lipophilic and hydrophilic compartments in the SC. There has been both theoretical and histochemical evidence to support this; evidence demonstrated that diffusion through intercellular lipids was more likely for most solutes. For the transcellular route, it is still controversial even for lipophilic solutes in spite of reaffirmations of the importance of this route. With the majority of work centred on the hair follicles, the delivery of particles and drugs through the appendageal route is considered a sensible substitute to delivery across the SC (Prow *et al.*, 2011)

1.2.5 Hair follicles

Hair follicles (HF) have recently been studied as a substitute pathway for dermal absorption. Regardless of their relatively low surface coverage of around 0.1%, they are frequently considered to enable permeation (Otberg *et al.*, 2004). Hair follicles also provide considerable assistance to the absorption of (sub)micron particles and small molecules, particularly small molecules with octanol-water partition coefficients varying between low to intermediate (Frum, Eccleston and Meidan, 2008; Patzelt *et al.*, 2011).

Furthermore, HFs are considered to serve as interesting target sites for drug delivery. For example, nanoparticles (NP) form a depot within the HF; this is because of the slow clearance rate by hair growth

and sebum-flow and can provide protection against removal by washing or from contact with clothing (figure 1.3).

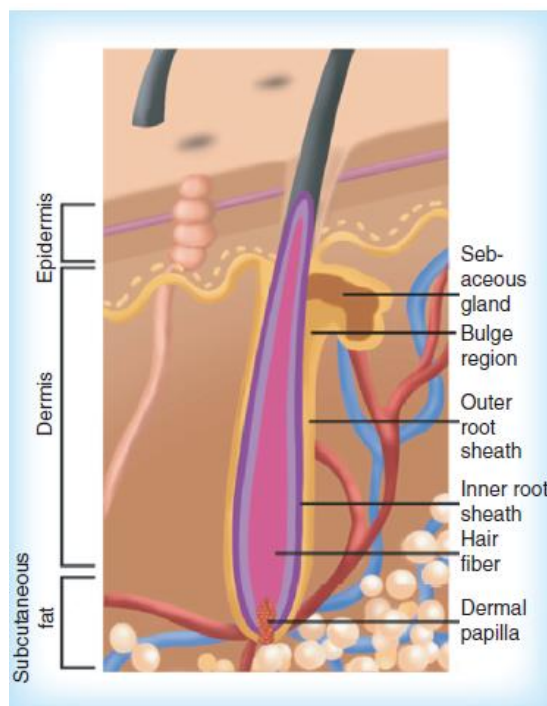


Figure 0.3 structure of hair follicles (Fang *et al.*, 2014)

Moreover, in the lower third of the HF, the stratum corneum (SC) is not present, facilitating the penetration of substances (Raber *et al.*, 2014). However, it has been shown by Otberg *et al.* (2004) that the follicle density varies in various body sites. For example, this is observed for the forehead and the calf regions; a high density of small hair follicles is present on the forehead, whereas the follicles are larger with smaller density on the calf region (Otberg *et al.*, 2004).

Lademann *et al.* (2006) reported that time-dependent differences were displayed for the retention of nanoparticles in both the stratum corneum and the hair follicles. The nanoparticles remained in the stratum corneum for 24 hours, whereas in the hair follicle nanoparticles were observed even after the 10-day period. At 30 min after nanoparticle application, the actual values reached were eight times

higher in the SC than within the hair follicle (Lademann *et al.*, 2006). One important consideration is that an oily substance is secreted by sebaceous glands into the hair follicle making it very important to study the diffusion properties and drug partition in the sebum for the targeted delivery of therapeutic agents into the sebum-filled hair follicle (Valiveti and Lu, 2007).

1.3 Wounds

1.3.1 Wounds definition and classification

A wound can be defined as destruction or disturbance to the skin in its functionality in providing protection; this occurs due to the epithelium losing its ability as a barrier as a result of one or more factor such as surgery, cuts, frictional forces, chemicals or even as a consequence of a disease. Wounds have been categorised into multiple types based on several factors including injury leading to wound, wound location and the healing time needed for the wounds. According to the healing time necessary for wounds, they can be categorised into acute or chronic wounds.

1.3.1.1 Acute Wounds

This type of wound is relatively common, and the healing time required is usually no more than 30 days as the tissue repair process begins instantly after the occurrence of the injury. The damage in acute wounds only affects the epidermis layer and the superficial dermis, and these types of wounds can be further classified in relation to the cause of the wound into many categories including surgical wounds, thermal burns, lacerations and abrasions. Another classification can be based on the type of the wound in relation to its depth and size (HC Korting & C Schollmann, 2011)

Surgical incision wounds

This type of wound occurs through surgery, and the duration of damage is dependent on the surgery and some surgical incision wounds can cause pain to the patient and are life-threatening. This type of wound can be particularly harmful if made in the heart, lungs or blood vessels.

Burns

Burns can occur due to contact with heat, electricity, radiation or friction; this can lead to damage of skin tissue in its surface layer and deeper into other layers depending on the severity of the burn. Some burns can be treated by simple measures, whereas others must be treated in hospitals. These wounds may cause a large loss of skin functions and damage to the skin which may subsequently cause infection, and in some cases, they may cause the skin to lose its functionality including its normal thermoregulation and immunity (Li, Chen and Kirsner, 2007)

Abrasion wounds

These types of wounds lead to damage or removal of the epidermis due to contact with other surfaces in the form of friction or small cuts. Abrasion wounds are usually painless and do not generally cause bleeding (HC Korting & C Schollmann, 2011)

Lacerations

Lacerations lead to deeper cuts than those in abrasion wounds and this type of wound generally causes bleeding and severe pain. The cause of laceration wounds is normally due to a sudden accident or trauma (Monaco & W. Thomas Lawrence, 2003)

1.3.1.2 Chronic Wounds

Acute wounds will often develop into chronic wounds if they are subjected to one of the following factors: systemic disease, long-term inflammation or a toxic environment. In some cases, wound healing

is impaired, and this lead to the development of chronic wounds (Eming and Krieg, 2002) These wounds are also classified into various types including: ischemic wounds, infectious wounds and surgical wounds. (Degreef, 1998)(Robson, 2001)(Szycher and Lee, 1992)

Ischemic wounds

These chronic wounds can be identified by their appearance as they will usually be cold and pale. The reason behind the development of these wounds is a reduced blood supply reaching the tissue which delays the wound healing process due to undersupply of nutrients and oxygen to the tissue.

Infected wounds

Infected wounds can generally be identified by the encompassing of pus and debris and the release of bad odours, these wounds occur due to bacteria, fungi or viruses and result in symptoms of inflammation including redness, pain and high fever.

Surgical wounds

As mentioned in 1.2.1.1.1, surgical wounds are normally acute; however, they may transition into chronic wounds when necessary treatments are not followed. The most likely consequence of this lack of required treatment is an ulcer and ulcers can also be further divided into venous ulcers, diabetic and pressure ulcers.

Various diabetes disorders, including vascular, metabolic and neurological, may lead to the development of ulcers. The way these disorders cause ulcers is that they first lead to damage in the nerves and a lack of adequate blood supply in addition to impairing immune functions which will all subsequently lead to damage of the skin and eventually ulceration. However, these chronic ulcers are painless.

The main location for the development of pressure ulcers is the bony areas in the body that are near the skin, and they arise due to friction or pressure which causes a disturbance in the blood flow reaching the

soft tissue. This then causes an injury to the skin and/or tissue beneath the skin. Pressure ulcers can be identified by the redness and itching they cause in addition to the swelling and discolouration.

Venous ulcerations are the most frequently developed type of vascular ulceration and are particularly common in lower limbs like deep vein thrombosis, venous hypertension and varicose veins. It is not unusual for patients who develop venous ulcers to have previously been subjected to lower limb oedema or damage and leaking in veins.

1.3.2 Wound infection

These are infections that occur in and/or surrounding the wound area, therefore, causing an interruption in the wound healing process, and the reason behind wound infections is due to the presence of microorganisms within the wound site or around it. Microorganisms most commonly present in the skin arise from external sources and are harmless if the skin is undamaged, however, when the skin is damaged, in the case of a wound, the skin loses its protective ability in that area, and the microorganisms gather and colonise the wound site, subsequently leading to a delay in the healing process of the wound.

Various types of microorganisms lead to the infection of wounds and the most frequent bacteria causing these infections are *Staphylococcus aureus* in addition to different groups of *Streptococci* (Phillip M & Williford, 1999) Other well-known microorganisms which contribute in skin infections include *Pseudomonas aeruginosa*, *Staphylococcus epidermis* and *Escherichia coli* (Percival *et al.*, 2012)

Wound infection can cause the loss of soft tissue which may lead to the need for amputation and can also be fatal in some severe cases. It has been reported that similar types of microbial infections are the

reason behind the death of around 10 thousand wound patients in every million. (Edwards and Harding, 2004)(Percival *et al.*, 2012)

1.3.3 Wound healing

Wound healing is arranged into four continuous and overlapping phases, haemostasis, inflammation, proliferation and finally, the remodelling phase (Diegelmann, 2004) (figure 1.4).

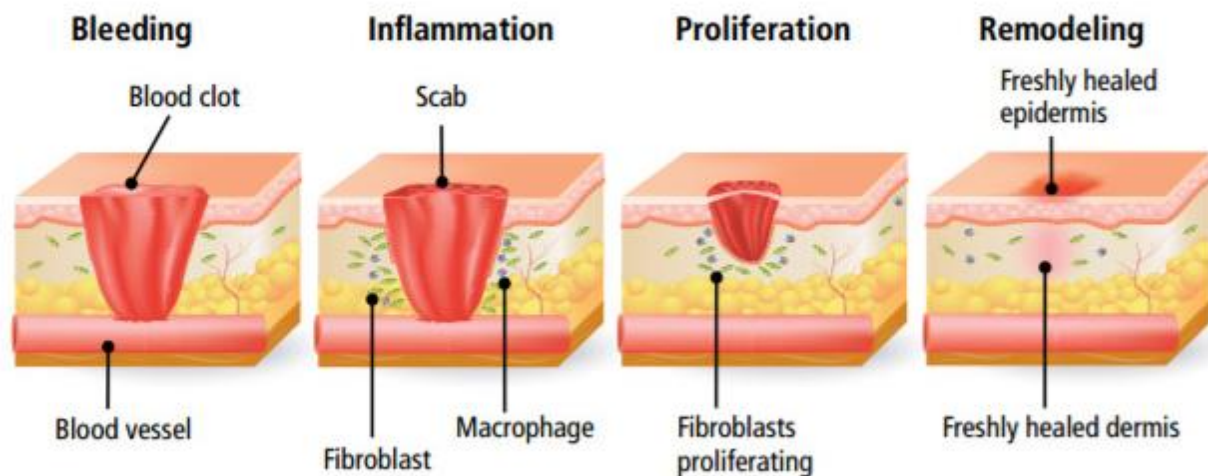


Figure 0.4 Four phases of wound healing (Hemmila, M.R., Mattar, A., Taddonio, M.A., Arbabi, S., Hamouda, T., Ward, P.A., Wang, S.C., Baker, 2010)

1.3.3.1 Haemostasis

This is the first phase which takes place immediately after the occurrence of an injury and can simply be described as the phase in which the wound is closed through clotting. The aim of this phase is to stop more tissue from being lost from damaged blood vessels. This phase generates the supporting matrix needed for migrating cells which plays an important role in the upcoming healing phases. (Broughton, 2006) (Robson, 2001) Haemostasis is accomplished when the synthesis of insoluble fibrin results in the

adhesion and accumulation of platelets; where adhesive molecules like fibronectin and vitronectin are stored on a fibrin mesh. The fibrin clots that are formed within the damaged blood vessels promote the termination of haemorrhage and the surrounding tissue with the blood vessels discharged into it form a provisional matrix used by migrating cells that are involved in the repair. The last stages of this phase are completed when inflammatory cells are activated by platelet-derived growth factors alongside fibrin degradation products.

1.3.3.2 Inflammation

This is the second phase of the healing process which immediately follows haemostasis. In this phase, an immune barrier for protection against microbial colonisation is created by cellular inflammation, and blood vessels release various leucocytes as a response to the cellular signals. This phase of wound healing can be divided into two stages based on the dominant type of leucocytes; these two phases are known as the early stage and the late stage (Hart, 2002). The early stage of the inflammation phase is dominated by neutrophils which facilitate phagocytosis and subsequent destruction of bacteria, therefore, leading to debridement of the wound. In the late stage, the predominant leucocytes are macrophages; the stage is completed when the lymphocytes infiltrate into the wound site.

1.3.3.3 Proliferation

The proliferation phase is characterised by the migration and growth of dermal and epidermal cells from neighbouring sites to the wound site, fibroblasts migrate, and new extracellular matrix (ECM) is deposited to replace the temporary network consisting of fibrin and fibronectin lasting around two weeks. The proliferation of the fibroblasts, in addition to the migration and the differentiation all take place due to the influence of growth factors. Other important characteristics of this phase are the formation of granulation tissue in addition to wound contraction which happens through the activity of

differentiated myofibroblasts which originate from mesenchymal fibroblast cell lines. (Gilbane, Denton and Holmes, 2013)

1.3.3.4 Remodelling

The remodelling phase in wound healing is considered the last stage; therefore, in this phase, the new epithelium is formed in addition to final scar tissue. This is the longest phase of wound healing and can last for up to two years after the occurrence of the injury (Witte and Barbul, 1997 & Ramasastry, 2005). Various actions take place during this phase such as the further organisation of collagen, and fibronectin is eliminated, glycosaminoglycans and hyaluronic acid are substituted with proteoglycans. Other factors occurring in this phase include: ECM is actively reorganised, new capillaries are formed, and proliferation and inflammation are reduced, these factors lead to a reduced need for nutrients in this phase. (Guo and Dipietro, 2010)

1.3.4 Wound Dressings

Traditionally, wound dressings were designed with the purpose of absorbing excretions from wounds in addition to maintaining a dry atmosphere. However, it is now recognised that it is important for the wound site to remain hydrated and moisturised to facilitate faster healing of wounds. To maintain hydration and retain moisture, new types of wound dressings were introduced which accomplished the necessary atmosphere through the occlusion. (Boateng *et al.*, 2008) (Schultz *et al.*, 2002)

Wound dressings are used for various type of injuries ranging from minor superficial wounds to more complicated infected wounds and play multiple roles in stopping wound bleeding, preventing worsening of wounds by protecting them from bacteria in the surrounding environment in addition to expediting the healing of wounds through the prevention of excessive wound exudate being present. Any ideal dressing must, therefore, perform the following functions: preserving the ideal humid environment,

forming a physical barrier from other infections and absorbing microorganisms and wound excretions.

(Quinn *et al.*, 1985)(Diegelmann, 2004)

1.3.4.1 Wound dressing types

Wound dressings are mainly split into two categories, the first category is the traditional dressings which include cotton wool, natural and synthetic bandages and gauzes. The second category, modern dressings, includes hydrogels, foam dressings, hydrocolloids, adhesive film dressings and alginates. These can be further subdivided into more categories regarding the dressing's function and can be categorised into antimicrobial, absorbent, occlusive, adherence and debridement dressings. Another categorisation for dressings is based on the level of contact the dressing has with the wound where primary dressings are the first type, and these dressings have direct physical contact with the surface of the wound, whereas secondary dressings do not have direct physical contact with the wound and normally cover primary dressings(K and Babu, 2000 & A NNA F. F ALABELLA, 2006).

1.3.4.1.1 Gauze Dressings

Traditionally, gauze dressings were dry and did not maintain moisture which was proven to be inadequate for wounds which produce a small amount of exudate, in addition to causing discomfort and trauma during removal. Therefore, newer designs of gauze dressings aim to maintain a moist atmosphere for the wound leading to improved results and less discomfort when serving as a primary dressing, whereas, traditional designs can be used for secondary dressings and they can also be used for wounds that are dry and clean. Gauze dressings comprise materials such as cotton fibres or rayon polyester and can sometimes be a combination of both materials.

1.3.4.1.2 Foam Dressings

Modern foam dressings are suitable for covering wounds which have little to moderate amounts of exudate as they can absorb moderate fluid levels. This absorbing ability is due to their porous polyurethane components which make these dressings adequate for treating granulating wounds. However, since foam dressings are dependent on exudates, they are unsuitable for the treatment of dry scars or wounds. (Ramos-e-silva, 2002) Branded foam dressings available include Lyofoam® (ConvaTec, UK) and Allevyn® (Smith and Nephew).

1.3.4.1.3 Hydrocolloid Dressings

Hydrocolloid dressings are usually made from pectin, gelatin and carboxymethylcellulose and are available in a range of forms such as films, sheets and gel forms where the gel form is an adhesive hydrocolloid gel. (Bethell, 2003) Hydrocolloid dressings are considered to be the most popular type of dressings; they are mostly suitable for wounds with little to moderate levels of exudate as the outer layer of the dressing is initially impermeable to oxygen, water vapour and bacteria when it is fully intact and gradually become more permeable as the gelling process occurs. (Barnea *et al.*, 2004) There are various brands of hydrocolloid dressings which include Tegisorb® (3M Healthcare, UK), Aquacel® (ConvaTec, UK) and Comfeel® (Coloplast, UK)

1.3.4.1.4 Hydrogel Dressings

These dressings are hydrophilic materials which are insoluble and made from synthetic polymers such as polyvinylpyrrolidone and are capable of transferring vapour and water, while also providing required moisture to the wound. (Fan *et al.*, 2011) The mechanism these hydrogel use is to rehydrate dead tissues and enhance the autolytic debridement for treating dry wounds, without causing irritation and without reacting to the biological tissue while providing permeability to metabolites. (Wichterl, 1960)

1.3.4.1.5 Alginate Dressings

Alginate dressings are made of sodium and calcium salts of alginic acid. Alginate dressings form a protective gel film by exchanging calcium ions in the alginate fibre with sodium ions in blood when treating wounds. Commercially available products of this dressing type include Kalostat® (ConvaTec, UK) and Sorbsan® (Maersk, UK)

1.3.4.1.6 Biological Dressings

Biological dressings, also referred to as bioactive dressings, are composed of biomaterials with important roles in the process of healing as they form sections of the natural tissue matrix and are made using various polymers including collagen, chitosan, hyaluronic acid and elastin. (Ishihara *et al.*, 2002)(Ueno *et al.*, 1999)

1.3.4.1.7 Antimicrobial Dressings

The main role of antimicrobial dressings is to eliminate or limit microorganism growth within a wound. Using antimicrobial dressings for topical treatment will minimise wound infection risk, and this type of dressing can be used for various infected injuries ranging from acute wounds to chronic wounds. There are multiple characteristics that the optimal antimicrobial for local treatment should have which include being non-toxic and non-allergenic, having a wide range of activity in addition to being microbicidal. (Flores, 2007) Various antiseptics have been applied in antimicrobial dressings including chlorhexidine, silver, polyhexamethyl biguanide (PHMB) and iodine. (Gerald McDonnell, 1999)

1.4 Antiseptics

1.4.1 Alcohol

Alcohols are considered effective antimicrobials with broad-spectrum against bacteria, viruses, and fungi. Ethyl, isopropyl alcohol, and n-propanol are the most commonly used. However, they are not the

best option for sterilisation as they are not sporicidal but recommended for disinfection and skin antiseptics. Products with a combination of alcohol and a low concentration of another antiseptic (like chlorhexidine) increase the efficacy of antimicrobials since the other antiseptic agent remains in the skin after the alcohol evaporates (Small *et al.*, 2013). At high concentrations of alcohol (60 to 90% v/v), an antimicrobial effect will be optimum, whereas below 50% will be considerably low (McDonnell & Russell, 1999). Not much is clear about the mechanism of action of alcohol. However, it causes membrane damage, protein denaturation and cell lysis. (Fraise *et al.*, 2013)

1.4.2 Biguanides

1.4.2.1 Chlorhexidine

Chlorhexidine has a broad spectrum of uses, low irritation and high efficacy and does not cause high irritation to the skin and has high substantivity in the skin, due to these characteristics, it is the most commonly used antiseptic product as a biocide (Day and Russell, 1993). The interaction of chlorhexidine with bacteria was studied for the first time by Hugo *et al.* 2013 . in which it was found that *E. coli* and *S. aureus* can take up chlorhexidine (Gerald McDonnell, 1999).

Since this antiseptic is not sporadic, the viability of *Bacillus* spores is not affected by chlorhexidine, even at its higher concentrations. The effect chlorhexidine has on the germination of bacterial spores is very small. However, it restricts outgrowth. The reason behind this, although not known definitely, could theoretically be due to the relative uptake of chlorhexidine as germination of cells in comparison with outgrowing require much less of the bisbiguanide (Fraise *et al.*, 2013).

1.4.2.2 Alexidine

This antiseptic has different Ethylhexyl end groups from chlorhexidine (figure 1.5), the bactericidal ability of alexidine is faster, and the alteration produced in bactericidal permeability is also significantly more rapid (Gerald McDonnell, 1999).

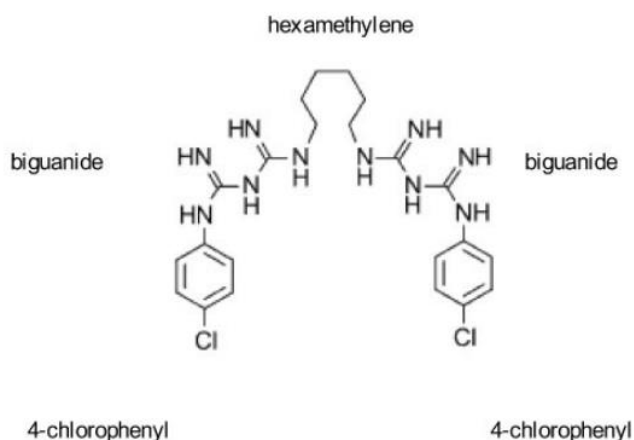


Figure 0.5 structure of chlorhexidine (K.S. Lim & P.C.A. Kam, 2008)

1.4.2.3 Polymeric biguanides

These types of antiseptic have a wide range of applications including in the food industry as well as being very effective in disinfecting swimming pools. Polyhexamethylene biguanide (PHMB) is an agent that is membrane-active and causes impairment in the stability of the outer membrane of gram-negative bacteria and can also operate as a barrier for permeability. The level of activity of PHMB rises with its weight which leads to higher polymerisation levels; this has been associated with improved perturbation of the inner membrane (Gilbert, Collier and Brown, 1990).

1.4.3 Iodine-releasing agents

Iodine has been used as an antiseptic for over a century in both its aqueous and alcoholic forms. Iodine has the advantages of being highly bactericidal, sporicidal and fungicidal. However, it has challenges associated with its use including high staining and irritation of the skin. Aqueous solutions are relatively

unstable. Due to these downfalls, iodine-releasing agents were developed which are complexes of iodine in addition to a solubilising agent. The iodine-releasing agents maintain the germicidal ability but reduce the fungicidal activity. Although the exact mechanism is unknown, iodine has a fast antimicrobial ability even when it is at a low concentration, the microorganism can be quickly penetrated by iodine, and key groups of proteins are then attacked (Gottardi, 1991).

1.4.4 Silver compounds

Various forms of silver have been used for many years as an antimicrobial agent, The most popular in current use is silver sulfadiazine (AgSD), although other silver compounds are also still in use and have antimicrobial properties; these include silver nitrate, silver protein and silver metal. Silver antiseptics in their various forms have been used in many applications; recent applications include the prevention of burns infections, eye infections, and to overcome warts. Other medical functions include their use in dental applications and catheters (Klasen, 2000).

1.4.5 Phenols

Phenolic antimicrobials have been used in various applications including perseveration, antiseptic and disinfectant usages. The membrane-active properties of these compounds are large contributors to their general activity (Denyer, 1995).

Phenol acts as a promoter for the gradual leaking of the constituents within a cell which includes the release of K^+ ; this is thought to be the first sign of damage to the membrane. Low concentrations of phenol and different non-phenolic agents have been shown to cause break down of quickly growing cultures of various bacteria including *E. coli*, streptococci and staphylococci which led to the conclusion that no autolytic enzymes were involved. It has also been proposed that phenol's action is solely at the

separation point of daughter cell pairs, therefore, leading to higher sensitivity to phenol in young bacteria cells than old cells.

Phenols have antifungal and antiviral characteristics; the antifungal properties of phenol are believed to include destroying the plasma membrane which consequently leads to leaking in the intercellular constituents. Phenols, however, do not have any impact on phage DNA in the capsid, and only have a small impact on various phage band proteins, except for those who are treated for a minimum of 20 minutes (Maillard *et al.*, 1995).

1.4.6 Bis-phenols

These are hydroxy-halogenated products from two phenolic groups which are connected to one another through different bridges. They are generally known to have broad range efficacy. However, their activity towards *P. aeruginosa* and moulds is very limited in addition to only having a sporostatic effect on bacterial spores. The two main and most commonly used biocides within this group, particularly in antiseptic soaps and hand washes are triclosan and hexachlorophene. These two compounds have been proven to have a very high and persistent impact on the skin (Gerald McDonnell, 1999).

1.4.6.1 Triclosan

Triclosan (2,4,4,9-trichloro-2-hydroxy diphenyl ether) has specific activity towards gram-positive bacteria, and its efficacy towards bacteria, yeasts and gram-negative bacteria can be notably improved through formulation effects. This has been proven in various cases, one of these was the addition of EDTA to triclosan which led to higher permeability in the outer membrane. Suggestions have been made to triclosan may have anti-inflammatory activity in addition to its established antibacterial properties (Rølla, 1994).

Although the exact action mechanism of triclosan remains unknown, suggestions have been made which state that its main effects are on the cytoplasmic membrane. Low concentrations of triclosan, when tested with *E. coli*, caused inhibition to the intake of required nutrients, and higher concentrations led to a fast release of cellular components in addition to leading to the death of cells (Gerald McDonnell, 1999).

1.4.7 Halophenols

1.4.7.1 Chloroxylenol

The main halophenol that is in use for antiseptic and disinfectant purposes is chloroxylenol (4-chloro-3,5-dimethylphenol; p-chloro-m-xyleneol). Although bactericidal, many moulds are resistant to its action, as is *P. aeruginosa*, and its mode of action is not yet fully understood, but since it is phenolic, it is expected that it affects microbial membranes (McDonnell and Russell, 1999).

1.5 Nanotechnology

Nanotechnology is an interesting development across engineering, biology and pharmaceutical fields and is relatively considered a new Nano-scale was defined from 1 nm to 1000 nm (Forrest and Kwon, 2008). One of the reasons behind applying nanotechnology in the pharmaceutical field is enhancing the bioavailability by improving the solubility and permeability of the API (Roduner, 2006). Moreover, at the same time nanotechnology reduced the side effects of an API by reducing the amount of drug as the surface area was increased (Agrawal *et al.*, 2013). With the development of this technology, the skin has become a potential route for these nanoformulations. (Prow *et al.*, 2011). Most of these nanoformulations are lipids carriers, or nanoemulsions with droplet size around 300 nm. And by using this nanoformulation, it is possible to increase the amount of drug that penetrates through the skin without inducing significant irreversible alterations to this barrier (skin) (Kreilgaard, 2002). This thesis

focuses on the developing formulations designed to deliver antiseptic agents to target sites within the skin to prevent the development of SSIs.

1.5.1 Nanoemulsions

A nanoemulsion is a system that consists of two immiscible liquids where one (the disperse phase) is dispersed in the other (the continuous phase) as a small droplet with a size ranging from 10-600 nm. In addition, a third component (emulsifying agent) is added which surrounds the droplets to prevent collapsing and segregation by reducing the interfacial tension between the two phases, therefore, choosing a suitable surfactant is a critical step in formulation and stability of the nanoemulsion (Solans *et al.*, 2005).

Nanoemulsions can be oil in water (o/w) or water in oil (w/o) or can have multiple phases, depending on which is the disperse phase and which is the continuous phase (Mason *et al.*, 2006). Unlike microemulsions which are thermodynamically stable, nanoemulsions are not spontaneously formed. However, they are kinetically stable, with no apparent flocculation or coalescence (Tadros *et al.*, 2004). However, the main issue of stability of nanoemulsions is Ostwald ripening which happens when the disperse phase has some limited solubility in the continuous phase. It can be overcome by adding a second disperse phase which is totally insoluble in the continuous phase or by using a different surfactant or a mixture of surfactants which is strongly adsorbed on dispersing droplets (Tadros *et al.*, 2004). There are also other advantages other than stability: nanoemulsion production is easy to scale up, and are less likely to cause irritation than microemulsions due to requiring a lower amount of surfactant. (Bouchemal *et al.*, 2004). Thus, nanoemulsion formulations may have applications in topical delivery.

1.5.1.1 Role of surfactant

As mentioned above, in addition to oil and water, surfactants are the third component in the formulation of a nanoemulsion. They play a vital role by preventing coalescence between droplets by forming an interfacial film around the new droplets. It is formed during the production process and prevents re-coalescence (Fletcher and Horsup, 1992). For dermal formulations, non-ionic surfactants are preferred as they are less irritant to the skin than ionic surfactants. An example of non-ionic surfactant is Tween[®] 80, and Span[®] 80 and in addition to the role of improving the stability of nanoemulsion, the surfactant has a role in enhancing the penetration of the formula through the skin. According to Kushal and Zatz, (1991) when the role of cationic surfactant in the enhancement of water and lidocaine flux was explored, a high concentration of surfactant the flux of both water and lidocaine was found to be preferable. Therefore choosing the appropriate emulsifier is very important in the process of production of a nanoemulsion.

1.5.1.2 Role of HLB

The hydrophile-lipophile balance is a system designed to categorise emulsifying agents according to their polarity with hydrophilic surfactants favouring o/w emulsions and the lipophilic surfactant favouring w/o emulsions. Figure 1.4 shows the HLB scale for the classification of surfactant functions.

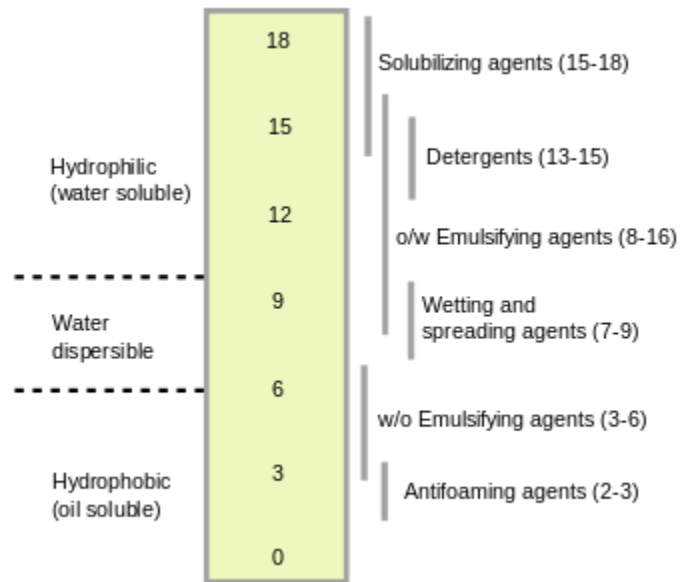


Figure 0.1 HLB scale for the classification of surfactant functions (D.Attwood, 2013)

There are various formulae for calculating the HLB value, one of which depends on the chemical structure of the surfactant and each group contribution has a specific value (Appendix 1). The HLB value for the determined surfactant can be obtained using equation 1.1.

$$HLB = 7 + \sum(\text{hydrophilic group numbers}) - \sum(\text{lipophilic group numbers}) \text{ equation 1.1}$$

It has been reported that some surfactants with given HLB values work best with specific oils, which led to the concept that all oils should have a specific required HLB value. So, to improve the stability of the emulsion, this value must be obtained. Therefore, the mixture of surfactant shows better stability than the singular as it easy to achieve the required HLB value for this oil by changing the percentage of surfactant,also due to complex interfacial layer formation (Tadros *et al.*, 2004).

1.5.1.3 *Enhancement of skin penetration*

There are various strategies and materials which help with the enhancement of the penetration and absorption through, and within the skin, these are known as penetration enhancers. Two types of approaches can be used: physical approaches such as stratum corneum stripping, and stratum corneum hydration and chemical approaches such as synthesis of lipophilic analogue, delipidation of stratum corneum, and coadministration of penetration enhancers (Sapra, Jain and Tiwary, 2008). Examples of these enhancers are surfactant (Tween), fatty acids/esters (oleic acid), solvents (ethanol) and terpenes (eucalyptol).

1.5.1.3.1 Eucalyptus oil

Essential oils are aromatic oily liquids collected from several plants, most commonly by steam distillation. They have been used as a flavouring, antiseptic, and antibacterial agents (Burt, 2004). Eucalyptus oil is obtained from leaves of eucalyptus, a genus of the plant family *Myrtaceae*. The mechanism of antimicrobial activity of eucalyptus oil is not yet fully understood, but as reported by Cowan (1999) eucalyptus may act on the plasma membranes of microorganisms, and enhance the permeability of the cell membrane (Cowan, 1999). According to Cromwell *et al.* (1995) terpenes such as eucalyptol, the major component of eucalyptus oil, and d-limonene show significantly enhanced penetration within the skin for hydrophilic and hydrophobic compounds (Cornwell, 1996). In addition to enhancing penetration, a study by Hendry *et al.* (2009) reported a synergic antimicrobial effect between eucalyptol and chlorhexidine digluconate against some clinical isolates including *S.aureus* and *E.coli* (Hendry *et al.*, 2009).

1.5.2 Production of nanoemulsions

Production methods for of nanoemulsions may be classified into two groups: high energy methods and low energy methods and both can produce nanoemulsions with small droplets and uniform distribution (Campos, Ricci-júnior and Mansur, 2012). Examples of high energy methods include:

Microfluidisation- the droplet size in this technique can be modified by changing the pump pressure or by altering the number of times it passes through the chamber (Seid Mahdi Jafari & Yinghe He, 2007),

Ultrasonication- although this technique can produce very small droplets, to produce a nanoemulsion with a good Polydispersity index (PDI), the run must be repeated multiple times because the samples close to the vibrating probe are often smaller (Fraise *et al.*, 2013).

High-pressure homogeniser- this method was used in this thesis (section 3.1.4.1). The advantages of this method are that it is easily scaled up, and it is a continuous process.

Low energy methods include *phase inversion temperature*; this is a preferred method in the industry as it does not require high energy levels. However, all the compounds must be able to withstand high temperatures (Hessien *et al.*, 2011).

1.5.3 Analysis methods for detection of retained drug in the skin

Various experimental techniques are used to study absorption from different formulations into skin; these techniques allow measuring of *in vivo* penetration or *ex vivo* penetration or permeation characteristics of elements penetrating through the SC barrier.

1.5.3.1 Tape stripping technique

This famous technique was first proposed by Pinkus in 1951, it is commonly used to study and evaluate the localisation of various elements within the SC and their distribution and is a minimally-invasive method (Hermann Pinkus, 1951). The tape-stripping technique was later developed to a combination of

tape-stripping and superglue stripping and was known as differential stripping; this facilitated evaluating the process of hair follicle penetration quantitatively (Teichmann *et al.*, 2005).

The differential stripping method is performed by applying the substance to the skin then performing the tape-stripping method to extract the substance portion that is within the SC; this is followed by the superglue stripping technique to remove the remaining substance which is located within the orifices of the hair follicle. This, therefore, enables the quantitative evaluation by region of substances within multiple pathways, intercellular, transcellular and transfollicular (Teichmann *et al.*, 2006)

For *ex-vivo* evaluations, the skin fixed onto Franz diffusion cells is exposed to the drug for set times before it is removed and studied and the penetration of the drug is quantified; this evaluation can be for full-thickness skin or defined thicknesses of skin as horizontal sections. HPLC is usually used after this to analyse the amount of drug in the receiver fluid. Other methods such as infrared imaging, Raman spectroscopy and confocal laser scanning microscopy are other forms of quantification methods which can be used (Anja Gysler, 1999, Naik *et al.*, 2004).

However, it is important to note that at the subcellular level, spatial resolution is not achieved by most of these approaches; therefore, some studies for skin absorption replace the drug with dyes to visualise the substance within the skin and the transport of the substances using fluorescence microscopy (Küchler *et al.*, 2009). High sensitivity is achieved with confocal laser scanning, and two-photon microscopy as single-molecule detection is possible, however, since fluorescence microscopy requires drugs to show fluorescence, this method cannot usually be used to examine the uptake of drugs in the skin (Peter T *et al.*, 2000)

1.5.3.2 X-ray microtomography (Micro CT scan)

In the field of materials science, the understanding of a material's microstructure provides an in-depth understanding of its mechanical and physical properties. The characterisation of these properties is usually shown using two-dimensional images through optical or electronic microscopy, resulting in a limitation of the measurable parameters and may require destruction of specimens. These two difficulties can be overcome using three-dimensional imaging with x-ray microtomography which facilitates more measurable parameters of the internal microstructure without requiring destruction of the samples (Salvo *et al.*, 2010).

X-ray microtomography can be defined as "A radiographic imaging technique that can produce 3D images of a material's internal structure at a spatial resolution better than 1 micrometre" (Govender *et al.*, 2003). This is also commonly referred to as micro-CT and has been used in various medical applications for over 40 years (Hsieh, 2009).

The principle of micro CT requires the specimen to be fixed on an x-ray beam trajectory, a section of the x-rays is transmitted and converted to visible light with the use of a scintillator, whereas, the rest is absorbed. The light corresponding to sample projections is recorded using optics such as CCD (charge-coupled device) and CMOS (complementary metal-oxide-semiconductor) cameras, this is followed by a 180° or 360° rotation of the sample during which several hundreds of projections are recorded. This series of projections is usually known as a scan; this scan is used for reconstruction of a sample 3D image (Figure 1.3) (Deckman *et al.*, 1990; Kinney and Nichols, 1992).

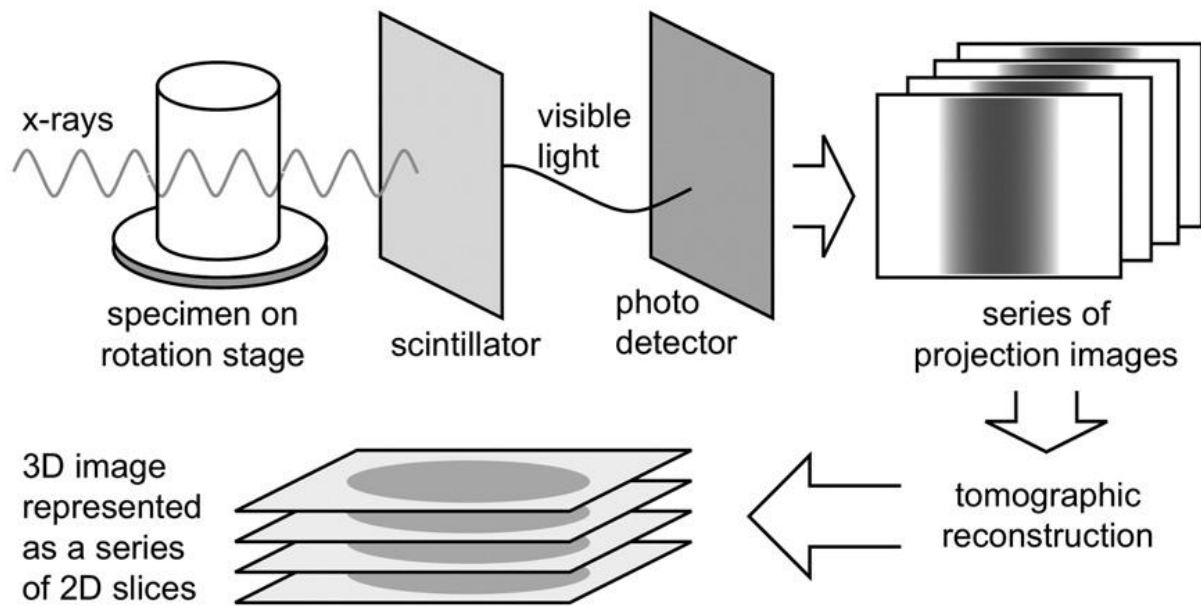


Figure 0.2 - Stages of micro CT principle(Kinney and Nichols, 1992)

The coefficient of absorption varies depending on a few factors such as material density, X-ray energy and atomic number. This variation is reflected by a contrast in the image due to the various characteristics of the microstructure in the material (Salvo *et al.*, 2010).

X-ray microtomography has multiple applications including *the* analysis of phases; this is used to find the different phases within a material and their distribution within it. *Micromechanical measurements*; this is the study of a sample subjected to mechanical loading, using micro CT, the relationship can be found between the sample, the load it is subjected to, the external deformation and the internal damaged caused. This technique is an ideal choice for these measurements as it does not cause destruction of the samples (Govender *et al.*, 2003).

In conclusion, the advantages of micro CT are the facilitation of high spatial resolution 3D images of the internal features of material without requiring any deformation of the samples. These advantages were

exploited in this thesis, as micro CT was used to qualitatively study the distribution of nanoemulsion within the skin based on the variation in density between the nanoemulsion and the skin.

Aims of the thesis

The aim of this thesis is to develop and characterize relevant pharmaceutical formulations designed to deliver antiseptic agents to target sites within the skin.

Many infections of wounds and surgical sites arise due to contamination of the site by the patient's bacterial flora. This project will explore the ability of nanoparticles containing antiseptics to effectively penetrate the skin more than current skin disinfection methods.

- To develop and characterise an optimum Nanoemulsion NE by using two techniques: a high-pressure homogeniser technique and a high-shear homogeniser followed by ultrasonication.
- To study the effect of changing parameters in both techniques such as the number of cycles in HPH and the sonication time in HSH on NE formulation.
- Find and explore novel analysis methods for detection of the retained drug in the skin
- To predict the miscibility of the antiseptic nanoemulsion formulations with artificial sebum by using HSPs as a determination tool.

Chapter 2 -Methodology and Materials

2.1 Instruments and Apparatus

2.1.1 High-pressure homogeniser

The high-pressure homogeniser which was used in this work is an EmulsiFlex-C5 from Avestin. (Figure 2.1). Samples are introduced to the cylinder body (1) then pushed to the motor pump (2). Subsequently, the high-pressure pump pushes the sample through an adjustable homogenising value(3) which is connected to the homogenising pressure gauge. Finally, it is collected in a beaker and completion of all these steps is considered as one cycle.

The minimum sample volume for the apparatus is 7 ml, and maximum pressure is 30000 Psi/207 MPa, the flow rate is changed according to pressure (1 -5 L/h), and it is possible to regulate the pressure by increasing or decreasing the homogeniser pressure (Avestin, 2010)



Figure 2.1 High-pressure homogeniser (Avestin, 2010)

2.1.2 High shear homogeniser

The high shear homogeniser used was the Silverson L5M-A. In this method, a strong suction is exerted by the rotor with high-speed rotation which moves the liquid into the rotor-head. The material is then driven to a puncture of the rotor-head by a centrifuge force and mixed at a high speed between the blade and stator. Intense hydraulic shear then forces the material out as it returns to the mix. A circulatory mixing pattern is formed as fresh material is constantly driven to the rotor-head.

2.1.3 Ultrasound

A 3000MP Ultrasonic Homogenizer was used, and the chosen settings were amplitude of 25% and the pulse timer alternated between 5 seconds on and off. The mechanism of this device is that line voltage is converted to high-frequency electrical energy at 20kHz using ultrasonic power. The electrical energy is then converted to mechanical energy after being transmitted to the probe. The probe vibrations are strengthened through a titanium tip which also causes coupling of the vibrations, this is then followed by the vibrations being passed on to the tip which is fully in solution. Cavitation then occurs which leads to instant formation and collapsing of vapour bubbles which in turn lead to strong shock waves radiating through solution closely to radiating tip face (BioLogics, no date).

2.1.4 Zetasizer

Malvern Zetasizer Nano –ZS is claimed to deliver accurate, reliable and repeatable size analysis of particles and molecules in solution. Size measurement can be undertaken from 0.3 nm (diameter) to 10 microns using patented NIBS (Non-Invasive Back Scatter) technology.

2.1.4.1 Particle size analysis and PDI

The Zetasizer Nano-ZS measures droplet sizes using a dynamic light scattering (DLS) technique, performed by measuring Brownian motion corresponding to particle size through particle illumination with a laser then analysing intensity fluctuations in scattered light.

Particles within a liquid are never static, and their constant motion is due to Brownian motion, which can be defined as the motion of particles because of collisions between random molecules surrounding the particle in the liquid. An essential characteristic of Brownian motion for Dynamic Light Scattering DLS is the faster movement of small particles in relation to larger particles which are slower. The Stokes-Einstein equation (equation 2.1) can be used to define the relationship between the particle size and its speed due to Brownian motion.

$$D = \frac{KT}{n\pi\eta r} \text{ equation 2.1}$$

Where D is the diffusion coefficient of a spherical particle of radius r in a fluid of dynamic viscosity η at absolute temperature T, and where K is the gas constant and n is Avogadro's Number.

The size of particles is calculated through the Zetasizer Nano system which determines the intensity rate of fluctuations which were formed due to light scattering, therefore, particle size can be found.

To determine PDI, the decay rates for various size classes can be extracted through algorithms by the Zetasizer software which in turn produce a distribution of sizes.

2.1.4.2 Zeta potential measurements

The electrophoretic mobility of the particles was measured using the Zetasizer and was then converted using the Helmholtz-Smoluchowski equation into the value of ZP. This equation is built into the Malvern Zetasizer software, and version 7.11 of this software was used. This measurement was repeated three times using 15 sub-runs for every measurement. The concentration and volume of diluted sample, in

addition to the equipment used and operating conditions, were kept constant for every batch, and an average of the three independent results were calculated and stated as the final measurement.

Each sample was diluted using ultrapure water at a concentration of 10 $\mu\text{m}/\text{ml}$ before the measurement was accomplished and 1ml of the sample after diluting was injected using a syringe in the disposable capillary cell; the cell was cleaned using deionised water at the end of every measurement in addition to between runs.

2.1.5 Franz diffusion cell

In vitro diffusion models either consist of “static” diffusion cells made up of two compartments or “flow-through” cells which are multi-jacketed. Inert materials are most widely used as the construction materials, and they are usually made of glass. The membrane is fixed as an obstruction in the diffusion cell between the donor compartment and the receptor compartment. In this incidence, the membrane is excised skin (figure 2.2). The amount of drug that diffuses from the donor cell to the receptor cell can be examined as a function of time.

Buffer solution or physiological saline is used to fill the receiver compartment; this can facilitate drug diffusion from the donor compartment by providing the needed ions and pH. The circulating water temperature is usually maintained at 37°C to maintain a temperature of 32°C at the surface of the skin. Continuous stirring is applied to the receiver compartment, to maintain sink conditions and prevent saturation of the receiver conditions. In this study, a PermeGear system (V6-CA-02) vertical glass diffusion cell system was used.

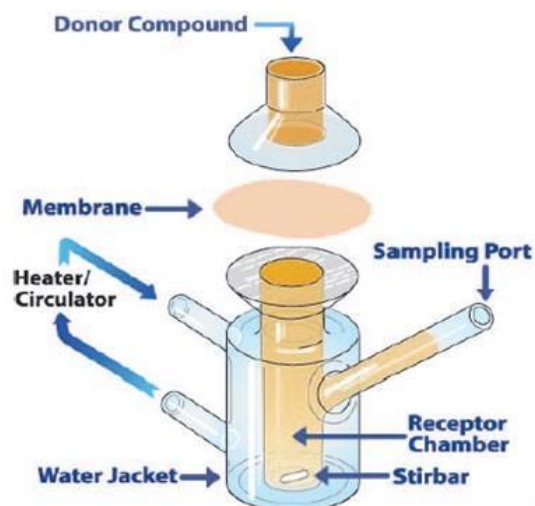


Figure 2.2 Standard Franz cells(Sonam Vats & Charu Saxena, 2014)

2.1.5.1 Membrane selection

The ideal and most suitable model for the evaluation and examination of drug delivery of different formulations is undoubtedly human skin which has commonly been used in *ex vivo* examination of drug penetration. It can be taken from multiple sources such as plastic surgery, cadavers and amputations, and from various sites within the human body and can vary in thickness. The most common sites include the abdomen and back in addition to the breast or leg. (Godin & Tuitou, 2007)

Another essential factor that widely varies between samples is the permeability of the skin, which not only varies between samples taken from different subjects and age groups but also greatly varies between multiple anatomical locations within the same subject (Haigh and Smith, 1994). The different anatomical locations in addition to health conditions, gender, race and age of donor are all factors that play a role in determining the lipid composition, hydration of the skin and the skin thickness which, therefore, lead to the differences in skin permeability (Gomes and Martins, 2014). After excising human skin from a donor, it is affected by metabolism and biotransformation of chemicals which is another

disadvantage with using human skin samples. These factors combined have led many *in vitro* studies on the permeation of skin using animal skin as an alternative to human skin and a wide variety of animals have been used for similar studies including rat, pig, rabbit and skin shed snake (Gomes and Martins, 2014)(Ngawhirunpat *et al.*, 2008).

Domestic porcine skin has a number of similarities with human skin including anatomical, histological and physiological resemblances, and it is therefore believed to be the most relevant animal model. The epidermal thickness of porcine skin is similar to that of human in addition to having a similar dermal-epidermal thickness ratio (Godin and Touitou, 2007). Another likeness is found in the density of both the hair follicles and blood vessels within the skin of pigs and humans, another important resemblance between the human model and the porcine model is in the content of SC glycosphingolipids, elastin, dermal collagen and ceramides(Dick & Scott, 1992; Godin and Touitou, 2007).

Another advantage of using porcine skin is its accessibility being readily available as a waste material from animals slaughtered for food. The drug permeability of human and porcine skin samples has been compared, and a good correlation has been found between the models specifically for lipophilic substances, with porcine skin found to have less donor variability than that found in human skin. The permeability of skin obtained from rodents was less representative being notably higher than the permeability of human skin (Barbero and Frasch, 2009).

2.1.6 Inverse gas chromatography (IGC)

IGC measurements were conducted using IGC Surface Measurement System (SMS), London, UK coupled with a flame ionization detector (FID). Methanol was used as an inert probe for the correction of deadtime retention. The selected carrier gas was helium with a flow rate of 10 ml/min. The columns were conditioned for 120 min at 20 °C and 0 RH%. Probes selected for the experiment were correlated

to interaction type and listed in Table 2.1. Target fractional surface coverage was selected at 0.05 n/nm at 20 °C and 0 RH%

Table 2.1 List of test probes used in the determination of HSPs using IGC

SP component	Interaction	Probe molecule
δ_D	Dispersive	HEXANE
		HEPTANE
		OCTANE
		NONANE
		DECANE
δ_P	Polar	DICHLOROMETHANE
		BENZENE
		ETHYL ACETATE
δ_H	Hydrogen bonding	ETHANOL
		1-BUTANOL

2.1.7 High-performance liquid Chromatography

2.1.7.1 HPLC system

A Shimadzu HPLC System was used, with an LC-20 AT pump which works on a series –type double plunger. The capacity to evacuate bubbles had been enhanced by changing the pump-head structure and the flow line. Maximum discharge pressure was 40 MPa, and the flow rate range was 0.001 – 10 ml/min, and the temperature range for the column oven was 4 – 80 °C. Injection volume of the autosampler (SIL-20A HT) was 0.1 – 100 μ l (High-per and Chromatograph, no date)

The SPD-M20A photo-diode array detector used has a high-resolution mode and high-sensitivity mode. It offers a noise level at 0.6×10^{-5} AU, which is comparable to that of UV-VIS detectors. Wavelength

ranged from 190 to 800nm. Workstation software is LC solution software was used – Version/ Release Number: 1.25

The columns which were used for detection triclosan and para-chloro-meta-xyleneol (PCMX) were:

- Phenomenex – pentafluorophenyl PFP, P/No. AJ0-8773. Size 250 X 4.60 mm, 5 µm which was used for triclosan.
- Phenomenex – C18, P/No. 00F-4361-E0. Size 150 X 4.60 mm, 5 µm which was used for PCMX

2.1.7.2 Preparation of HPLC system

2.1.7.2.1 Triclosan

The HPLC method used comprised an isocratic mobile phase of acetonitrile (ACN): water (65: 35) (v/v), a flow rate of 1.0 ml/min, and the wavelength of photo-diode array detector at 287 nm. The injection volume was 20 µl, and the run time was 10 min. the column used PFP (pentafluorophenyl) (250 mm x 4.6 mm ID, 5µm) from Phenomenex, UK

2.1.7.2.2 Chloroxyleneol

- The HPLC method used comprised an isocratic mobile phase of acetonitrile (ACN): water (60: 40) (v/v), a flow rate of 1.0 ml/min, the wavelength of photo-diode array detector at 288 nm. The injection volume was 20 µl, and the runtime was 6 min. the column used C18 (150 mm x 4.6 mm ID, 5µm) from Phenomenex, UK

2.1.8 UV Spectrometers

The UV spectrophotometer which used in this work was Agilent Cary 60 UV-Vis.

The wavelength range is 190 – 1100 nm

The cuvette was rectangular 10 mm, open-top, Quartz

2.1.9 Micro CT scan

After applying the formulation to the skin samples, the samples were removed and mounted onto a sample holder using double-adhesive tape. Imaging was recorded using X-ray microtomography (Nikon XT H 225, Nikon Corp. Tokyo, Japan) with the following specifications: tungsten targets, accelerating voltage of 75kV, current of gun of 250 μ A, copper filter thickness of 0.125 mm. Projections were then recorded for approximately two hours and CT-pro, and VG Studio 2.1 software were used to reconstruct and examine projected images respectively.

2.2 Materials

2.2.1 Analytes and general chemicals

- Tween 80 (POE (20) sorbitan monooleate), Span 80 (sorbitan monooleate), eucalyptol 99%, squalene, cottonseed oil, coconut oil, olive oil, paraffin wax (Sigma Aldrich, United Kingdom).
- Triclosan 96.0%, chloroxylenol, Tween 20, Span 20, Tween 40, Span 40, Tween 60, and Span 60 (TCI America, USA).
- Ultra-pure water from Milli-Q Direct 8 water purification system.
- Palmitoleic acid (Acros, United Kingdom).
- Cholesteryl oleate, Oleic acid, 99%, palmitic acid (Alfa Aesar, United Kingdom).
- Spermaceti wax (Croda Europe limited)

2.3 Methodology

2.3.1 Preparation of nanoemulsions

For triclosan/PCMX nanoemulsions, the hydrophilic and lipophilic phases were prepared independently. The hydrophilic phase was prepared by adding tween 80 (T80) and deionised water in a beaker, then stirring them for a 5 min on hot plate stirrer at 60 °C/ 500 RPM (to avoid the cloud point of T80 at 65°C). The same conditions were used for the lipophilic phase, containing S80 and triclosan/PCMX (lipophilic antiseptic) and eucalyptol oil in another beaker. After heating, the lipophilic phase was added to the hydrophilic phase slowly and stirred for a further 5 min on a hot plate at 60 °C/ 800 RPM. Then this milky emulsion was passed through the HPH- EmulsiFlex-C5/ HSH followed by ultrasound for several cycles until a nanoemulsion was formed.

2.3.2 Preparation of Artificial Sebum

All components of artificial sebum were weighed in a glass beaker (w/w %) and heated to 60 °C for 18 min with stirring until the liquid became clear.

2.3.3 Preparation the skin

Full-thickness porcine ear skin from freshly-slaughtered animals was isolated and stored frozen at -20°C a maximum of one week. Before using the skin, it was placed in PBS solution for one hour to defrost and hydrate, before being cut to size and left on Franz cells for one hour to equilibrate. The formulation was then applied onto the skin and left for 24 hours, the skin was then removed and shaken to remove excess formulation and left to dry for 10 minutes. Either the tape-stripping method was then applied to the skin to find the quantitative amount of antiseptic within the skin, or a CT scan was used to qualitatively study the distribution of the antiseptic within the skin.

Chapter 3 - Design and Development of Triclosan Nanoemulsion for Dermal Delivery

3.1 Introduction

Although the dermal drug delivery route is appealing, this route faces certain challenges in delivering the required amount of drug to the target site and overcoming skin barrier properties. Another challenge in utilizing this route is the difficulty in predicting the amount of drug delivered to the target site; this is even more of a challenge for drugs with poor solubility.

The focus of this chapter will be to examine the impact of preparation method on the properties of a nanoemulsion formulation. Triclosan was incorporated into a nanoemulsion using two methods: high-pressure homogenisation and high shear homogenisation followed by ultrasonication. The ideal ratio of different surfactant mixtures; T80/S80, T60/S60, T40/S40 and T20/S20 was obtained based on the required hydrophilic-lipophilic balance of eucalyptol oil, which was calculated and will be discussed. The critical parameters of nanoemulsion formulation (discussed in section 3.3.1), i.e., the effect of the amount and type of surfactant, the effect of the amount of oil and the sonication duration effect on MDS, and PDI of formulations were studied. Viscosity, pH and ZP were determined for each formulation. An HPLC method to determine the triclosan in NE formulation was developed and validated according to ICH guidelines and will also be reviewed in this chapter.

The stability of the NE formulation was monitored over three months at two different temperatures (4°C and 25°C). This chapter also includes determination of the amount of triclosan within the skin quantitatively by tape stripping method and qualitatively through CT scans.

Finally, all determined data in this chapter is used to find an optimised formulation with the highest stability and absorption into the skin.

3.1.1 Nanoemulsion and nanoemulsion formation

NEs are isotropic, unstable, thermodynamically dispersed systems of two non-miscible liquids, but are not formed spontaneously like microemulsions. Hence NEs need high energy input in order to form. The size of the dispersed droplets is in nanoscale dimensions (100 -600 nm). To prevent Ostwald ripening, which leads to creaming and flocculation of NEs, it is normal to add a surfactant to stabilise the formation of NEs. Figure 3.1 shows the steps of NE formation (Uchechi, Ogbonna and Attama, 2014). Unlike microemulsions, NE requires lower amounts of surfactant for successful formation, which gives NEs a commercial advantage with a reduced requirement for excipients (Mason *et al.*, 2006). Furthermore, high concentrations of surfactant (ionic) may cause skin irritation, and consequently may not be acceptable in dermal formulations (Uchechi, Ogbonna and Attama, 2014).

Primarily, there are three methods to formulate NEs, high-pressure homogenization, microfluidization, and phase-inversion temperature methods (Mason *et al.*, 2006). As mentioned above, to form a NE, energy (pressure or shear) must be applied. When sufficient pressure is applied, large droplets are broken into small droplets in nanosize ranges, and the role of the surfactant is to coat these nanodroplets with a very thin film and prevent coalescence due to interfacial repulsion between the surfactant films (Mason *et al.*, 2006) (Figure 3.1).

Each spherical droplet is exposed to Laplace pressure (L_p), “the pressure difference between the inside and the outside of a curved surface” (Butt, Graf and Kappl, 2003). This is the pressure proportional to surface tension (σ) and inverse to the radius (a) of the droplet described by Equation 3.1:

$$L_P = \frac{2\sigma}{a} \quad \text{Equation 3.1}$$

From Equation 3.1, it can be deduced that small droplets require higher pressure to form than larger ones.

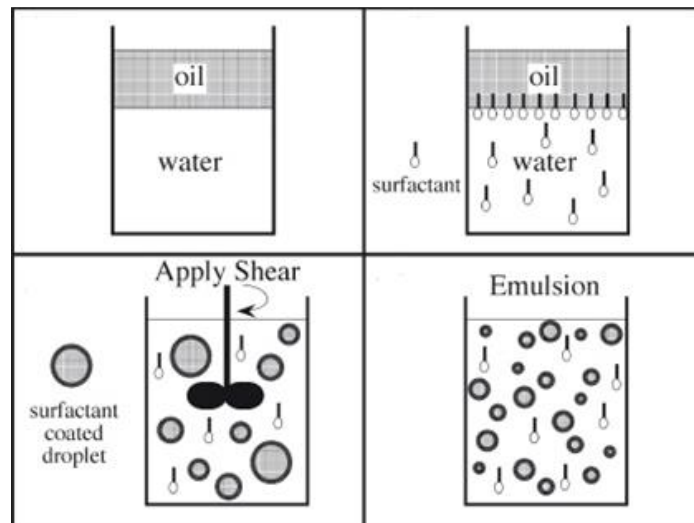


Figure 3.1 Steps for the formation of a NE (Mason *et al.*, 2006)

As mentioned above, to stabilise the NE for an extended period, a surfactant is required, and surfactant selection must take into account the Hydrophile-Lipophile balance (HLB), i.e., a “system of classification of the tendency of surfactants to disperse in polar or non-polar liquids” (Myers, 1999).

3.1.2 Hydrophile –Lipophile balance

In 1949, Griffin proposed a system able to identify the tendencies of non-ionic surfactants between oil and water, according to different regions in the molecule (functional groups); this system is called the Hydrophile-Lipophile balance (HLB) (Guo, Rong and Ying, 2006). Lipophilic surfactants are considered to have low HLB values, while hydrophilic surfactants have high HLB values. According to theory, o/w NEs generally require the use of surfactants with high HLB, and in contrast, a low value of HLB should be used in w/o NEs (Schmidts *et al.*, 2010). For a stable NE, it was found that a combination of low HLB and high HLB surfactants like Span 80 (HLB=4.3) and T80 (HLB=15) were more effective in stabilising a NE than a single surfactant (Croda Europe Ltd, 2009); (Orafidiya and Oladimeji, 2002).

Equations 3.2 is used to calculate the percentage of each surfactant according to the required HLB value (X) of the oil phase

$$\% (A) = \frac{(X - HLB_B) \times 100}{HLB_A - HLB_B} \text{ Equation 3.2}$$

$$\%(B) = 100 - \%(A)$$

Where (A) is the first surfactant, and (B) is the second surfactant.

3.1.3 Physicochemical characterisation of nanoemulsion formulations

3.1.3.1 Droplet size and PDI measurement

The size and PDI for NE formulations were measured using Zetasizer Nano Zs (Malvern Instruments Ltd, UK). The polydispersity of the NE describes the distribution of the droplets in the continuous phase. The ratio of PDI increases as the size distribution increases, and above the value 0.5, the NE is considered

unstable due to the variability in size of droplets which leads to coalescence and cracking (separation of emulsion into its constituent phases)(Laouini, Fessi and Charcosset, 2012).

3.1.3.2 Zeta potential measurement:

The ZP of NE formulations was measured using Zetasizer Nano Zs (Malvern Instruments Ltd, UK). ZP measurement is a critical parameter in disperse systems which measures the electrostatic charges of repulsion and attraction between dispersed droplets to predict whether the droplet will cause coalescence or whether it will be dispersed in the continuous phase. Araujo et al. found that if the value of ZP is greater than ± 30 mV, then generally, the emulsion can be considered stable (Araújo *et al.*, 2011). Each sample (100 μ l) was diluted with 10 ml of deionised water, and all analyses carried out in triplicate to determine the mean value.

3.1.3.3 Stability studies

All NE formulations were stored in sealed glass vials at two different temperatures (25°C and 4°C) for three months to study the stability. Samples were taken every month to check MDS, PDI and ZP. All measurements were carried out in triplicate.

3.1.3.4 pH determination

The pH of the NEs formulations was measured by using a pH meter at 25°C. All measurements were carried out in triplicate.

3.1.3.5 Determination of viscosity

The viscosity of NEs was measured in triplicate using a Bohlin cone and plate rheometer at 25°C and shear ramp between 0.1 and 100 s⁻¹. Methods of production of nanoemulsions

There are three methods to produce nanoparticles and NEs, such as high shear homogenization and ultrasound, high-pressure homogenization, and solvent emulsification/evaporation. Each of these methods has relative advantages and disadvantages (Mehnert and Mäder, 2001).

3.1.3.6 The principle of high-pressure homogenization

High-pressure homogenization (HPH) is a technique involving application of high pressure (100 – 2000 bar) on a liquid to push it through a very narrow gap (in the micron range) in a homogeniser, and as a result, the fluid crosses this distance at a very high speed (1000 km/h). This cycle is repeated several times. Due to this process, high shear stress and cavitation forces arise, and consequently, the macro droplets rupture to form nanodroplets (Lippacher & Muller, 2000). In practice, the pressure must be gradually increased to prevent clogging of the narrow homogeneity gap (Kipp, 2004). Particle size and particle size distributions are mainly affected by the number of cycles through the homogeniser, and the pressure applied. Figure 3.2 shows a schematic diagram of HPH.

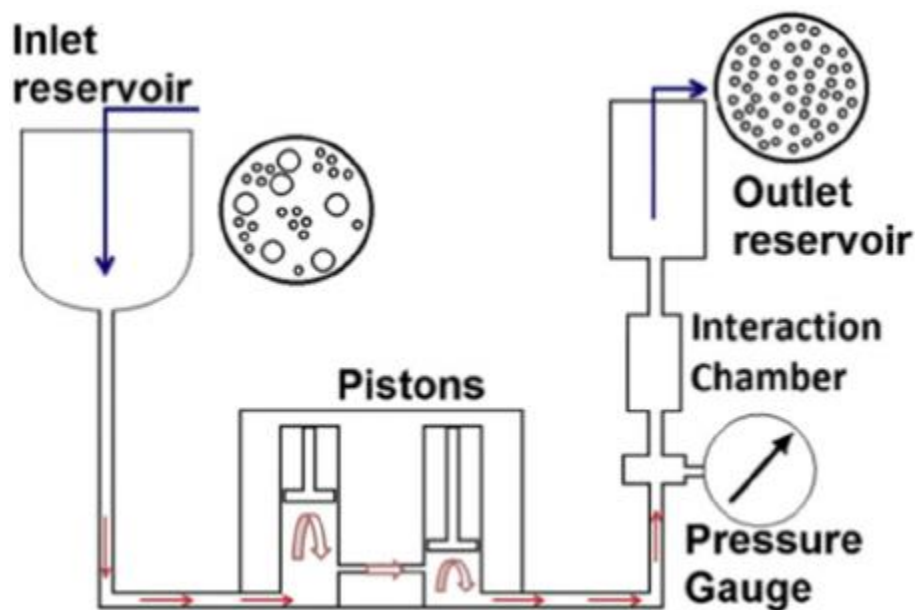


Figure 3.2 Schematic diagram of high-pressure homogenization (Fontes *et al.*, 2015)

3.1.3.7 The principle of high-shear homogenization and ultrasound

This technique of nanoemulsion preparation needs two steps; the first step is homogenising a NE by HSH and second step is sonicating it to minimise the size distribution and improve the stability.

A high shear mixer can reduce mixing time by 90% when compared with a conventional method. High-speed rotation of the rotor exerts a powerful suction driving the liquid upward into the rotor head. Then a centrifugal force drives the material towards a perforation in the rotor head where it is rapidly mixed between the rotor blade and stator (a stationary component around the rotor). This is followed by intense hydraulic shear as the material is forced out through the perforation and back into the bulk mix. Fresh material is continually driven to the rotor head resulting in a circulation pattern of mixing.

Figure 3.3 shows a schematic diagram of the high-shear homogenization and ultrasound technical steps.

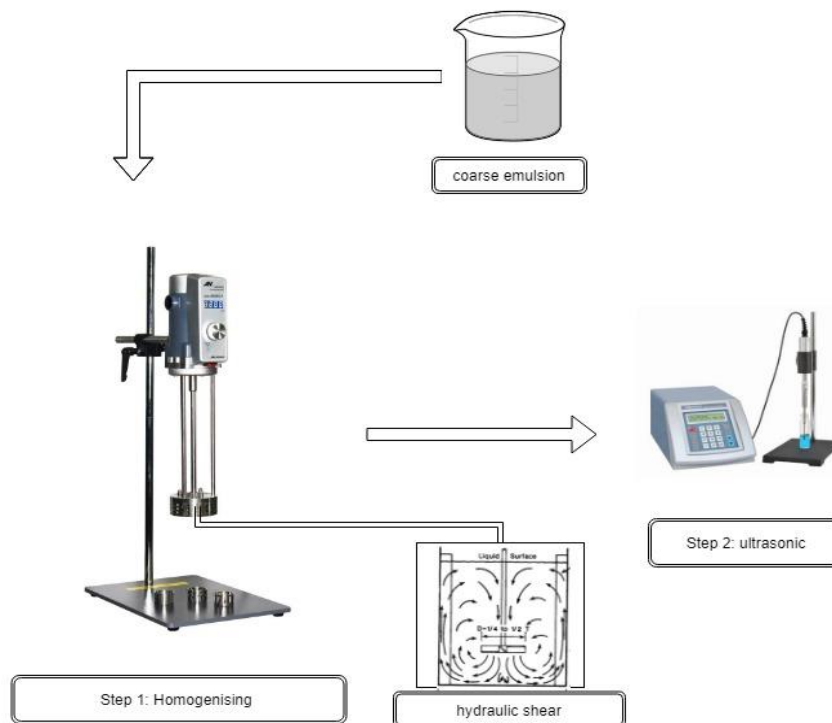


Figure 3.3 Schematic diagram of high-shear homogenization and ultrasounds technique

3.1.4 Triclosan and mechanisms of action

Antiseptics and disinfectants are utilised widely in hospitals and are found in many examples of topical formulations. Since 1999, antiseptics are considered a crucial part of infection control practices and can help in the avoidance of nosocomial infections (McDonnell & Russell, 1999).

Triclosan (2, 4, 4'-trichloro-2'-hydroxy diphenyl ether; Irgasan DP 300), as shown in Figure 3.4, is a broad-spectrum antimicrobial agent, with activity against both gram-positive and gram-negative bacteria (Waller, 1993).

Triclosan is insoluble in water but soluble in most organic solvents; ($pK_a = 7.9$), $\log P = 4.76$ and molecular weight = 289.5 Da (Ramos, 2009)

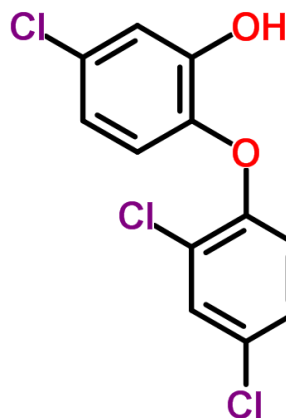


Figure 3.4 Chemical structure of triclosan (Ramos, 2009)

Triclosan mainly exerts its effects on the cytoplasmic membrane of bacteria in which it inhibits the uptake of essential nutrients, which occurs at low concentrations. It plays a bacteriostatic role, while at high concentrations it is considered bactericidal causing a rapid release of cellular components and cell death (McDonnell & Russell, 1999)

3.1.5 Analysis and characterisation of nanoemulsions

3.1.5.1 HPLC - method validation

In accordance to the ICH (International Committee on Harmonization, 1996); the process through which it is established that performance characteristics of methods meet requirements for the envisioned analytical application using laboratory studies is known as the validation. There are multiple parameters which are used for this which are; linearity, sensitivity, precision, accuracy, and stability.

3.1.5.1.1 Linearity

The linearity parameter is a representation of the directly proportional relationship between the known concentration of analytes and the instrumental response. Linearity is indicated by the correlation coefficient (R^2) of the curve, when the correlation coefficient is equal to one this means the curve is completely linear, the linearity also decreases with the decrease in value of the correlation coefficient.

For a linearity test to be completed, this requires a minimum of five concentrations of analytes, it is preferable that one of these is the limit of quantitation, the test must also be repeated five times.

3.1.5.1.2 Sensitivity

There are two factors that represent the sensitivity parameter, the first of these factors is *the limit of quantification (LOQ)*; the lowest analyte concentration within a sample which can be determined with an adequate level of accuracy and precision. The second factor is *the limit of detection (LOD)*; The lowest detectable concentration within a sample, this does not necessarily mean it is quantifiable.

These two factors LOD and LOQ can be calculated according to ICH using equations 3.3 and 3.4 respectively.

$$LOD = \frac{3.3 \sigma}{S} \text{ Equation 3.3}$$

Where (σ) standard deviation of the intercept

And (S) mean of the slope

$$LOQ = \frac{10 \sigma}{S} \text{ Equation 3.4}$$

Where (σ) standard deviation of the intercept

And (S) mean of the slope

3.1.5.1.3 Precision

When an analytical method is applied to various sampling of a homogenous sample, the degree of agreement obtained amongst individual test results is known as the precision of the method (Rockville 1985). For this precision test to be completed, a minimum of five various analyte concentrations are required, a minimum of five replications of the test must also be performed on the same day for the determination of intra-day precision. As for inter-day precision, this is determined by repeating the test for five days. To express precision, the Relative Standard Deviation (RSD) is then calculated, RSD percentage is given by equation 3.5

$$\%RSD = \frac{\text{standard deviation} \times 100}{\text{mean of concentration}} \text{ Equation 3.5}$$

3.1.5.1.4 Accuracy

The degree of closeness of a measurement to the true or actual value is referred to as the accuracy, the accuracy increases with the closeness to the true value and decreases as it grows further away, indicating poor accuracy. Accuracy can be calculated by Equation 3.6

$$\text{Relative error} = \frac{\text{true}-\text{observed}}{\text{true}} \times 100 \text{ Equation 3.6}$$

3.1.6 Determination of triclosan in skin quantitatively and qualitatively

3.1.6.1 *In vitro skin diffusion study*

Even though human skin is the best model to study the penetration through/in the skin, pig ear skin according to many authors shows a high similarity with human skin in histological, physiological and permeation characteristics compared with other animal models (DICK & SCOTT, 1992; Flaten *et al.*, 2015). In the present study, fresh, full-thickness porcine skin was obtained from a local abattoir (J.& E Medcalf Ltd, Huddersfield) and used immediately or frozen at -20°C and used within one week. The standard 15 mm jacketed Franz cell vertical glass diffusion cell with an orifice area of 1.77 cm² and 12 ml receptor volume (PermeGear, USA) was used for diffusion studies. Skin samples were examined for any punctures or defects before use, and all skin samples were immersed in PBS (pH 7.4) for an hour. Then the hydrated skin was put into Franz cell for 30 min to equilibrate before applying 1 ml of triclosan NE formulation (equivalent to 10mg/g) in the donor chamber. The donor chamber was covered with parafilm to prevent evaporation. The receiver chamber was filled in PBS solution with 1% w/v of SLS to improve the solubility of triclosan. The water bath of jacketed Franz cell was maintained at 37°C, so the surface of the skin sample was kept 32°C, to mimic the human skin temperature. Each experiment was run for 24 hours, and then triclosan was determined quantitatively by using an adhesive tape stripping method and qualitatively by using CT scan.

3.1.6.2 *Quantitatively by using an adhesive tape stripping method*

There is a consensus among many authors that the differential tape stripping method is a successful method to determine the amount of drug quantitatively in the skin (Ossadnik *et al.*, 2007; Thielitz *et al.*,

2001; Wosicka & Cal, 2010). In this method, the tape isolates the stratum corneum layer by layer to determine the amount of the drug in stratum corneum and is followed by cyanoacrylate adhesive step to determine the amount of drug in hair follicles. Subsequently, the skin sample is cut into small pieces to determine the amount of drug in the entire sample (Ossadnik *et al.*, 2007). In the current study after 24 hours of diffusion in the Franz cell, skin samples were removed and shaken to remove the excess triclosan NE which had not been absorbed, then skin samples were left for 20 min to dry and after that a 2X2 cm² pieces of tape (3M Transpore[®]) were used to strip the layers of stratum corneum following application of an even pressure. This process was repeated 15 times, and then tapes were placed in 5 ml methanol according to the following distribution tape 1, tapes 2-5, tapes 6-10, tapes 11-15. Subsequently, a cyanoacrylate adhesive step was applied to determine the amount of triclosan in hair follicles. A small amount of cyanoacrylate was placed on the stripped skin and the cyanoacrylate was covered by a 2X2 cm² of tape and was left for 10 min then removed quickly. This step was repeated twice, and these two tapes were put in 5 ml methanol. The final step involved cutting the skin to small pieces and placing them in 5 ml of methanol. All these tubes were sonicated for 30 min and then were centrifuged at 400 rpm for 20 min. Then the supernatant was analysed by HPLC to determine the amount of triclosan in each tube.

3.1.6.3 *Qualitatively by using CT Scan*

After leaving the samples in Franz cells for 24 hours, they were removed and left to dry for 1 hour; the samples were then placed on the CT scan to obtain 3D images of each sample. The density of triclosan and the skin was determined and used to find the distribution of triclosan within the skin, which subsequently determined the triclosan qualitatively.

Various formulations were examined using this method, and these results were found to agree with results from the previous tape stripping method, where formulations that showed high amounts of triclosan in the skin quantitatively also qualitatively showed a high density of triclosan using 3D imaging.

3.2 Aim and Objectives

The aim of this chapter was to develop and characterise relevant pharmaceutical formulations designed to deliver antiseptic agents, in this case, triclosan, to target sites within the skin.

Many infections of wounds and surgical sites arise due to contamination of the site by the patient's own bacterial flora. This chapter explores the ability of nanoparticles containing triclosan to effectively penetrate the skin compared to solution formulations.

- To develop and character an optimum triclosan NE using two techniques: a high-pressure homogeniser technique and a high-shear homogeniser followed by ultrasonication.
- To study the effect of processing parameters such as the number of cycles in HPH and the sonication time in HSH on NE formulation on the formulation
- To determine the relative stability of triclosan NEs
- To determine the amount of triclosan in the skin quantitatively using tape stripping and qualitatively using CT.

- To compare both techniques and find the optimum one by the amount of triclosan determined in the skin.

3.3 Results and Discussion

3.3.1 Formulation study of triclosan nanoemulsion

3.3.1.1 Development of triclosan nanoemulsion

As outlined previously, NEs are thermodynamically unstable, so to extend stability for long periods (up to years), the optimum type and concentration of surfactants should be used. It is, therefore, useful to determine the required HLB value for eucalyptol and the solubility of triclosan in it.

A triclosan NE was prepared by two different methods , HPH as a continuous processing method, and HSH followed by ultrasound as an alternative.

3.3.1.2 Determining the required HLB value for eucalyptol

To formulate stable emulsions, it is recommended that the HLB value of surfactants or combinations of surfactants should be close to the HLB value of the oil phase (Orafidiya and Oladimeji, 2002). To determine the required HLB value of eucalyptol, a matched pair of Tween and Span, such as T80 with S80 was used. Seven batches of emulsifier combinations with different HLB values according to Equation 3.7, ranging from HLB =4.3 (S80) to HLB = 15 (tween 80) were prepared. Table 3.1 shows the calculated HLB values for seven batches (Chemmunique, 2004)

$$\% (A) = \frac{(X-HLB_B) \times 100}{HLB_A-HLB_B} \quad \text{Equation 3.7}$$

$$\%(B) = 100 - \%(A)$$

Where (X) is the required HLB value of the oil, (A) is T80, and (B) is S80

Table 3.1 The HLB values of different percentages of emulsifier blend used to determine HLB of eucalyptol

Sample No	Emulsifier Blend		Calculated HLB
	Span 80	Tween 80	
1	100%	---	4.3
2	85%	15%	6
3	65%	35%	8
4	46%	53%	10
5	28%	72%	12
6	9%	91%	14
7	---	100%	15

All vials were stirred by using a magnetic stirrer for 30 min at 25°C.

The most stable one is that which does not cause separation of the oil and water phases, it is considered as the primary optimum one, and as shown in Figure 3.5 is sample 5 (HLB=12). Once this was determined, values in a closer range to this were then studied to produce a more accurate value. Table 3.2 shows the calculated HLB values of the surfactant mixes ranging from 11 to 13.

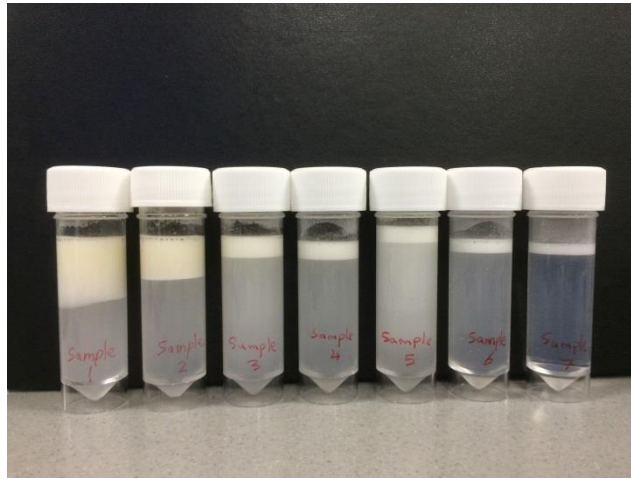


Figure 3.5 Proposed emulsion formulations using a wide range of HLB mixtures to determine the most stable (sample 5=12 HLB)

Table 3.2 The HLB values of different percentages of emulsifier blend range 11-13

Sample No	Emulsifier Blend		Calculated HLB
	Span 80	Tween 80	
8	37%	63%	11
9	33%	67%	11.5
10	28%	72%	12
11	23%	77%	12.5
12	19%	81%	13

As shown in Figure 3.6, the most stable emulsion was sample 11, with an HLB value of 12.5. Thus the HLB value of eucalyptol is predicted to be 12.5.

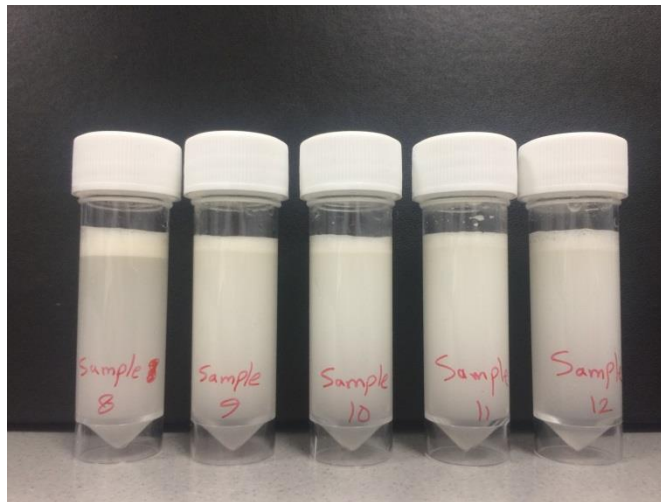


Figure 3.6 Proposed NEs formulation using a narrow range from 11 to 13 of HLB mixtures to determine the most stable (sample 11=12.5 HLB)

Using Equation 3.8 and the determined HLB value for eucalyptol, the ratio of surfactant mixture is determined as 3:1 T80: S80.

$$\% (\textit{Tween } 80) = \frac{(12.5-4.3) \times 100}{15-4.3} = 76.63 \% \quad \textit{Equation 3.8}$$

$$\% (\textit{span } 80) = 100 - 76.63 = 23.37 \%$$

3.3.1.3 The solubility of triclosan in eucalyptol

Determination of the solubility of triclosan (drug) in eucalyptol (oil phase) is an important factor in developing a triclosan NE formulation (Zhao, 2013). To determine the solubility of triclosan, three vials were prepared according to Table 3.3 containing an excess of triclosan.

Table 3.3 The amount of triclosan in each vial

	Eucalyptol (g)	Triclosan(g)	Span 80(g)	Tween 80(g)	Water (g)
Vial 1	1.80	0.33	-----	-----	-----
Vial 2	1.78	0.32	0.07	0.05	-----
Vial 3		0.09			5

The three vials were mixed using a vortex mixer at speed 1500 rpm and then were maintained in an isothermal shaker at $25 \pm 1^\circ\text{C}$ for 72 h to equilibrate. Following centrifugation at 3000 rpm for 15 min, the supernatant was removed, filtered using a $0.45\mu\text{m}$ filter and analysed by HPLC, after dilution by methanol (Shafiq *et al.*, 2007). The solubility of triclosan is shown in Table 3.4

Table 3.4 The solubility of triclosan after 72 h equilibration at $25 \pm 1^\circ\text{C}$.

	Solubility of triclosan (mg/ml)
Triclosan in eucalyptol only	122.85
Triclosan in eucalyptol + T80 + S80	141.29
Triclosan in water	0.35

3.3.1.4 Determination of minimal surfactant concentration

If it is assumed that T80 and S80 form a thin film around each droplet in a monolayer, so according to geometric calculations, it possible to estimate sufficient amounts of these surfactants to stabilise any emulsion.

For example, for 2.5g of eucalyptus oil (density is 0.912 g/ml)(Silva *et al.*, 2011).

Volume = mass / density

$$= 2.5 \text{ g} / 0.912 \text{ g/ml}$$

$$= 2.7412 \text{ ml (cm}^3\text{)}$$

For a droplet diameter of 33 nm (section 3.3.1), thus:

Droplet diameter=33 nm= 3.3×10^{-6} cm, and if assumed that the droplet is spherical, so

$$\text{Volume of droplet} = \frac{4}{3} \pi r^3 = \frac{\pi d^3}{6} = 1.882 \times 10^{-17} \text{ cm}^3$$

where r: radius

d: diameter

Total number of drops in 2.5 g = volume of eucalyptus oil/volume of the droplet

$$= 2.7412 / 1.882 \times 10^{-17}$$

$$= 1.457 \times 10^{17}$$

Surface area of each droplet = πd^2

$$= 3.422 \times 10^{-11} \text{ cm}^2$$

Total surface area of droplets = Surface area of each particle x Total number of drops

$$= 3.422 \times 10^{-11} \times 1.457 \times 10^{17}$$

$$= 4.984051 \times 10^6 \text{ cm}^2$$

The molecular weight of T80 = 604.41 g/mol

Surface area = $133 \text{ \AA} = 1.33 \times 10^{-14} \text{ cm}^2$ (PubChem, n.d.-b)

Molecular weight of S80 = 428.31 g/mol

Surface area = 96.2 Å = $9.62 \times 10^{-15} \text{ cm}^2$ (Pub chem, no date a)

Number of required molecules of T80 = Total surface area of droplets/surface area of T80

$$= 4.984051 \times 10^6 / 1.33 \times 10^{-14}$$

$$= 3.7474 \times 10^{20}$$

Number of required molecules of S80 = Total surface area of droplets/surface area of S80

$$= 4.984051 \times 10^6 / 9.62 \times 10^{-15}$$

$$= 5.18093 \times 10^{20}$$

Amount of required surfactant (g) = $\frac{\text{(Number of required molecules} \times \text{molecular weight)}}{\text{Avogadro's number}}$

$$\text{Amount of required tween 80 (g)} = \frac{(3.7474 \times 10^{20} \times 604.41)}{6.0221415 \times 10^{23}} = 0.376107 \text{ g}$$

$$\text{Amount of required span 80 (g)} = \frac{(5.18093 \times 10^{20} \times 428.31)}{6.0221415 \times 10^{23}} = 0.368481 \text{ g}$$

So according to the formula and using a ratio of surfactant mixture (T80: S80) (3:1), 0.28208 g of T80 and 0.09212 g of S80 would be the minimum needed to emulsify 2.5 g of eucalyptol oil in water.

3.3.1.5 Physicochemical characterisation of the nanoemulsion formulations

Physicochemical characterisation was carried out(zeta potential, pH, and viscosity) for all NE formulations using both techniques (HPH and HSH) (Table 3.5). As mentioned in section 3.1.3.2, the zeta

potential is an important parameter for stability, and as the charge increases the repulsion between droplets increases and decreases the chance of coalescence. In the present study, the values of zeta potential for the HPH technique and HSH technique range between -23.4 ± 2.5 mV to -37.5 ± 3.5 mV and -20.3 ± 3.4 mV to -41.2 ± 3.4 mV, respectively. So in both techniques, the values of zeta potential were high, and according to different studies (Yang and Benita, 2000; Zhao *et al.*, 2010; Laouini, Fessi and Charcosset, 2012) with a high value of zeta potential the charged droplets will repel one another more than droplets with a low value of zeta potential and thus prevent coalescence. The negative charge in triclosan arises from the chlorinated polyaromatic phenol groups, and thus the droplets acquire a negative overall charge.

Since all NEs formulations in this study are O/W, they have low viscosity water forms the continuous phase and is in a higher ratio than the oil. However, formulations which have a higher percentage of oil have a slight increase in viscosity, as shown in Table 3.5 (Solans *et al.*, 2005). The increased viscosity of the continuous phase decreases the movement of the droplets, consequently reducing the chance of coalescence between droplets (Jafari *et al.*, 2008).

According to Schmid *et al.*, a change in skin pH plays a role in the pathogenesis of skin conditions like irritant contact dermatitis, to avoid that, the pH of detergents and antiseptics formulations should be around 5.5 (Schmid-Wendtner and Korting, 2006) as the pH of healthy human skin ranges between (5.4 – 5.9) (Braun-Falco and Korting, 1986) In the present study, all NE formulations in both techniques HPH and HSH are within the mentioned range (5.27 ± 0.3 to 5.97 ± 0.1) and (5.12 ± 0.1 to 5.82 ± 0.4) respectively.

Table 3.5 Physicochemical characterisation of the NE formations for both technique HPH & HSH (n=3; mean±sd)

NE			High Shear Homogenizer			High-pressure Homogenizer		
Surfactant		Oil	pH	ZP (mV)	Viscosity (cP)	pH	ZP (mV)	Viscosity (cP) ±SD
Type	Amount(%w/w)	Amount(%w/w)						
Tween 80/Span 80	0.34%	5%	5.32 ±0.2	-37.57 ±3.5	20.05 ± 1.25	5.21 ±0.3	-38.01±5.6	19.67 ± 0.98
	2%	5%	5.78 ±0.3	-23.45±2.5	21.36 ± 0.63	5.47 ±0.1	-26.62±2.6	20.58± 1.11
	5%	5%	5.63 ±0.1	-27.95±4.5	19.85 ± 0.87	5.60 ±0.3	-28.63±4.7	19.08 ± 1.85
	10%	5%	5.42 ±0.3	-24.73±3.8	23.65 ± 1.09	5.82 ±0.4	-26.15±1.6	22.69 ± 1.25
Tween 60/Span 60	0.34%	5%	5.38 ±0.2	-32.71±3.4	20.25 ± 1.12	5.39 ±0.2	-36.64±5.9	20.85 ± 1.62
	2%	5%	5.95 ±0.1	-28.32±4.7	22.22 ± 1.01	5.34 ±0.1	-23.38±3.4	21.69 ± 1.24
	5%	5%	5.49 ±0.1	-31.75±8.6	22.07 ± 0.87	5.12 ±0.1	-28.49±3.7	20.58 ± 0.95
	10%	5%	5.27 ±0.3	-30.79±3.6	23.85 ± 0.96	5.64 ±0.3	-24.74±3.9	24.05 ± 1.50
Tween 40/Span 40	0.34%	5%	5.67 ±0.2	-24.83±1.8	20.30 ± 1.52	5.34 ±0.3	-32.76±3.7	21.58 ± 1.26
	2%	5%	5.24 ±0.3	-28.44±6.2	20.29 ± 1.43	5.87±0.3	-25.42±5.6	19.98 ± 1.43
	5%	5%	5.39 ±0.3	-29.27±1.2	19.58 ± 1.58	5.49 ±0.3	-27.38±4.6	23.25 ± 1.21
	10%	5%	5.97 ±0.1	-30.48±2.8	22.10 ± 0.97	5.68 ±0.1	-30.60±2.6	21.25 ± 0.57
Tween 20/Span 20	0.34%	5%	5.67 ±0.3	-37.19±1.8	21.58 ± 1.13	5.29 ±0.5	-41.29±3.4	20.29 ± 1.65
	2%	5%	5.34 ±0.2	-27.82±4.7	21.36 ± 1.29	5.75 ±0.2	-20.38±3.4	21.69 ± 1.01
	5%	5%	5.97 ±0.1	-28.83±3.9	23.02 ± 0.90	5.64 ±0.1	-27.45±5.8	19.20 ± 1.20
	10%	5%	5.74 ±0.3	-28.09±5.9	21.08 ± 1.23	5.35 ±0.6	-24.35±7.6	22.34 ± 0.84
Tween 80/Span 80	2%	2.5%	5.36 ±0.1	-28.30±1.9	19.85 ±0.67	5.99 ±0.3	-34.16±1.5	18.65 ±0.97
	2%	5%	5.34 ±0.3	-32.74±6.7	21.47 ± 1.19	5.37 ±0.0	-32.69±6.3	20.42 ± 0.58
	2%	7.5%	5.76 ±0.3	-30.33±4.5	22.87 ± 1.49	5.54 ±0.7	-34.34±6.4	21.99± 1.85
	2%	10%	5.48 ±0.3	-25.93±5.6	26.03 ± 1.85	5.60 ±0.1	-34.85±4.2	25.18 ± 2.49

3.3.1.6 Effect of concentration of oil on triclosan nanoemulsions

3.3.1.6.1 High-pressure Homogenizer technique

Formulations were prepared with different concentrations of oil (2.5%, 5%, 7.5% and 10% (%w/w)). All other variables were fixed to examine the effect of varying concentrations of oil on particle size, i.e. 2% mixture of surfactant T80: S80 (3:1), 0.5% triclosan and deionised water and at a homogeniser pressure of 20K psi. Table 3.6 shows the impact of the concentration of oil on particle size and size distribution following 3 and 5 cycles.

Table 3.6 Size and PDI of NEs prepared with different oil concentrations following 3 and 5 cycles using HPH

No of cycles	Property	concentration of oil (% w/w)			
		2.50	5	7.5	10
After 3 Cycles	Size (nm)	113.90	70.02	62.15	101.38
	PDI	0.27	0.26	0.33	0.27
After 5 Cycles	Size (nm)	83.28	69.59	58.92	80.96
	PDI	0.25	0.26	0.20	0.24

From the results in Table 3.6, it can be seen the smallest particles with a relatively narrow PDI were produced at a concentration of 7.5% oil. The increase in size at 10% w/w oil can be explained by the reduced efficacy of surfactant at this concentration, due to the amount of surfactant not being enough to cover this amount of oil, or the increased the oil in formulation obstructed the movement of surfactants. However, in order to choose the best concentration, the stability of formulations must also be considered (section 3.3.4).

3.3.1.6.2 High Shear Homogenizer followed by ultrasound technique

As outlined in paragraph 3.3.1.6.1, four formulations were prepared to study the effect of the amount of oil on MDS and PDI. Results in Table 3.7 and Figure 3.7 show that the MDS increases with the amount of oil, indicating that the amount of surfactant is not enough to prevent the coalescence between droplets in emulsification zone resulting in an increase in the MDS beyond a concentration of 10% w/v. This is as expected as the amount of surfactant used was optimised to stabilise 7.5%.

Table 3.7 Size and PDI of NEs prepared with different oil concentrations (n=3; mean±sd)

Amount of oil (w/w%)	Tween 80/span 80	
	Size ±SD	PDI±SD
2.5	34.87±0.76	0.25±0.01
5	76.60±1.76	0.18±0.02
7.5	99.04±2.15	0.15±0.01
10	116.80±2.36	0.15±0.01

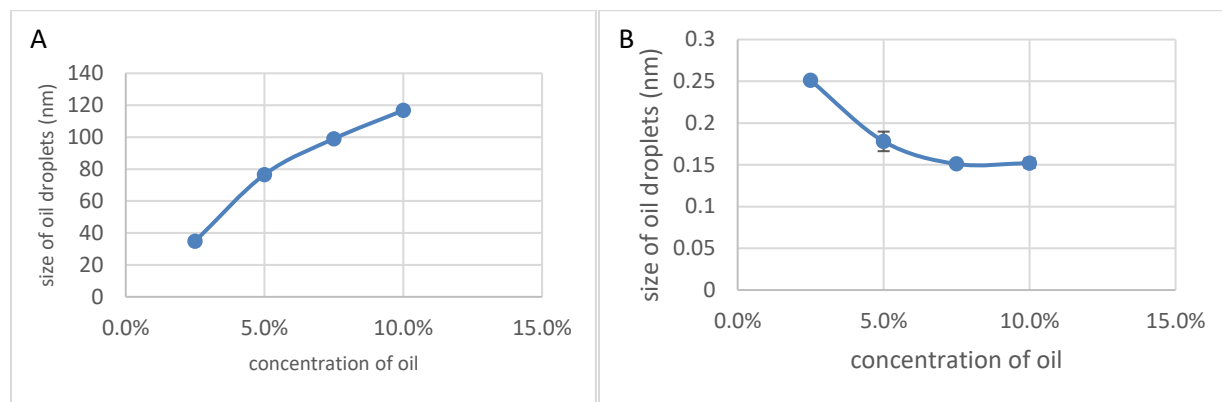


Figure 3.7 Size (A) and PDI (B) of NEs prepared with different oil concentrations

3.3.1.7 Effect of type and concentration of surfactant on triclosan nanoemulsions

3.3.1.7.1 High-pressure Homogenizer technique

To study the effect of type of surfactant on triclosan NEs, formulations using a blend of emulsifiers were prepared as detailed in Table 3.8. As mentioned above the required HLB value of eucalyptol was calculated to be 12.5, to get that the ratio of surfactants in the emulsifier blend was varied to match this using a range of Tween and Span (Table 3.8).

Table 3.8 Ratio of blend emulsifier at HLB = 12.5 using a range of Tween and Span

	T20 : S20	T40 : S40	T60 : S60	T80 : S80
HLB =12.5	50% : 50%	33.5% : 66.5%	22.5% : 77.5%	22.5% : 77.5 %
Ratio	1 : 1	1 : 2	1 : 3	1 : 3

For each formulation, a range of surfactant concentrations (0.34 %, 2%, 5% and 10% w/w) was prepared. All other variables were kept constant: 5% w/w oil (eucalyptol), 0.5% w/v triclosan and deionised water at a homogeniser pressure of 20Ksi. Samples were taken after 3 and 5 cycles to check the size, PDI, and ZP. Tables 3.9 and 3.10 and figures 3.8, 3.9, 3.10, and 3.11 show the size and PDI of NEs prepared with different emulsifiers after 3 and 5 cycles, respectively.

Table 3.9 Size and PDI of NEs prepared by HPH with different emulsifiers at 3 cycles

After 3 cycles					
Surfactant mixture	Property	Concentrations of surfactant % w/w			
		0.34	2	5	10
Tween 80/ Span 80	Size (nm)	105.47	62.37	70.02	94.93
	PDI	0.12	0.19	0.26	0.26
Tween 60/ Span 60	Size (nm)	71.06	76.43	127.00	142.39
	PDI	0.19	0.27	0.37	0.43
Tween 40/ Span 40	Size (nm)	98.04	60.67	68.59	80.19
	PDI	0.19	0.26	0.39	0.46
Tween 20/ Span 20	Size (nm)	121.97	66.75	87.87	83.75
	PDI	0.17	0.19	0.23	0.29

Table 3.10 Size and PDI of NE prepared with different emulsifiers at 5 cycles

At 5 cycles					
Surfactant mixture	Property	Concentrations of surfactants % w/w			
		0.34	2	5	10
Tween 80/ Span 80	Size (nm)	104.94	53.51	69.59	74.57
	PDI	0.09	0.12	0.26	0.267
Tween 60/ Span 60	Size (nm)	73.58	60.92	85.25	73.19
	PDI	0.14	0.25	0.29	0.45
Tween 40/ Span 40	Size (nm)	81.34	48.84	43.21	52.87
	PDI	0.12	0.22	0.37	0.42
Tween 20/ Span 20	Size (nm)	87.55	55.35	71.38	61.27
	PDI	0.10	0.17	0.21	0.25

For all emulsifiers, the smallest sizes were produced at 2% surfactant, which indicates that there is enough surfactant at this concentration to cover all oil droplets and prevent collapsing of droplets. The increase in size after 2% indicates that this exceeded the critical micelle concentration (CMC) and the emulsifier itself may form a micelle, or aggregates may form. This hypothesis is supported by the increase in PDI in all formulations with increasing concentration. The T40/S40 combination produced the smallest size at all concentrations but not the lowest PDI, whereas the T20/S20 and T80/S80 produced small sizes and narrow PDI profiles. This variation between the emulsifier pattern is due to differences in the hydrophilicity and chemical structure of each one (Yuan and Gao, 2008). When the HPH breaks large droplets of oil into smaller ones, the role of the surfactant is to prevent the cohesion of droplets again. The more effective the surfactant is, the smaller the particle size. In order to choose the best emulsifier, the stability of formulas must be considered, and this is discussed in section 3.3.4.

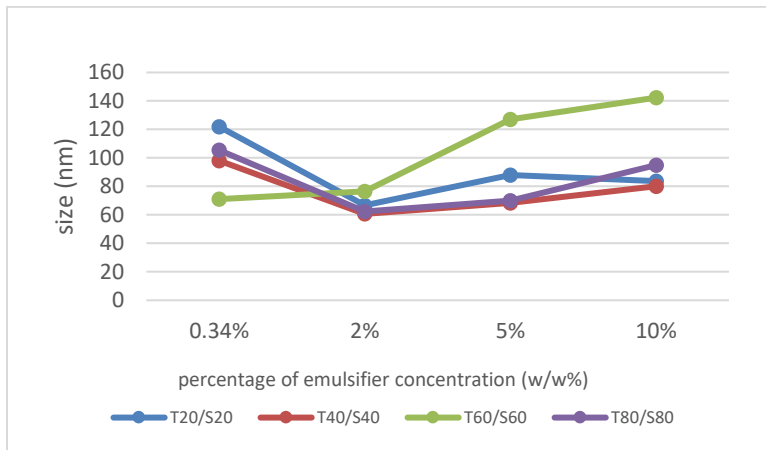


Figure 3.8 Size of NE with different emulsifiers at 3 cycles

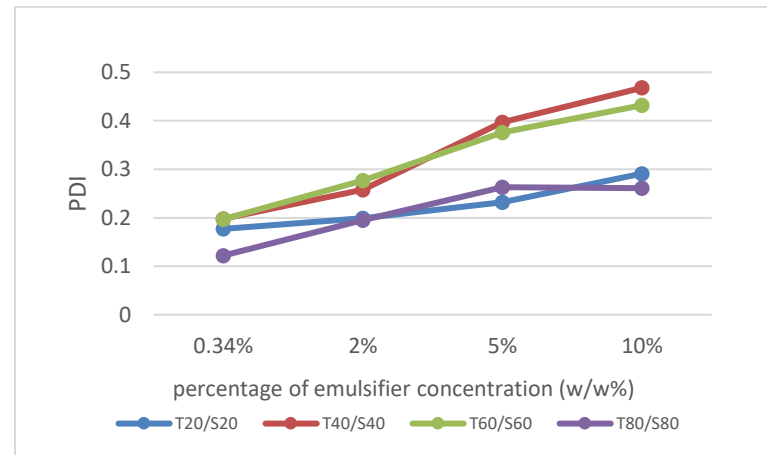


Figure 3.10 Size distribution of NE with different emulsifiers at 3 cycles

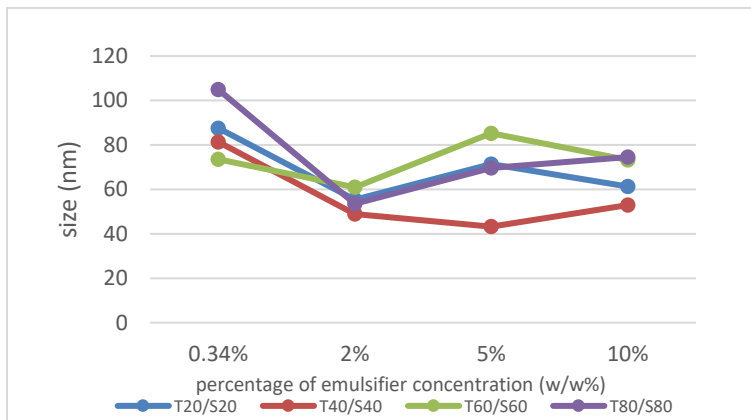


Figure 3.9 Size of NE with different emulsifiers at 5 cycles

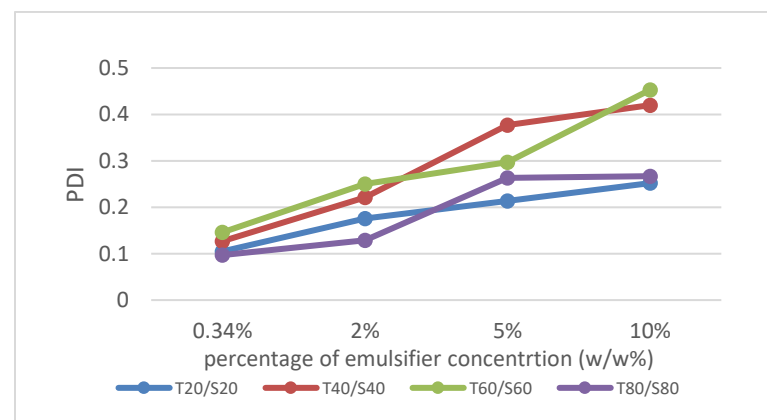


Figure 3.11 Size distribution of NE with different emulsifiers at 5 cycles

3.3.1.7.2 High Shear Homogenizer followed by Ultrasound Technique

As mentioned above, different formulations were prepared to study the effect of type and amount of surfactant harmonised with the required HLB value for each surfactant. Table 3.11 and Figure 3.12 show that the MDS decreases as the concentration of surfactant increases which corresponds with previous reports (Jafari *et al.*, 2008) as more surfactant is adsorbed onto the surface of the new disrupted droplets and prevents coalescence. Increasing the amount of surfactant can increase the cost and potential toxicity, albeit that nonionic surfactants are considered safer than ionic one (D.Attwood, 2013), and smaller MDS will be more susceptible to stability issues like Ostwald's ripening (Klang and Valenta, 2011).

Table 3.11 Size and PDI of NE prepared with different amounts of emulsifiers (n=3; mean±sd)

Amount of surfactant(w/w%)	tween 80/span 80	
	Size ± SD (nm)	PDI ± SD
0.3	163.56 ± 4.38	0.14+ 0.01
2	76.67 ±1.76	0.17 ± 0.02
5.0	32.65 ±0.73	0.22 ±0.00
10	28.25 ± 0.46	0.17 ±0.00

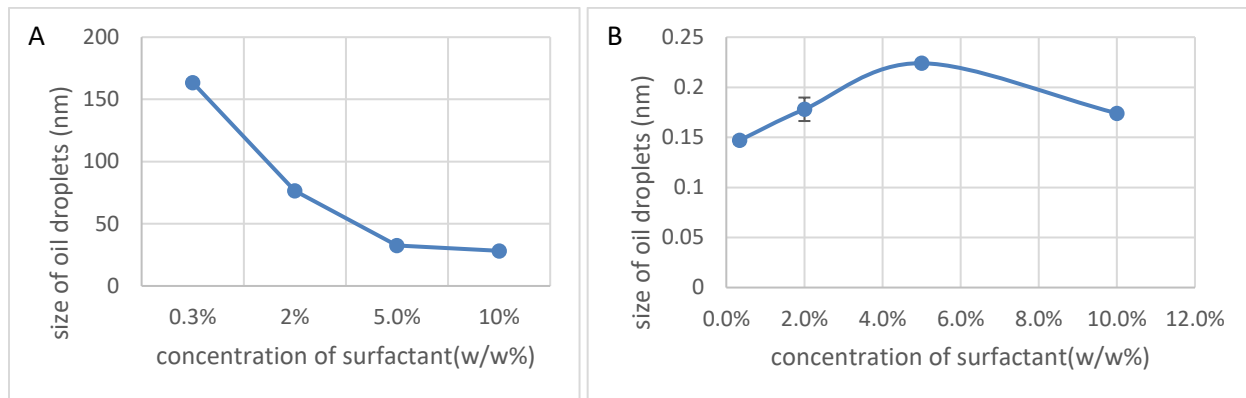


Figure 3.12 size (A) and PDI (B) of NE prepared with different amounts of emulsifiers

In addition to the concentration of surfactant, the MDS is also affected by the rate of adsorption of surfactant on the interfacial surface of the droplet which depends on the viscosity of the continuous phase and how the surfactant moves within the continuous phase to cover the droplet. So a different type of surfactant has a different pattern and movement, and therefore, a different effect on MDS.

Table 3.12 and Figure 3.13 show the effect of different types of surfactant on the MDS.

Table 3.12 size and PDI of NE prepared with different types of emulsifiers (n=3; mean±sd)

type of surfactant	size ± SD (nm)	PDI± SD
Tween 80/ Span 80	76.61±1.76	0.17± 0.01
Tween 60/ Span 60	82.42 ± 1.3	0.25± 0.00
Tween 40/ Span 40	109.43 ± 2.87	0.20± 0.02
Tween 20/ Span 20	130.84 ± 2.4	0.15± 0.01

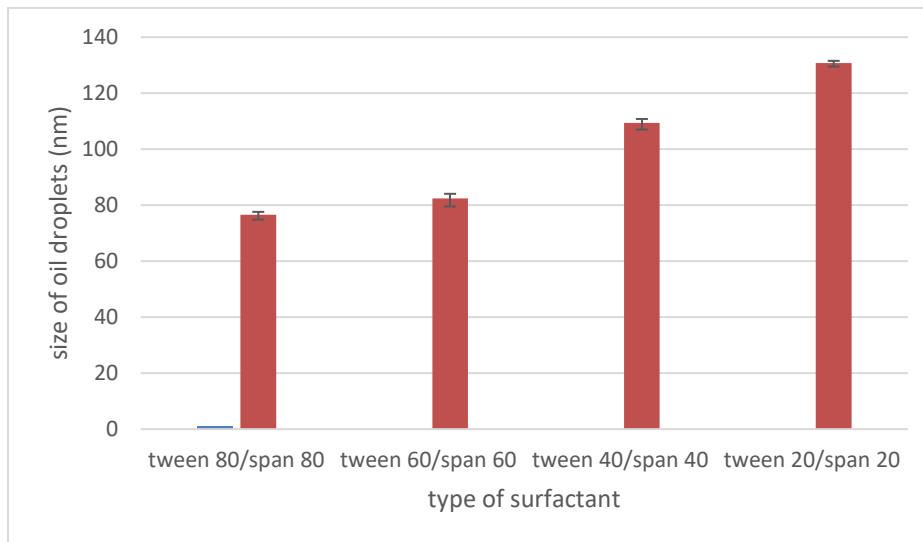


Figure 3.13 Size and PDI of NE prepared with different types of emulsifiers
 In comparison with the NE prepared by HPH, the MDS was smaller for most formulations due to the residence time in dispersing zone (when the droplets break-up) being shorter for HPH than HSH, which reduces the probability of coalescence. (Jafari *et al.*, 2008).

3.3.2 Parameters used for High-Pressure Homogenisation

3.3.2.1 Effect of the number of cycles of HPH

According to Müller & Peters (1998), increasing the number of cycles (passing of a NE through an HPH) will reduce both mean particle size and the polydispersity index of NEs. Thus, the effect of the number of cycles on the size of droplets using a homogeniser pressure of 20 ksi, was studied and PSD and PDI determined after 3, 5, 7 and 9 cycles.

Table 3.13 shows the effect of the number of cycles on size and PDI. To measure the effect of the number of cycles on size, OLS (ordinary least square) single regression was carried out using EViews software. There is a negative association between size and number of cycles increased by 1 unit, and size decreased by 1.42 units. This relationship is statistically significant at the empirical significance level

of 1% (P-value < 0.001). And the P-value of F-statistics is less than 1%, so our model is overall significant. The explanatory power of this model is high ($R^2=79\%$ of the variation in size can be attributed to the variation in a number of the cycle).

The average size decreased sharply as the number of cycles increased from 3 to 7 and it decreased slightly from 7 till 9. A T-test was conducted to compare the average size along 5 cycles with the average size of 7 cycles and another T-test to compare the average size along 7 cycles with the average size of 9 cycles. The null hypothesis of the T-tests proposes that the difference between the two groups is not significant. If the P-value < 5%, we reject the null hypothesis and therefore, the difference is statistically significant. The P-value for 5 till 7 cycles are 0.036, which means the decrease was significant, whereas the P-value for 7 to 9 cycles is 0.281, which means the impact on particle size was not significant. Therefore, 7 cycles were used for standard formulations.

Table 3.13 The effect of the No of the cycle on size and PDI

No. of cycles	Average size (nm)	PDI
3 cycles	100.44	0.135
5 cycles	99.43	0.099
7 cycles	94.45	0.065
9 cycles	92.51	0.060

3.3.3 Parameters for High Shear Homogenisation followed by Ultrasound

In this research, three parameters were varied: homogenization time, the speed of mixer and sonication time to determine the impact on NE properties.

3.3.3.1 Impact of homogenization time

To check the optimum homogenization time, MDS and PDI were used as indicators of formulation success. Both are considered as the main parameters in NE formulation due to their effect on delivery through skin and stability. Figure 3.14 shows that as duration increased, the MDS decreased. A significant decrease was found between 5 and 15 minutes, after which time there was no further significant impact. The same trend was found for PDI but with no impact after 10 minutes. Therefore a standard homogenization time of 15 min was adopted.

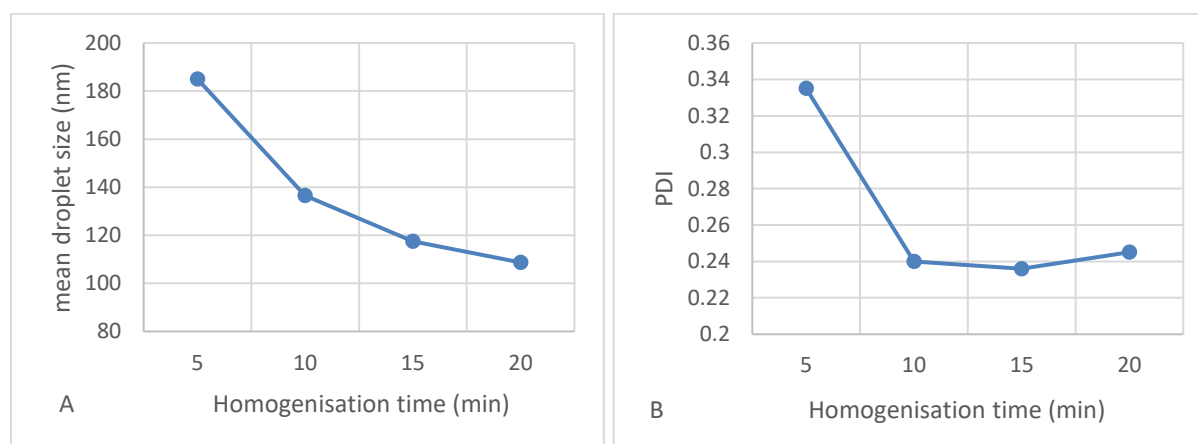


Figure 3.14 Effect of homogenization time on mean droplet size (A) and PDI (B)

3.3.3.2 Impact of mixing speed

Mixer speed was varied from 3000 -10000 RPM. Results (Figure 3.15) showed that there is no significant change in the MDS of resultant NEs above 5000 rpm, whereas PDI was similar for all speeds. According to that, the optimum speed was 5000 rpm. The formulation used to study the speed was 5% w/w of oil and 2% w/v of a mixture of T80/ S80 and 0.5% w/v of triclosan.

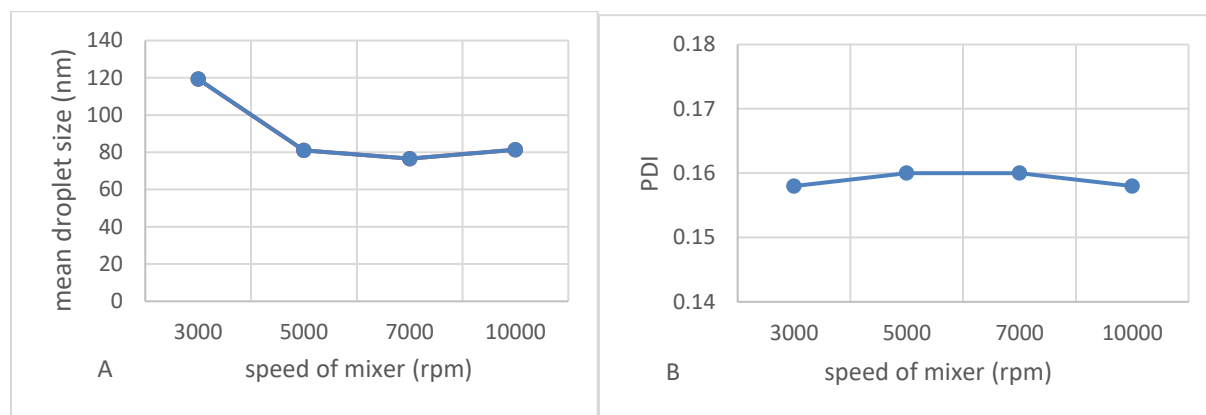


Figure 3.15 Effect of Speed of mixer on mean droplets size (A) and PDI (B)

3.3.3.3 Impact of ultrasonication time

To determine the effect of ultrasonication time on the MDS and PDI of triclosan NE an amplitude of 50% was used and the duration varied from 2 to 10 minutes, with a formulation of 5% w/v of oil and 2% w/v of a mixture of T80/ S80 and 0.5% w/v of triclosan PSD and PDI decreased with increasing sonication time (Figure 3.16). This is expected with an increase in shear force on droplet size, which causing deformation of the droplet and reduction in size. These results are comparable to Shahavi et al., which found sonication time has a considerable effect on the droplet size (Shahavi *et al.*, 2015).

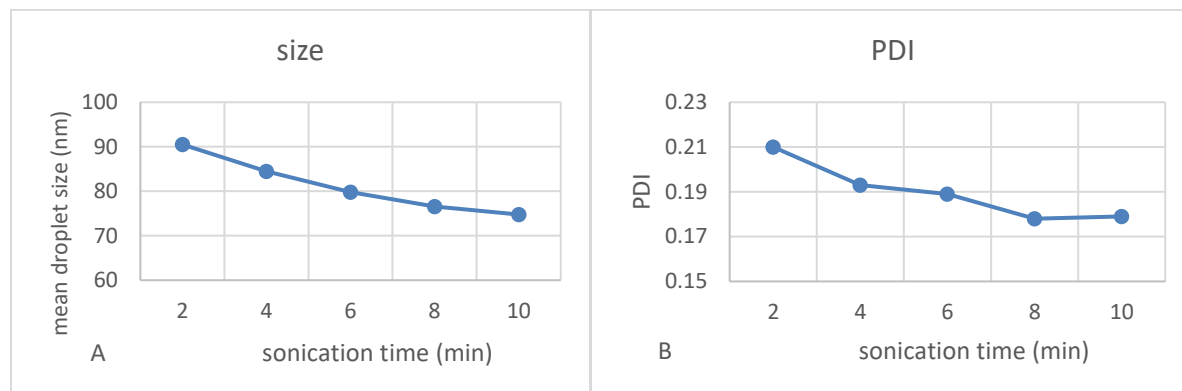


Figure 3.16 Effect of sonication time on mean droplets size (A) and PDI (B)

3.3.4 Long-term stability of triclosan nanoemulsion

3.3.4.1 High-pressure Homogenizer technique

NEs, in general, have better stability than emulsions, as flocculation and coalescence decrease with decreasing the particle size (Qian and McClements, 2011). In this thesis, the stability of samples was studied at two different temperatures, 4°C and 25°C over three months. For samples having a different type and concentration of surfactant, Figure 3.17 and Figure 3.18 show the effect of storage on particle size. These figures show that formulation containing surfactants at 2% w/w is generally stable except the T20/S20 at 25°C in which particle size increased after four weeks.

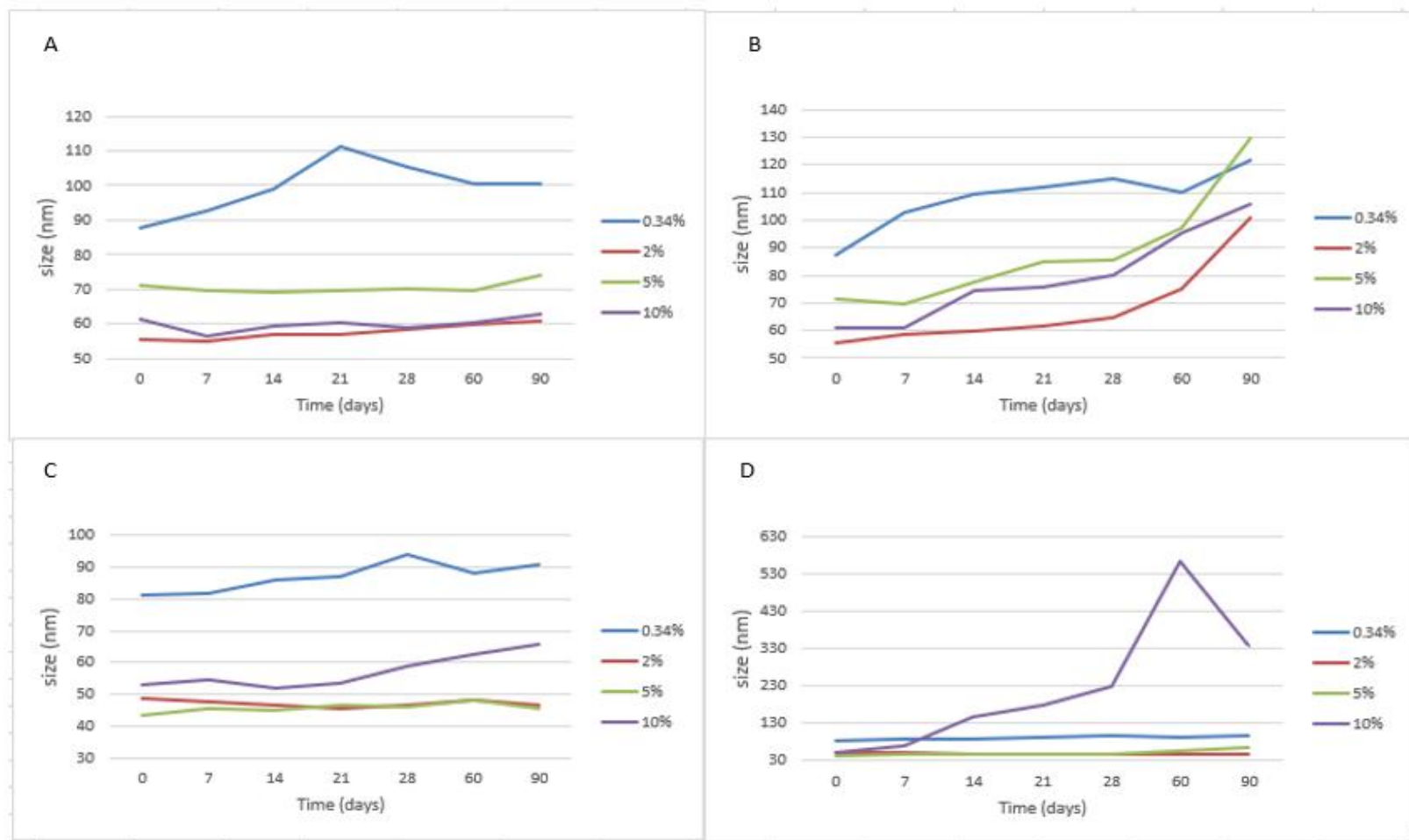


Figure 3.17 The effect of surfactant on triclosan NE during storage at 4 and 25°C for 3 months (A)effect of surfactant (T20/S20)at 5 cycles/4°C (B) effect of surfactant (T20/S20)at 5 cycles /25°C (C) effect of surfactant (T40/S40)at 5 cycles /4°C(D) effect of surfactant (T40/S40)at 5 cycles /25°C

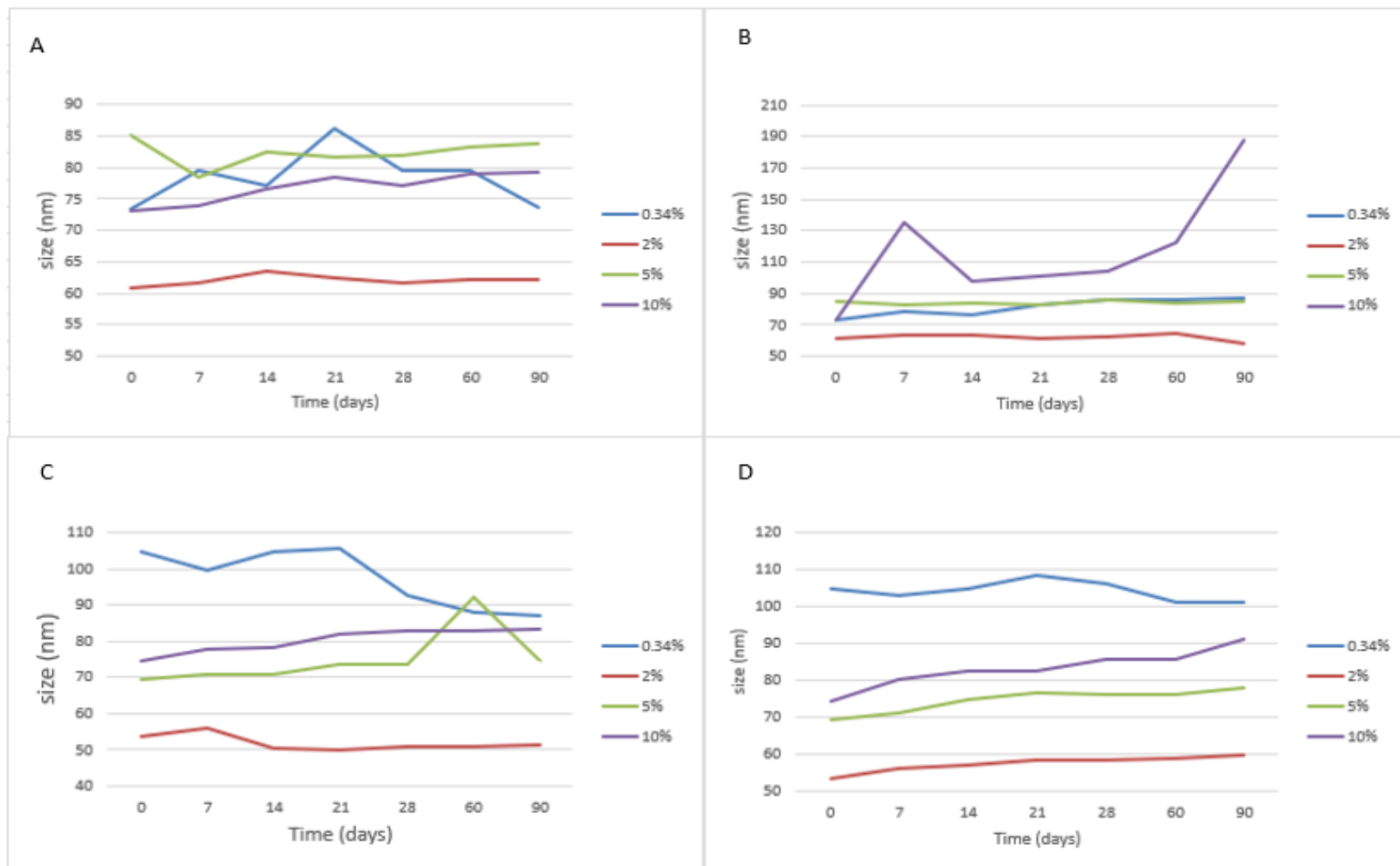


Figure 3.18 The effect of surfactant on triclosan NE during storage at 4 and 25°C for 3 months (A)effect of surfactant (T60/S60)at 5 cycles/4°C (B) effect of surfactant (T60/S60)at 5 cycles /25°C (C) effect of surfactant (T80/S80)at 5 cycles /4°C(D) effect of surfactant (T80/S80)at 5 cycles /25°C

3.3.4.2 High shear homogenisation followed by ultrasound technique

The stability of all formulations was studied over a 3 month period. When assessed visually only samples prepared at low mixing speeds (3000 and 5000 rpm) and without sonication appeared to exhibit some cracking behaviour. This implies that sonication aids stabilisation of batches prepared at slower mixing speeds., This was also reported by Baspinar *et al.* who found that the effect of the number of cycles on particle size is greater at lower pressures is greater than the effect on high pressure (Baspinar, Keck and Borchert, 2010). Figure 3.20 shows the stability results for different concentrations and types of surfactant. These graphs show that the MDS and PDI were more stable compared with the formulation prepared by HPH technique. Nevertheless, the optimum formulation is not only determined by the smallest droplet size or highest stability; the determining parameters for the optimised formulation will be the formulations with the fast release and skin absorption.

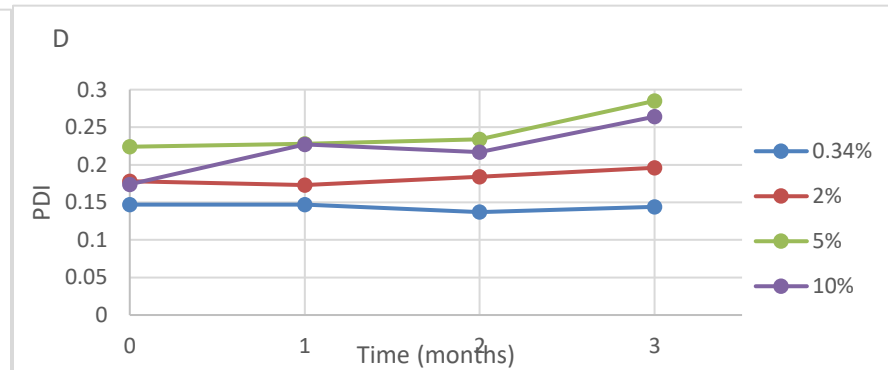
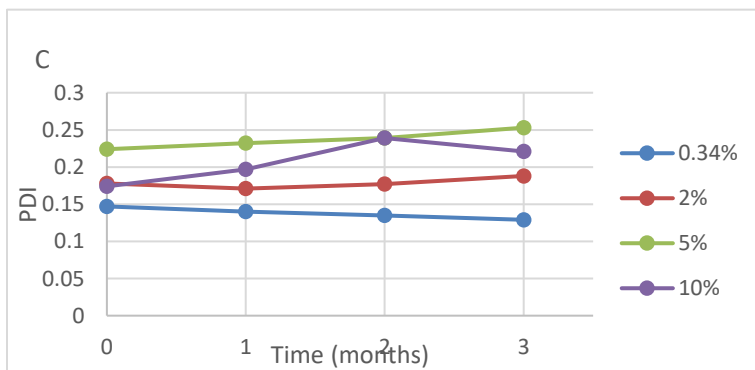
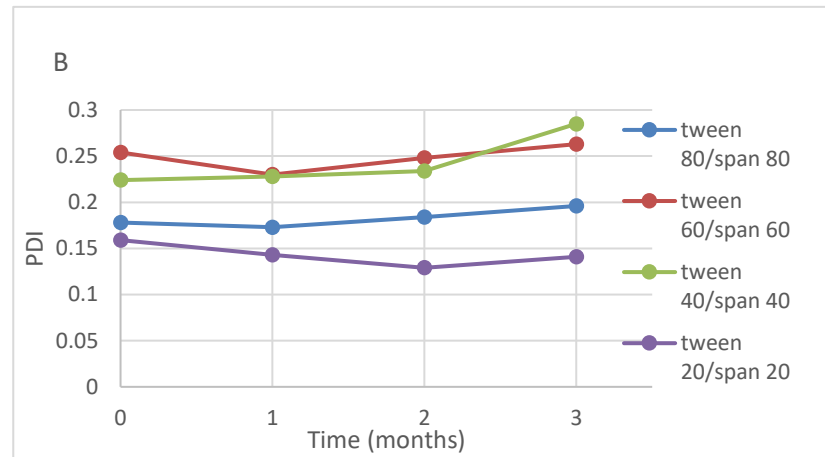
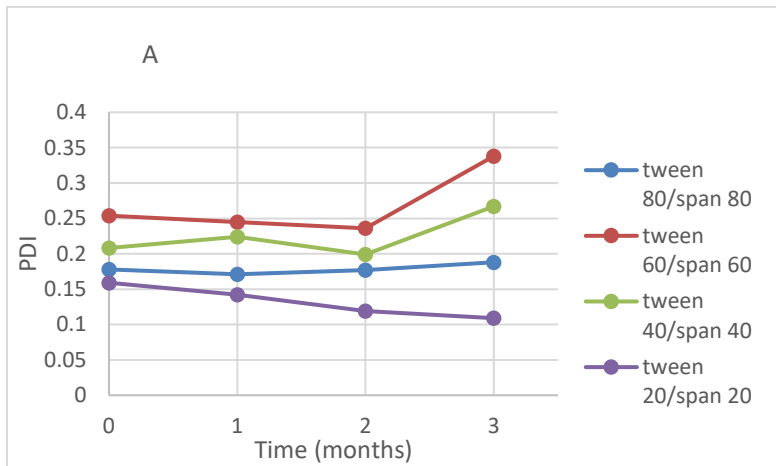


Figure 3.19 PDI result for the stability study of different type and amount of surfactant for triclosan NE storage at 4 and 25°C for 3 months (A) Different type of surfactant At 25° C (B) Different type of surfactant At 4° C (C) Different amount of surfactant At 25° (D) Different amount of surfactant At 4° C

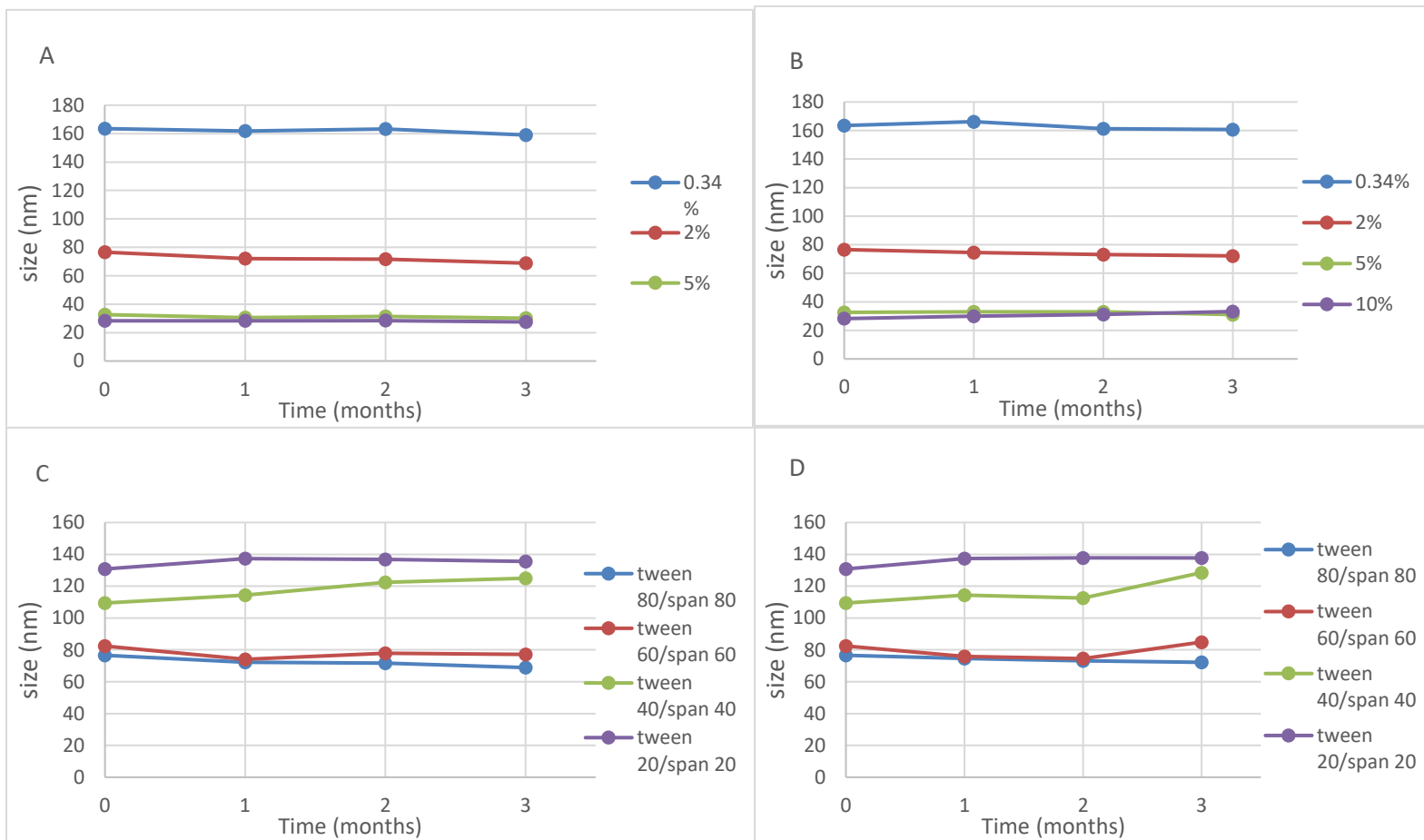


Figure 3.20 MDS result for stability study of different type and amount of surfactant for triclosan NE storage at 4 and 25°C for 3 months (A) Different amount of surfactant at 4°C (B) Different amount of surfactant At 25°C (C) Different type of surfactant At 4°C (D) Different type of surfactant At 25°C

3.3.5 Development and validation method of HPLC determination of triclosan in nanoemulsion

3.3.5.1 Development method

In order to obtain the optimum separation and resolution, various ratios of solvents in the mobile phase acetonitrile (ACN) and water were considered, the optimum ratio was found to be 60:40 ACN:water. There were two different columns that were also studied, these are; C18 and pentafluorophenyl (PFP), the peaks formed by the PFP column had a higher intensity than the C18, this is because of the fluorine atoms in the PFP which cause a unique aromatic selectivity. The maximum wavelength (λ max) for triclosan was determined using a UV-visible spectrophotometer, this was found to be 287 nm and is shown in Figure 3.21.

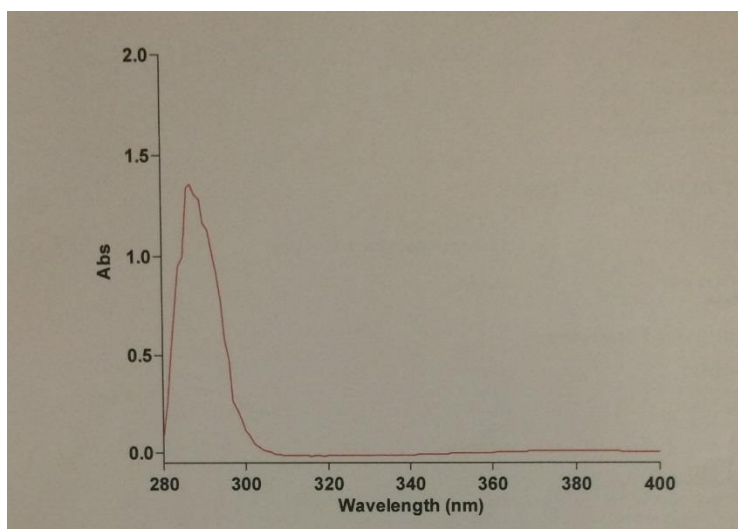


Figure 3.21 UV spectrum for triclosan in methanol, showing the λ max at 287nm

3.3.5.2 Validation method

Validation of each method is required, the process to achieve this throughout this study was performed in accordance to the ICH 1996 guidelines

3.3.5.2.1 Linearity

Six different concentrations of triclosan were prepared in order to establish linearity, these concentrations were; (1, 5, 10, 20, 50, 100 µg/ml), covering the expected range and including the limit of quantification. This test was performed five times, the ratio of peak area of triclosan concentration was then plotted. Figure 3.22 shows linearity in one of the five tests performed (group A, B, C, D and E), whereas other graphs can be found in Appendix A. The correlation coefficient (R^2) in the five groups was studied and the average R^2 was 0.9996; this was found using statistical methods along with visual examination and is an indication of a very high linearity relationship, suggesting that all triclosan concentration alterations will lead to a corresponding change in peak area.

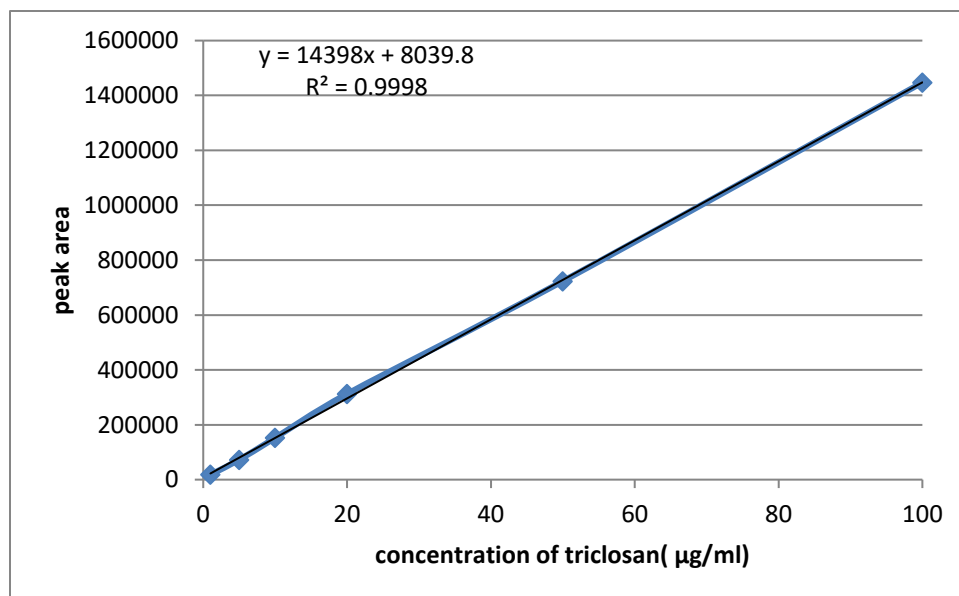


Figure 3.22 Linearity curve of group A for triclosan (n=3; mean±sd)

3.3.5.2.2 Sensitivity

The limit of detection (LOD) and the limit of quantification (LOQ) are the two factors used to determine sensitivity, the equations for these are expressed in Equation 3.3 and 3.4. The LOD and LOQ were calculated in this study.

Table 3.14 shows the mean of slopes in the linearity curves in the five groups as well as the standard deviation of the intercept of these groups.

Table 3.14 Standard deviation of intercept and slopes mean

	Intercept	Slope
Group A	8039.85	14398
Group B	3114.45	16477
Group C	3154.36	16463
Group D	14324	15625
Group E	14611	15601
Standard Deviation	5677.71	
Mean		15712.88

The limit of detection and limit of quantification were subsequently calculated and found to be 1.192 $\mu\text{g/ml}$ and 3.613 $\mu\text{g/ml}$ respectively.

3.3.5.2.3 Selectivity

As shown in Figure 3.24, this method leads to good selectivity for triclosan and has good separation for triclosan as it was eluted at 6.737 min.

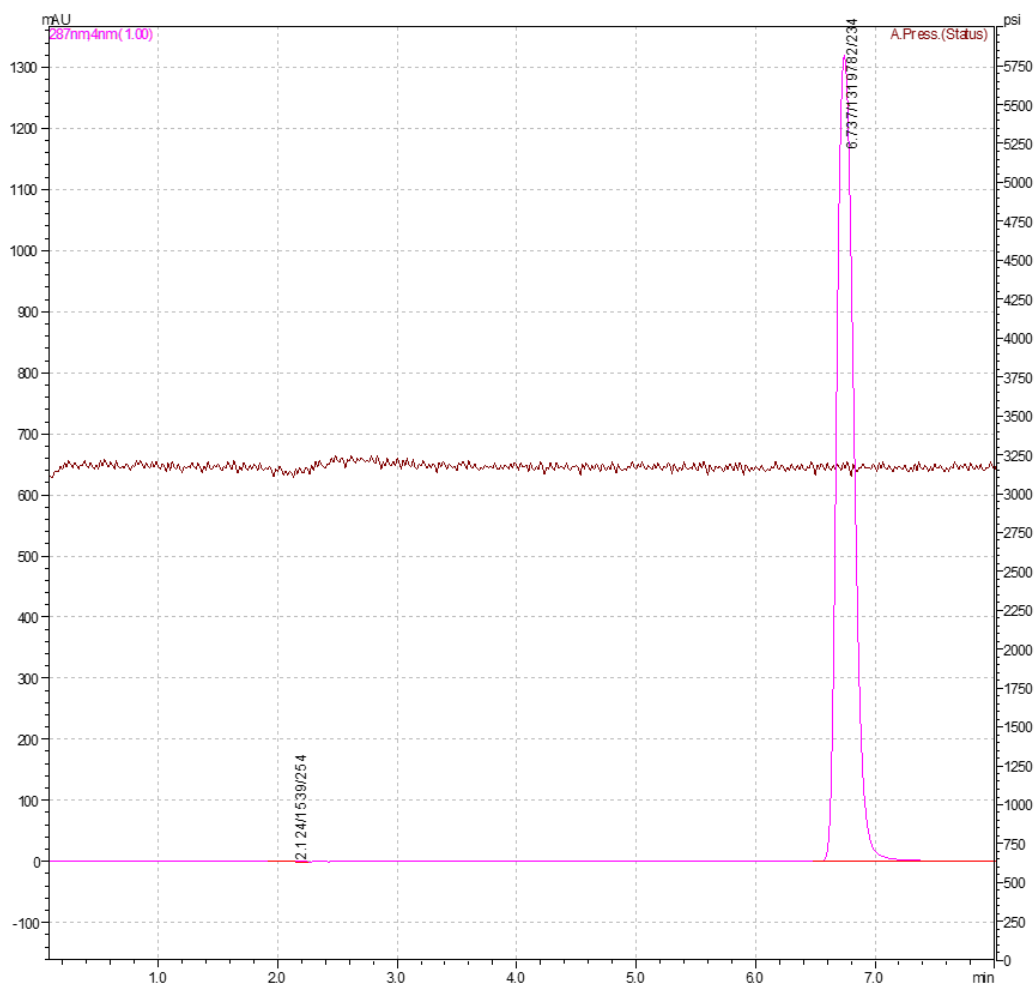


Figure 3.23 Peak of triclosan at 6.737 min

3.3.5.2.4 Accuracy

Low, medium and high concentrations were prepared for this accuracy test, different to the concentrations used for the linearity test. These concentrations were; (10, 40, 80) $\mu\text{g/ml}$. This test was

performed five times and the average was calculated. The final found concentration was then calculated by a calibration curve and plotting peak area on the curve. Equation 3.6 was the equation used to calculate the accuracy.

The range of accuracy was from 99.25 to 102.58%, according to the ICH guidelines (1996), this is an acceptable accuracy range, these results are shown in Table 3.15

Table 3.15 Range of accuracy for HPLC method for triclosan

Actual concentration ($\mu\text{g/ml}$)	Observed concentration ($\mu\text{g/ml}$)	% Accuracy
10	10.25	102.58
40	40.17	100.44
80	79.40	99.25

3.3.5.2.5 Precision

Three varying triclosan concentrations were needed for the calculation of precision. Low, medium and high concentrations were used these were; (4, 40, 80) $\mu\text{g/ml}$. The relative standard deviation (RSD) must be calculated for the determination of precision, If the RSD is equal to or less than 2% this is a confirmation of the precision of the method. There are two parts to the precision test; the first is the intra-day precision that is replicated five times within the same day to find the RSD between every two injections, the second is the inter-day precision in which the process is performed and repeated over five days to find the RSD between the days. (All precision data is found in Appendix B) Table 3.16 shows the RSD range of the inter-day precision as well as the intra-day precision. Inter-day precision was found to be between 0.06% and 0.18%, as for the intra-day precision this was between 0.83 and 1.47%. Since both the inter-day precision and intra-day precision were both found to be lower than 2%, this confirms the precision of the method in accordance to the definitions by ICH (1996).

Table 3.16 Range of RSD for both intra-day and inter-day precision

Nominal concentration ($\mu\text{g/ml}$)	% Relative Standard Deviation (RSD)	
	Intra-day	Inter-day
low =4	0.18	1.46
medium = 40	0.12	1.13
high = 80	0.06	0.82

3.3.6 *In vitro* skin permeation study

3.3.6.1 *Quantitative determination using an adhesive tape stripping method*

As mentioned in section 3.1.7.2, an adhesive tape stripping method is a successful method to determine triclosan within the skin. Permeation of a number of triclosan formulations into the skin was studied.

3.3.6.1.1 Effect of amount of surfactant

To study the effect of the amount of surfactant used in NE formation on skin permeation, four different formulations were prepared using HSH technique as shown in table 3.17, and a control (triclosan in oil) to compare with these formulations. Figure 3.25 shows that the four formulations have better release and penetration in the skin compared with the control. Therefore, it can be concluded that the triclosan NE was successful in improving the penetration of triclosan (increasing overall amount, and reaching deeper layers) into the skin. On the other hand, there are significant differences between these formulations ($P < 0.05$), the formula (H1-P031) which has the lowest amount of surfactant showed the best release (increasing overall amount) and retention (deeper layers) of triclosan within the skin. This result could be due to a monolayer surfactant film around an oil droplet, which made the release of triclosan from eucalyptol to skin easier than other formulations where the film consists of multilayers.

Table 3.17 parameters of different triclosan NE to study the effect of the amount of surfactant

High shear homogeniser - the effect of the amount of surfactant					
Formula code	Oil(w/w%)	surfactant		Triclosan (w/w%)	Water (w/w%)
		type	amount(w/w%)		
control	5	----	----	0.5	----
H3-P031	5	T80/S80	10.00	0.5	84.5
H2-P031	5	T80/S80	5	0.5	89.5
H1-P028	5	T80/S80	2	0.5	92.5
H1-P031	5	T80/S80	0.34	0.5	94.15

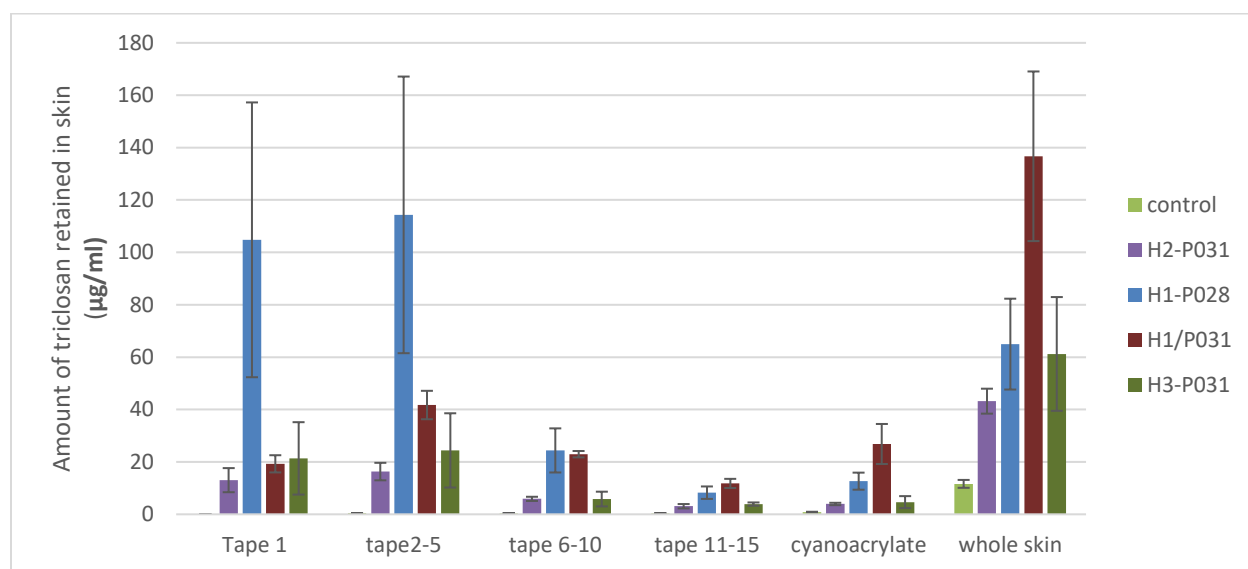


Figure 3.24 Effect of the different amount of surfactant on skin permeation (mean \pm SD n=3)

3.3.6.1.2 Effect of type of surfactant

As mentioned above, four different mixtures of surfactants were tested to study the effect of type of surfactant on skin permeation, as shown in Table 3.18. The better release (increasing overall amount) was in formulation with a mixture of T20/S20, that could be explained by two reasons; firstly, to get the required HLB of eucalyptol 12.5 which was determined in section 3.3.1.2 the ratio of T20/ S20 should be 1:1 (section 3.3.1.7.1). So, the lipophilic surfactant in this formulation is higher than the rest of the formulations. Secondly, could be the chemical structure of surfactant; where S20 (sorbitan

monolaurate) the alkyl group of the fatty acid in it is shorter than S40, S60, S80 (sorbitan monolmitate, sorbitan monostearate, sorbitan monooleate respectively) and that will reduce the hindering of the movement of molecules. so as shown in figure 3.26 the formulation with T20/S20 shows the best retainment and releases.

Table 3.18 Parameters of different NE to study the effect of the type of surfactant

High-pressure homogeniser - the effect of type of surfactant					
Formula code	Oil(w/w%)	surfactant		Triclosan (w/w%)	Water (w/w%)
		Type	Amount(w/w%)		
Control	5	----	----	0.5	----
F3-P032	5	T80/S80	2	0.5	92.5
F1-40/P024	5	T40/S40	0.34	0.5	94.15
F2-40/P024	5	T40/S40	2	0.5	92.5
F2-20/P024	5	T20/S20	2	0.5	92.5
F2-60/P024	5	T60/S60	2	0.5	92.5

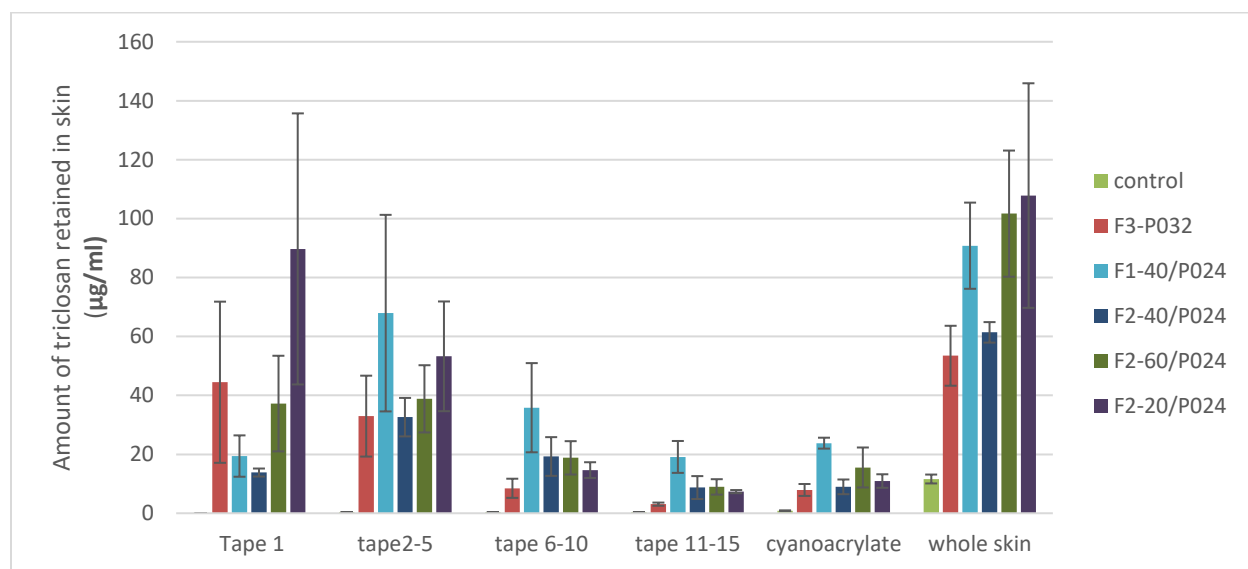


Figure 3.25 Effect of the different type of surfactant on skin permeation (mean \pm SD n=3)

3.3.6.1.3 Effect of amount of oil

To study the effect of the amount of oil on skin permeation, three formulations were prepared, as shown in table 3.19. All formulations had the same parameter except the H1-P030 the amount of triclosan 0.25% w/w as the solubility of triclosan in eucalyptol 122.85mg/ml (section 3.3.1.4). Figure 3.27

shows that there is no significant difference in permeation at all levels between formulations ($P>0.05$).

For that, a 5% w/w consider an optimum amount for this formulation.

Table 3.19 Parameters of different NE to study the effect of the type of surfactant

High-shear homogeniser - the effect of the amount of oil					
Formula code	Oil(w/w%)	surfactant		Triclosan (w/w%)	Water (w/w%)
		Type	Amount(w/w%)		
control	5	----	----	0.5	----
H1-P030	2.5	T80/S80	2	0.25	95.25
H1-P028	5	T80/S80	2	0.5	92.5
H2-P030	7.5	T80/S80	2	0.5	90

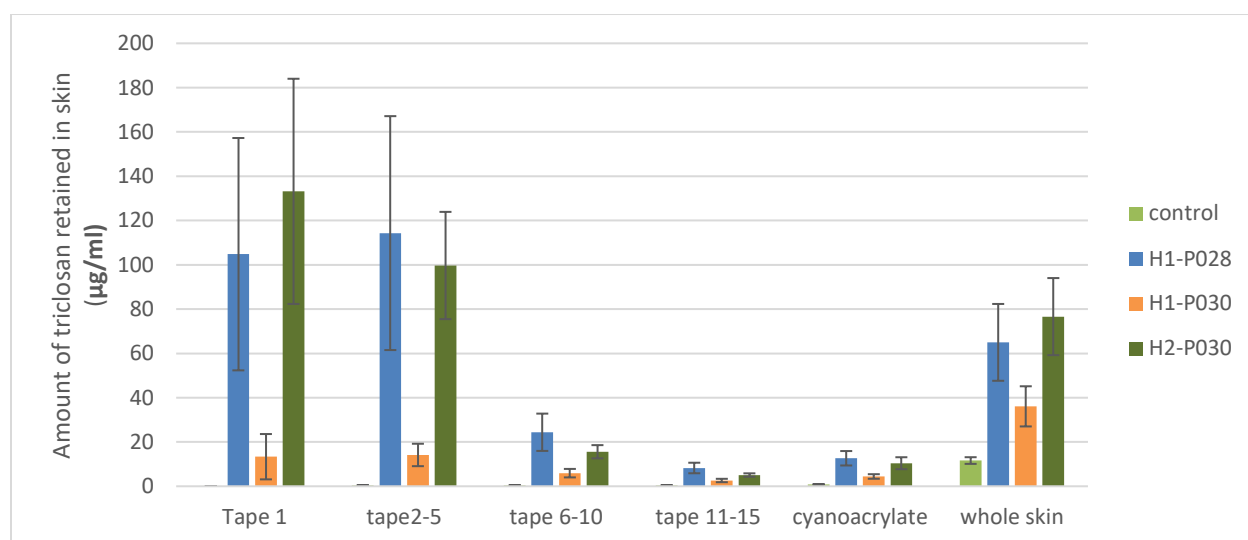


Figure 3.26 Effect of the different amount of oil on skin permeation (mean \pm SD n=3)

3.3.6.2 Qualitative determination using CT Scan

After quantitatively determining the amount of triclosan within the skin using the tape stripping method, the triclosan was also tested qualitatively using CT scans to find the distribution of triclosan within the skin.

As explained in section 3.1.7.3, the skin sample was left on Franz cells for 24 hours then removed and left to dry for 1 hour, then placed on the CT scan. False-colouring was applied to the samples based on the various densities within each sample. A video and 3D images were recorded for the samples; the video records the 3D movement across the skin samples and screenshots were taken every three seconds in the sagittal plane video. The sagittal plane was chosen since it views the triclosan penetration from the surface to the bottom of the samples, making it the clearest view out of the three possible planes. Three samples were tested using this method; skin without formulation (Figure 3.28 a and b), and skin with H1-P031 formulation (Figure 3.29a and Figure 3.29b) and F3-P032 formulation (Figure 3.0a and Figure 3.30b).

As seen in Figure 3.28, only one colour appeared when applying false-colouring on skin samples without formulation, indicating that only one density was found. Whereas in Figure 3.29 and Figure 3.30. Two colours appeared on the skin sample, indicating the presence of triclosan within the skin. Figure 3.29 showed a larger red area than Figure 3.30, which indicates a greater amount of triclosan in this sample. This result correlates with the result found in the quantitative tape stripping method where the H1-P031 was found to have better penetration and retention within the skin.

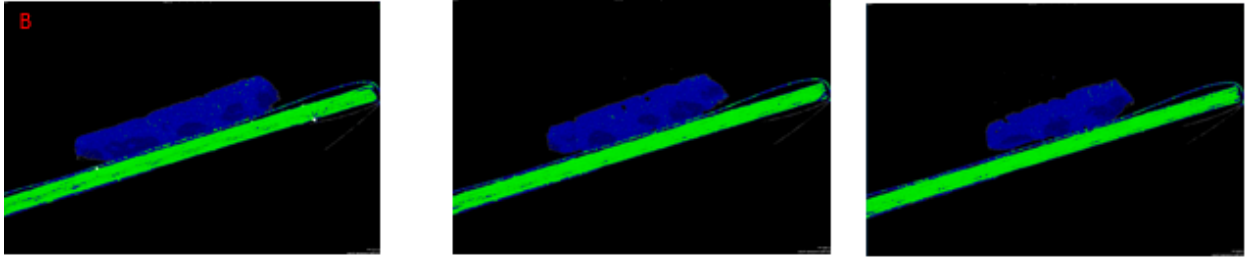
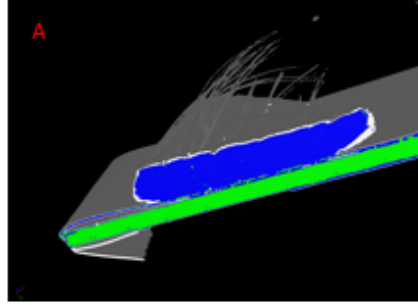


Figure 3.27(a) 3D image of the skin sample without formulation (b) screenshots from video every 10 seconds of skin sample without formulation (blue; skin, green; plate)

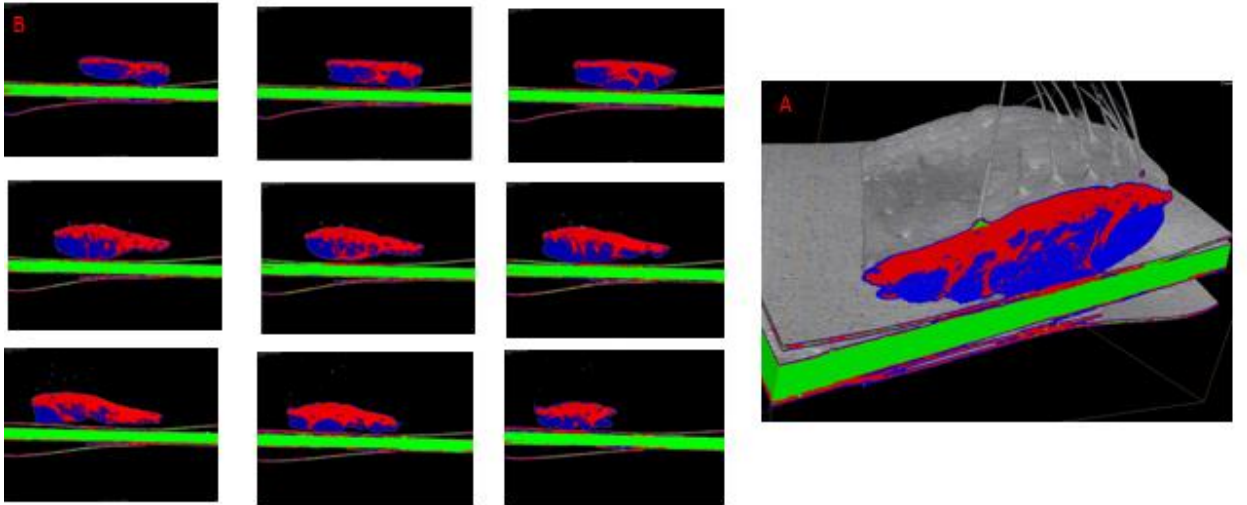


Figure 3.28 3D image of the skin sample with H1-P031 formulation (b) screenshots from video every 3 seconds of skin sample with H1-P031 formulation (blue; skin, red; triclosan, green; plate)

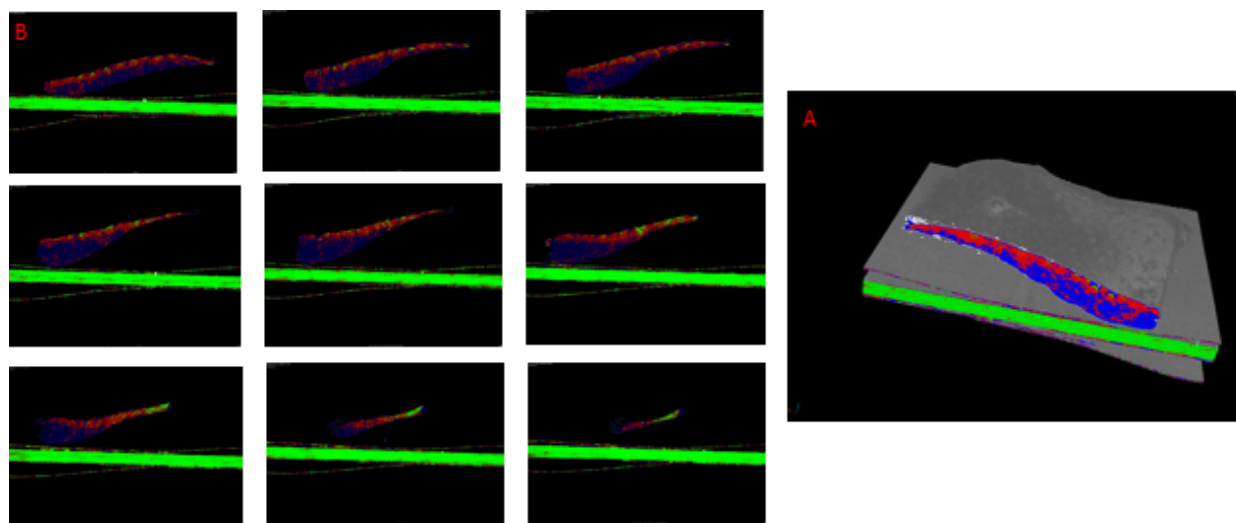


Figure 3.29 3D image of the skin sample with F3-P032 formulation (b) screenshots from video every 3 seconds of skin sample with F3-P032 formulation (blue; skin, red; triclosan, green; plate)

3.3.6.3 Impact of preparation method on skin permeation

To study the effect of preparation technique on penetration and retention of triclosan in the skin, three formulations prepared using an HPH technique (F3-P032, F2-40/P024, F1-40/P024) were compared with two formulations made using an HSH technique (H1- were prepared as shown in table 3.20). All formulations which were prepared by HSH show better release and retain within the skin than the formulations were prepared by HPH as shown in figure 3.31, despite smaller size and PDI. The MDS and PDI of NE which prepared by HPH lesser than HSH. In view of that, there are other parameters must be studied and a further investigation to understand the penetration within the skin.

Table 3.20 Parameters of different NE to compare between two techniques

Comparison of two techniques					
Formula code	Oil(w/w%)	surfactant		Triclosan (w/w%)	Water (w/w%)
		type	amount(w/w%)		
control	----	----	----	0.5	99.5
F3-P032	5	T80/S80	2	0.5	92.5
F2-40/P024	5	T40/S40	2	0.5	92.5
H1-P028	5	T80/S80	2	0.5	92.5
F1-40/P024	5	T40/S40	0.34	0.5	94.15
H1-P031	5	T80/S80	0.34	0.5	94.15

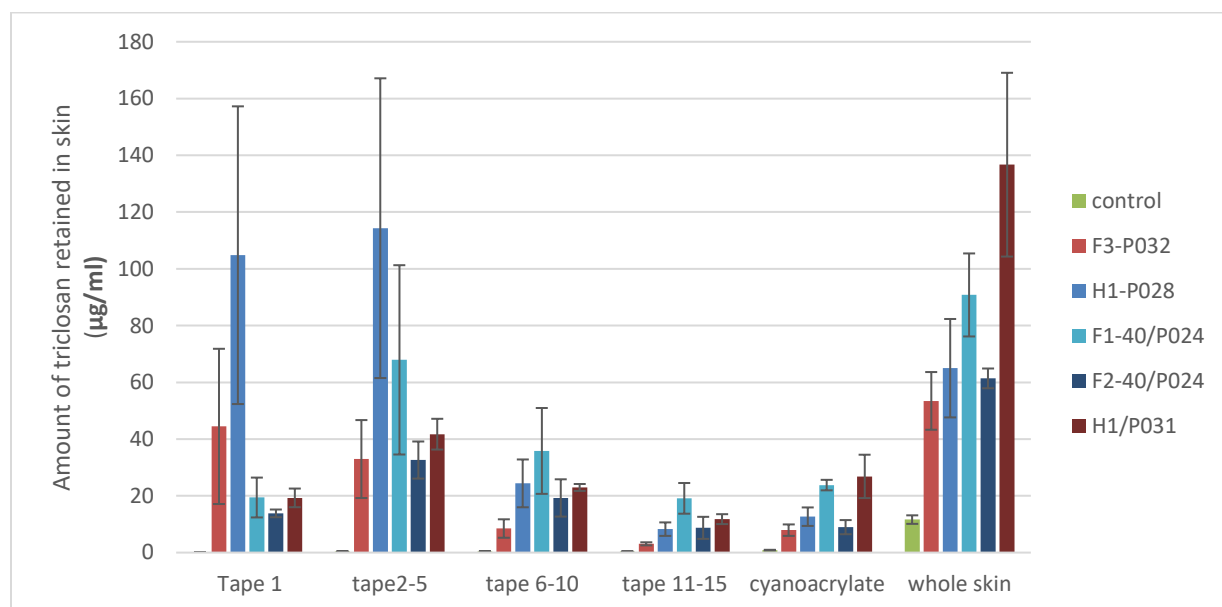


Figure 3.30 Comparison between two techniques (mean \pm SD n=3)

3.3.6.4 The optimum formulation

From studying the effect of the amount of surfactant in the penetration of triclosan into the skin (section 3.3.6.1.1), it was concluded that the lowest amount of surfactant showed the highest level of penetration and retention of triclosan within the skin, which was 0.34% w/w. From studying the type of surfactant (section 3.3.6.1.2), the best was found to be T20/S20, which resulted in the highest penetration and retention of triclosan within the skin. The amount of oil in formulations did not show

significant differences. Therefore, 5% was chosen to minimise the amount of surfactant needed to cover the oil. By comparing both techniques (section 3.3.6.3), high-shear homogenisation was found to produce NE with better penetration than the high-pressure technique.

From the mentioned studies, it was concluded that the F1-20/P024 formulation is the optimum formulation which resulted in the highest level of penetration and retention of triclosan within the skin, this formulation was prepared by high-shear homogeniser and has surfactant mixture 0.34% w/w T20/S20, 5% oil and 0.5% triclosan and is shown in Figure 3.32.

Table 3.21 Variables Summary of all formulations used in skin

All formulations					
Formulation code	Oil(w/w%)	surfactant		Triclosan (w/w%)	Water (w/w%)
		type	amount(w/w%)		
control	----	----	----	0.5	99.5
H2-P031	5.0	T80/S80	5.00	0.5	89.5
F3-P032	5.0	T80/S80	2.00	0.5	92.5
H1-P028	5.0	T80/S80	2.00	0.5	92.5
F1-40/P024	5.0	T40/S40	0.34	0.5	94.15
H1-P030	2.5	T80/S80	2.00	0.25	95.25
F2-40/P024	5.0	T40/S40	2.00	0.5	92.5
H1-P031	5.0	T80/S80	0.34	0.5	94.15
F1-20/P024	5.0	T20/S20	0.34	0.5	94.15
F2-20/P024	5.0	T20/S20	2.00	0.5	92.5
H2-P030	7.5	T80/S80	2.00	0.5	90
F2-60/P024	5.0	T60/S60	2.00	0.5	92.5
H3-P031	5.0	T80/S80	10.00	0.5	84.5

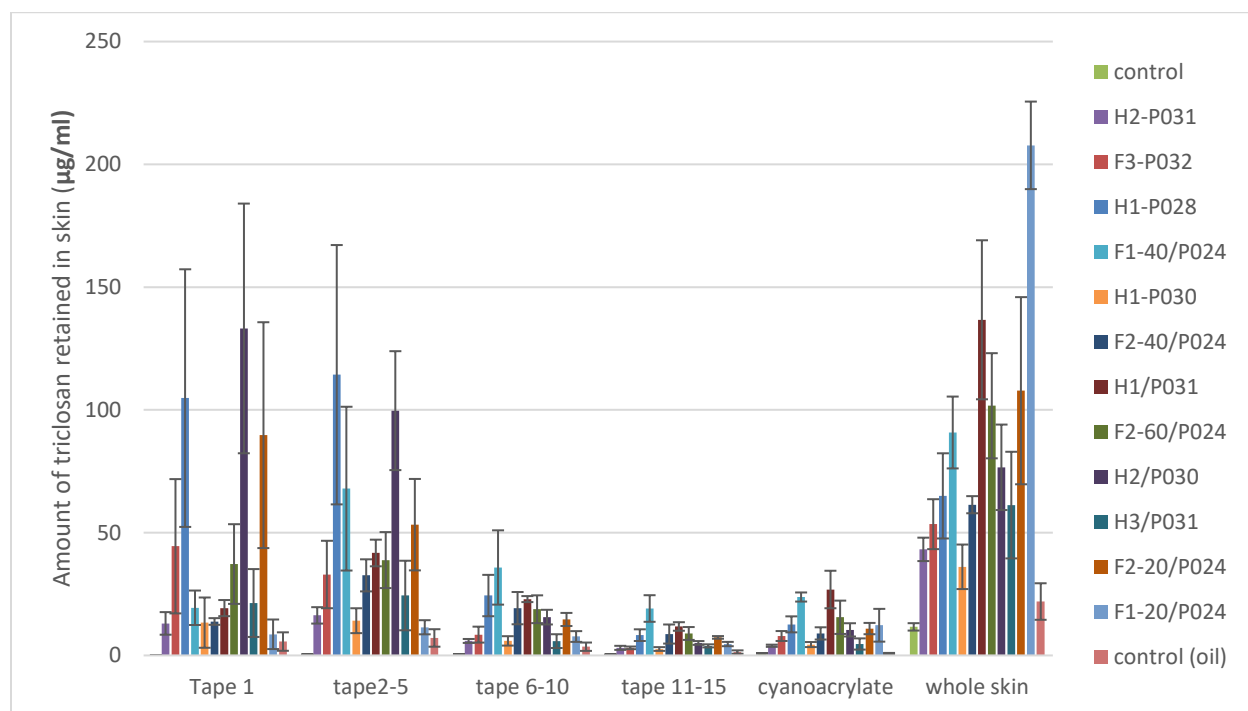


Figure 3.31 graph of all formulations (mean \pm SD n=3)

3.4 Conclusion

In conclusion, triclosan NE was successfully designed and developed using two techniques; a high-pressure homogeniser and a high-shear homogeniser followed by ultrasonication. The physicochemical characterisation of the formulations was studied, which includes; MDS, PDI, ZP, PH and viscosity. The amount and type of surfactant in addition to the amount of oil were explored to determine the optimum formulation, specific parameters for each technique were also considered including; the effect of the number of cycles for the high-pressure homogeniser and the sonication time for the high-shear homogeniser. A stability study was carried out for all formulations in both techniques over three months.

The HLB for the eucalyptol was calculated and found to be 12.5. The formulation with the lowest amount of surfactant (0.34%w/w), T20/S20 ratio 1:1 showed the best penetration and retention within the skin.

The number of cycles for HPH did not have a significant effect on MDS and PDI after seven cycles, according to t-test (P -value < 0.05). In the HSH technique, the sonication had an important role in minimizing the PDI and improving stability.

The use of the tape-stripping method was successful in quantitatively determining the triclosan within the skin, and the micro CT scan was successful in the qualitative determination and correlation was found between both these methods.

Chapter 4- Design and Development of Chloroxyleneol Nanoemulsion for Dermal Delivery

4.1 Introduction

Microbes are frequently able to access the preferred environment for infections, which is a moist, nutritious and warm environment, due to a rupture in the skin, more commonly known as a wound which can subsequently lead to infection due to the presence of bacteria, fungi, etc. MRSA, for example, is generally found in open wounds and abrasions to the skin and is frequently the result of infections within hospitals. These types of infections lead to complications and result in a lengthened illness, which subsequently leads to the requirement for prolonged treatment and higher treatment costs. To limit wound infection, it is therefore essential in wound management to generate an ideal environment for the regeneration of the epidermal layer of the skin while considering the avoidance of possible further injury to the skin throughout the renewal period of the epidermis. This leads to the requirement and importance of antimicrobial dressings in wound treatment; the current most commonly used topical antimicrobial dressings are iodine and silver sulfadiazine (Shupp *et al.*, 2010). However, there are challenges with the design of antimicrobial dressings which include the possibility of toxicity to host cells, low adherence to skin and low duration of activity against both gram-positive and gram-negative bacteria (Hemmila *et al.*, 2010).

These disadvantages have led to the drive for development of improved and enhanced delivery systems that can control drug release over a prolonged period and penetrate the antimicrobial agent further into the skin than current solutions.

Nanoemulsions can generally be defined as the liquid dispersion of both an oil phase and a water phase combined with a surfactant; this liquid dispersion is thermodynamically stable or kinetically stable.

When oil droplets are dispersed into an aqueous phase, this is referred to as an O/W NE and is the

preferred system for delivery for hydrophobic substances. The favourable delivery system for hydrophilic substances, however, is W/O NEs.

In this thesis, various NE formulations with varying types of surfactant mixtures and different amounts of the mixtures and eucalyptol oil were studied. Eucalyptol oil was chosen for two reasons; it is considered an antimicrobial agent and it has a role in enhancing the permeability of formulation within the skin.

Therefore, these studies were performed to achieve the optimum formulation to find the highest amount of antiseptic which can penetrate the skin.

4.1.1.1 . Physicochemical characterisation of the nanoemulsion formations:

The following tests were mentioned in Chapter 3 and thoroughly explained.

4.1.1.1.1 *Accelerated stability studies*

Three steps were used for the accelerated stability study which are; heating-cooling cycle followed by centrifugation and finally the freeze-thaw cycle.

- 1- Heating-cooling cycle: The samples were placed in the refrigerator at 4°C for 48 hours then heated at 45°C for another 48 hours. Six cycles were performed, and the samples that remained stable throughout this step moved onto to the next step.
- 2- Centrifugation: The samples which remained stable were then centrifuged at 3500rpm for half an hour, the samples which showed no segregation between phases or creaming were then tested in the final step.
- 3- Freeze-thaw cycle: The samples which passed the centrifugation step were then frozen at -21°C then placed at room temperature of 25°C for 48 hours at each temperature, this was repeated three times.

The samples which passed all three stages were considered to pass the accelerated stability study (Shafiq *et al.*, 2007).

4.1.1.2 Droplet size and PDI measurement:

Zetasizer Nano ZS (Malvern Instruments Ltd, UK) was used to find the size and PDI of NE formulations and the measurements were carried out in triplicate to find the mean value and sd.

4.1.1.3 Zeta potential measurement:

Zetasizer Nano ZS (Malvern Instruments Ltd, UK) was used to find the ZP to find the droplet's electrostatic charge, and this was repeated three times to find the mean value and sd.

4.1.1.4 Stability studies:

All formulations were placed at two temperatures of 4°C and 25°C for three months to study their stability, a sample was taken each month and repeated three times to measure the size and PDI and find the mean value and sd.

4.1.1.5 pH determination:

pH was found using pH meter at 25°C; this was carried out in triplicate to find the mean pH value and the sd.

4.1.1.6 Determination of viscosity:

The viscosity was measured using Bohlin cone and plate rheometer at 25°C and shear ramp between 0.1 and 100 s⁻¹. The mean value and sd of three of these measurements were found.

4.1.2 Chloroxylenol and mechanisms of action

Chloroxylenol is a disinfectant and antiseptic, first used in the 1920s. It is also known as para-chloro-meta-xyleneol (PCMX) (see figure 4.1) and has a molecular weight of 156.609 g/mol and a pKa of 9.7.

Its main use is in skin disinfection, disinfection of surgical instruments and wounds and as a household cleaning product. PCMX is mainly active against gram-positive bacteria and functions by disrupting the cell wall and suspending the functionality of enzymes (Fraise *et al.*, 2013).

Chloroxylenol is relatively cheap and accessible; it is available as a liquid and, the most common brand name for this antiseptic is Dettol®.

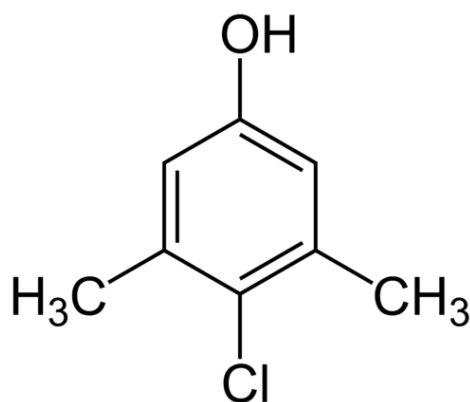


Figure 4.1 Chemical structure of PCMX

4.1.3 Analysis and characterisation of PCMX nanoemulsions

4.1.3.1 HPLC - method validation

In this study, the guidelines adopted in the validation process were those, according to ICH (International Committee on Harmonization, 1996). The analytical parameters used are linearity, sensitivity, precision, accuracy, and stability outlined in section 3.1.6.1.

4.1.4 Physicochemical characterisation of nanoemulsion formulations

The following tests were fully described in section 3.1.3 in Chapter 3.

4.1.5 Determination of PCMX in skin quantitatively and qualitatively

4.1.5.1 *In vitro skin diffusion study*

The in-vitro diffusion studies for PCMX NE formulations were performed using Franz cells to find the optimum formulation for skin retention, as outlined in section 3.1.7.1.

4.1.5.2 *Quantitatively by using an adhesive tape stripping method*

To quantitatively determine the PCMX within the skin, an adhesive tape stripping method was used, as described in section 3.1.7.2

4.1.5.3 *Qualitatively by using CT Scan*

Microtomography was used as described in section 3.1.7.3

4.2 Aim and Objectives

The aim of this chapter was to develop appropriate pharmaceutical formulations designed for the delivery of PCMX to target sites, i.e. hair follicle in the skin in addition to characterising the formulations.

- To develop and characterise an optimum PCMX NE using a high-shear homogeniser followed by ultrasonication and to determine the relative stability of PCMX NEs
- To study the effect of processing parameters such as the sonication time during HSH on NE formulation on the formulation
- To determine the amount of PCMX in the skin using an in vitro Franz cell method following topical application quantitatively using tape stripping and qualitatively using CT.
- To compare the penetration of PCMX NE in human skin and porcine skin.

4.3 Results and Discussion

4.3.1 Formulation study of PCMX nanoemulsion

4.3.1.1 Development of PCMX nanoemulsion

As nanoemulsions stability is affected by many parameters, including the type and amount of surfactant, it was necessary to design a system to investigate the relative stability of emulsion formulations (see section 3.3.1.2).

A PCMX NE was prepared by using an HSH method followed by ultrasound as described in section 3.3.3

4.3.1.2 Solubility of PCMX in eucalyptol

The solubility of PCMX in eucalyptol, water and PBS with 1% SLS was determined by adding an excess of PCMX to the solutions which were mixed using a vortex mixer at 1500 rpm. Then these were maintained in an isothermal shaker at $25 \pm 1^\circ\text{C}$ for 72 h to equilibrate. Following centrifugation at 3000 rpm for 15 min, the supernatant was removed, filtered using a $0.45 \mu\text{m}$ filter and analysed by HPLC, after dilution by methanol (Shafiq *et al.*, 2007). The solubility of PCMX is shown in Table 4.1.

Table 4.1 The solubility of PCMX in eucalyptol, water, and PBS

	Solubility of PCMX (mg/ml)
PCMX in eucalyptol only	510.19
PCMX in BPS+1% of SLS	320.04
PCMX in water	0.53

4.3.1.3 Determination of minimal surfactant concentration

If it is assumed that T80 and S80 form a thin film around each droplet in a monolayer, so according to geometric calculations, it possible to estimate sufficient amounts of these surfactants to stabilise any emulsion.

For example, for 2.5g of eucalyptol oil (density is 0.912 g/ml)(Silva *et al.*, 2011).

Volume = mass / density

$$= 2.5 \text{ g} / 0.912 \text{ g/ml}$$

$$= 2.7412 \text{ ml (cm}^3\text{)}$$

For a droplet diameter of 30 nm (section 4.3.1), thus:

Droplet diameter=30 nm= 3×10^{-6} cm, and if assumed that the droplet is spherical, so

$$\text{Volume of droplet} = \frac{4}{3} \pi r^3 = \frac{\pi d^3}{6} = 1.439 \times 10^{-17} \text{ cm}^3$$

where r: radius

d: diameter

Total number of drops in 2.5 g = volume of eucalyptus oil/volume of the droplet

$$= 2.7412 / 1.882 \times 10^{-17}$$

$$= 1.457 \times 10^{17}$$

Surface area of each droplet = πd^2

$$= 2.828 \times 10^{-11} \text{ cm}^2$$

The total surface area of droplets = Surface area of each particle x Total number of drops

$$= 3.422 \times 10^{-11} \times 1.457 \times 10^{17}$$

$$= 5.482456 \times 10^6 \text{ cm}^2$$

The molecular weight of T80 = 604.41 g/mol

Surface area = $133 \text{ \AA} = 1.33 \times 10^{-14} \text{ cm}^2$ (PubChem, n.d.-b)

Molecular weight of S80 = 428.31 g/mol

Surface area = $96.2 \text{ \AA} = 9.62 \times 10^{-15} \text{ cm}^2$ (Pub chem, no date a)

Number of required molecules of T80 = Total surface area of droplets/surface area of T80

$$= 5.482456 \times 10^6 / 1.33 \times 10^{-14}$$

$$= 4.122 \times 10^{20}$$

Number of required molecules of S80 = Total surface area of droplets/surface area of S80

$$= 5.482456 \times 10^6 / 9.62 \times 10^{-15}$$

$$= 5.699 \times 10^{20}$$

Amount of required surfactant (g) = $\frac{\text{(Number of required molecules} \times \text{molecular weight)}}{\text{Avogadro's number}}$

$$\text{Amount of required tween 80 (g)} = \frac{(3.7474 \times 10^{20} \times 604.41)}{6.0221415 \times 10^{23}} = 0.41371 \text{ g}$$

$$\text{Amount of required span 80 (g)} = \frac{(5.18093 \times 10^{20} \times 428.31)}{6.0221415 \times 10^{23}} = 0.32786 \text{ g}$$

So according to the formula and using a ratio of surfactant mixture (T80: S80) (3:1), 0.311 g of T80 and 0.082 g of S80 would be the minimum needed to emulsify 2.5 g of eucalyptol oil in water.

4.3.1.4 Physicochemical characterisation of the nanoemulsion formulations

A range of formulations was prepared as detailed in Table 4.2 and zeta potential, pH and viscosity were measured for NE formulations prepared using HSH followed by sonication method. from Table 4.2, the

ZP value ranged between -14 ± 5.9 mV to -28.5 ± 3.5 mV. Various studies (Yang and Benita, 2000; Zhao *et al.*, 2010; Laouini, Fessi and Charcosset, 2012) have confirmed that higher values of ZP cause more repulsion for charged droplets than lower values, therefore stopping coalescence between the droplets.

The negative charge in the ZP values of PCMX shows the chlorinated polyaromatic phenol groups.

The NE formulations in this study are all O/W; therefore, are of low viscosity as the continuous phase is formed by water. The results shown in Table 4.3 show the viscosity ranges between 19.08 ± 1.25 cP to 23.74 ± 1.63 cP. The high viscosity in the continuous phase in these results leads to a decrease in the droplet motion, which subsequently leads to increased stability (Jafari *et al.*, 2008).

As mentioned in section 3.3.1.5, an alteration in pH of skin contributes to the pathogenesis of skin diseases such as irritant contact dermatitis. Therefore it is reported that the pH of formulations should be around 5.5 to minimise irritation (Schmid-Wendtner and Korting, 2006). In this study, the pH results range between 5.34 ± 0.3 to 6.92 ± 0.3 ; these results are close to the recommended value of 5.5 without exceeding neutral pH.

Table 4.2 Physicochemical characterisation of PCMX NE formulations (n=3; mean±sd)

Surfactant		Oil	pH ±SD	ZP (mV) ±SD	Viscosity (cP) ±SD
Type	Amount (%w/w)	Amount (%w/w)			
T80/S80	0.34	5	6.87 ±0.2	-28.5 ±3.5	19.58 ± 1.25
T80/S80	2	5	6.69 ±0.3	-16.4±2.5	21.36 ± 0.63
T80/S80	5	5	5.63 ±0.1	-27.9±4.5	22.81 ± 0.89
T80/S80	10	5	6.92 ±0.3	-24.7±3.8	23.65 ± 1.09
T60/S60	2	5	6.52 ±0.3	-28.1±1.8	20.54 ± 1.23
T40/S40	2	5	6.52 ±0.2	-22.8±4.7	22.36 ± 1.29
T20/S20	2	5	5.88 ±0.1	-22.8±3.9	21.02 ± 0.80
T80/S80	2	2.5	5.74 ±0.3	-14±5.9	19.08 ± 1.25
T80/S80	2	7.5	5.36 ±0.1	-25.3±1.9	23.85 ±0.87
T80/S80	2	10	5.34 ±0.3	-25.7±6.7	23.47 ± 1.63

4.3.1.5 Effect of concentration of oil on PCMX nanoemulsions

Formulations were prepared with different concentrations of oil (2.5%, 5%, 7.5% and 10% (%w/w)). All other variables were fixed to examine the effect of varying concentrations of oil on particle size, i.e. 2% mixture of surfactant T80: S80 (3:1), 0.24% PCMX and deionised water. The mixer speed was set at 7000 rpm for 10 min and then 8 mins sonication.

Table 4.3 Size and PDI of PCMX NEs prepared with different oil concentrations

amount of oil (% w/w)	Size \pm SD	PDI \pm SD
2.5	39.89 \pm 0.17	0.43 \pm 0.01
5	62.58 \pm 1.31	0.36 \pm 0.03
7.5	89.17 \pm 0.55	0.28 \pm 0.01
10	99.02 \pm 0.56	0.28 \pm 0.00

From Table 4.3, it can be inferred that as oil concentration increased, the size of the droplet increased, and the PDI decreased. The increase in size can be explained by way of the measurement method of zetasizer. Since the zetasizer determines the average volumes of the droplets, it is possible that there are micelles of surfactant with a very small range (20-30 nm) that are causing a reduction in the average sample size. That is confirmed by the high value of PDI with a low value of MDS as shown in the sample with 2.5% oil, which means there is a wide range in the droplet sizes. As the concentration of oil is increased, more surfactant is needed to cover each droplet, and fewer micelles are formed, which reduces the PDI, which is shown in the sample with 10% oil. However, in order to choose the best concentration the stability of formulations must also be considered (section 3.3.4)

4.3.1.6 Effect of type and concentration of surfactant on PCMX nanoemulsions

As surfactants alter the interface between the oil phase and the aqueous phase, therefore controlling the adsorption and coalescence rate, they are essential components in the formation of NEs (Qian and McClements, 2011). The surfactant molecules play multiple roles in the NE formation using the HSH

technique as they adsorb onto the oil droplets that are newly formed, subsequently preventing coalescence and aggregation of the droplets and lowering the surface tension (Guzey and McClements, 2006).

In this study, the effect of the type and concentration of surfactant on PCMX NEs was investigated. To study the effect of type of surfactant on PCMX NEs, formulations using a blend of emulsifiers were prepared as detailed in Table 4.4. As mentioned in Chapter 3 section 3.3.1.2, the HLB value of eucalyptol was calculated to be 12.5, and a range of ratios of Tween and Span were used to match that HLB (Table 4.4).

Table 4.4 Ratio of blend emulsifier at HLB = 12.5

	T20: S20	T40: S40	T60: S60	T80: S80
HLB =12.5	50%: 50%	66.5% : 33.5%	77.5% : 22.5%	77.5% : 22.5%
Ratio	1: 1	2: 1	3: 1	3: 1

All other variables were kept constant: 5% w/w oil (eucalyptol), mixture of surfactant 2% w/w, 0.24% w/w PCMX and 92.76% w/w deionized water. A blend of T80/S80 produced the smallest droplet size (62.58 nm) in relation to the other surfactant types, whereas T40/S40 resulted in the largest size (142.94 nm) (Figure 4.2). This could be due to the surfactant nature and solubility in water, as T80/S80 has the highest ratio of hydrophilic to hydrophobic characteristics at 3:1, whereas, T40/S40 has a lower ratio which could facilitate faster motion of surfactant (T80/S80 blend) in the aqueous phase which could allow the surfactant to adsorb onto the newly formed oil droplets preventing aggregation. This fits with the smaller droplet size in T80/S80 blend in comparison with other surfactants and has also been observed in other studies (Jafari *et al.*, 2008; Ziani *et al.*, 2011).

The T80/S80 blend was therefore chosen for future studies and used to find the optimum surfactant amount.

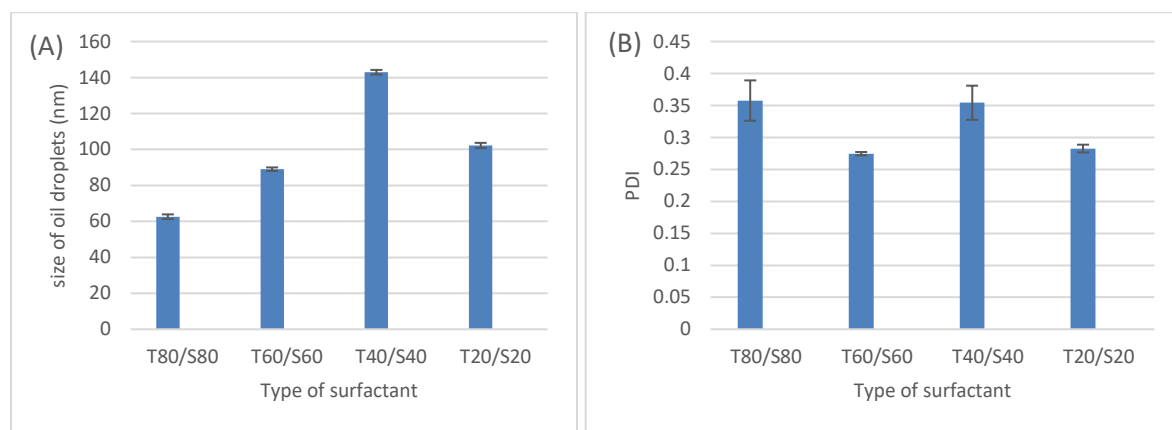


Figure 4.2 Effect of type of surfactant on mean droplet size (A) and PDI (B)

To study the effect of the amount of surfactant on particle size, a range of surfactant concentrations (0.4 %, 2%, 5% and 10% w/w) was prepared. The size of droplets decreased as the amount of surfactant is increased between 0.4% to 5%, then the droplet size slightly increased until 10% (Table 4.5) which is likely to be due to the increase in amount of surfactant leading to formation of micelles and this can be confirmed through the high value of PDI (0.53 ± 0.01) at this percentage of surfactant. Although the 5% amount of surfactant resulted in the smallest droplet size, it is important to note that using a minimal amount of surfactant is preferable for cost and reduction of any potential toxicity or irritant risks of surfactant. Another essential factor to consider is the optimum surfactant amount to enable permeation into the skin which is shown in section 4.3.5.1.1

Table 4.5 Size and PDI of NEs prepared with different surfactant concentrations

Amount of surfactant w/w%	Size (nm) \pm SD	PDI \pm SD
0.4	98.97 \pm 1.96	0.32 \pm 0.02
2	62.58 \pm 1.31	0.36 \pm 0.03
5	30.72 \pm 0.35	0.38 \pm 0.01
10	49.64 \pm 0.26	0.53 \pm 0.01

4.3.2 Optimisation of homogenization and sonication parameters

To study the impact of homogenization time, the speed of mixer and impact of sonication a prepared nanoemulsion containing 5% w/w eucalyptol as oil, 2% w/w of mixture surfactant 3:1 T80: S80, 0.24% w/w PCMX and 92.76% w/w water was used.

4.3.2.1 Impact of homogenization time

To check the impact of homogenization time on formulation characteristics, MDS and PDI were used as indicators of formulation success. Both are considered as important parameters in NE formulation due to their effect on delivery through skin, appearance and stability of the formulation. Results, summarized in Table 4.6, show a significant decrease in both MDS and PDI from 5 min to 10 min; this was followed a by a plateau until 15 min and then an increase from 15 to 20 min. The increase can be explained by the additional energy which caused droplets to collapse. A study by Shahavi et al. also shows similar results when preparing a NE using clove oil as during the sonication time increase from 1 to 10 min, a droplet size decreased from 160 nm to 40 nm. This was then followed by a stage when there was no further reduction in the droplet size until after 15 min (Shahavi *et al.*, 2015). Therefore, the chosen homogenization time in this study was 10 min.

Table 4.6 Effect of homogenization time on mean droplet size and PDI

Homogenization duration (min)	tween 80/span 80			
	Size-Ave (nm)	standard error	PDI	standard error
5	26.96	0.39	0.34	0.01
10	21.47	0.09	0.28	0.01
15	22.57	0.18	0.27	0.01
20	43.73	1.01	0.43	0.01

4.3.2.2 Impact of Mixing Speed

Mixing speeds were varied between 3000 – 10000 RPM and results are shown in Figure 4.3. A speed of 7000 RPM was chosen since it resulted in the smallest droplet size while maintaining acceptable PDI results of less than 0.5.

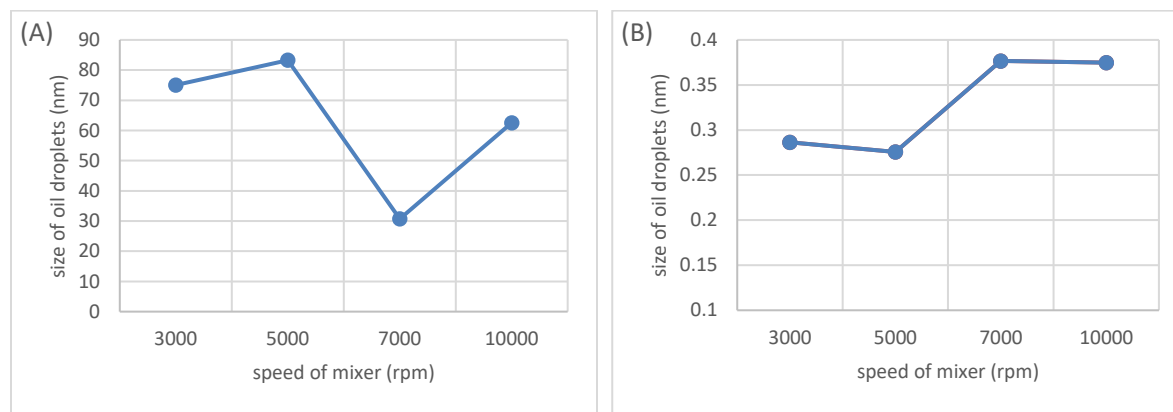


Figure 4.3 Effect of speed of mixer on mean droplet size (A) and PDI (B) for PCMX NE

4.3.2.3 Impact of sonication

Sonication has a significant effect on MDS and PDI, which can be seen in Figure 4.4. The samples were sonicated using a sonication probe for 8 minutes after homogenisation with the mixer. A sonication stage was introduced to minimise droplet size and reduce the PDI, which should ultimately lead to improved stability as similar droplet sizes eliminate the collapsing of larger droplets to smaller droplets. Therefore, the adopted method for the preparation of NE was sonication after homogenisation.

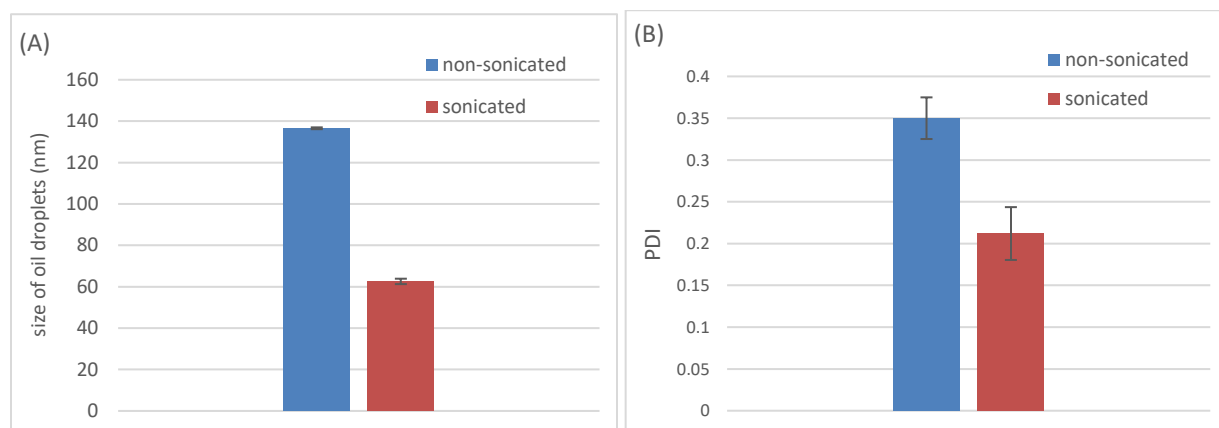


Figure 4.4 Effect of sonication on mean droplet size (A) and PDI (B) for PCMX NE

4.3.3 Stability of PCMX nanoemulsion

Two stability studies were performed, one long-term study and an accelerated stability study. The long-term stability study was performed at two temperatures for 3 months; the two temperatures were 25°C and 4°C.

4.3.3.1 Accelerated stability studies

To consider the NE formula stable, it should pass all three stages in the accelerated stability study; these are a heat-cooling cycle, centrifugation and a freeze-thaw cycle (Hung *et al.*, 2011). The heat-cooling cycle stage was performed to accelerate the motion and increase collisions between the oil droplets as higher temperatures lead to higher kinetic energy in the Brownian motion of oil droplets. All prepared formulations were stable under these conditions (Table 4.7) as no creaming or sedimentation was observed, and all formulations were progressed onto the centrifugation stage of the study. Again, there was no evidence of phase separation (Figure 4.5). Gravitational forces may be the cause of emulsion instability during centrifugation as the centrifugation phase has been found to accelerate creaming and sedimentation rate s(Hung *et al.*, 2011). In this study, since the NE is O/W, creaming is expected to occur rather than sedimentation as the density of the oil phase is lower than the density of water.

Formulation C3/P061, with a high percentage of surfactant (10%w/w), separated into two layers on centrifugation, and formulations C2/P064 and C3/P064 with high percentages of oil (7.5% and 10% respectively) resulted in a small amount of creaming. When separation occurred, the reason could be due to the amount of surfactant used being too high, and when creaming occurred, this could be due to the amount of surfactant being insufficient for covering the oil droplets.

In the final stage of the freeze-thaw cycle, during freezing, segregation of the oil droplets occurs due to the formation of a crystalline ice particle which leads to breaking of the surfactant film. During thawing, the droplets melt and can collide with other droplets. Formulations C2/P061, C3/061, C2/P063, C1/P064 and C3/P064 did not pass this stage as creaming or separation occurred (Table 4.7 and Figure 4.6), and these formulations were considered as potentially unstable.



Figure 4.5 NE formulations after heat-cooling cycle - accelerated stability study



Figure 4.6 NE formulations after the freeze-thaw cycle- accelerated stability study

Table 4.7 Effect of type and concentration of surfactant and oil in accelerated stability study for NE

Formula code	parameter				Accelerated stability studies steps		
	Surfactant		Oil	Mixer speed (RPM)	Heating cooling cycle	Centrifugation	Freeze-thaw cycle
	Type	Amount (% w/w)	Amount (% w/w)				
C1/P061	T80/S80	0.4	5	7000	stable	stable	stable
C2/P061	T80/S80	5	5	7000	stable	stable	creaming
C3/P061	T80/S80	10	5	7000	stable	two layers	two layers
C1/P062	T60/S60	2	5	7000	stable	stable	stable
C2/P062	T40/S40	2	5	7000	stable	stable	stable
C3/P062	T20/S20	2	5	7000	stable	stable	stable
C1/P063	3000 rpm	2	5	3000	stable	stable	stable
C2/P063	5000 rpm	2	5	5000	stable	stable	creaming
C3/P063	10000 rpm	2	5	10000	stable	stable	stable
C1/P064	T80/S80	2	2.5	7000	stable	stable	creaming
C2/P064	T80/S80	2	7.5	7000	stable	Little creaming	stable
C3/P064	T80/S80	2	10	7000	stable	Little creaming	creaming
C1/P060	T80/S80	2	5	7000	stable	stable	stable

4.3.3.2 Long-term stability

The long-term stability of NE was studied for 3 months at two different temperatures for formulations of NE with varying types and amounts of surfactant. Samples were observed for a separation every month and size, and PDI determined.

There was no change in droplet size or PDI on storage for 3 months (Figures 4.7 and 4.8). The reason behind these results can be due to one of two reasons at 25°C; either the NE was highly stable or the 25°C was not high enough to increase the movement of the droplets, therefore, no collapsing occurred.

As for the 4°C temperature, the reason could be that the low temperature caused a reduction in movement of the droplets, therefore, reducing the risk of collapsing between droplets and subsequently maintaining stability.

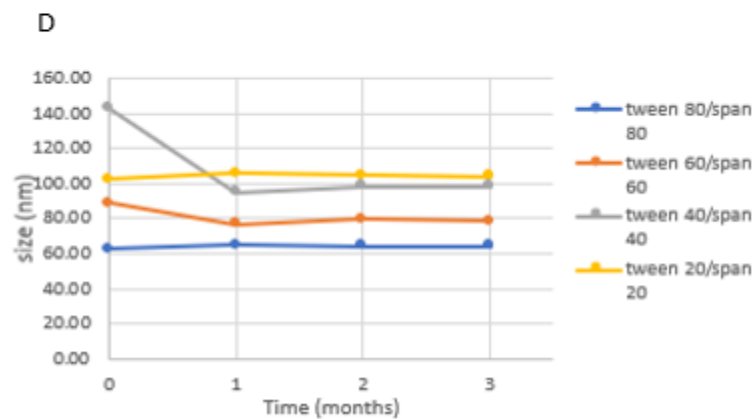
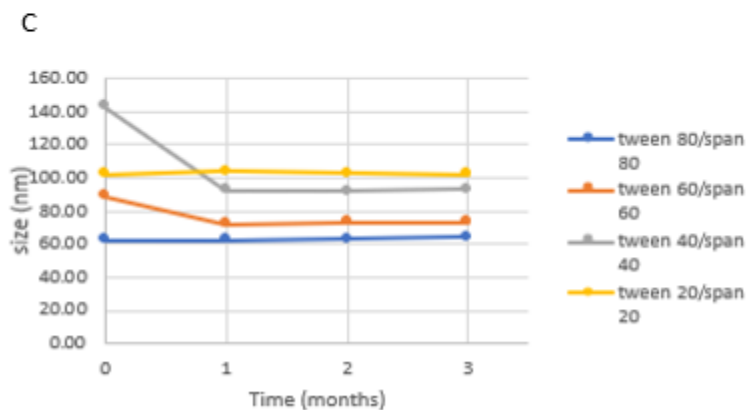
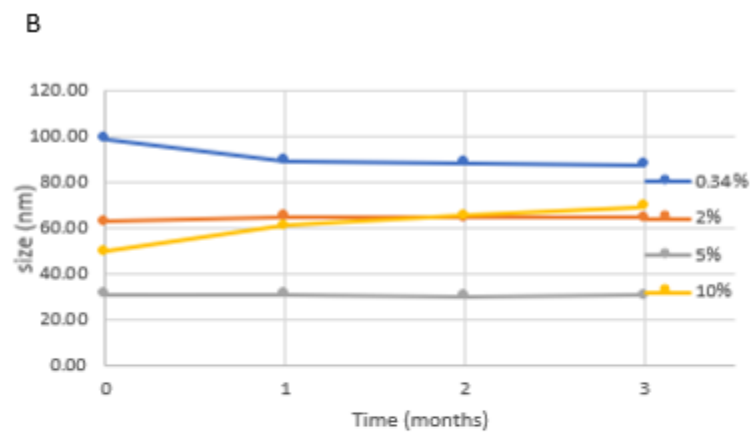
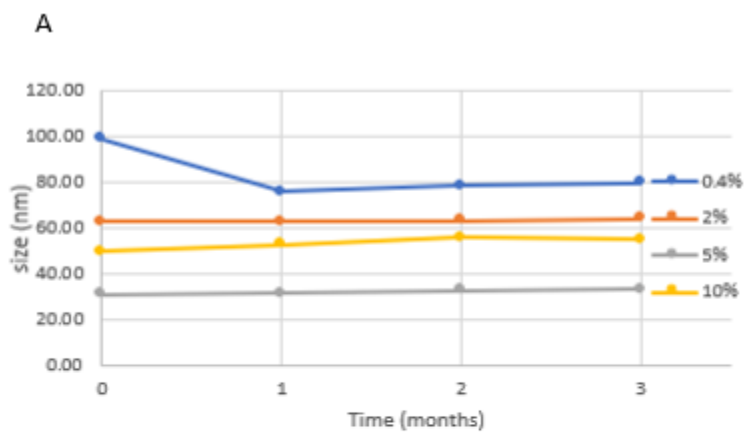


Figure 4.7 The effect of surfactant on size of PCMX NE during storage at 4 and 25°C for 3 months (A)effect of surfactant concentration at 4°C (B) effect of surfactant concentration at 25°C (C) effect of type of surfactant at 4°C(D) effect of type of surfactant at 25°C

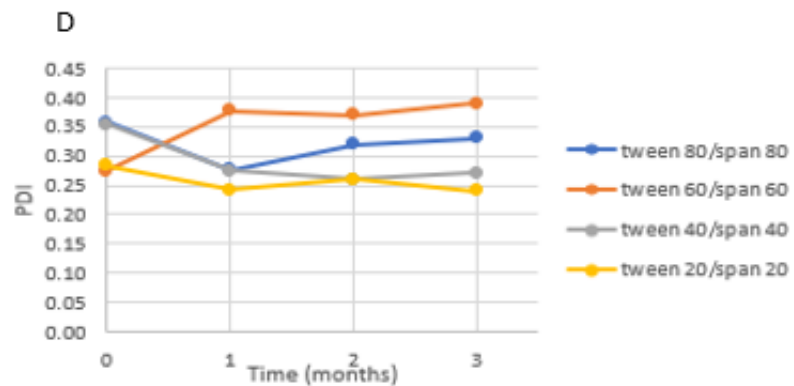
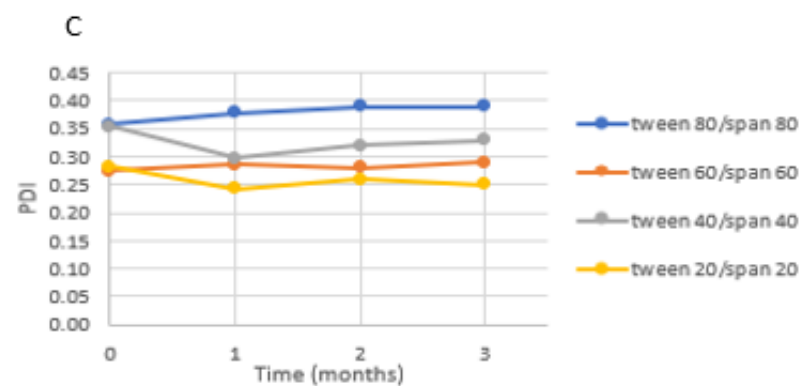
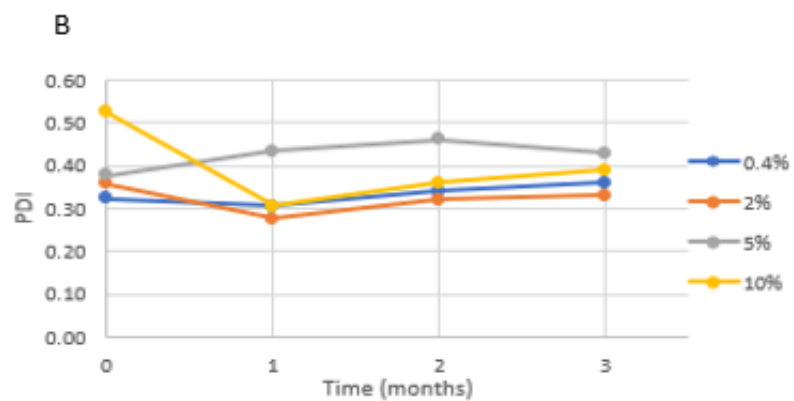
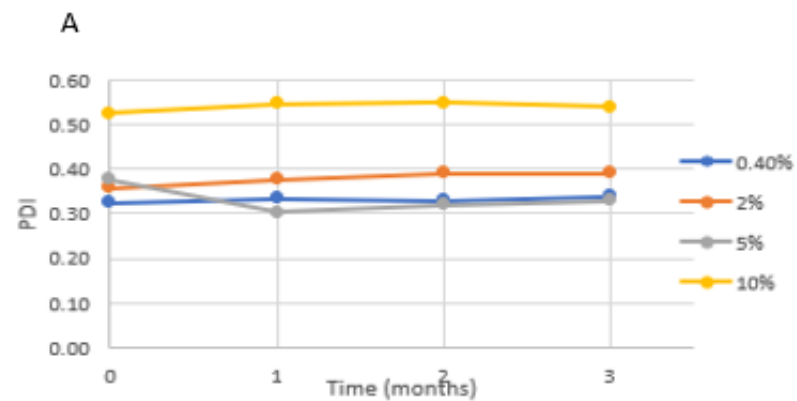


Figure 4.8 The effect of surfactant on PDI of PCMX NE during storage at 4 and 25°C for 3 months (A) effect of surfactant concentration at 4°C (B) effect of surfactant concentration at 25°C (C) effect of type of surfactant at 4°C (D) effect of type of surfactant at 25°C

4.3.4 Development and validation method of HPLC for the measurement of PCMX

4.3.4.1 Development method

A 60: 40 ratio of ACN: water was found to be the optimum ratio. The C18 column was the first to be tested, followed by a pentafluorophenyl (PFP) column, the peaks of the two columns were compared and the C18 column was found to produce peaks with higher intensity than the PFP column as well as having better resolution. There is a highly hydrophobic stationary phase for C18, which shows great methylene selectivity. For the determination of PCMX's maximum wavelength (λ max) UV-visible spectrophotometry was the method used, λ max was found to be 288 nm, this is shown in Figure 4.9.

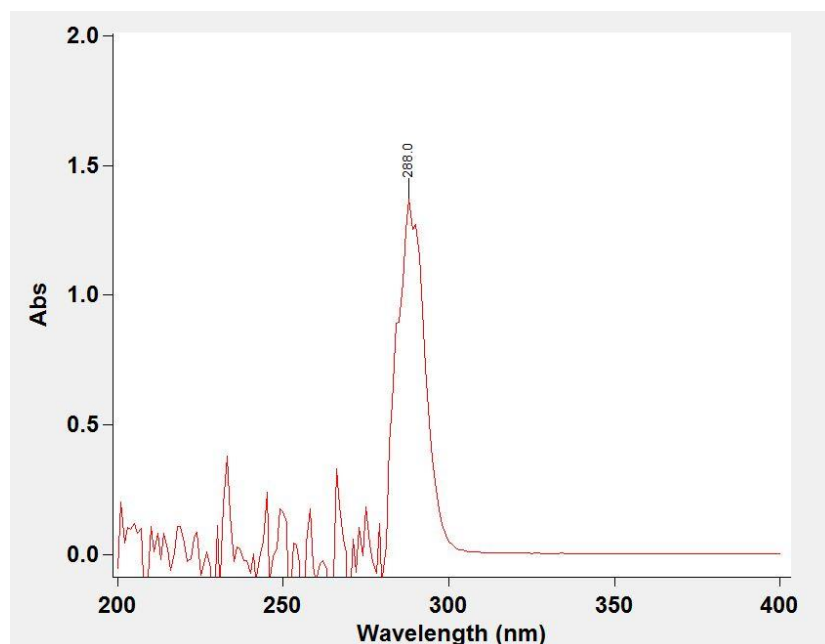


Figure 4.9 UV spectrum for PCMX, showing the λ max at 288nm

4.3.4.2 Validation method

It is a requirement that each method developed should be validated, in this study, the validation method performed was in accordance to the ICH guidelines 1996.

4.3.4.2.1 Linearity

Six various concentrations of PCMX were used to find linearity, all of which were within the expected range in addition to including the limit of quantification, the six concentrations used were (2, 5, 10, 20, 50, 100 µg/ml). Measurements were performed and replicated five times, after which a plot was made of the ratio of peak area with PCMX concentration. The results of one of the five repetitions of the linearity test (group A, B, C, D and E) is shown in Figure 4.10, (all remaining graphs can be seen in Appendix A). The correlation coefficient (R^2) average between the five groups was calculated and found to indicate a high linearity relationship through visual inspection as well as the use of statistical methods (R^2) was found to be 0.9996.

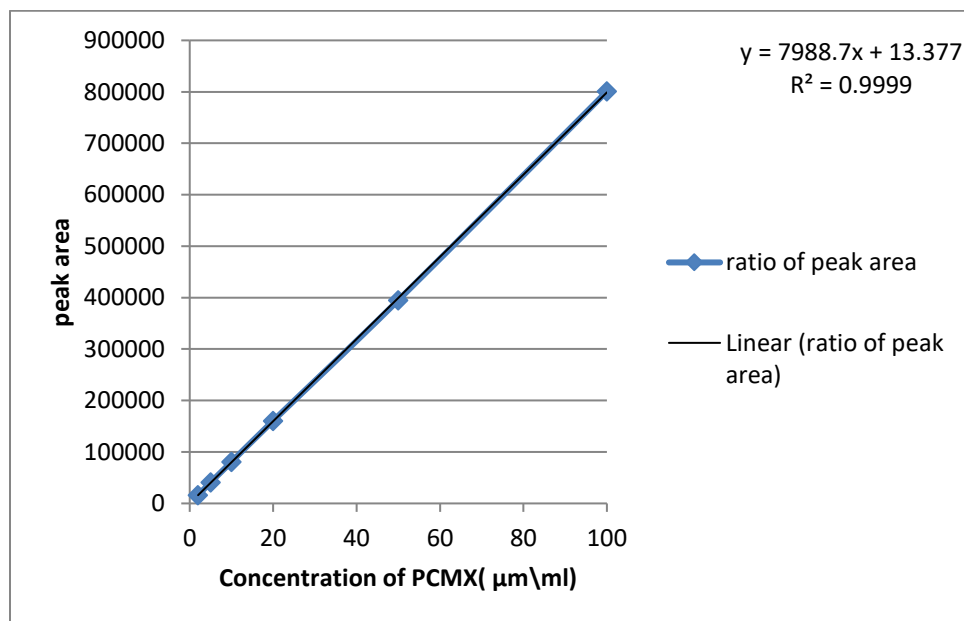


Figure 4.10 Linearity curve of group A (one graph of the five graphs of linearity) For PCMX

4.3.4.2.2 Sensitivity

There are two different factors that can be used for expressing sensitivity, the first of these is the limit of detection (LOD) whereas the second is the limit of quantification (LOQ), to calculate these two factors equations 3.3 and 3.4 were used.

The mean of the slopes in the linearity curves as well as the standard deviation of the intercept in the five groups are shown in Table 4.8

Table 4.8 Standard deviation of intercept and slopes mean of the five group of linearity for PCMX

	Intercept	Slope
Group A	2984.75	7448.95
Group B	3151.16	7446.96
Group C	3136.87	7509.37
Group D	13.37	7988.79
Group E	190.84	7984.64
Standard Deviation	1639.51	
Mean		7675.68

The limit of detection was therefore found to be 0.71 $\mu\text{g/ml}$ whereas the limit of quantification was calculated to be 2.14 $\mu\text{g/ml}$.

4.3.4.2.3 Selectivity

From Figure 4.11 it is concluded that this method proves good selectivity for PCMX as well as having good separation as it was eluted at 6.737 min.

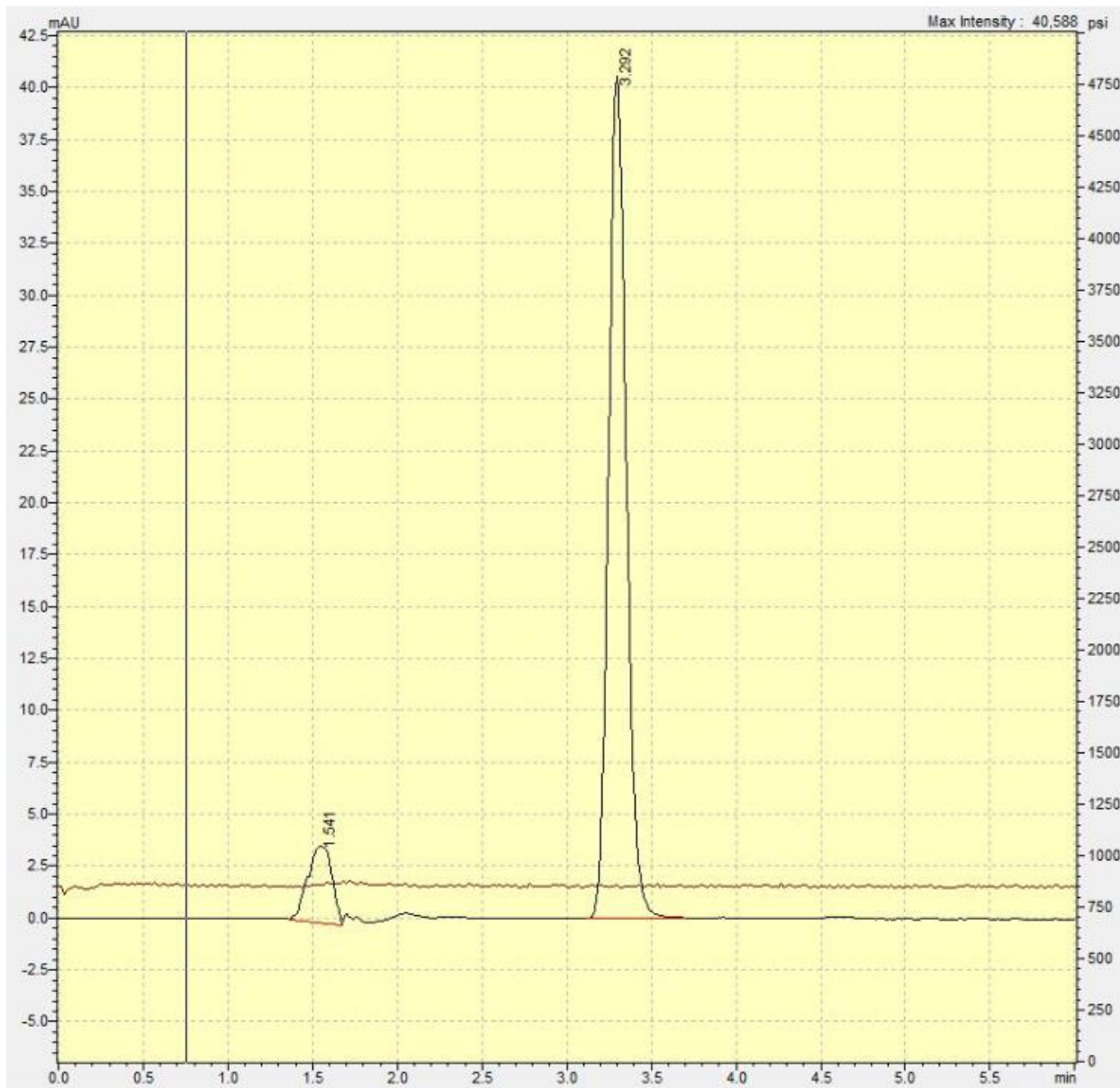


Figure 4.11 Selectivity test shows the resolution of the method - Peak of PCMX at 3.29 min

4.3.4.2.4 Accuracy

To establish the accuracy, three various PCMX concentrations were prepped, these were; 10, 40 and 80 $\mu\text{g/ml}$ taken from the concentration used in the linearity test. Five repetitions of this test were performed before determining the mean result. This was then followed by calculating the observed

concentration through a plot of the peak area on a calibration curve and accuracy was calculated with Equation 3.6.

The range of accuracy was found to be between 97.35% and 98.48% as shown in table 4.9 which is an acceptable accuracy range in accordance to the ICH guidelines (1996).

Table 4.9 Range of accuracy for HPLC method for PCMX

Actual concentration ($\mu\text{g/ml}$)	Observed concentration ($\mu\text{g/ml}$)	% Accuracy
10	9.73	97.35
40	39.39	98.48
80	78.57	98.22

4.3.4.2.5 Precision

As for the precision test, PCMX concentrations of 4, 40 and 80 $\mu\text{g/ml}$ were used and the test was split into two parts; the first of these is the intra-day precision test which is performed five times within one day and the RSD is then calculated between every two injections. The second part of the precision test is the inter-day precision, in which the process performed for the intra-day test is repeated over five days and the RSD is then calculated between the days. (see appendix B to show all the dates the precision test was performed on). For a method to be considered of satisfactory precision, the PSD must be lower than or equal to 2%. The range for the RSD in the intra-day tests was found to be between 0.02– 0.19%, as for the RSD range for the inter-day precision test, this was between 0.29 -0.58% as shown in table 4.10. Since all values in both the tests were between 2%, this is a confirmation that the precision of the method in accordance to the ICH guidelines (1996).

Table 4.10 Precision test - Range of RSD for both intra-day and inter-day precision

Nominal concentration ($\mu\text{g/ml}$)	% Relative Standard Deviation (RSD)	
	Intra-day	Inter-day
low =4	0.19	0.29
medium = 40	0.09	0.41
high = 80	0.02	0.58

4.3.5 *In vitro* skin permeation study

As previously mentioned, the amount of drug retained within the skin was determined quantitatively using the tape-stripping method and qualitatively using a micro CT scan.

4.3.5.1 **Quantitative determination by using an adhesive tape stripping method**

4.3.5.1.1 Effect of amount of surfactant

To quantify the amount of drug retained within the skin following application of PCMX nanoformulations, a tape-stripping method was used. The superficial layer of SC was removed using adhesive tape; the drug was quantified using HPLC as described in section 3.3.6.1 (Lademann *et al.*, 2009)

Formulations, as detailed in Table 4.11, were used, and Dettol[®] was used as the control (Figure 4.12). Tape 1 contains an excess formulation that did not penetrate the skin. As for Tape 2-5 and Tape 6-10 and Tape 11-15 were performed to ensure that no excess formulation remained on the surface of the skin. Whereas the super-glue step was performed to study the amount of drug in the hair follicle, as for the full skin (homo) was performed to study the amount of drug penetrated deeper into the skin. Formulation C1-P061, which contained the lowest amount of surfactant, had the highest amount of drug in Homo level (full thickness skin), even exceeding the amount of PCMX in the control (Dettol[®]). This indicates that even small amounts of surfactant helped the oil droplet of eucalyptol containing the drug

to penetrate further into the skin. This could be because eucalyptol modifies the barrier properties of SC, therefore facilitating the penetration process (Femenía-Font, 2005). A second reason is that as the formulation is NE, which has a large surface area that enhances the penetration and NE also helps hydrate the skin, therefore, improving the delivery. (Tadros *et al.*, 2004)

For the remaining formulations with higher amounts of surfactant than the C1-P061 formula, the amount of PCMX NE was lower which may be due to the higher amount of surfactant which could possibly reduce the role the eucalyptol plays in improving penetration, another possible reason could be due to the multi-layer of surfactant surrounding the oil droplet which could obstruct the penetration within the skin.

Table 4.11 Parameters of different NE to study the effect of the amount of surfactant

High shear homogeniser - the effect of the amount of surfactant					
Formula code	Oil (w/w%)	surfactant		PCMX (w/w%)	water(w/w%)
		type	Amount (w/w%)		
Dettol®	----	----	----	0.50	99.50
C1-P061	5	T80/S80	0.4	0.24	94.56
C1-P060	5	T80/S80	2.0	0.24	92.76
C2-P061	5	T80/S80	5.0	0.24	89.76
C3/P061	5	T80/S80	10.0	0.24	84.76

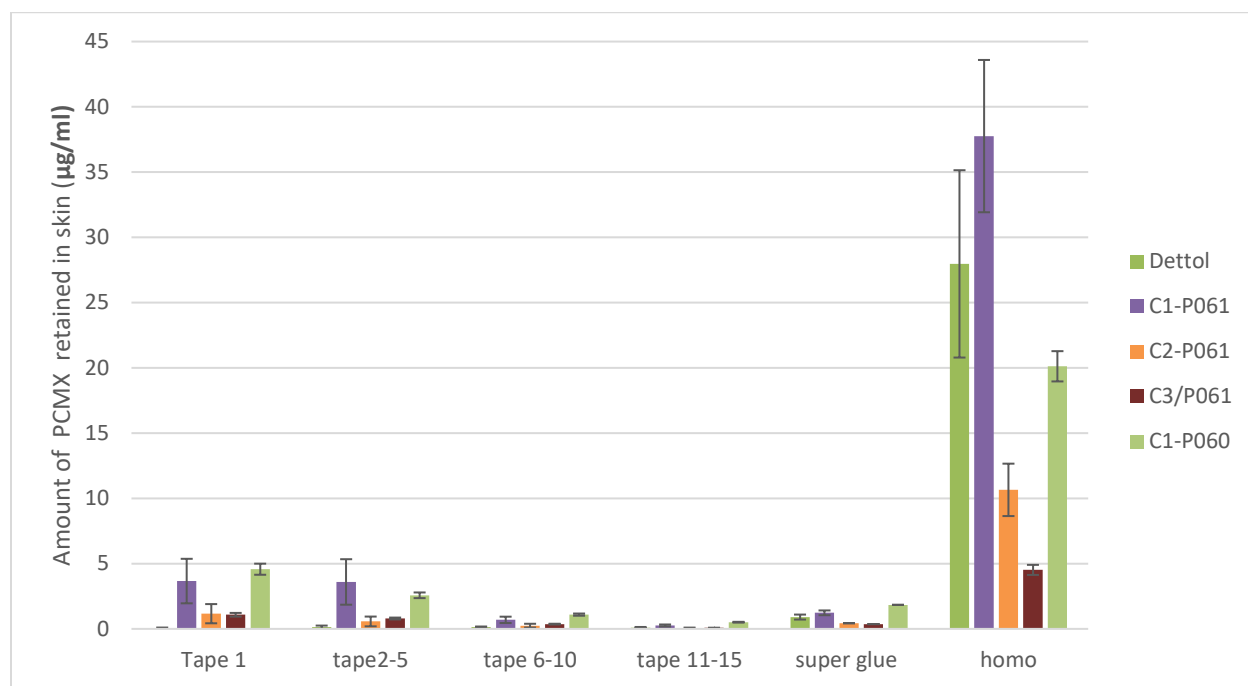


Figure 4.12 Effect of the different amount of surfactant on skin permeation of PCMX NE (mean \pm SD n=3)

4.3.5.1.2 Effect of type of surfactant

To study the type of surfactant, four formulations with varying types of surfactants were prepared, as shown in Table 4.12. Figure 4.13, it shows formulations containing T80/S80 showed the highest amount of drug retainment (permeation uptake through the skin) into the skin on both the hair follicle level and in full skin (homo). This may be due to compatibility between the PCMX and T80/S80, and as mentioned in section 4.3.1.6, the smallest droplet size was in this mixture., This is similar to the findings of Shafat et al., (2013) which states that the formulations with smaller droplet size and low viscosity have higher permeation uptake through the skin.

Table 4.12 Parameters of different NE to study the effect of the type of surfactant

High-pressure homogeniser - the effect of type of surfactant					
Formula code	Oil (w/w%)	Surfactant		PCM X (w/w%)	Water(w/w%)
		Type	Amount(w/w%)		
C1-P060	5	T80/S80	2	0.24	92.76
C1-P062	5	T60/S60	2	0.24	92.76
C2-P062	5	T40/S40	2	0.24	92.76
C3-P062	5	T20/S20	2	0.24	92.76

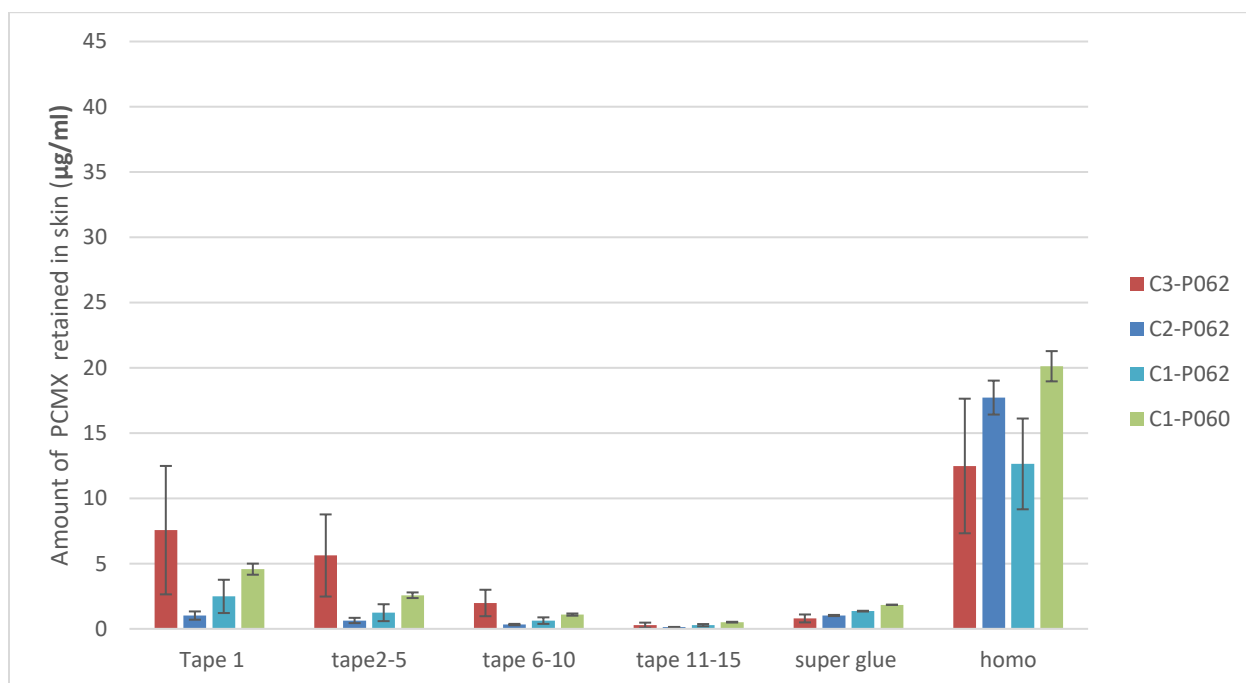


Figure 4.13 Effect of the different type of surfactant on skin permeation (mean \pm SD n=3)

4.3.5.2 Qualitative determination by using Micro CT

Qualitative determination of the distribution of PCM X in the skin was performed using micro CT according to the method detailed in section 3.1.7.3.

3D images in addition to a video were recorded, and the video shows 3D motion for PCM X NE through the skin samples and screenshots were captured in the sagittal plane video with 3-second intervals. The sagittal plane was used as it shows the penetration of PCM X from the top of the sample to the bottom.

Two formulations were studied, C1-P061 and C2-P062 and results are shown in figures 4.15 and 4.16, respectively.

As mentioned in section 3.2.6.2 and seen in Figure 3.28, when the skin sample did not have any formulation and using the false-colouring technique, only one colour appeared, therefore, indicating a similar density throughout the sample. In Figure 4.14 and Figure 4.15, two colours are present in the sample after using false-colouring, this indicates the presence of PCMX within the skin.

Figure 4.14 with the C1-P061 formulation showed a larger area of red than in Figure 4.15 with the C2-P061 formulation meaning a higher amount of PCMX in the C1-P061 sample. Therefore, this sample is thought to have higher levels of penetration through the skin; the same conclusion was found in the quantitative evaluation using the tape-stripping method.

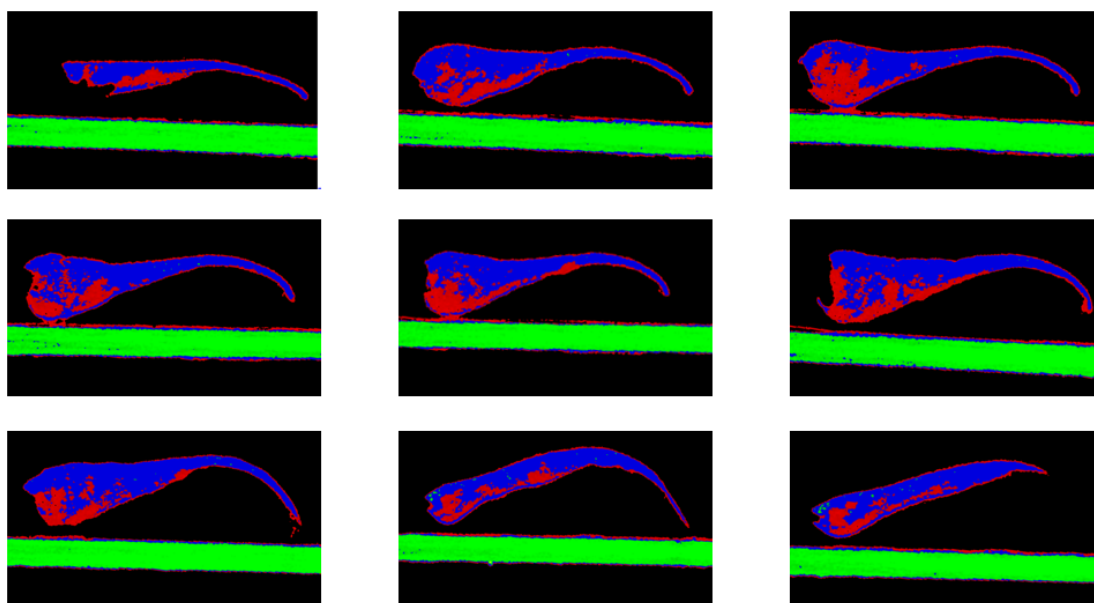


Figure 4.14 screenshots from video every 3 seconds of skin sample with C1-P061 formulation (blue; skin, red; PCMX, green; plate)

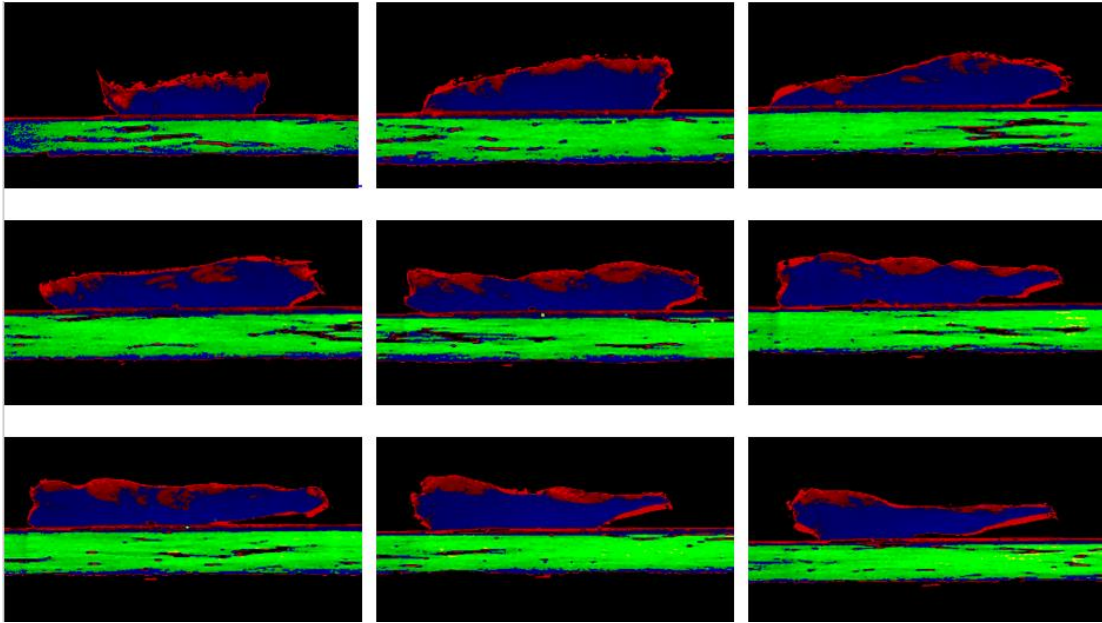


Figure 4.15 screenshots from video every 3 seconds of skin sample with C2-P061 formulation (blue; skin, red; PCMX, green; plate)

4.3.5.3 Comparison of penetration of PCMX nanoemulsion in human and porcine skin

As mentioned in section 2.1.5.1, porcine skin is considered a suitable model for human skin but selected studies were repeated using human skin (Table 4.13 and Figure 4.16) From Figure 4.16, the high similarity between both skin samples was shown, however, the permeation of the drug in the porcine sample was slightly higher than that in the human sample. This could be due to a slightly higher density of pores in the porcine sample.

Table 4.13 Parameters of NE to study the effect of the type of Skin

Formula code	Oil (w/w%)	Surfactant		PCMX (w/w%)	Water(w/w%)
		Type	Amount (w/w%)		
C1-P061/human skin	5	T80/S80	0.4	0.24	94.56
C1-P061/Pig skin	5	T80/S80	0.4	0.24	94.56

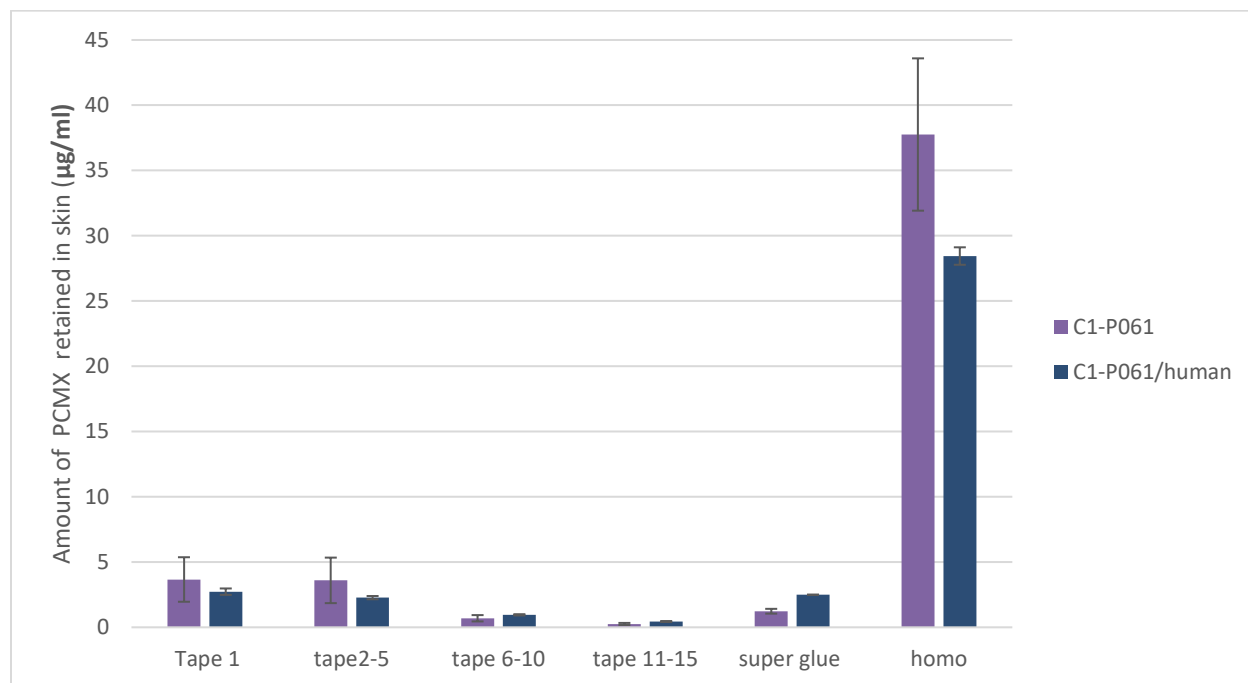


Figure 4.16 Effect of the different type of Skin (human and porcine) on permeation (mean \pm SD n=3)

4.3.5.4 The optimum formulation

Through the studies for finding the effect the amount and type of surfactants have on the penetration of PCMX through the skin, the lowest amount of surfactant was found to have the highest penetration levels. This is similar to the results found when studying the effect of the amount of surfactant on the penetration of triclosan through the skin where the highest penetration was also found with the lowest amount of surfactant. Therefore both results support the suggested hypothesis claiming that the lowest amount of surfactant results in the highest penetration level. For PCMX nanoemulsion, the concentration and combinations of surfactants resulting in highest penetration were 0.4% surfactant and T80/S80; C1/P061 formulation. These results are shown in Figure 4.17, and Table 4.14 shows the variables for the formulations tested.

Table 4.14 Formulations variables for PCMX

All formulations					
Formula code	Oil (w/w%)	surfactant		PCMX (w/w%)	water(w/w%)
		type	amount(w/w%)		
Dettol®	----	----	----	0.24	99.50
C1-P060	5	T80/S80	2.0	0.24	92.76
C1-P062	5	T60/S60	2.0	0.24	92.76
C2-P062	5	T40/S40	2.0	0.24	92.76
C3-P062	5	T20/S20	2.0	0.24	92.76
C2-P061	5	T80/S80	5.0	0.24	89.76
C1-P061	5	T80/S80	0.4	0.24	94.56
C3-P061	5	T80/S80	10.0	0.24	84.76

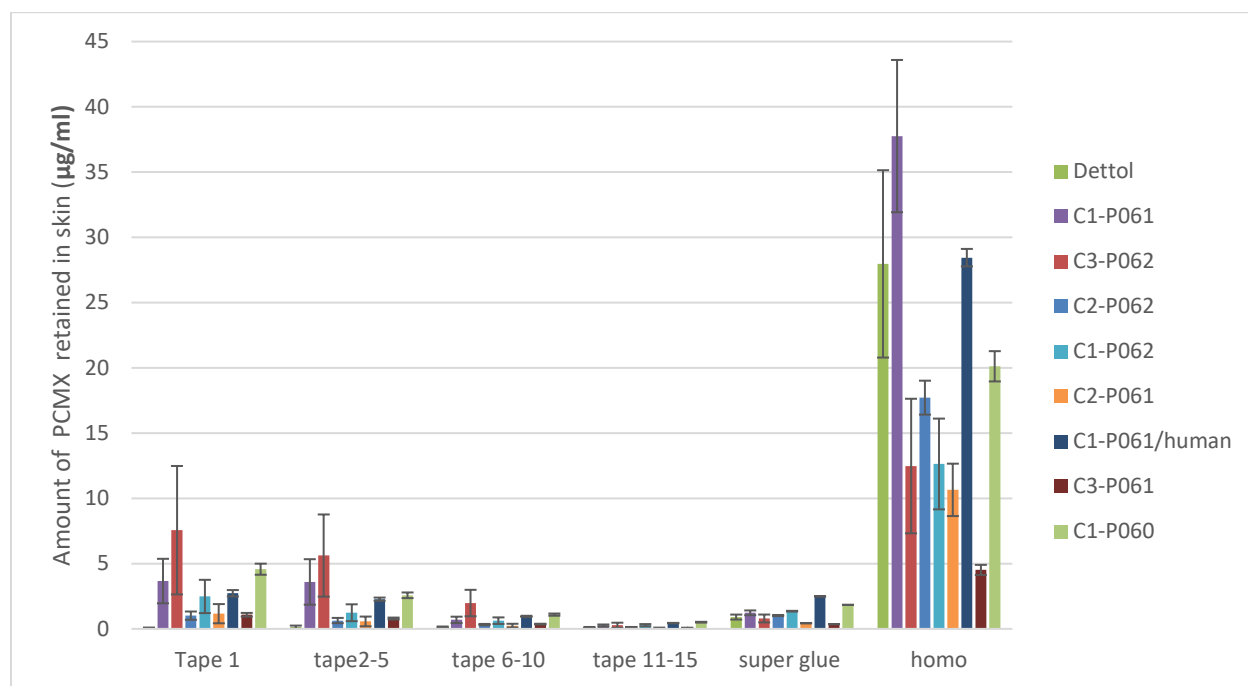


Figure 4.17 Graph of all PCMX formulations (mean \pm SD n=3)

4.4 Conclusion

In conclusion, high-shear homogenisation followed by ultrasonication was a successful method for the design and development of a PCMX NE. Various parameters and variables were studied for this NE, including MDS, PDI, ZP, pH and viscosity. Several types and amount of surfactant were investigated to find the optimum formulation, the effect of the amount of oil was also explored and other factors that were tested include the sonication time, mixing time and mixer speed of the high-shear homogeniser. An accelerated and long-term stability study was carried out for all formulations over three months. The results showed that the formulation with the lowest amount of surfactant was found to be (0.4%w/w) and T80/S80 with a ratio of 3:1 showed the best penetration and retention within the skin.

The use of the tape-stripping method was successful in quantitatively determining the PCMX within the skin, and the micro CT scan was successful in the qualitative determination, which confirmed what tape stripped method showed.

Chapter 5-Hansen solubility parameters (HSPs) as a tool to predict miscibility of nanoemulsion formulations with artificial sebum

5.1 Introduction

The hair follicle is considered an important route for delivering drugs into and through the skin. However, there are some difficulties associated with this route such as the presence of sebum which prevents the formulation from reaching the target site. It is therefore important to study the miscibility of the formulation with the sebum.

In this chapter, HSPs are used to predict the miscibility of nano-formulations with artificial sebum, and for this to be achieved the HSP for artificial sebum was calculated using three different methods: contribution group method (Van Krevelen method), Y-MB method using HSPiP software and the third method using the solubility and miscibility of known HSPs and regression statistics.

The miscibility of nano-formulations with artificial sebum was then studied using their HSPs values using a miscibility equation according to Greenhalgh approaches.

5.2 The composition of artificial sebum and similarity with human sebum

The composition of triglycerides and fatty acids in sebum varies from one human to another and varies over time due to triglyceride degradation and these changes lead to differences in the exact human sebum composition from site to site, person to person as well as temporally. Thus, the average human sebum composition as obtained by Valiveti (2008) was used to formulate artificial sebum as shown in Figure 5.1. In artificial sebum, the wax esters in the human sebum were replaced by a paraffin wax and spermaceti wax. Triglycerides in the human sebum were substituted with olive oil, cottonseed oil and coconut oil, having carbon chain lengths of fatty esters similar to components in serum(Valiveti, Wesley and Lu, 2008).

The extent of triglyceride degradation which takes place during the secretion of sebum from the sebaceous glands up towards the surface of the skin is the reason for the variation in the percentage of fatty acids in human sebum. There are no fatty acids in the sebum that is secreted from the glands while levels can reach up to 45% fatty acids content when the sebum reaches the surface of the skin. Since the sebum of most relevance in this study is in the upper duct of the hair follicle, a 11% of fatty acid was incorporated into the artificial sebum.

Valiveti (2008) tested this artificial sebum in comparison with human sebum using DSC and NMR methods and established the similarity between the two. A high correlation was also found in the diffusion and partition property between the human sebum and the artificial sebum; this was achieved through the execution of partition and diffusion studies. In this study, this composition of artificial sebum was adopted to study the miscibility of nanoemulsion with it.

Composition	Human sebum-I (Wertz, 2001) (lumen/surface)	Human sebum-II (Rosenthal, 1964)	Human sebum-III (Greene et al., 1970)	Human sebum-IV (Nordstrom et al., 1986)	Artificial sebum
Squalene	15/15	13	12	19.9	15
Wax esters	25/25	26	26	25.3	
Paraffin wax					10
Spermaceti wax					15
Triglycerides	57/42	32	57.5	16.1	
Olive oil (C16–18)					10
Cotton seed oil (C16–18)					25
Coconut oil (C12–16)					10
Fatty acids	0/15 (C16)	23	–	33.0	
Oleic acid					1.4
Palmitic acid					5
Palmitoleic acid					5
Cholesterol	1/1	1.6	1.5	3.8	1.2
Cholesteryl esters	2/2	3.5	2.0	2.0	
Cholesterol oleate					2.4

Figure 5.1 The composition of artificial sebum (Valiveti, Wesley and Lu, 2008)

5.3 Overview of chemical bonds

The calculation of HSPs is highly dependent on the energy of chemical bonds, therefore, to reach an understanding of HSPs a short summary of the various chemical bonds and interactions between atoms and molecules is presented.

5.3.1 Intra-molecular bonds

5.3.1.1 Covalent bonds

When two atoms with equal electronegativity share one or more electrons, a pure covalent bond is formed between them. An example of this is the hydrogen molecule which has two atoms of hydrogen sharing an electron, and since both have the same electronegativity, it is shared equally between them. Whereas if the two atoms have differing electronegativity and the difference in electronegativity is less than 1.7, the covalent bond will be a polar covalent bond. In this case, the shared electron will be closer to the atom with higher electronegativity and give the atom a small negative charge, whereas the other atom is given a small positive charge, this is known as the electric dipole. An example of this is the water molecule in which the oxygen atom has a higher electronegativity than the hydrogen atom and the bond between them is a polar covalent bond (Manning, 2009).

5.3.1.2 Ionic bonds

This type of bond is formed between two atoms with large and clear differences in electronegativity between both atoms. An example of this difference is found between alkali metals of Group 1 of the periodic table which easily lose electrons and halogens of Group 17 which are likely to gain electrons, and a strong ionic bond is usually formed as a result, and an example of this bond is sodium chloride (NaCl). The ionic bond is considered the strongest bond and a very large amount of energy is needed to break this bond; this explains the reason behind the very high melting point for materials with this bond. The strength of the bond is variable based on the difference in electronegativity between the two atoms (Manning, 2009).

5.3.2 Inter-molecular bonds

5.3.2.1 Van der Waals interactions

This type of bond connects between two dipole molecules, where the small positive charge of the first molecule attracts the small negative charge in the other molecule (see Figure 5.2). Van der Waals

interactions have a clear effect on liquids, but also affect solids and gases, although the effect is much reduced. An example of this is the bond that connects hydrogen chloride, the HCl molecules align themselves in a way that the positive end of one molecule is close to the negative end of the other molecule, and this configuration, known as a Van der Waals interaction, results in an intermolecular force which holds two molecules together.

Van der Waals interactions are weak interactions where HCl is a gas at room temperature and changes to liquid at -85°C and freezes at -114°C (Manning, 2009).

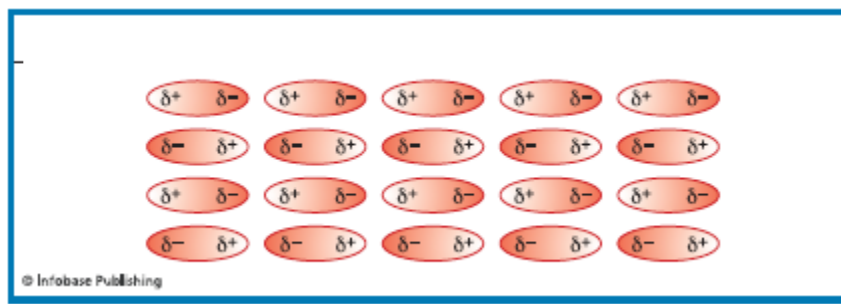


Figure 5.2 Molecules held together by dipoles (Manning, 2009)

5.3.2.2 Hydrogen bonds

The energy required to dissociate the polar covalent bond of H-Cl is 431 kJ/mol, whereas only 3.3 kJ/mol is needed to break a dipole-dipole bond of the same compound (HCl – HCl) which is 130 times less than the energy required in a polar covalent bond, thus exemplifying the variation between the strength of bonds. However, the dipole bond between water molecules is stronger than that in hydrogen chloride molecules, where a 19 kJ/mol energy is required to break a dipole bond between two water molecules. This bond is called a hydrogen bond; a hydrogen bond is formed as a result of the ability of a hydrogen atom to form a strong dipole bond with one of the following high electronegativity atoms: fluoride,

oxygen and nitrogen, and that explains why water has a higher boiling point (100°C) in comparison with hydrogen chloride (-85 °C) (Manning, 2009).

5.4 Overview of Hansen Solubility Parameters (HSP) and miscibility theory

The first scientists who worked on the concept of development of a solubility parameter (δ) were Hildebrand and Scott, followed by Hansen who developed his theory in 1967.

In 1950, Hildebrand and Scott proposed a theory stating that the chemical and physical interaction for every material is basically energy, which can be calculated in different ways, and is called cohesion energy. Dividing this cohesion energy by molar volume, (i.e. the volume occupied by one mole of substance at a given temperature and pressure, and the unit is m^3/mol) for any material will yield a cohesion energy density, which can be represented by the solubility parameter (δ). Materials that have the same δ values would be miscible, according to the basic rule “like dissolves like” (Hildebrand and Scott, 1950). However, one of the most important limitations of the Hildebrand parameter was that it was based on a single parameter (i.e. total cohesive energy) whereas the Hansen solubility parameter (HSP), which was developed from the Hildebrand parameter, uses the individual components of the total cohesive energy. For example, epoxies are not soluble in nitromethane or butanol, although both have the same value (δ) Hildebrand parameters. A 50:50 blend of these two solvents, however, is a good solvent for epoxies and this is effortlessly clarified by Hansen parameters and is not explained with Hildebrand (Abbott, Hansen and Yamamoto, 2013)

The Hansen solubility parameter (HSP) model consists of three important types of interaction, one at the atomic level and two at molecular levels. The atomic one is dispersion cohesive energy, (ED), like van der Waals interactions which are found in any molecule, as a molecule is built from atoms. The second type is polar cohesive energy (EP) which represents electrical attractions arising from dipole moments. A

third important one, a hydrogen bonding cohesive energy (EH), is a type of polar force, and it is also referred to as an electron exchange parameter (Hansen, 1967). There are more types of energy such as ionic energy, or electrostatic interactions, that may play a role, but the three energies mentioned above are the major ones.

There are a lot of applications for HSP in different fields like coating, paints and plastics manufacturing (Krauskopf, 1999). Also, HSPs have been considered a vital criterion to check the miscibility of a drug with excipients and carriers in solid dispersions (Greenhalgh *et al.*, 1999). Furthermore, HSPs have been broadly used to anticipate liquid-liquid miscibility, miscibility of polymer mixes, surface wettability, and the adsorption of colours to surfaces (Hansen, 2014). This study aims to predict the miscibility of different materials in artificial sebum according to their HSP values.

5.4.1 Theory and miscibility models

Thermodynamics can determine if a reaction is possible or not. For example, sodium chloride dissolves in water because the solvated sodium and chloride ions are thermodynamically more stable than crystalline form. Conversely, barium sulfate is insoluble in water because its crystals are thermodynamically more stable than the ionized form. Kinetics describes how quickly the reaction proceeds if it is thermodynamically possible. The strength of HSPs is that they are based on thermodynamics. They are about whether reactions are fundamentally possible or not (Abbott, Hansen and Yamamoto, 2013). To consider whether a solute dissolves in a solvent, it is necessary to compare two energy losses with one energy gain, and in the case where the gained energy is greater than energy loss, then the solute will dissolve in a solvent.

Some physicochemical properties of a material can be determined using the solubility parameter which is also known as the cohesion energy parameter; these properties include the solubility and melting

point of a material (Hancock, York and Rowe, 1997). The cohesive energy is considered to be the sum of a number of forces holding the material together, as well as the energy required to break these forces within the atoms and molecules of a material, the main forces being van der Waals interactions, covalent bonds and hydrogen bonds (Hancock, York and Rowe, 1997). To calculate the solubility parameter (δ), the cohesive energy density (CED) which is the cohesive energy per unit volume is used; this is accomplished based on regular solution theory and can only be used in non-polar systems (equation 5.1), (Mohammad, Alhalaweh and Velaga, 2011):

$$\delta = (\text{CED})^{0.5} = \left(\frac{\Delta E_V}{V_m} \right)^{0.5} \text{ Equation 5.1}$$

ΔE_V : Energy of vaporization

V_m : Molar volume

δ : Solubility parameter, measured in units of $(\text{J}/\text{cm}^3)^{0.5}$, $\text{MP}_a^{0.5}$ or $(\text{cal}/\text{cm}^3)^{0.5}$

$1 (\text{cal}/\text{cm}^3)^{0.5} = 2.0421 \text{ MP}_a^{0.5}$ or $(\text{J}/\text{cm}^3)^{0.5}$.

One of the most important attempts made to develop the previous approach was to extend the approach to include polar systems and strongly interacting species using an HSP theory. This theory proposes that the total force of the interactions can be split into partial solubility parameters representing the possibility of intermolecular interactions between similar or different molecules; these partial solubility parameters are: dispersion (δ_d), polar (δ_p) and hydrogen bonding (δ_h). The total solubility parameter (δ_t) which is also known as the three-dimensional solubility parameter, can be calculated using the following equation (equation 5.2):

$$\Delta\delta t = (\delta_d^2 + \delta_p^2 + \delta_h^2)^{0.5} \text{ Equation 5.2}$$

Multiple methods have been used to estimate the HSPs of materials using both theoretical approaches like the Small method, Fedors methods, Van Krevelen–Hoftyzer methods and Hoy's methods and

experimental approaches such as using inverse gas chromatography (IGC), solubility and miscibility with compounds with already known values of δ . The most regularly used theoretical method is the group contribution method, and this merely requires knowledge of the compound's chemical structure to calculate the HSP (Hansen, 2014; Subrahmanyam, Prakash, & Rao, 1996).

According to the principle of 'like dissolves like', Van Krevelen and others had found compounds with similar δ values are likely to be miscible. Van Krevelen and Hoftyzer determined the miscibility of two

compounds using the $\overline{\Delta\delta}$ factor, which can be calculated using equation 5.3:

$$\overline{\Delta\delta} = \left[(\delta_{d2} - \delta_{d1})^2 + (\delta_{p2} - \delta_{p1})^2 + (\delta_{h2} - \delta_{h1})^2 \right]^{0.5} \quad \text{Equation 5.3}$$

Van Krevelen and Hoftyzer found that to accomplish good miscibility between liquids, the $\overline{\Delta\delta}$ should be less or equal 5 MPa^{0.5} (Van Krevelen, 1997; Güner, 2004). Subsequently, Bagley and co-workers found a volume-dependent solubility parameter (δ_v) which is described by equation 5.4

$$\delta_v = (\delta_d^2 + \delta_p^2)^{0.5} \quad \text{Equation 5.4}$$

Because they found the effect of δ_d and δ_p are thermodynamically similar, therefore $R_{a(v)}$ the miscibility of two compounds, can be calculated using the following (equation 5.5):

$$\text{Equation 5.5} \quad R_{a(v)} = \left[4(\delta_{v2} - \delta_{v1})^2 + (\delta_{h2} - \delta_{h1})^2 \right]^{0.5}$$

It can be plotted in two dimensions, δ_v against δ_h (Breitkreutz, 1998). According to Albers, studies have suggested that if $R_{a(v)}$ is less or equal to 5.6 MPa^{0.5} the two compounds will be miscible (Albers, 2008).

Greenhalgh et al. (1999) also described another method to calculate miscibility depending on the differences between the total solubility parameters (Equation 5.6)

$$\Delta\delta_t = |\delta_{t1} - \delta_{t2}| \text{ Equation 5.6}$$

Where t1 and t2 are solvent and drug, respectively. It was found that if $\Delta\delta_t$ was less than $7 \text{ MPa}^{0.5}$ the two compounds would be miscible, and if it is greater, then they would not be miscible (Greenhalgh et al., 1999).

In this study, HSPs of components of artificial sebum and antiseptic compounds were calculated by three different theoretical methods (the Van Krevelen–Hoftyzer method, Yamamoto-Molecular Break (Y-MB) using HSPIP software and using a multiple regression model), and then the miscibility was checked according to three scientific approaches (Van Krevelen–Hoftyzer, Bagley, and Greenhalgh). Finally, the miscibility was determined experimentally using HPLC to determine the amount of active in sebum.

5.5 Methods to calculate Hansen solubility parameters (HSPs)

Unfortunately, researchers have not yet developed a direct method to determine the value of the component of HSPs δ_d , δ_p , δ_h , so the researchers endeavoured to calculate these values using complicated methods, some theoretical and other experimental methods.

5.5.1 Theoretical methods in calculating HSPs

The theoretical methods for calculating HSPs are based on the tables of group contributions which were found using the theory that states that large molecules with complicated compositions can be divided into smaller sections with known HSPs values and the HSPs for the whole material can, therefore, be calculated by adding these sections together (Scott, 1992). Consequently, it is only necessary to know the chemical structure of the compound for the group contributions to be calculated; then the HSPs can

be determined. As the chemical structure of most compounds is widely known it is therefore not difficult to determine HSPs using these methods.

The values of the group contributions may vary between studies due to the use of different methods for calculation. Figure 5.3 shows some of the important group contributions as calculated by various researchers.

Group	H ₂ ^o Bondi	E _{coh} (298)					E _{coh} (T _b) Bunn	E _{coh} (298) Hoflyzer and Van Krevelen
		Rheineck and Lin	Dunkel	Di Benedetto	Hayes	Fedors		
-CH ₃	10,560	4150	7460	-	-	4710	7120	9640
-CH ₂ -	6350	5150	4150	3600	4150	4940	2850	4190
$\begin{array}{c} \text{H} \\ \\ -\text{C}- \\ \end{array}$	(-270)	4060	-1590	-	-	3430	(-1840)	420
>C<	(-8000)	-	(-7340)	-	-	1470	(-6280)	-5580
-CH(CH ₃)-	(10,290)	(8210)	(5870)	-	7120	(8140)	5700	(10,060)
-C(CH ₃) ₂ -	(13,120)	-	7580	10,390	11,900	(10,890)	7960	(13,700)
-CH=CH-	-	-	8300	7210	7500	(8620)	7120	10,200
$\begin{array}{c} \text{H} \\ \\ -\text{C}=\text{C}- \\ \end{array}$	-	-	(2560)	-	-	(8620)	(2940)	4860
-C(CH ₃)=CH-	-	-	10,020	10,900	11,480	(13,330)	10,060	(14,500)
cyclopentyl	33,770	-	-	-	-	(24,240)	-	-
cyclohexyl	38,210	29,500	-	-	-	(29,180)	-	-
phenyl	41,060	31,220	30,920	-	-	31,940	22,630	31,000
p-phenylene	35,950	-	-	-	23,880	31,940	16,340	25,140
-F	-	-	8630	-	-	4190	(4730)	4470
-Cl	-	11,690	14,250	-	-	11,550	11,730	12,990
-Br	-	-	-	-	-	15,490	12,990	15,500
-I	-	-	-	-	-	19,050	17,600	-
-CN	-	-	-	-	-	25,530	-	25,000
-CHCN-	-	-	-	-	24,130	28,960	-	25,420
-OH	-	32,810	30,380	-	-	29,800	24,300	-
-O-	-	-	6830	-	6830	3350	4190	6290
-CO-	-	-	17,890	-	-	17,370	11,150	-
-COOH	-	32,810	37,580	-	-	27,630	23,460	-
-COO-	-	(19,530)	(16,010)	-	14,160	18,000	12,150	3410
$\begin{array}{c} \text{O} \\ \\ -\text{O}-\text{C}-\text{O}- \\ \end{array}$	-	-	-	-	-	17,580	-	-
$\begin{array}{c} \text{O} \quad \text{O} \\ \quad \\ -\text{C}-\text{O}-\text{C}- \\ \quad \end{array}$	-	-	-	-	-	30,560	16,340	-
$\begin{array}{c} \text{O} \quad \text{H} \\ \quad \\ -\text{N}-\text{N}- \\ \quad \end{array}$	-	-	67,880	-	44,750	33,490	35,620	60,760
$\begin{array}{c} \text{O} \quad \text{H} \\ \quad \\ -\text{O}-\text{C}-\text{N}- \\ \quad \end{array}$	-	-	-	-	26,310	26,370	36,620	-
-S-	-	-	-	-	-	14,150	9220	8800

Figure 5.3 Some group contributions as calculated by various researchers (Scott, 1992).

5.5.1.1 Small method

In 1953 a definition of molar attraction constant was proposed by Small which can be calculated using the following, (Equation 5.7).

$$F = \sqrt{(E_{coh}/V_{(298 K)})} \text{ Equation 5.7}$$

5.5.1.2 Fedors method

This method was published by Fedors in 1974, and the accuracy of this method was found to be lower than other methods. However, the advantage of it is that it included many functional groups (Hansen, 2014).

5.5.1.3 Hoftyzer- van Krevelen method

Hoftyzer-van Krevelen based this method on the known values of polymers.

In 1976 three relationships were established to calculate the partial HSPs; δ_d , δ_p and δ_h using the group contributions of the tested molecule (Fedors, 1974; Van Krevelen, 1976):

$$\delta_d = \frac{\sum_i F_{d_i}}{\sum_i V_i} \text{ Equation 5.8}$$

$$\delta_p = \frac{\left(\sum_i F_{p_i}^2\right)^{0.5}}{\sum_i V_i} \text{ Equation 5.9}$$

$$\delta_h = \left(\frac{\sum_i E_{h_i}}{\sum_i V_i}\right)^{0.5} \text{ Equation 5.10}$$

i: a Structural group within the molecule

F_{d_i} : Group contributions to the dispersion forces

F_{p_i} : Group contributions to the polar forces

E_{h_i} : Group contributions to the hydrogen-bonding energy

V_i : Group contributions to the molar volume

5.5.2 Experimental methods for calculating HSPs

5.5.2.1 The heat of vaporisation method

The heat of vaporisation of a material can be used to determine the total solubility parameters if the tested material is stable at a temperature higher than its boiling point. Therefore, the heat of vaporisation of the material can be directly measured using the following equation (equation 5.11).

$$\delta = \sqrt{\frac{\Delta E_{\text{vaporisation}}}{V}} = \sqrt{\frac{(\Delta E_{\text{vaporisation}} - RT)}{V}} \quad \text{Equation 5.11}$$

However, this method can only be used for determining the total solubility parameters and cannot be used for pharmaceutical materials or excipients due to instability at high temperatures (Hancock, York and Rowe, 1997).

5.5.2.2 Surface free energy

Another method used to determine the solubility parameters of a material is to determine the material's surface free energy as the surface free energy of material has been found to have a directly proportional relationship with its cohesive energy. The following equation (equation 5.12) shows this relationship.

$$\delta^2 = \left(\frac{\gamma}{\sqrt[3]{V}}\right)^n \quad \text{Equation 5.12}$$

δ^2 : cohesive energy of the material

γ : surface free energy of the material

n: constant relating to atom and molecule arrangement in space

Therefore, using surface free energies, solubility parameters can directly be calculated. This method has been found to have a very good correlation with other approaches used to find solubility parameters and has consequently been commonly used for a broad number of pharmaceutical materials. Due to this direct relationship between a material's surface free energy and its cohesive energy, it is, therefore, feasible to find a material's solubility parameters through any approach that obtains the material's surface energetic properties such as the contact angle analysis method (Hancock, York and Rowe, 1997).

5.5.2.3 Inverse Gas chromatography

The use of inverse gas chromatographic (IGC) is another method used to establish the solubility parameters for various liquids and solids. For this method, the retention times of gases of known cohesive energies are used. The solubility parameters for a large selection of pharmaceutical drugs and excipients have been calculated using this method (King, 1995).

This method has been found to result in solubility parameters that are both precise and reproducible, however, it cannot be considered a true equilibrium method and a heterogeneous distribution of active sites on the stationary phase could influence the acquired results. It has also previously been suggested that the measured cohesive energy may be affected by the essential manipulation of the stationary phase and its extended exposure to carrier gases throughout the experiment. The infrequent differences that can be found between this IGC method and other more straightforward methods are most likely due to the higher sensitivity of this method to surface heterogeneities in comparison with methods determining cohesive energy in bulk (Hancock, York and Rowe, 1997).

5.5.2.4 Solubility and miscibility

Another common method for finding the partial and total solubility parameters is through the determination of the miscibility and solubility of the materials in liquids; this is achieved using the known cohesive energies of these liquids. The liquid in which the tested material dissolves most completely and without involving heat or a change in temperature is obtained, and the solubility parameter of this liquid is accepted as the solubility parameter of the tested material. The directness and practicality of this method in addition to its possible application to gases, liquids and solids have led to this being a very common and well-known approach (Hancock, York and Rowe, 1997). This method has also been used for a few pharmaceutical film-coating polymers by Archer as the solubility parameters of these polymers was obtained using their miscibility (Archer, 1992).

5.6 Aim and objectives

This chapter aims to predict the miscibility of the antiseptic nanoemulsion formulations with artificial sebum. As mentioned in the introduction, the hair follicle is considered one of the most important routes to deliver the drug within and through the skin and the presence of sebum may obstruct this route. Therefore, it is important to know the miscibility of the drug to find out whether the drug will reach the target site. To achieve this, HSPs were used as a tool to determine whether the antiseptic nanoemulsion formulation is miscible with sebum.

The objectives of this chapter to accomplish the mentioned aim include:

- To calculate the sebum's HSPs using three different methods:
 - a. Hoftyzer- Van Krevelen group contribution method
 - b. Y-MB method using HIHSP software
 - c. Using regression statistics to calculate HSPs of sebum from different chemical compounds with known HSP that are soluble within it

- To calculate HSPs for triclosan and PCMX using two method methods;
 - a. Hoftyzer- Van Krevelen group contribution method
 - b. Y-MB method using HIHSP software

- To study the miscibility between the nanoemulsion formulations with artificial sebum

5.7 Results and Discussion

5.7.1 Hansen Solubility Parameter calculations for antiseptic compounds and artificial sebum

As mentioned in the introduction, targeting the HF is a promising potential pathway for dermal and transdermal delivery. However, one of the biggest obstacles restricting this route is the presence of sebum, the oily secretion from sebaceous glands that fills the hair follicle and can prevent particles reaching the target site in the hair follicle. This study was carried out to investigate the miscibility of artificial sebum with antiseptic nanoemulsion formulations containing triclosan and PCMX. The HSPs for artificial sebum were calculated using three methods, and one of the methods was calculated using regression statistics via the solubility of different chemical structures known as δ in artificial sebum. The solubility of these chemical structures in artificial sebum was gathered from the literature (Valiveti & Lu, 2007; Valiveti, & Lu, 2008) and the HSPs were calculated. Table 5.1 shows the HSPs and solubility of different chemical structures in artificial sebum.

Table 5.1 The HSPs and solubility of different chemical structures in artificial sebum (Valiveti and Lu, 2007)

Compounds	Molecular weight	K sebum	Solubility in water ($\mu\text{g/mL}$)	Solubility in Sebum ($\mu\text{g/mL}$)	Y-MB				VKH			
					δ_D	δ_P	δ_H	δ_{tol}	δ_D	δ_P	δ_H	δ_{Total}
Ketoconazole	531.43	9111.28	22.17	201995.30	21.6	11.9	6.2	25.4	20.7	5.9	9.6	23.5
Minoxidil	209.25	5.17	2483.87	12837.11	21.1	14.9	24.0	35.3	24.5	12.8	20.0	34.1
Salicylic acid	138.12	3.17	6972.45	21613.29	19.6	8.3	15.1	26.1	20.6	6.2	16.8	27.2
2,5-Dihydroxyl benzoic acid	154.12	2.11	23816.76	50251.76	20.6	9.5	18.8	29.4	20.6	7.1	20.7	30.1
Lidocaine	234.34	192.43	23318.34	4487082.74	17.2	5.5	4.7	18.6	17.2	4.4	6.3	18.8
Phenyl 4-hydroxybenzoate	214.22	91.93	23.19	2131.85	19.8	7.2	8.9	22.8	19.0	4.1	12.4	23.1
4-Hydroxybenzoic acid	138.12	2.38	6531.03	15543.78	20.1	8.8	16.1	27.2	20.6	6.2	16.8	27.2
Methyl 4-hydroxybenzoate	152.15	5.74	1641.05	9419.34	19.0	9.1	11.0	23.8	19.1	5.5	14.4	24.5
Ethyl 4-hydrooxybenzoate	166.17	13.66	640.16	8743.76	18.6	8.5	10.0	22.8	18.8	4.9	13.6	23.7
Propyl 4-hydroxybenzoate	180.20	51.96	245.65	12730.27	18.3	7.7	9.2	21.9	18.6	4.4	12.9	23.1
Butyl 4-hydroxybenzoate	194.23	151.54	177.25	26852.88	18.2	7.3	8.1	21.2	18.5	4.0	12.3	22.5
Amyl 4-hydroxybenzoate	208.25	471.18	103.16	48578.65	18.0	7.0	7.7	20.8	18.3	3.6	11.8	22.1
Hexyl 4-hydroxybenzoate	222.20	1768.05	24.29	42945.93	17.9	6.5	7.3	20.4	18.2	3.4	11.3	21.7
Heptyl 4-hydroxybenzoate	236.31	3818.15	11.45	43717.24	17.9	6.2	6.9	20	18.1	3.1	10.9	21.4
Octyl 4-hydroxybenzoate	250.33	11078.49	0.93	10302.99	17.6	5.9	9.2	20.8	18.0	2.9	10.5	21.1

5.7.1.1 Solubility parameters calculation of artificial sebum, antiseptics compounds using Hoftyzer –Van Krevelen group contributions

Using the three equations of Hoftyzer –Van Krevelen (equations 5.8, 5.9, 5.10) to calculate the partial solubility parameters (δ_d , δ_p and δ_h) and Fedors table to determine the molar volumes, it was possible to determine HSPs for triclosan and the components of artificial sebum and the value of the group contributions according to Hoftyzer –Van Krevelen are shown in Figure 5.4.

As mentioned in section 5.2, the triglycerides in human sebum were replaced with olive oil, cottonseed oil and coconut oil in artificial sebum and to calculate the HSPs for oils the composition of these oils should be determined Table 5.3 shows the composition of each oil.

Table 5.2 and Figure 5.5 shows how HSPs were calculated for triclosan and for the components of artificial sebum (see appendix A). Table 5.3 shows the value of the HSPs for PCMX and all components of artificial sebum, determined according to Hoftyzer –Van Krevelen methods.

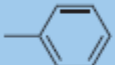
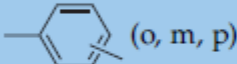
Structural group	F_{di} (MJ/m ³) ^{1/2} · mol ⁻¹	F_{pi} (MJ/m ³) ^{1/2} · mol ⁻¹	E_{hi} J/mol
-CH ₃	420	0	0
-CH ₂ -	270	0	0
>CH-	80	0	0
>C<	-70	0	0
=CH ₂	400	0	0
=CH-	200	0	0
=C<	70	0	0
	1620	0	0
	1430	110	0
 (o, m, p)	1270	110	0
-F	(220)	-	-
-Cl	450	550	400
-Br	(550)	-	-
-CN	430	1100	2500
-OH	210	500	20,000
-O-	100	400	3000
-COH	470	800	4500
-CO-	290	770	2000
-COOH	530	420	10,000
-COO-	390	490	7000
HCOO-	530	-	-
-NH ₂	280	-	8400
-NH-	160	210	3100
>N-	20	800	5000
-NO ₂	500	1070	1500
-S-	440	-	-
=PO ₄	740	1890	13,000
Ring	190	-	-

Figure 5.4 Solubility parameter component group contributions (method Hoftyzer–Van Krevelen) (Scott, 1992)

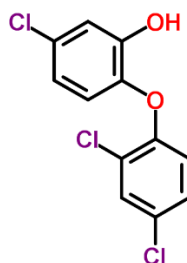


Figure 5.5 Chemical structure of triclosan

Table 5.2 Calculation of HSPs and molar volume for triclosan according to the Hoftyzer-van Krevelen methods)

Group	Frequency	F _d (J ^{1/2} .cm ³ /2.mol ⁻¹)	F _p (J ^{1/2} .cm ³ /2.mol ⁻¹)	E _h (J/mol)	V _m (cm ³ /mol)
(o,m,p) phenylene	2	2540	24200	0	104.8
ring	2	380	0	0	32
-Cl	3	1350	907500	1200	72
-OH	1	210	250000	20000	10
-O-	1	100	160000	3000	3.8

Applying equations 5.8, 5.9 and 5.10 , a solubility parameter can be calculated for triclosan:

$$\delta_d = \frac{\sum_i F_{d_i}}{\sum_i V_i} = 20.58 \text{ MP}_a^{0.5}$$

$$\delta_p = \frac{\left(\sum_i F_{p_i}^2 \right)^{0.5}}{\sum_i V_i} = 5.20 \text{ MP}_a^{0.5}$$

$$\delta_h = \frac{\left(\sum_i E_{h_i} \right)^{0.5}}{\sum_i V_i} = 10.43 \text{ MP}_a^{0.5}$$

$$\delta_t = (\delta_d^2 + \delta_p^2 + \delta_h^2)^{0.5} = 23.65 \text{ MP}_a^{0.5}$$

The same process can be used to determine solubility parameters for all the components of artificial sebum.

Table 5.3 Calculated HSPs for PCMX and artificial sebum components according to Hoftzyer –Van Krevelen methods

	Oil composition		VK-H				
	Fatty acids	percentage	molecular Volume	δ_D	δ_P	δ_H	δ_{tot}
PCMX			153.49	18.06	4.90	11.53	21.98
Squalene			477.05	16.11	0.00	0.00	16.15
Oleic acid			314.40	16.32	1.39	5.60	17.32
Palmitic acid			287.40	16.54	1.59	5.92	17.54
Palmitoleic acid			282.28	16.33	1.53	6.00	17.41
Cholesterol oleate			675.14	17.01	0.74	3.25	17.44
Cholesterol			381.22	17.75	1.32	7.26	19.16
Coconut oil (C12–16)(ZAMBIAZI, 2007)	Lauric acid	45.46	223.04	16.37	1.88	6.70	17.78
	Myristic acid	18.82	255.25	16.42	1.65	6.26	17.65
	Palmitic acid	10.08	287.47	16.53	1.51	5.97	17.54
	Caprylic acid	6.38	158.65	16.20	2.65	7.94	18.24
	Capric Acid	5.56	190.87	16.30	2.20	7.24	17.97
	Stearic acid	4.31	319.68	16.53	1.33	5.63	17.53
	Arachidic acid	0.08	351.89	16.51	1.24	5.34	17.42
	Oleic acid	7.45	314.40	16.37	1.35	5.63	17.36
	Linoleic acid	1.80	309.24	16.14	1.36	5.69	17.16
	gadoleic acid	0.06	346.62	16.36	1.21	5.37	17.26
Cotton seed oil (C16–C18)(Carlos Zambiasi <i>et al.</i> , 2007)	Palmitic acid	21.87	287.44	16.53	1.52	5.91	17.57
	Stearic acid	2.27	319.62	16.56	1.35	5.63	17.53
	Myristic acid	0.77	255.25	16.42	1.65	6.26	17.65
	behenic acid	0.36	384.03	16.54	1.10	5.10	17.31
	Arachidic acid	0.26	351.84	16.55	1.24	5.33	17.43
	Lignoceric acid	0.12	416.27	16.67	1.02	4.92	17.35
	Margaric acid	0.08	303.59	16.52	1.44	5.73	17.56
	Linoleic acid	56.35	309.22	16.14	1.36	5.69	17.16
	Oleic acid	16.61	314.49	16.33	1.31	5.65	17.38
	Palmitic acid	0.47	282.22	16.34	1.53	6.06	17.41
	Linolenic acid	0.33	304.09	15.95	1.38	5.74	17.01
	Nervonic acid	0.16	411.00	16.42	1.02	4.93	17.18
	gadoleic acid	0.14	346.66	16.36	1.21	5.37	17.26
	Myristoleic acid	0.11	250.00	16.20	1.68	6.32	17.47
	eicosadienoic acid	0.10	341.43	16.20	1.23	5.41	17.12
Olive oil (C16–18)(Carlos Zambiasi <i>et al.</i> , 2007)	Palmitic acid	10.84	287.44	16.52	1.5	5.92	17.55
	Stearic acid	3.59	319.65	16.54	1.3	5.63	17.57
	Arachidic acid	0.50	351.81	16.55	1.2	5.34	17.42
	behenic acid	0.15	384.03	16.57	1.1	5.15	17.37
	Margaric acid	0.14	303.55	16.57	1.4	5.72	17.52
	Lignoceric acid	0.12	416.23	16.62	1.0	4.96	17.37
	Oleic acid	75.55	314.46	16.35	1.3	5.62	17.31
	Linoleic acid	7.01	309.27	16.14	1.36	5.69	17.16
	Palmitic acid	0.92	282.24	16.35	1.5	6.03	17.48
	Linolenic acid	0.66	304.05	15.95	1.38	5.74	17.01
	gadoleic acid	0.32	346.62	16.36	1.21	5.37	17.26
	Myristoleic acid	0.21	250.00	16.20	1.68	6.32	17.47
	docosadienoic acid	0.05	373.67	16.25	1.12	5.17	17.09

5.7.1.2 Calculation of artificial sebum and antiseptic solubility parameters using Y-MB methods

To calculate an HSP for artificial sebum component and antiseptics according to Y-MB method, HSPiP (Hansen Solubility Parameters in Practice) software was used. The HSPiP was developed by Steven Abbott, Charles M. Hansen and Hiroshi Yamamoto. It has more than 10,000 chemical compounds in the dataset. To calculate a partial solubility parameter of any chemical compound, the structure is entered in SMILES format (e.g. www.chemspider.com). This method is fast and accurate. One of the limitations of this method however, is that it is not suitable for large molecules such as large polymers (more than 120 atoms). The way that is used to overcome this limitation is to split the molecules to two regions (Abbott, Hansen and Yamamoto, 2013). Table 5.4 shows the HSPs for triclosan, PCMX and components of artificial sebum calculated according to Y-MB methods.

Table 5.4 HSPs for Triclosan, PCMX and artificial sebum components according to Y-MB method.

	Oil composition		Y-MB				
	Fatty acids	percentage	δ_D	δ_P	δ_H	δ_{tol}	
Triclosan			21.2	7.0	8.3	23.8	
PCMX			18.8	4.1	8.8	19.2	
Squalene			17.0	0.9	3.1	17.3	
Oleic acid			16.4	3.0	5.5	17.6	
Palmitic acid			16.2	3.3	5.8	17.5	
Palmitoleic acid			16.5	3.4	6.3	18.0	
Cholesterol oleate			17.2	1.0	1.7	17.3	
Cholesterol			17.2	2.1	3.9	17.7	
Coconut oil (C12–16)(Carlos Zambiasi <i>et al.</i> , 2007)	Lauric acid	45.46	16.3	4.0	7.5	18.3	
	Myristic acid	18.82	16.3	3.3	6.6	17.8	
	Palmitic acid	10.08	16.2	3.3	5.8	17.5	
	Caprylic acid	6.38	16.3	5.2	10.1	19.8	
	Capric Acid	5.56	16.3	4.2	8.6	18.9	
	Stearic acid	4.31	16.2	2.8	5.2	17.2	
	Arachidic acid	0.08	16.1	2.7	4.7	17.0	
	Oleic acid	7.45	16.4	3.0	5.5	17.6	
	Linoleic acid	1.8	16.7	3.1	6.1	18.0	
	gadoleic acid	0.06	16.4	2.9	5.1	17.4	
	Palmitic acid	21.87	16.2	3.3	5.8	17.5	
	Stearic acid	2.27	16.2	2.8	5.2	17.2	
	Myristic acid	0.77	16.3	3.3	6.6	17.8	
	behenic acid	0.36	16.2	2.3	4.3	16.9	
Cotton seed oil (C16–C18)(Carlos Zambiasi <i>et al.</i> , 2007)	Arachidic acid	0.26	16.1	2.7	4.7	17.0	
	Lignoceric acid	0.12	16.1	2.4	3.9	16.7	
	Margaric acid	0.08	16.2	2.8	5.4	17.3	
	Linoleic acid	56.35	16.7	3.1	6.1	18.0	
	Oleic acid	16.61	16.4	3.0	5.5	17.6	
	Palmitic acid	0.47	16.5	3.4	6.3	18.0	
	Linolenic acid	0.33	16.9	3.3	5.8	18.2	
	Nervonic acid	0.16	16.3	2.2	4.2	17.0	
	Gadoleic acid	0.14	16.4	2.9	5.1	17.4	
	Myristoleic acid	0.11	16.5	3.6	6.9	18.3	
	eicosadienoic acid	0.1	16.6	2.8	5.3	17.6	
	Olive oil (C16–18)(Carlos Zambiasi <i>et al.</i> , 2007)	Palmitic acid	10.84	16.2	3.3	5.8	17.5
		Stearic acid	3.59	16.2	2.8	5.2	17.2
		Arachidic acid	0.5	16.1	2.7	4.7	17.0
Behenic acid		0.15	16.2	2.3	4.3	16.9	
Margaric acid		0.14	16.2	2.8	5.4	17.3	
Lignoceric acid		0.12	16.1	2.4	3.9	16.7	
Oleic acid		75.55	16.4	3.0	5.5	17.6	
Linoleic acid		7.01	16.7	3.1	6.1	18.0	
Palmitic acid		0.92	16.5	3.4	6.3	18.0	
Linolenic acid		0.66	16.9	3.3	5.8	18.2	
gadoleic acid		0.32	16.4	2.9	5.1	17.4	
Myristoleic acid		0.21	16.5	3.6	6.9	18.3	
docosadienoic acid		0.05	16.5	2.4	4.8	17.4	

5.7.1.3 Calculation of artificial sebum using multiple regression model

The HSPs of artificial sebum were calculated by using a multiple regression model, and an equation was used to predict the partition coefficient of a drug between two solvents (Equation 5.13) (Al balkhi *et al.*, 2016) by rearranging the equation to the form $Y = aX_1 + bX_2 + C$ as seen in Equation 5.14

$$\ln K_{S2S1} = \frac{V_m^D}{RT} [(\delta_t^{S1} - \delta_t^D)^2 - (\delta_t^{S2} - \delta_t^D)^2] + \ln \frac{V_m^{S1}}{V_m^{S2}} \quad \text{Equation 5.13}$$

$$RT \ln K_{S2S1} = V_m^D [(\delta_t^{S1} - \delta_t^D)^2 - (\delta_t^{S2} - \delta_t^D)^2] + RT \ln \frac{V_m^{S1}}{V_m^{S2}}$$

$$RT \ln K_{SW} = V_m^D (\delta_t^W)^2 + V_m^D (\delta_t^D)^2 - 2V_m^D \delta_t^W \delta_t^D - V_m^D (\delta_t^S)^2 - V_m^D (\delta_t^D)^2 + 2V_m^D \delta_t^S \delta_t^D + RT \ln \frac{V_m^W}{V_m^S}$$

$$RT \ln K_{SW} = V_m^D (\delta_t^W)^2 - V_m^D (\delta_t^S)^2 + 2V_m^D \delta_t^S \delta_t^D - 2V_m^D \delta_t^W \delta_t^D + RT \ln \frac{V_m^W}{V_m^S}$$

$$RT \ln K_{SW} = [(\delta_t^W)^2 - (\delta_t^S)^2] V_m^D + [2\delta_t^S - 2\delta_t^W] V_m^D \delta_t^D + RT \ln \frac{V_m^W}{V_m^S} \quad \text{Equation 5.14}$$

$$Y = [(\delta_t^W)^2 - (\delta_t^S)^2] X_1 + [2\delta_t^S - 2\delta_t^W] X_2 + C$$

Where V_m is the molar volume, T is the temperature (in degrees Kelvin), R is the gas constant, and superscripts S, W, D indicate sebum, water, and the drug, respectively. Positive values of $\ln K_{SW}$ mean that the concentration of the drug in sebum is higher than in water; the higher the value, the higher the concentration of the drug in sebum compared to water.

From Table 5.1 $\ln K_{SW}$ and $V_m^D \delta_t^D$ can be calculated as shows in Table 5.5

Table 5.5 $\ln K_{sw}$ and $V_{m*}^D \delta_t^D$ for different chemical compounds

Compounds	K _{sebum}	Ln k _{sebum}	molar Volume (cm ³ /mol)	Y-MB		VK-H	
				$\delta_{Total}(J/cm^3)^{0.5}$	$V_m * \delta_{Total}$	$\delta_{Total}(J/cm^3)^{0.5}$	$V_m * \delta_{Total}$
Ketoconazole	9111.24	9.18	396.70	25.43	10076.18	23.55	8184.79
Minoxidil	5.17	1.64	162.68	35.35	5739.78	34.16	3967.35
Salicylic acid	3.14	1.13	106.64	26.16	2782.26	27.28	2912.99
2,5-Dihydroxyl benzoic acid	2.11	0.75	108.12	29.43	3178.14	30.13	3513.06
Lidocaine	192.43	5.26	231.99	18.66	4313.34	18.85	4839.54
Phenyl 4-hydroxybenzoate	91.93	4.52	175.83	22.87	4008.24	23.17	4029.06
4-Hydroxybenzoic acid	2.38	0.86	105.99	27.23	2880.48	27.29	2912.99
Methyl 4-hydroxybenzoate	5.74	1.74	128.73	23.82	3063.06	24.52	3187.46
Ethyl 4-hydrooxybenzoate	13.66	2.61	146.35	22.87	3335.64	23.74	3465.07
Propyl 4-hydroxybenzoate	51.96	3.95	163.49	21.97	3578.46	23.17	3741.56
Butyl 4-hydroxybenzoate	151.54	5.02	180.62	21.28	3828.72	22.54	4017.17
Amyl 4-hydroxybenzoate	471.18	6.16	196.38	20.82	4083.04	22.13	4292.07
Hexyl 4-hydroxybenzoate	1768.05	7.48	213.06	20.41	4345.26	21.72	4566.38
Heptyl 4-hydroxybenzoate	3818.10	8.24	229.54	20.09	4590.08	21.48	4840.22
Octyl 4-hydroxybenzoate	11078.49	9.312760669	246.47	20.84	5125.12	21.18	5113.64

$\ln K_{SW}$ can be considered a dependent variable and V_m^D , and $V_m^D \delta_t^D$ can be considered independent variables and $RT \ln \frac{V_m^W}{V_m^S}$ is an intercept. By applying multiple regression analysis on Equation 5.14, the value of $((\delta_t^W)^2 - (\delta_t^S)^2)$ and $(2\delta_t^S - 2\delta_t^W)$ according to each method (Y-MB and VK-H) were determined as shown in Table 5.6, and according to Hansen, the solubility parameter for water is 18.1, 17.1, and 16.9 (δ_d), (δ_p) and (δ_h) respectively (Hansen, 2014). From Equation 5.2 the total solubility parameter of water can be calculated

$$\delta_t = (\delta_d^2 + \delta_p^2 + \delta_h^2)^{0.5}$$

$$\delta_t^W = ((18.1)^2 + (17.1)^2 + (16.9)^2)^{0.5}$$

$$\delta_t^W = 30.09 \text{ MPa}^{0.5}$$

Table 5.6 Output of Regression statistics

Y-MB				VK-H			
Regression Statistics output				Regression Statistics output			
Intercept	$((\delta_t^W)^2 - (\delta_t^S)^2)$	$(2\delta_t^S - 2\delta_t^W)$	R ²	Intercept	$((\delta_t^W)^2 - (\delta_t^S)^2)$	$(2\delta_t^S - 2\delta_t^W)$	R ²
-1.5917	0.068142895	-0.00151789	0.87	2.717264	0.11079928	-0.00443946	0.87

For the Y-MB method, the value of the total solubility parameter of artificial sebum is:

As shown in Equation 5.13 $\ln k_{sebum}$ is multiplied by RT so the value of the output of regression statistics must also be multiplied by RT (8.314 * 298.15)

$$(\delta_t^W)^2 - (\delta_t^S)^2 = 0.068142895 (8.314 * 298.15)$$

$$(\delta_t^S)^2 = (\delta_t^W)^2 - 168.9139$$

$$(\delta_t^S)^2 = 736.49$$

$$\delta_t^S = 27.1$$

$$(2\delta_t^S - 2\delta_t^W) = -0.00151789 (8.314 * 298.15)$$

$$2\delta_t^S = 2\delta_t^W - 3.76258$$

$$2\delta_t^S = 56.4174$$

$$\delta_t^S = 28.2$$

So, the values of both ways are close.

For the VK-H method, the value of the total solubility parameter of artificial sebum is:

$$(\delta_t^W)^2 - (\delta_t^S)^2 = 0.11079928 (8.314 * 298.15)$$

$$(\delta_t^S)^2 = (\delta_t^W)^2 - 274.6514$$

$$(\delta_t^S)^2 = 630.75$$

$$\delta_t^S = 25.1$$

$$(2\delta_t^S - 2\delta_t^W) = -0.00443946 (8.314 * 298.15)$$

$$2\delta_t^S = 2\delta_t^W - 11.0046$$

$$2\delta_t^S = 49.17538$$

$$\delta_t^S = 24.6$$

The total solubility parameters by using this method are 27.1, 28.2 for Y-MB method and 25.1, 24.6 for VK-H method, which shows a relatively similar value as the previous methods. And as R^2 of regression statistics was 0.87 (table 5.6) that explain the difference value of δ_t^S in each method.

5.7.2 Limitations in the calculation of HSPs for artificial sebum components

One of the main challenges in this study was the calculation of HSPs for paraffin wax, and spermaceti wax (the wax esters in artificial sebum, see Figure 5.1). As these are natural products, their constitution tends to be complex and variable. Exact compositions have not been defined for either paraffin wax or spermaceti wax, except one paper which claimed that paraffin comprised 67 different compounds, but these were not identified (Levy, 1961). Determination of the composition of paraffin wax or spermaceti wax would require column chromatography to separate the components, then NMR spectroscopy to define the components, thereafter HPLC to know the percentage of each component, and this is beyond the scope of this project and the value is somewhat limited. Therefore, HSPs of paraffin wax and spermaceti wax were estimated using IGC (section 2.1.6 Inverse gas chromatography) (Adamska and Voelkel, 2005). Table 5.7 shows the HSPs of paraffin wax and spermaceti wax determined using IGC.

Table 5.7 The HSPs of paraffin wax and spermaceti wax by using IGC method

	δ_D	δ_P	δ_H	δ_{Total}
Paraffin wax	55.78	18.80	4.08	59.01
Spermaceti wax	47.58	9.82	6.80	49.05

The calculation of HSPs is based on the experimental retention data of test solutes called probes and the targeted material. More specifically, measured retention volumes using IGC can be used to calculate Flory-Huggins interaction parameters ($\chi_{1,2}^{\infty}$). Subsequently, the total solubility parameter (δ_T) and its components, dispersive (δ_D), polar (δ_P), and hydrogen bonding (δ_H) can be determined. The selection of test probes is crucial in measuring solubility parameters using IGC as each type of solvent represents a certain type of interaction. The measurement of solubility parameters and Flory-Huggins values using

IGC was firstly reported by Price *et al.* (1986). Several researchers have reported solubility parameter calculations using IGC measurement data (Price, Guillet and Purnell, 1986; Voelkel and Fall, 1996; Adamska and Voelkel, 2005).

$\chi_{1,2}^{\infty}$ can be calculated using retention volume measured at infinite dilution after being transformed into a mass activity coefficient using equation 5.15:

$$\ln \Omega^{\infty} = \ln \left(\frac{273.15R}{p_1^0 V_r M_1} \right) - \frac{p_1^0 (B_{11} - V_1)}{RT} \quad \text{Equation 5.15}$$

Where Ω^{∞} is the mass activity coefficient. V_r is the retention volume, p_1^0 , V_1 , and M_1 are saturation pressure, molecular mass, and molecular volume of the probe molecule. B_{11} is the second virial coefficient. B_{11} value was calculated using Guggenheim and McGlashan approach (McGlashan and Wormald, 1964). Then $\chi_{1,2}^{\infty}$ can be calculated using the following equation 5.16:

$$\chi_{1,2}^{\infty} = \ln \Omega^{\infty} + \ln \left(\frac{\rho_1}{\rho_2} \right) - \left(1 - \frac{V_1}{V_2} \right) \quad \text{Equation 5.16}$$

Where ρ_1 , and ρ_2 are true densities of the probe and sample, respectively. V_1 and V_2 are the molecular volume of probe and sample, respectively. Finally, the calculation of solubility parameter was performed using DiPaolo and Guillet equation 5.17:

$$\frac{\delta_1^2}{RT} - \frac{\chi_{1,2}^{\infty}}{V_1} = \frac{\delta_1^2}{RT} - \left(\frac{2\delta_2\delta_1}{RT} + \frac{\chi_s^{\infty}}{V_1} \right) \quad \text{Equation 5.17}$$

Where δ_1 , and δ_2 are solubility parameter of test probe, and sample, respectively. $\chi_{1,2}^{\infty}$ is Flory-Huggins parameter, V_1 is the molecular volume of probe. χ_s^{∞} , is the entropic contribution of the Flory-Huggins parameter. Using multiple probes set in the measurement, a linear relationship can be obtained if $\left(\frac{\delta_1^2}{RT} - \frac{\chi_{1,2}^{\infty}}{V_1} \right)$ vs. δ_1 is plotted. Subsequently, solubility parameter of the sample (δ_2) can be calculated from slope value $\left(\frac{2\delta_2}{RT} \right)$.

For the dispersive component (δ_D) n-alkanes were used as probes according to equation 5.18:

$$\delta_D = \frac{S_{n-alkanes} \times RT}{2} \text{ Equation 5.18}$$

Whereas, aromatic hydrocarbons, ketones, or nitropropanes were selected for determination of the polar component (δ_p) using equation 5.19:

$$\delta_p = \frac{(S_{polar} - S_{n-alkanes}) \times RT}{2} \text{ Equation 5.19}$$

Alcohol, or pyridines were used to measure hydrogen bonding component (δ_H) using equation 5.20:

$$\delta_H = \frac{(S_{alcohols} - S_{n-alkanes}) \times RT}{2} \text{ Equation 5.20}$$

Where $S_{n-alkanes}$, S_{polar} , and $S_{alcohols}$ are the slopes of $(\frac{\delta_1^2}{RT} - \frac{\chi_{1,2}^\infty}{V_i})$ vs. δ_1 from DiPaolo and Guillet equation calculated from retention volumes of n-alkanes, polar, and alcohol probes.

5.7.3 Hansen Solubility Parameters of artificial sebum

According to the composition of artificial sebum in Figure 5.1, HSPs of artificial sebum calculated using both VK-H and Y-MB methods are shown in Tables 5.8 and 5.9 respectively. These two methods show a similarity in partial solubility parameters, dispersion (δ_d), polar (δ_p) and hydrogen (δ_h).

Table 5.8 HSPs of artificial sebum according to Hoftzyer –Van Krevelen method

Hoftzyer–Van Krevelen method									
composition	Percentage of artificial sebum %	HSPs				HSPs of artificial sebum			
		δ_D	δ_P	δ_H	δ_{Total}	δ_D	δ_P	δ_H	δ_{Total}
Squalene	15	2.41	0	0	2.41	24.94	4.21	4.91	26.13
Oleic acid	1.4	0.22	0.01	0.07	0.24				
Palmitic acid	5	0.82	0.07	0.29	0.87				
Palmitoleic acid	5	0.81	0.07	0.29	0.86				
Cholesterol oleate	2.4	0.40	0.01	0.07	0.41				
Cholesterol	1.2	0.21	0.01	0.08	0.22				
Coconut oil (C12–16)	10	1.63	0.17	0.64	1.77				
Cotton seed oil (C16–C18)	25	4.06	0.34	1.43	4.32				
Olive oil (C16–18)	10	1.63	0.13	0.56	1.73				
Paraffin wax	10	5.57	1.88	0.41	5.90				
Spermaceti wax	15	7.13	1.47	1.02	7.35				

Table 5.9 HSPs of artificial sebum according to Yamamoto-Molecular Break method

Yamamoto-Molecular Break method									
composition	Percentage of artificial sebum %	HSPs				HSPs of artificial sebum			
		δ_D	δ_P	δ_H	δ_{Total}	δ_D	δ_P	δ_H	δ_{Total}
Squalene	15	2.55	0.13	0.46	2.59	25.08	4.57	5.31	26.32
Oleic acid	1.4	0.22	0.04	0.07	0.24				
Palmitic acid	5	0.81	0.16	0.29	0.87				
Palmitoleic acid	5	0.82	0.17	0.31	0.90				
Cholesterol oleate	2.4	0.41	0.02	0.040	0.41				
Cholesterol	1.2	0.20	0.02	0.04	0.21				
Coconut oil (C12–16)	10	1.63	0.17	0.64	1.77				
Cotton seed oil (C16–C18)	25	4.06	0.34	1.43	4.32				
Olive oil (C16–18)	10	1.63	0.13	0.56	1.73				
Paraffin wax	10	5.57	1.88	0.40	5.90				
Spermaceti wax	15	7.13	1.47	1.02	7.35				

5.7.4 Miscibility of antiseptic with artificial sebum

5.7.4.1 Theoretical miscibility of antiseptic with artificial sebum

In this study, the miscibility of triclosan and PCMX with artificial sebum was calculated according to the Greenhalgh equation 5.6 with good miscibility having values of $\Delta\delta_t \leq 7 \text{ MPa}^{0.5}$. Table 5.10 shows the miscibility results of triclosan and PCMX with artificial sebum and eucalyptol considering two methodologies VK-H and Y-MB.

Table 5.10 the miscibility of triclosan and PCMX with artificial sebum considering two methodologies VK-H and Y-MB

	Phase 1				Phase 2				Miscibility tool
	δ_d	δ_p	δ_h	δ_t	δ_d	δ_p	δ_h	δ_t	$\Delta\delta_{\text{total}} \text{ MPa}^{0.5}$
Triclosan_artificial sebum Y-MB	21.2	7.0	8.3	23.8	25.1	4.6	5.3	26.3	2.5
Triclosan_artificial sebum VK-H	20.6	5.2	10.4	23.6	24.9	4.2	4.9	26.1	2.5
Triclosan_eucalyptol Y-MB	21.2	7.0	8.3	23.8	16.6	2.5	2.5	16.9	6.9
Triclosan_eucalyptol VK-F	20.6	5.2	10.4	23.6	17.1	2.5	4.3	17.8	5.8
PCMX_artificial sebum Y-MB	18.8	4.1	8.8	21.2	25.1	4.6	5.3	26.3	5.2
PCMX_artificial sebum VK-H	18.1	4.9	11.5	22.0	24.9	4.2	4.9	26.1	4.2
PCMX_eucalyptol Y-MB	18.8	4.1	8.8	21.2	16.6	2.5	2.5	16.9	4.3
PCMX_eucalyptol VK-F	18.1	4.9	11.5	22.0	17.1	2.5	4.3	17.8	4.2

$\Delta\delta_{\text{total}}$ Using both methodologies VK-H and Y-MB, triclosan and PCMX are miscible with artificial sebum, being less than $7 \text{ MPa}^{0.5}$ in all cases. The affinity of triclosan to be released from eucalyptol to artificial sebum higher than the affinity of PCMX as shown the value of $\Delta\delta_{\text{total}}$ for triclosan with artificial sebum is 2.5 in both methods (VK-H and Y-MB) whereas the value $\Delta\delta_{\text{total}}$ for triclosan with eucalyptol is 6.9 and 5.8 for VK-H and Y-MB respectively. This means triclosan will be released from nanoemulsion formulation (eucalyptol oil) into artificial sebum more easily than PCMX, although the affinity of both antiseptics is acceptable.

5.7.4.2 Experimental miscibility of antiseptic with artificial sebum

The miscibility of triclosan and artificial sebum was determined experimentally. Artificial sebum (14 mg) was combined with 1 ml of triclosan nanoemulsion in a vial. The vials were shaken for 15 h at 37 °C, then centrifuged at 8000 rpm for 15 min, and the supernatant was analysed by HPLC. To measure how much of the amount of triclosan partitioned into artificial sebum, the amount of triclosan in the supernatant was subtracted from the amount in the initial triclosan nanoemulsion (Valiveti, Wesley and Lu, 2008). Two different formulations of triclosan nanoemulsion (Table 5.11) were studied, and the miscibility results are shown in Table 5.12.

Table 5.11 Two formulations of triclosan nanoemulsion used in miscibility studies

Formulation code	Oil (%w/w)	Surfactant (T80/S80 3:1)	Triclosan (%w/w)	Water (%w/w)
F1-80	5	0.34%	1	94.16
F3-80	5	5.00%	1	89.00

Table 5.12 The results of miscibility of two triclosan formulations with artificial sebum

	Triclosan concentration (µg/ml)
F1-80	7.47
F1-80 + 14 mg artificial Sebum	0.72
F3-80	12.94
F3-80 + 14 mg artificial Sebum	3.31

Table 5.12 confirmed the theory of the HSPs miscibility of triclosan and artificial sebum by moving the most amount of triclosan from nanoemulsion formulation to artificial sebum. In addition, it showed the formulation with a lower amount of surfactant (F1-80) was more miscible than the other formula (F3-80). This can be attributed to the fact that increasing surfactant reduces miscibility, which may be because a multilayer of surfactant obstructs the release of triclosan from a droplet of eucalyptol which

was found in chapter 3 to be the optimum formulation. The same study was carried out using PCMX formulations to determine the miscibility of PCMX with artificial sebum. Table 5.13 shows the two different formulations of PCMX Nanoemulsions and table 5.14 shown the miscibility results

Table 5.13 Two formulations of PCMX Nanoemulsion used in miscibility studies

Formulation code	Oil (%w/w)	Surfactant (T80/S80 3:1)	PCMX (%w/w)	Water (%w/w)
C1/P061	5	0.4%	0.24	94.56
C1/P060	5	2.0%	0.24	92.76

Table 5.14 The results of miscibility of two PCMX formulations with artificial sebum

	PCMX concentration ($\mu\text{g/ml}$)
C1/P060	35.11
C1/P060+ 14 mg artificial Sebum	2.81
C1/P061	32.67
C1/P061+ 14 mg artificial Sebum	2.58

The difference in miscibility was not as clear as the in triclosan formulations as the difference in the amount of surfactant in PCMX formulations was lower than the triclosan formulations. However, there is a difference which that supports the theory that the multilayer of surfactant decreases the amount of releasing the antiseptics from the oil droplet.

5.8 Conclusion

To calculate the HSPs for the artificial sebum, the HSPs for its components were calculated, and to validate these results; three various methods were used; VK-H method using contribution group method, Y-MB using HSPiP software and the third method using regression statistics with different soluble chemical compounds in artificial sebum with known HSPs.

In the first two methods, the components of HSPs δ_d , δ_p and δ_h were calculated.

The results are 24.94, 4.21, 4.91, 25.08, 4.57, 5.31 MPa^{0.5} for the VK-H method and Y-MB method, respectively.

In a third method, the total HSPs for the artificial sebum were calculated, this method showed similar results to the total HSPs found using the first two methods (26.13,26.32 VK-H method and Y-MB methods respectively).

The miscibility of the antiseptic with the artificial sebum was then calculated in accordance to the Greenhalgh equation; the results showed the affinity of triclosan to be released from eucalyptol to artificial sebum, whereas the affinity of PCMX was less than that of triclosan.

These results were confirmed experimentally and showed the miscibility between antiseptic compounds and artificial sebum.

Chapter 6- General Conclusion and Future Work

Infections resulting from surgery and other medical incisions of the skin generally known as healthcare-associated infections (HAIs), these types of infections have detrimental effects on healthcare services and are extremely costly to these types of services as they result in patients requiring additional and more extensive care and longer occupancy within hospitals, these infections have also been found to be linked to increased morbidity rates. The burden these HAIs form means that effective antisepsis of the skin before any incision is made is crucial to avoid these unfavourable effects. Surgical site infections (SSIs) are believed to make up around 15% of all HAIs making them the most likely type of infection within patients undertaking surgery. The care given to patients after the surgery they undergo has been found to lead to a decrease in the number of infections, however this alone is not enough and efficient and adequate procedures prior to surgery is essential for the prevention of surgical related infections. (Vilela et al., 2007) (Stevens, 2009)

The most frequent pathogens to be involved in SSIs are *S. aureus* and *S. epidermidis*, these microorganisms are often found in surgical sites, when incisions are performed on the skin, the tissue underneath the incision is exposed to the endogenous flora above which leads to a higher rate of SSIs (Piette and Verschraegen, 2009). The issue with these microorganisms is their ability to grow within the skin regardless of the use of antiseptic agents leading to further complicating these infections. Current recommendations state that 2% w/w CHG 70% (v/v) isopropyl alcohol (IPA) should be used as the ideal antisepsis before incisions are made to the skin. (Loveday et al., 2014) However, it is essential to note that prior to antisepsis of the skin, microorganisms have been found to linger in the skin, this in addition to inadequate penetration of most antiseptic agents are major contributing factors to SSIs. (Hendley and Ashe, 2003; Karpanen et al., 2008)

Therefore, it is essential to develop a carrier system which enhances the penetration of antimicrobial agents within the skin long-term, this would be applied to the skin prior to any surgical incisions to prevent the growth of bacteria in the surgical site and consequently limit infections of the skin.

In this thesis, the efficiency of nanoemulsion NE was studied to improve the amount of antimicrobial agent penetrating to the target site within the skin.

In chapter 3 of this thesis, two different techniques were used for the design and development of triclosan NE, the first technique was using a high-pressure homogeniser, as for the second technique it was using a high-shear homogeniser followed by ultrasonication. The design and development of triclosan NE was achieved successfully, and a study of various parameters of physiochemical characterisation of the formulation was performed including; MDS, PDI, ZP, pH and viscosity. In order to find the optimum formulation, the amount and type of surfactant were explored as well as the amount of oil. Different parameters for each of the two techniques were explored which included the effect of a number of cycles for the first technique and the sonication time for the second. A stability study was performed on all formulations in each of the techniques over a period of three months.

The HLB for the eucalyptol was calculated and found to be 12.5. The best penetration and retainment within the skin was achieved by the formulation with the lowest amount of surfactant (0.34%w/w), T20/S20 ratio 1:1.

As for chapter 4, high-shear homogenisation followed by ultrasonication was used and found to be a successful method for designed and developing PCMX NE. for this nanoemulsion the same physiochemical characterisations were explored as in the triclosan NE. Similarly to the triclosan NE, various types and amounts of surfactants were explored this was carried out to find the optimum formulation. The effect of different amounts of oil was also tested in addition to sonication time, mixing

time and speed of mixer in the high-shear homogeniser. Over three months, a long-term accelerated stability study was performed on all formulations.

Results of this chapter indicated that the formulations with the least surfactant showed the best penetration and skin retention which was (0.4%w/w) and T80/S80 with a ratio of 3:1.

The hair follicle HF is an essential drug delivery route within the skin, and through it, hair follicles also play a large role in leading to infections as they harbour microorganisms. Drug delivery is sometimes obstructed from reaching the target site within the HF, this obstruction may occur due to the presence of sebum. In order to prevent the sebum from obstructing drug delivery to target sites, Chapter 5 of this thesis focused on calculating HSPs of artificial sebum, this was tested to find the miscibility of antiseptic with artificial sebum.

The HSPs for the different components of artificial sebum were calculated to find the overall HSP of the artificial sebum, these results were also validated, three different methods were used which are; VK-H method using contribution group method, Y-MB using HSPiP software and the third method using regression statistics with different soluble chemical compounds in artificial sebum with known HSPs.

In the first two methods, the components of HSPs δ_d , δ_p and δ_h were calculated.

The results are 24.94, 4.21, 4.91, 25.08, 4.57, 5.31 MPa^{0.5} for the VK-H method and Y-MB method respectively.

In a third method, the total HSPs for the artificial sebum were calculated, this method showed similar results to the total HSPs found using the first two methods (26.13, 26.32 VK-H method and Y-MB methods respectively).

The Greenhalgh equation was then used to calculate the miscibility of the antiseptic with the artificial sebum, the affinity of triclosan was found to be released from eucalyptol to the artificial sebum, as for the PCMX, the affinity was found to be less than the affinity of triclosan. Results were then

experimentally supported and demonstrated the miscibility between the antiseptic compounds and the artificial sebum.

Future work

- This study showed that the lower concentration of surfactant results in better penetration for triclosan and PCMX, to further investigate and support this finding, the same method could be applied to other nanoemulsion formulations.
- Transmission electron microscopy TEM could be used to present the actual shape of the nanoemulsion droplet when surrounded by the surfactant to support the finding of the monolayer of the surfactant.
- Micro CT scan was successfully used in this study to show the distribution of the nanoemulsion within the skin qualitatively, this could be applied to other nanoemulsion formulations to support this finding.
- Atomic force microscopy could be used to study the changes occurring on the surface of the skin when applying nanoemulsion

Chapter 7 – References

- A. Lippacher, R.H. Muller, K. M. (2000) 'Investigation on the viscoelastic properties of lipid based colloidal drug carriers', *International Journal of Pharmaceutics*, 196(2), pp. 227–230..
- A.nna F.F alabella (2006) 'Debridement and wound bed preparation', *Dermatology and Therapy*, 19, pp. 317–325.
- Abbott, S., Hansen, C. M. and Yamamoto, H. (2013) *Hansen solubility parameters in practice*, 5th edition, pp.1-236 .
- Adamska, K. and Voelkel, A. (2005) 'Inverse gas chromatographic determination of solubility parameters of excipients', 304, pp. 11–17. .
- Agrawal, U. et al. (2013) 'Multifunctional nanomedicines: Potentials and prospects', *Drug Delivery and Translational Research*, 3(5), pp. 479–497..
- Al-Tawfiq, J. A. and Tambyah, P. A. (2014) 'Healthcare associated infections (HAI) perspectives', *Journal of Infection and Public Health. King Saud Bin Abdulaziz University for Health Sciences*, 7(4), pp. 339–344.
- Albers, J. (2008) 'Hot-melt extrusion with poorly soluble drugs', pp.1-150
- Anja Gysler, Burkhard Kleuser, Wolfgang Sippl, Katharina Lange, Hans Christian Korting, Hans-Dieter Höltje, M. S.-K. (1999) 'Skin Penetration and Metabolism of Topical Glucocorticoids in Reconstructed Epidermis and in Excised Human Skin', *Pharmaceutical Research*, 16(9), pp. 1386–1391.
- Araújo, F. A. et al. (2011) 'Development and characterization of parenteral nanoemulsions containing thalidomide', *European Journal of Pharmaceutical Sciences*, 42(3), pp. 238–245..
- Archer, W. L. (1992) 'hansen solubility parameters for selected cellulose ether', *Drug Development and Industrial Pharmacy*, 8, pp. 599–616.
- Avestin (2010) 'Operating Instructions for the EmulsiFlex -C5 High Pressure Homogenizer', pp. 1–12.
- Al balkhi, M. H. et al. (2016) 'Development of a liquid-liquid extraction method of resveratrol from cell culture media using solubility parameters', *Separation and Purification Technology*. , 170, pp. 138–145. .
- Barbero, A. M. and Frasc, H. F. (2009) 'Toxicology in Vitro Pig and guinea pig skin as surrogates for human in vitro penetration studies : A quantitative review', *Toxicology in Vitro*. , 23(1), pp. 1–13..
- Barnea, Y. et al. (2004) 'Clinical Comparative Study of Aquacel and Paraffin Gauze Dressing for Split-Skin Donor Site Treatment', *Annals of Plastic Surgery*, pp. 132–136..
- Baspinar, Y., Keck, C. M. and Borchert, H. H. (2010) 'Development of a positively charged prednicarbate nanoemulsion', *International Journal of Pharmaceutics*, 383(1–2), pp. 201–208..
- Peter m. elias. (1975) 'The permeability barrier in mammalian epidermis', pp. 180–191.
- Boateng, J. S. et al. (2008) 'Wound Healing Dressings and Drug Delivery Systems : A Review', *Journal of Pharmaceutical Sciences*., pp. 2892–2923..
- Bouchemal, K. et al. (2004) 'Nano-emulsion formulation using spontaneous emulsification: Solvent, oil and surfactant optimisation', *International Journal of Pharmaceutics*., pp. 241–251..
- Braun-Falco, O. and Korting, H. C. (1986) '[Normal pH value of human skin].', *Der Hautarzt; Zeitschrift für Dermatologie, Venerologie, und verwandte Gebiete*.

- Breitkreutz, J. (1998) 'Prediction of intestinal drug absorption properties by threedimensional solubility parameters'. *Pharm. Res.*
- Broughton, G. J. E. J. (2006) 'The Basic Science of Wound Healing', *Plastic and Reconstructive Surgery*, 117, pp. 12–34. .
- Burt, S. (2004) 'Essential oils : their antibacterial properties and potential applications in foods — a review', *International Journal of Food Microbiology*, 94, pp. 223–253.
- Butt, H.-J., Graf, K. and Kappl, M. (2003) *Physics and Chemistry of Interfaces*, Wiley-VCH GmbH & Co. KGaA. .
- Campos, V. E. B. De, Ricci-júnior, E. and Mansur, C. R. E. (2012) 'Nanoemulsions as Delivery Systems for Lipophilic Drugs', *American Scientific Publishers*, 12(3), pp. 2881–2890..
- Carlos Zambiasi, R. et al. (2007) 'fatty acid composition of vegetable oils and fats', 25(1), pp. 111–120.
- Caubet, C. et al. (2004) 'Degradation of Corneodesmosome Proteins by Two Serine Proteases of the Kallikrein Family, , *Journal of Investigative Dermatology*, 122, pp. 1235–1244. .
- Chemmunique (2004) *The HLB System: a time-saving guide to emulsifier selection*, ICI Americas Inc.
- Cole, M. (2011) 'Patient safety and healthcare-associated infection', *British Journal of Nursing*, 20(17).
- Cornwell, P. (1996) 'Modes of action of terpene penetration enhancers in human skin ; differential scanning calorimetry , small-angle X-ray diffraction and enhancer uptake studies', *International Journal of Pharmaceutics*, 127, pp. 9–26.
- Cowan, M. M. (1999) 'Plant Products as Antimicrobial Agents', *American Society for Microbiology*, 12(4), pp. 564–582.
- Croda Europe Ltd (2009) 'Span and Tween', *Www.Croda.Com/Europe*, 44(0), pp. 6–11.
- D.Attwood (2013) *Aulton's Pharmaceutics..*
- Day, M. J. and Russell, A. D. (1993) 'Antibacterial activity of chlorhexidine', *Journal of Hospital Infection*, 25(4), pp. 229–238.
- Deckman, H. W. et al. (1990) 'Development of Quantitative X-Ray Microtomography', *MRS Proceedings*. Cambridge University Press, 217, p. 97..
- Degreef, H. J. (1998) 'how to heal a wound fast', *Dermatologic Clinics*, 16(2), pp. 365–375.
- Denyer, S. P. (1995) 'Mechanisms of Action of Antibacterial Biocides', *International Biodeterioration & Biodegradation*, 36(3–4).
- DICK, I. P. and SCOTT, R. C. (1992) 'Pig Ear Skin as an In-vitro Model for Human Skin Permeability', *Journal of Pharmacy and Pharmacology*, 44(8), pp. 640–645. .
- Diegelmann, R. F. M. C. E. (2004) 'wound healing: an overview of acute, fibrotic and delayed healing', *Frontiers in Bioscience*, (4), pp. 283–289.
- Edwards, R. and Harding, K. G. (2004) 'Bacteria and wound healing', *Current Opinion in Infectious Diseases*, pp. 91–96.
- Eming, S. A. and Krieg, T. (2002) 'Treatment of Chronic Wounds : State of the Art and Future Concepts',

Cells Tissues Organs, pp. 105–117..

Fan, K. et al. (2011) 'State of the Art in Topical Wound-Healing Products', *Plastic and Reconstructive Surgery*, 127, pp. 44–59. .

Fang, C. L. et al. (2014) 'Delivery and targeting of nanoparticles into hair follicles', *Therapeutic Delivery*, 5(9), pp. 991–1006. .

Fedors, R. F. (1974) 'A method for estimating both the solubility parameters and molar volumes of liquids', *Polymer Engineering and Science*, 14(2), pp. 147–154. .

Femenía-Font, A. et al. (2005) 'Effect of chemical enhancers on the in vitro percutaneous absorption of sumatriptan succinate', *European Journal of Pharmaceutics and Biopharmaceutics*, 61(1–2), pp. 50–55. .

Flaten, G. E. et al. (2015) 'In vitro skin models as a tool in optimization of drug formulation', *European Journal of Pharmaceutical Sciences*. Elsevier B.V., 75, pp. 10–24. .

Fletcher, P. D. and Horsup, D. (1992) 'Droplet Dynamics in Water-in-oil Microemulsions and Macroemulsions stabilised by Non-ionic Surfactants Correlation of Measured Rates with Monolayer Bending Elasticity', *Journal of the Chemical Society*, 88(6), pp. 855–864.

Flores, A., Kingsley, A. (2007) 'topical antimicrobial dressings : an overview', *wound essential*, 2, pp. 182–185.

Fontes, D. D. H. et al. (2015) 'Experimental evaluation of thermal conductivity, viscosity and breakdown voltage AC of nanofluids of carbon nanotubes and diamond in transformer oil', *Diamond and Related Materials*. Elsevier B.V., 58, pp. 115–121. .

Forrest, M. L. and Kwon, G. S. (2008) 'Clinical developments in drug delivery nanotechnology', *Advanced Drug Delivery Reviews*, 60(8), pp. 861–862..

Fraise, A. et al. (2013) *Russel, Hugoe & Ayliffe's principles and practice of disinfection, preservation and sterilization*, 5th Edition. .

Frum, Y., Eccleston, G. M. and Meidan, V. M. (2008) 'In-vitro permeation of drugs into porcine hair follicles: is it quantitatively equivalent to permeation into human hair follicles?', *Journal of Pharmacy and Pharmacology*, 60(2), pp. 145–151. .

Gelfuso, G. M. et al. (2013) 'Iontophoresis-targeted, follicular delivery of minoxidil sulfate for the treatment of alopecia', *Journal of Pharmaceutical Sciences*, 102(5), pp. 1488–1494..

Gerald McDonnell, A. D. R. (1999) 'Antiseptics and Disinfectants : Activity , Action , and Resistance', *American Society for Microbiology*, 12(1), pp. 147–179.

Gilbane, A. J., Denton, C. P. and Holmes, A. M. (2013) 'Scleroderma pathogenesis : a pivotal role for fibroblasts as effector cells', *Arthritis Research & Therapy*.

Gilbert, P., Collier, P. J. and Brown, M. R. W. (1990) 'MINIREVIEW Influence of Growth Rate on Susceptibility to Antimicrobial Agents : Biofilms , Cell Cycle , Dormancy , and Stringent Response', *American Society for Microbiology*, 34(10), pp. .

Godin, B. and Touitou, E. (2007) 'Transdermal skin delivery : Predictions for humans from in vivo , ex vivo and animal models ☆', 59, pp. 1152–1161. .

Gomes, M. J. and Martins, S. (2014) 'Lipid nanoparticles for topical and transdermal application for alopecia treatment: development, physicochemical characterization, and in vitro release and penetration studies', pp. 1231–1242.

Gottardi, W. (1991) 'Iodine and iodine compounds', in *Disinfection, Sterilization, and Preservation*. 4th ed. Lea & Febiger, Philadelphia, Pa., pp. 152–166.

Govender, S. et al. (2003) 'A scalable membrane gradient reactor for enzyme production using *Phanerochaete chrysosporium*', *Biotechnology Letters*, 25(2), pp. 127–131.

Greenhalgh, D. J. et al. (1999) 'Solubility parameters as predictors of miscibility in solid dispersions', *Journal of Pharmaceutical Sciences*, 88(11), pp.

Güner, A. (2004) 'The algorithmic calculations of solubility parameter for the determination of interactions in dextran/certain polar solvent systems', *European Polymer Journal*, 40(7), pp. 1587–1594.

Guo, S. and Dipietro, L. A. (2010) 'Factors Affecting Wound Healing', *Journal of Dental Research*, (859), pp. 219–229. .

Guo, X., Rong, Z. and Ying, X. (2006) 'Calculation of hydrophile-lipophile balance for polyethoxylated surfactants by group contribution method', *Journal of Colloid and Interface Science*, 298(1), pp. 441–450.

Guzey, D. and McClements, D. J. (2006) 'Formation, stability and properties of multilayer emulsions for application in the food industry', *Advances in Colloid and Interface Science*, 128–130(2006), pp. 227–248. .

Haigh, J. M. and Smith, E. W. (1994) 'The selection and use of natural and synthetic membranes for in vitro diffusion experiments', *European Journal of Pharmaceutical Sciences*. Elsevier, 2(5–6), pp. 311–330.

Hancock, B., York, P. and Rowe, R. (1997) 'The use of solubility parameters in pharmaceutical dosage form design', *International Journal of Pharmaceutics*, 148, pp. 1–21. .

Hansen, C. M. (1967) 'The Three Dimensional Solubility Parameter and Solvent Diffusion Coefficient. Their Importance in Surface Coating Formulation', *J. Paint Technology*, p. 104.

Hansen, C. M. (2014) *Hansen solubility parameters. A user's Handbook*, Igarss 2014..

Hart, J. (2002) 'Inflammation 1: its role in the healing of acute wounds', *Journal of Wound Care*, 11(6), pp. 205–209.

HC Korting, C Schollmann, R. W. (2011) 'Management of minor acute cutaneous wounds: importance of wound healing in a moist environment', *Journal of the European Academy of Dermatology and Venereology*, pp. 130–137. .

Hemmila, M.R., Mattar, A., Taddonio, M.A., Arbabi, S., Hamouda, T., Ward, P.A., Wang, S.C., Baker, J. . (2010) 'Topical nanoemulsion therapy reduces bacterial wound infection and inflammation after burn injury', *Surgery*, pp. 499–509.

Hemmila, M. R. et al. (2010) 'Topical nanoemulsion therapy reduces bacterial wound infection and inflammation after burn injury', *Surgery*. Mosby, Inc., 148(3), pp. 499–509..

Hendry, E. R. et al. (2009) 'Antimicrobial efficacy of eucalyptus oil and 1, 8-cineole alone and in

combination with chlorhexidine digluconate against microorganisms grown in planktonic and biofilm cultures', *Journal of Antimicrobial Chemotherapy*, (October), pp. 1219–1225. .

Hermann Pinkus (1951) 'Examination of the Epidermis by the Strip Method of Removing Horny Layers: I. Observations on Thickness of the Horny Layer, and on Mitotic Activity After Stripping', *Journal of Investigative Dermatology*, 16(6), pp. 383–386. .

Hessien, M. et al. (2011) 'Stability and Tunability of O / W Nanoemulsions Prepared by Phase Inversion Composition', *Langmuir*, pp. 2299–2307. .

High-per, S. and Chromatograph, L. 'Shimadzu High-Per for mance Liquid Chromatograph'.

Hildebrand, J. H. and Scott, R. L. (1950) *The solubility of nonelectrolytes*. 3rd ed. Reinhold, New York.

Hsieh, J. (2009) 'Computed Tomography: Principles, Design, Artifacts, and Recent Advances'. .

Hung, L. C. et al. (2011) 'An improved method for the preparations of nanostructured lipid carriers containing heat-sensitive bioactives', *Colloids and Surfaces B: Biointerfaces*. Elsevier B.V., 87(1), pp. 180–186.

Ishihara, M. et al. (2002) 'Photocrosslinkable chitosan as a dressing for wound occlusion and accelerator in healing process', *Biomaterials*, 23, pp. 833–840.

Jafari, S. M. et al. (2008) 'Re-coalescence of emulsion droplets during high-energy emulsification', *Food Hydrocolloids*, 22(7), pp. 1191–1202. .

K.S. Lim and P.C.A. Kam (2008) 'Chlorhexidine--pharmacology and clinical applications', *Anaesthesia and Intensive Care*, 36(4), p. 502.

K, P. S. and Babu, M. (2000) 'Collagen based dressings Ð a review', 26, pp. 54–62.

Khan, H. A., Baig, F. K. and Mehboob, R. (2017) 'Journal of Tropical Biomedicine', *Asian Pacific Journal of Tropical Biomedicine*. Elsevier B.V., 7(5), pp. 478–482. .

King, J. W. (1995) 'Determination of the Solubility Parameter of Soybean Oil by Inverse Gas Chromatography', 195, pp. 190–195.

Kinney, J. H. and Nichols, M. C. (1992) 'X-Ray Tomographic Microscopy (XTM) Using Synchrotron Radiation', *Annual Review of Materials Science*, 22(1), pp. 121–152..

Kipp, J. E. (2004) 'The role of solid nanoparticle technology in the parenteral delivery of poorly water-soluble drugs', *International Journal of Pharmaceutics*, 284(1–2), pp. 109–122..

Klang, V. and Valenta, C. (2011) 'Lecithin-based nanoemulsions', *Journal of Drug Delivery Science and Technology*. Elsevier Masson SAS, 21(1), pp. 55–76. .

Klasen, H. J. (2000) 'Historical review of the use of silver in the treatment of burns . I . Early uses', *Burns*, 26.

Kooi, T. Van Der et al. (2017) 'Prevention of hospital infections by intervention and training (PROHIBIT): results of a pan - European cluster - randomized multicentre study to reduce central venous catheter - related bloodstream infections', *Intensive Care Medicine*. Springer Berlin Heidelberg..

Krauskopf, L. G. (1999) 'Prediction of plasticizer solvency using hansen solubility parameters', *Journal of Vinyl and Additive Technology*, 5(2), pp. 101–106. .

Kreilgaard, M. (2002) 'Influence of microemulsions on cutaneous drug delivery', *Advanced Drug Delivery Reviews*, 54(SUPPL.). .

Van Krevelen, D. W. (1976) *Properties of Polymers: Their Estimation And Correlation with Chemical Structure*. 2nd ed. Elsevier Scientific Publ.

VAN KREVELEN, D. W. (1997) *Acoustic Properties*. 3rd ed., *Properties of Polymers*. 3rd ed. Amsterdam,; Elsevier Scientific Publ.

Küchler, S. et al. (2009) 'Nanoparticles for skin penetration enhancement – A comparison of a dendritic core-multishell-nanotransporter and solid lipid nanoparticles', *European Journal of Pharmaceutics and Biopharmaceutics*. Elsevier B.V., 71(2), pp. 243–250.

Lademann, J. et al. (2006) 'Hair follicles - A long-term reservoir for drug delivery', *Skin Pharmacology and Physiology*, 19(4), pp. 232–236.

Lademann, J. et al. (2009) 'Determination of the cuticula thickness of human and porcine hairs and their potential influence on the penetration of nanoparticles into the hair follicles', *Journal of Biomedical Optics*, 14(2), pp. 021014-1-021014-4.

Laouini, A., Fessi, H. and Charcosset, C. (2012) 'Membrane emulsification: A promising alternative for vitamin E encapsulation within nano-emulsion', *Journal of Membrane Science*. Elsevier, 423–424, pp. 85–96.

Levy, E. J. et al. (1961) 'Identification of Components in Paraffin Wax by High Temperature Gas Chromatography and Mass Spectrometry', *Analytical Chemistry*, 33(6), pp. 698–704.

Li, J., Chen, J. and Kirsner, R. (2007) 'Pathophysiology of acute wound healing', *Clinics in Dermatology*, 25, pp. 9–18.

Maillard, J. et al. (1995) 'Effects of biocides on the transduction of *Pseudomonas aeruginosa* P A 0 by F116 bacteriophage', *Letters in Applied Microbiology*, pp. 19–22.

Mangram, J. A. et al. (1999) 'Guideline for prevention of surgical site infection', *Infection Control and Hospital Epidemiology*, 20(4), pp. 247–278.

Manning, P. (2009) *Chemical Bonds Essential chemistry*.

Mason, T. G. et al. (2006) 'Nanoemulsions: formation, structure, and physical properties', *Journal of Physics: Condensed Matter*, 18(41), pp. R635–R666.

Mcdonnell, G. and Russell, A. D. (1999) 'Antiseptics and disinfectants: Activity, action, and resistance', *Clinical Microbiology Reviews*, 12(1), pp. 147–179.

McGlashan, M. L. and Wormald, C. J. (1964) 'Second virial coefficients of some alk-1-enes, and of a mixture of propene + hept-1-ene', *Transactions of the Faraday Society*, 60(1 I), p. 646

Mehnert, W. and Mäder, M. (2001) 'Solid lipid nanoparticles: production, characterization and applications.', *Adv. Drug Del. Rev. Del Rev*, 47, pp. 165–196.

Mohammad, M. A., Alhalaweh, A. and Velaga, S. P. (2011) 'Hansen solubility parameter as a tool to predict cocrystal formation', *International Journal of Pharmaceutics*. Elsevier B.V., 407(1–2), pp. 63–71.

Monaco, J. L. and W. Thomas Lawrence (2003) 'Acute wound healing An overview', 30, pp. 1–12.

Morse, A. (2009) 'Reducing Healthcare Associated Infections in Hospitals in England', National Audit Office, (June), pp. 1–69.

Myers, D. (1999) *Surfaces, Interfaces and Colloids — Principles and Applications*, Talanta.

Naik, A. et al. (2004) 'Visualization of skin penetration using confocal laser scanning microscopy', *European Journal of Pharmaceutics and Biopharmaceutics*, 58, pp. 301–316

Ngawhirunpat, T. et al. (2008) 'Evaluation of Simultaneous Permeation and Metabolism of Methyl Nicotinate in Human, Snake, and Shed Snake Skin', *Pharmaceutical Development and Technology*, pp. 75–83

NICE guideline (2008) 'Surgical site infections : prevention and treatment', National Institute for Health and Care Excellence,

Orafidiya, L. O. and Oladimeji, F. A. (2002) 'Determination of the required HLB values of some essential oils', *International Journal of Pharmaceutics*, 237(1–2), pp. 241–249.

Ossadnik, M. et al. (2007) 'Differential stripping : introduction of a method to show the penetration of topically applied antifungal substances into the hair follicles', pp. 457–462.

Otberg, N. et al. (2004) 'Variations of hair follicle size and distribution in different body sites.', *The Journal of investigative dermatology*, 122(1), pp. 14–19.

Patzelt, A. et al. (2011) 'Selective follicular targeting by modification of the particle sizes', *Journal of Controlled Release. Elsevier B.V.*, 150(1), pp. 45–48.

Percival, S. L. et al. (2012) 'Microbiology of the skin and the role of biofilms in infection', *International Wound Journal*, 9(1).

Peter T et al. (2000) 'two-photon excitation fluorescence microscopy', *European Journal of Pharmaceutics and Biopharmaceutics*, 71(2), pp. 399–429.

Phillip M. Williford (1999) 'OPPORTUNITIES FOR MUPIROCIN CALCIUM CREAM IN THE EMERGENCY DEPARTMENT', *The Journal of Emergency Medicine*, 17(1), pp. 213–220.

Price, G. J., Guillet, J. E. and Purnell, J. H. (1986) 'Measurement of solubility parameters by gas-liquid chromatography', *Journal of Chromatography A*, 369(C), pp. 273–280.

Prow, T. W. et al. (2011) 'Nanoparticles and microparticles for skin drug delivery', *Advanced Drug Delivery Reviews. Elsevier B.V.*, 63(6), pp. 470–491.

Qian, C. and McClements, D. J. (2011) 'Food Hydrocolloids Formation of nanoemulsions stabilized by model food-grade emulsifiers using high-pressure homogenization : Factors affecting particle size', *Food hydrocolloids. Elsevier Ltd*, 25(5), pp. 1000–1008.

Quinn, K. J. et al. (1985) 'Principles of burn dressings', 6, pp. 369–377.

Raber, A. S. et al. (2014) 'Quantification of nanoparticle uptake into hair follicles in pig ear and human forearm', *Journal of Controlled Release. Elsevier B.V.*, 179(1), pp. 25–32.

Ramasasthy, S. S. (2005) 'Acute Wounds', *Clinical Plastic Suregry*, 32, pp. 195–208.

RAMOS-E-SILVA, R. M. C. R. (2002) 'New Dressings, Including Tissue-Engineered Living Skin', *Clinics in Dermatology*, 20, pp. 715–723.

- Ramos, A. I., Braga, S. S. and Almeida Paz, F. A. (2009) 'Triclosan', *Acta Crystallographica Section C Crystal Structure Communications*, 65(8), pp. o404–o405.
- Robson, M. C. D. L. S. (2001) 'Wound Healing: Biologic Features and Approaches to Maximize Healing Trajectories', *Current Problems in Surgery*, 38(2).
- Roduner, E. (2006) 'Size matters: Why nanomaterials are different', *Chemical Society Reviews*, 35(7), pp. 583–592.
- Rølla, P. B. G. (1994) 'Triclosan protects the skin against dermatitis caused by sodium lauryl sulphate exposure', *Journal of clinical Periodontology*, (III), pp. 717–719.
- Salvo, L. et al. (2010) '3D imaging in material science: Application of X-ray tomography', *Comptes Rendus Physique. Elsevier Masson SAS*, 11(9–10), pp. 641–649.
- Sapra, B., Jain, S. and Tiwary, A. K. (2008) 'Percutaneous Permeation Enhancement by Terpenes: Mechanistic View', *Journal of the American Association of Pharmaceutical Scientists*, 10(1), pp. 120–132.
- Schaberg, D. R. (1994) 'Resistant Gram-positive organisms', *Annals of Emergency Medicine*, 24(3), pp. 462–464.
- Scheuplein, R. J. (1965) 'mechanism of percutaneous adsorption sense the stratum corneum is a macroscopic Blank (I) and Blank and Scheuplcin (JJ) 1 and epidermal membranes makes possible a sion : stants so obtained arc truly representative of', 45(5), pp. 334–347.
- Schmid-Wendtner, M. H. and Korting, H. C. (2006) 'The pH of the skin surface and its impact on the barrier function', *Skin Pharmacology and Physiology*, 19(6), pp. 296–302.
- Schmidts, T. et al. (2010) 'Multiple W/O/W emulsions-Using the required HLB for emulsifier evaluation', *Colloids and Surfaces A: Physicochemical and Engineering Aspects. Elsevier B.V.*, 372(1–3), pp. 48–54.
- Schultz, G. S. et al. (2002) 'Wound bed preparation : a systematic approach to wound management', *Wound Repair and Reperation*,
- Scott, G. (1992) Properties of polymers. Their correlation with chemical structure; their numerical estimation and prediction from additive group contributions, *Endeavour*.
- Seid Mahdi Jafari, Yinghe He, B. B. (2007) 'Production of sub-micron emulsions by ultrasound and microfluidization techniques', *Journal of Food Engineering*, 82, pp. 478–488.
- Shafiq, S. et al. (2007) 'Development and bioavailability assesment of ramipril nanoemulsion formulation', *European Journal of Pharmaceutics and Biopharmaceutics*, 66(2), pp. 227–243.
- Shahavi, M. H. et al. (2015) 'Evaluation of critical parameters for preparation of stable clove oil nanoemulsion', *Arabian Journal of Chemistry. King Saud University*.
- Shupp, J. W. et al. (2010) 'A review of the local pathophysiologic bases of burn wound progression', *Journal of Burn Care and Research*, 31(6), pp. 849–873.
- Silva, S. M. et al. (2011) 'Essential oils from different plant parts of *Eucalyptus cinerea* F. Muell. ex Benth. (Myrtaceae) as a source of 1,8-Cineole and their bioactivities', *Pharmaceutics*, 4(12), pp. 1535–1550.
- Small, H. et al. (2013) 'Efficacy of Adding 2 % (w / v) Chlorhexidine Gluconate to 70 % (v / v) Isopropyl Alcohol for Skin Disinfection Prior to Peripheral Venous Cannulation', 29(10), pp. 17–20.

Solans, C. et al. (2005) 'Nano-emulsions', *Current Opinion in Colloid and Interface Science*, 10(3–4), pp. 102–110.

Sonam Vats and , Charu Saxena, TS Easwari, V. S. (2014) 'Emulsion Based Gel Technique: Novel Approach for Enhancing Topical Drug Delivery of Hydrophobic Drugs', *International Journal for Pharmaceutical Research Scholar*

Subrahmanyam, C. V. S., Prakash, K. R. and Rao, P. G. (1996) 'Estimation of the solubility parameter of trimethoprim by current methods', *Pharmaceutica Acta Helvetiae*, 71(3), pp. 175–183.

Szycher, M. and Lee, S. J. (1992) 'Modern Wound Dressings : A Systematic Approach to', *Journal of Biomaterials Applications*.

Tadros, T. et al. (2004) 'Formation and stability of nano-emulsions', *Advances in Colloid and Interface Science*, 108–109, pp. 303–318.

Teichmann, A. et al. (2005) 'Differential Stripping : Determination of the Amount of Topically Applied Substances Penetrated into the Hair Follicles', pp. 264–269.

Teichmann, A. et al. (2006) 'Follicular Penetration : Development of a Method to Block the Follicles Selectively against the Penetration of Topically Applied Substances', *Skin Pharmacology and Physiology*, 19(4), pp. 216–223.

Thiboutot, D. (2004) 'Regulation of Human Sebaceous Glands', *Journal of Investigative Dermatology*. Elsevier Masson SAS, 123(1), pp. 1–12.

Thielitz, A. et al. (2001) 'Lipid analysis of follicular casts from cyanoacrylate strips as a new method for studying therapeutic effects of antiacne agents', *British Journal of Dermatology*.

Tortora, G. J. and Derrickson, B. (2014) *Principles of Anatomy and Physiology*, Wiley.

Tregear, R. T. (1966) 'The Permeability of Mammalian Skin to Ions', *Journal of Investigative Dermatology*. Elsevier Masson SAS, 46(1), pp. 16–23.

Uchechi, O., Ogbonna, J. D. N. and Attama, A. a (2014) 'Nanoparticles for Dermal and Transdermal Drug Delivery', *Application of Nanotechnology in Drug Delivery*, pp. 193–235.

Ueno, H. et al. (1999) 'Accelerating effects of chitosan for healing at early phase of experimental open wound in dogs', *Biomaterials*, 20, pp. 1407–1414.

Valiveti, S. and Lu, G. W. (2007) 'Diffusion properties of model compounds in artificial sebum', *International Journal of Pharmaceutics*, 345(1–2), pp. 88–94.

Valiveti, S., Wesley, J. and Lu, G. W. (2008) 'Investigation of drug partition property in artificial sebum', 346, pp. 10–16.

Voelkel, A. and Fall, J. (1996) 'Influence of prediction method of the second virial coefficient on inverse gas chromatographic parameters', *Journal of Chromatography A*, 721(1), pp. 139–145.

Waalder, S. M. et al. (1993) 'Effects of oral rinsing with triclosan and sodium lauryl sulfate on dental plaque formation: a pilot study.', *Scandinavian journal of dental research*, 101(4), pp. 192–5.

Wichterle, O., Lim, D. (1960) 'Hydrophilic gels for biological use', *Nature*, 185, pp. 117–118.

Williams, A. C. (2007) 'Topical and transdermal drug delivery', in *Aulton's Pharmaceutics*. Elsevier Ltd,

pp. 675–697.

Witte, M. B. and Barbul, A. (1997) 'GENERAL PRINCIPLES OF WOUND HEALING', *Surgical Clinics of North America*, 77(3), pp. 509–528.

Wosicka, H. and Cal, K. (2010) 'Targeting to the hair follicles : Current status and potential', 57, pp. 83–89.

Yang, S. C. and Benita, S. (2000) 'Enhanced absorption and drug targeting by positively charged submicron emulsions', *Drug Development Research*, 50(3–4), pp. 476–486.

Yuan, Y. and Gao, Y. (2008) 'Characterization and stability evaluation of β -carotene nanoemulsions prepared by high pressure homogenization under various emulsifying conditions', 41, pp. 61–68.

Zhao, L. et al. (2013) 'Nanoemulsion improves the oral bioavailability of baicalin in rats: In vitro and in vivo evaluation', *International Journal of Nanomedicine*, 8, pp. 3769–3779.

Zhao, Y. et al. (2010) 'Self-nanoemulsifying drug delivery system (SNEDDS) for oral delivery of Zedoary essential oil: Formulation and bioavailability studies', *International Journal of Pharmaceutics*, 383(1–2), pp. 170–177.

Ziani, K. et al. (2011) 'Manipulating interactions between functional colloidal particles and polyethylene surfaces using interfacial engineering', *Journal of Colloid and Interface Science*. Elsevier Inc., 360(1), pp. 31–38.

Chapter 8 – Publications

These publications contributed towards partial aspects of this PhD

- Campanile, Antonella, Morral, Kim, Aljammal, Mohammad Khaled, Felix, Owusu-Kwarteng, Elena, Tillotson, Shabbir, Mohammed, Beadham, Ian G. and MorralCardoner, Jordi, (2015) "Development of a versatile laboratory experiment to teach the metabolic transformation of hydrolysis" *British Journal of Pharmacy*
- Maen Alshafiee; Mohammad K Aljammal; Daniel Markl; Adam Ward; Karl Walton; Liam Blunt; Sachin Korde; Sudhir Pagire; Adrian L Kelly; Anant Paradkar; Barbara R Conway, (2019) "Hot-melt extrusion process impact on polymer choice of Glyburide solid dispersions: The effect of wettability and dissolution" *International Journal of Pharmaceutics*
- M.KH. AL-Jammal, M. Bashimam, M.B. alserawan M. A. Mohammad, B. R. Conway, (2020) "Hansen solubility parameter as a tool to predict a miscibility of different materials in artificial sebum" manuscript ready for submission
- M.KH. AL-Jammal, Ghori, M. U,M. A. Mohammad, B. R. Conway, (2020) "Quantitative and Qualitative assessing follicular delivery of triclosan formulation using tape stripping techniques and CT scanning" manuscript ready for submission

Appendices

Appendix A

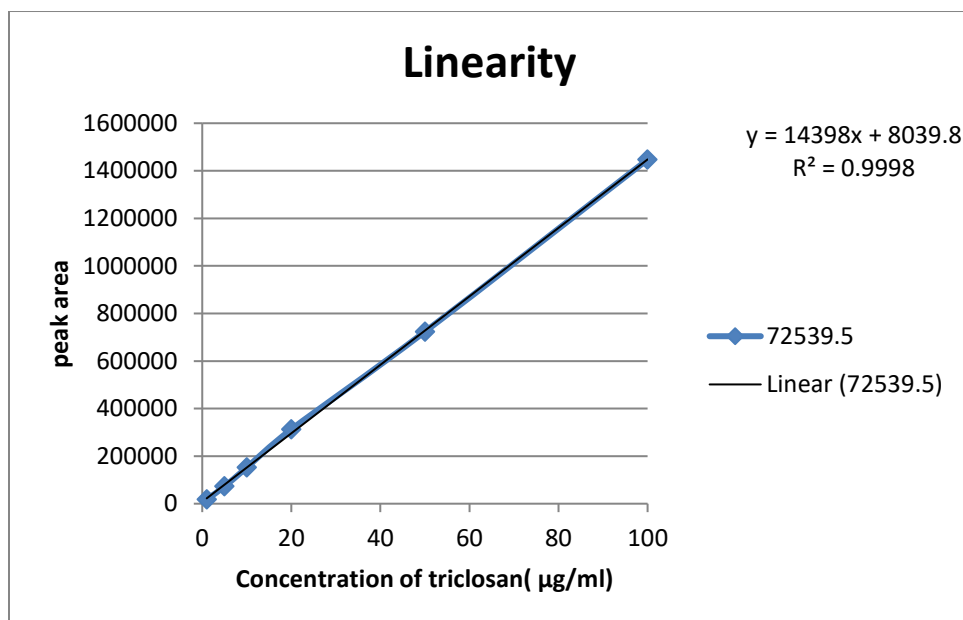
These are the linearity test for five groups (A, B, C, D, and E), all groups have a high regression coefficient (R2) more than 0.99

Group A

This table shows the peak area for each concentration of Triclosan.

Group A			
concentration of Triclosan(µg/ml)	peak area of triclosan		
	Run 1	Run 2	Average
100	1446164	1448123	1447143.5
50	723142	723558	723350
20	311980	313153	312566.5
10	151937	152746	152341.5
5	72566	72513	72539.5
1	18392	18082	18237

This graph shows the linearity curve of group A

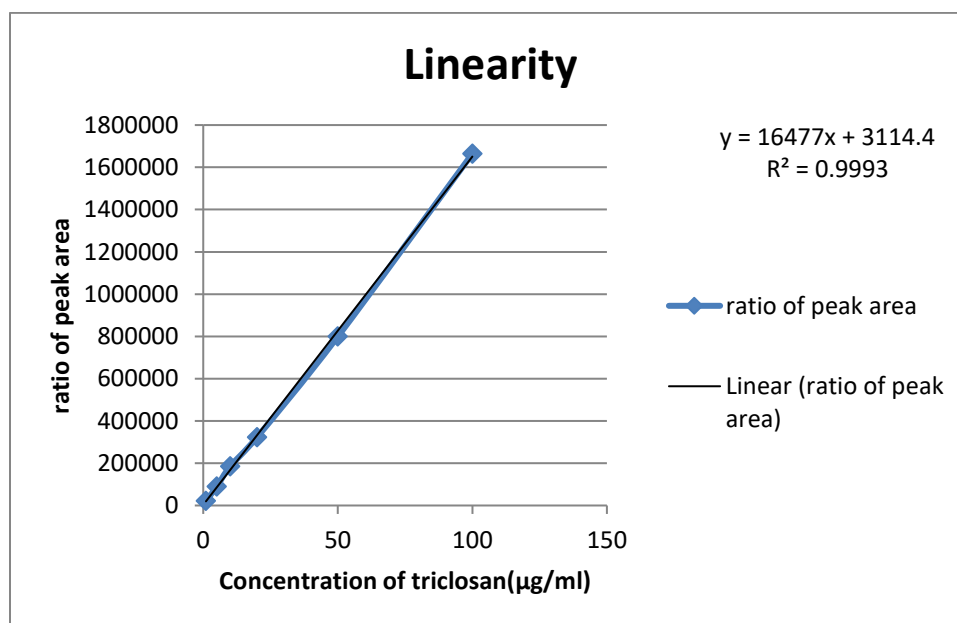


Group B

This table shows the ratio of peak area to each concentration of Triclosan.

Group B			
Concentration of Triclosan (µg/ml)	peak area of triclosan		
	Run 1	Run 2	Average
100	1665021	1664258	1664639.5
50	799664	798692	799178
20	323115	323367	323241
10	184160	186416	185288
5	88765	88966	88865.5
1	22309	22037	22173

This graph shows the linearity curve of group B

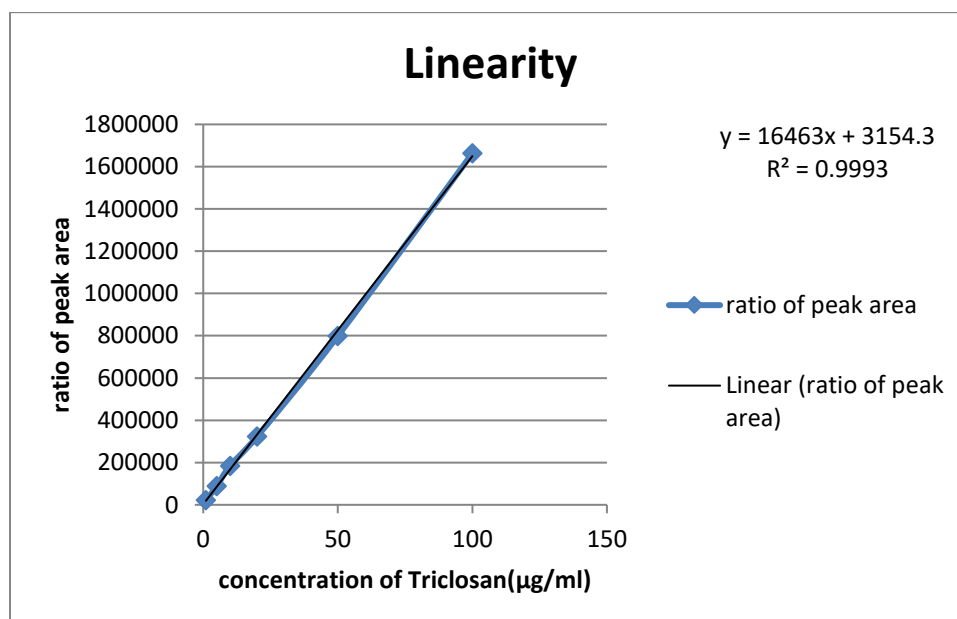


Group C

This table shows the ratio of peak area to each concentration of Triclosan.

Group C			
concentration of Triclosan($\mu\text{g/ml}$)	peak area of Triclosan		
	Run 1	Run 2	Average
100	1663627	1662768	1663197.5
50	798610	798971	798790.5
20	323629	322736	323182.5
10	184758	185397	185077.5
5	88917	88659	88788
1	22173	22014	22093.5

This graph shows the linearity curve of group C

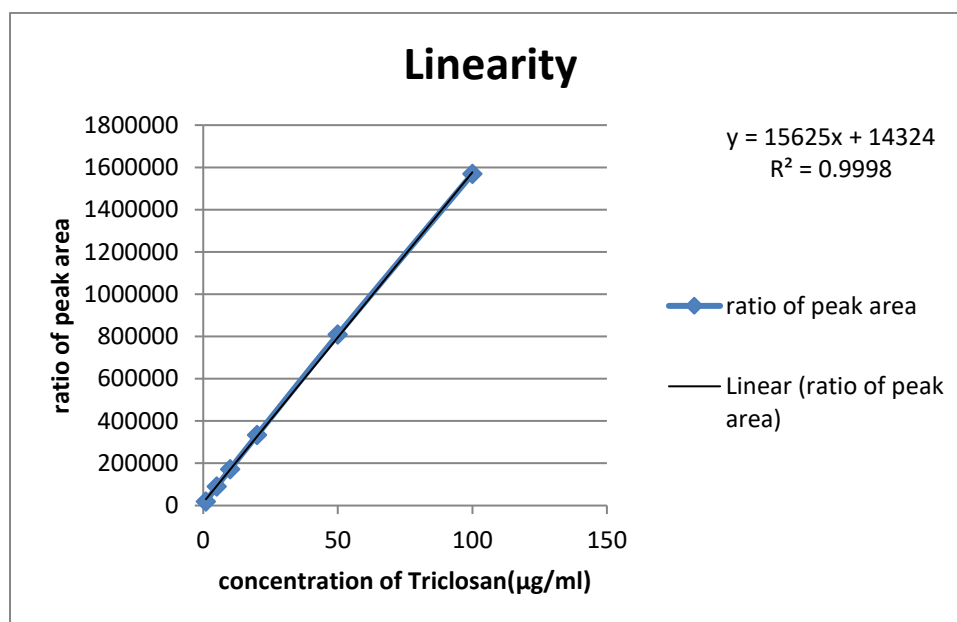


Group D

This table shows the ratio of peak area to each concentration of Triclosan.

Group D			
concentration of Triclosan($\mu\text{g/ml}$)	peak area of triclosan		
	Run 1	Run 2	Average
100	1569013	1569088	1569050.5
50	808935	808177	808556
20	333507	333582	333544.5
10	172550	171881	172215.5
5	89710	89751	89730.5
1	19010	19128	19069

This graph shows the linearity curve of group D

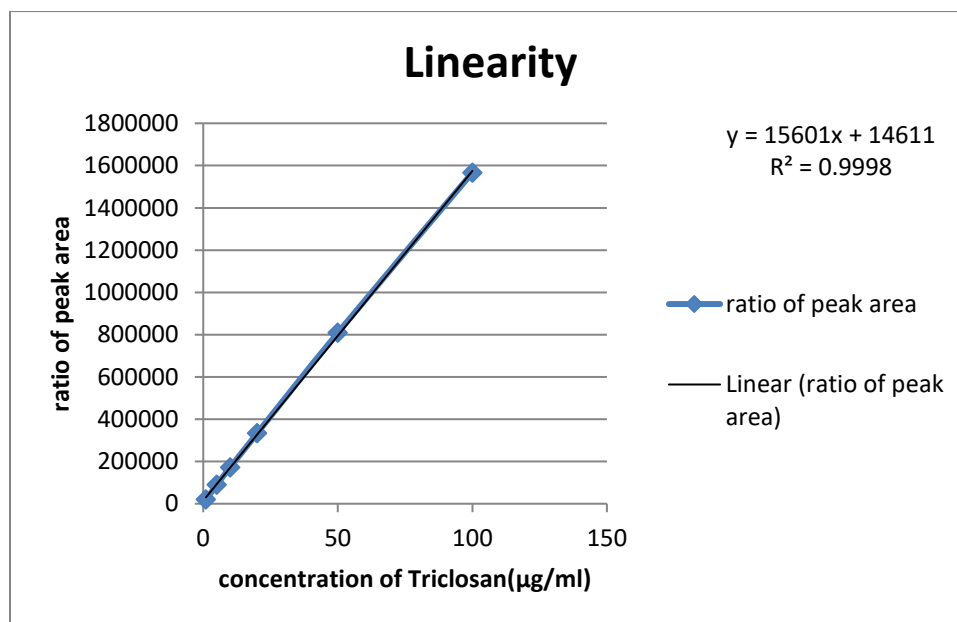


Group E

This table shows the ratio of peak area to each concentration of Triclosan.

Group E			
concentration of Triclosan($\mu\text{g/ml}$)	peak area of triclosan		
	Run 1	Run 2	Average
100	1566551	1566551	1566551
50	808407	809022	808714.5
20	332702	333217	332959.5
10	172145	171817	171981
5	89649	89933	89791
1	19843	19121	19482

This graph shows the linearity curve of group E



Appendix B

number of Run	High (80 µg/ml)	Medium (40 µg/ml)	Low (4 µg/ml)
	peak area of Triclosan	peak area of Triclosan	peak area of Triclosan
1	1293147	658114	80667
2	1292403	656896	80484
3	1291875	655941	80893
4	1292364	656542	80626
5	1290910	657072	80733
Mean	1292139.8	656913	80680.6
Standard Deviation	824.0932593	798.4979649	149.7307584
Relative standard Deviation (RSD)	0.063777407	0.121553077	0.185584587

This table shows the Relative standard Deviation (RSD) for intra-day precision

This table shows the Relative Standard Deviation (RSD) for inter-day precision for the first day.

First Day			
number of Run	High (80 µg)	Medium (40 µg)	Low (4 µg)
	peak area of Triclosan	peak area of Triclosan	peak area of Triclosan
1	1289595	657496	83654
2	1289054	657766	83854
3	1289627	657626	83298
4	1289465	656948	82987
5	1289765	656606	83169
Mean	1289501.2	657288.4	83392.4
Standard Deviation	271.8054451	491.6083807	355.2031813
Relative standard Deviation (RSD)	0.02107834	0.074793406	0.42594191

This table shows the Relative Standard Deviation (RSD) for inter-day precision for the second day.

Second Day			
number of Run	High (80 µg)	Medium (40 µg)	Low (4 µg)
	peak area of Triclosan	peak area of Triclosan	peak area of Triclosan
1	1293147	658114	80667
2	1292403	656896	80484
3	1291875	655941	80893
4	1292364	656542	80626
5	1290910	657072	80733
Mean	1292139.8	656913	80680.6
Standard Deviation	824.0932593	798.4979649	149.7307584
Relative standard Deviation (RSD)	0.063777407	0.121553077	0.185584587

This table shows the Relative Standard Deviation (RSD) for inter-day precision for the third day.

Third-Day			
number of Run	High (80 µg)	Medium (40 µg)	Low (4 µg)
	peak area of Triclosan	peak area of Triclosan	peak area of Triclosan
1	1304469	664987	83234
2	1305671	664794	83853
3	1305094	664209	83873
4	1304840	664062	82926
5	1305601	664686	83325
Mean	1305135	664547.6	83442.2
Standard Deviation	509.095767	394.7775323	411.6706208
Relative standard Deviation (RSD)	0.039007135	0.059405456	0.493360219

This table shows the Relative Standard Deviation (RSD) for inter-day precision for the fourth day.

fourth Day			
number of Run	High (80 µg)	Medium (40 µg)	Low (4 µg)
	peak area of Triclosan	peak area of Triclosan	peak area of Triclosan
1	1314925	672797	83490
2	1313902	666843	82808
3	1313706	672444	83050
4	1304024	672665	83113
5	1305098	671424	83720
Mean	1310331	671234.6	83236.2
Standard Deviation	5301.180057	2513.553719	364.5822267
Relative standard Deviation (RSD)	0.40456801	0.374467246	0.438009216

This table shows the Relative Standard Deviation (RSD) for inter-day precision for the fifth day.

Fifth Day			
number of Run	High (80 µg)	Medium (40 µg)	Low (4 µg)
	peak area of Triclosan	peak area of Triclosan	peak area of Triclosan
1	1314092	666534	83056
2	1313934	666235	83258
3	1313930	667342	83180
4	1312818	666424	82893
5	1313033	665428	83019
Mean	1313561.4	666392.6	83081.2
Standard Deviation	589.0847138	685.1334177	142.2522408
Relative standard Deviation (RSD)	0.044846378	0.102812279	0.171220734

Appendix C

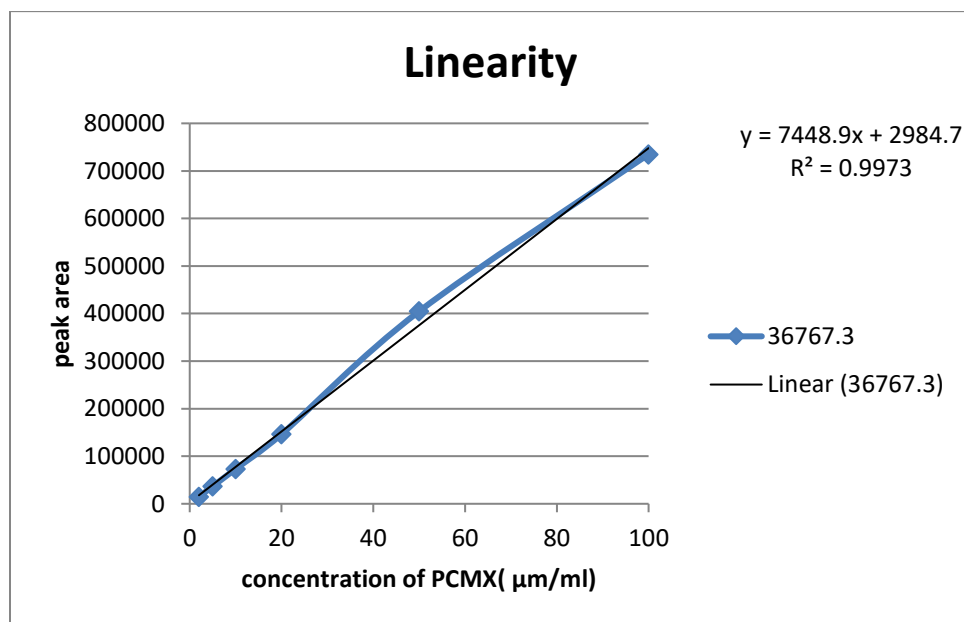
These are the linearity test for five groups (A, B, C, D, and E), all groups have a high regression coefficient (R2) more than 0.99

Group A

This table shows the peak area for each concentration of Triclosan.

Group A			
concentration of PCMX($\mu\text{g}/\text{ml}$)	Peak area of PCMX		
	Run 1	Run 2	Average
100	734949.2	734707.4	734993.8
50	404944.5	404835.5	404741.2
20	146449	146216.2	146329.9
10	73227.2	73178.2	73305
5	36688.4	36708.3	36767.3
2	14749.5	14806.7	14708

This graph shows the linearity curve of group A

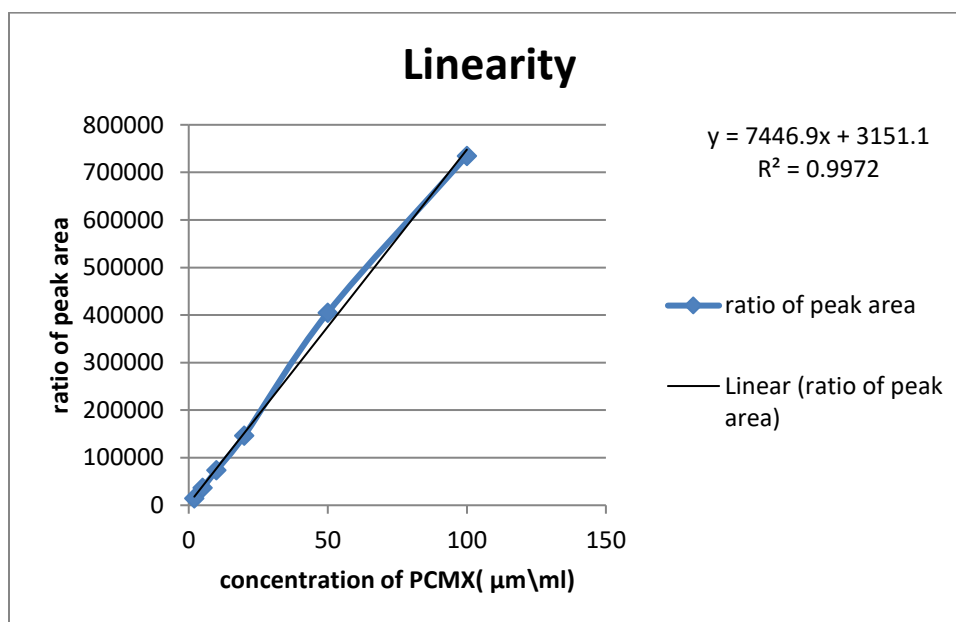


Group B

This table shows the ratio of peak area to each concentration of Triclosan.

Group B			
Concentration of PCMX ($\mu\text{g}/\text{ml}$)	Peak area of PCMX		
	Run 1	Run 2	Average
100	734910.9	734710.6	734812.6
50	404874.2	404982	405082.6
20	146051.5	146458.3	146602.6
10	73478.6	73460.8	73528.2
5	36476.8	36717.7	36598.4
2	14708	14846.6	14859.8

This graph shows the linearity curve of group B

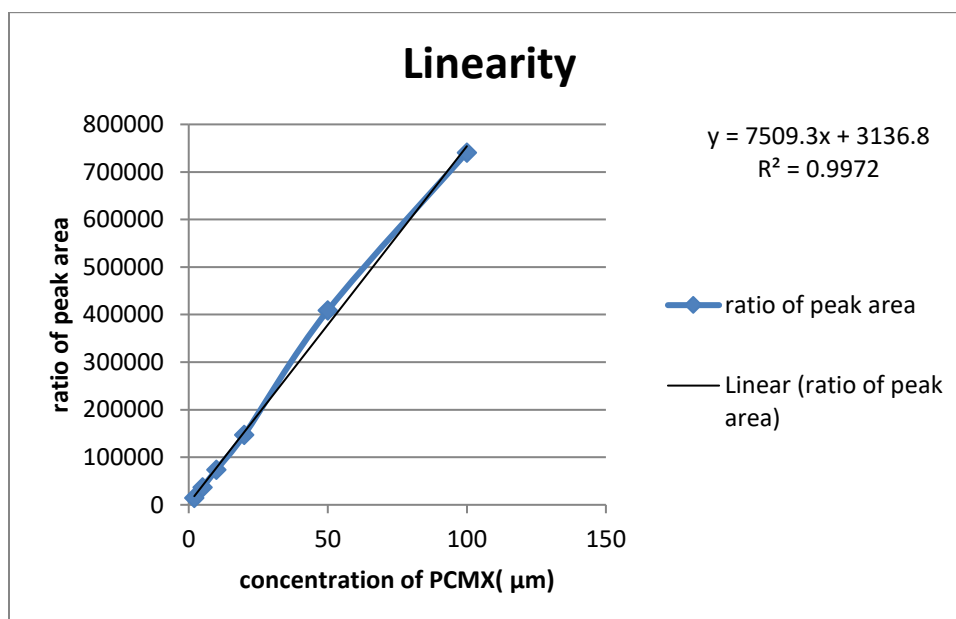


Group C

This table shows the ratio of peak area to each concentration of Triclosan.

Group C			
concentration of PCMX($\mu\text{g}/\text{ml}$)	Peak area of PCMX		
	Run 1	Run 2	Average
100	741532.8	741485.5	740835.2
50	407701.6	408114.5	408741.7
20	147562	147402.5	147502
10	74046.8	73699	73948.3
5	36973.3	36976.9	37178.6
2	15019.4	14917.1	14861.2

This graph shows the linearity curve of group C

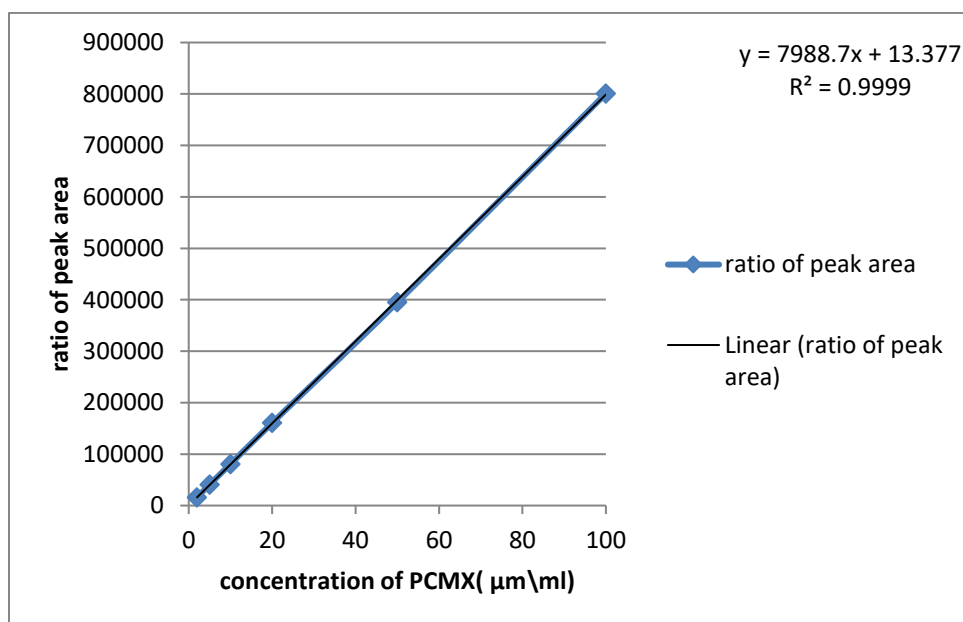


Group D

This table shows the ratio of peak area to each concentration of Triclosan.

Group D			
concentration of PCMX ($\mu\text{g}/\text{ml}$)	Peak area of PCMX		
	Run 1	Run 2	Average
100	801302.9	800532.4	800792.9
50	394499.7	395023.8	395023.8
20	160610.1	160607.8	160636.4
10	80696.1	80646.6	80750.7
5	40762.4	40913.8	40835.6
2	16216.3	16083.1	15920

This graph shows the linearity curve of group D

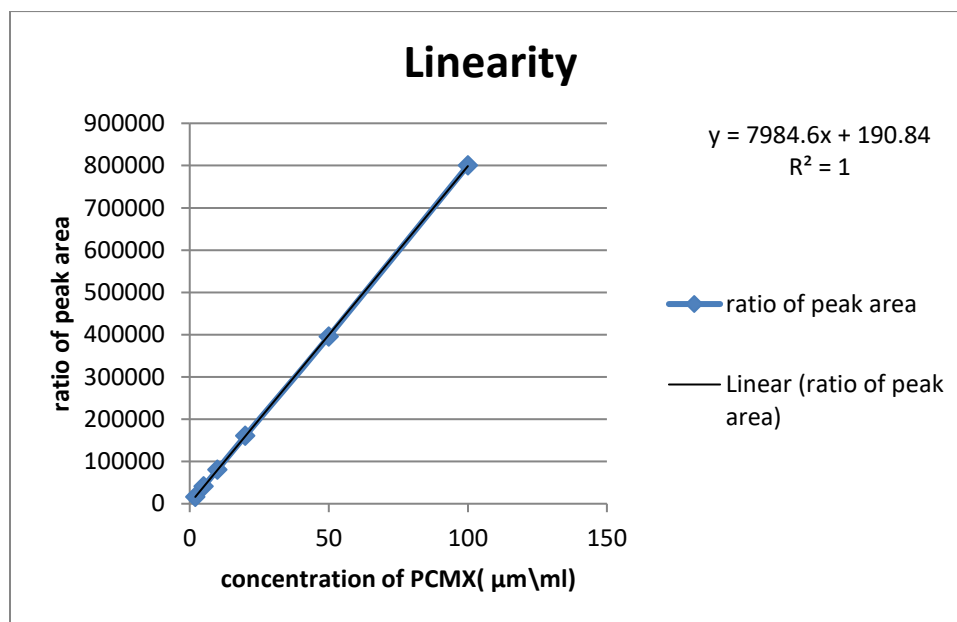


Group E

This table shows the ratio of peak area to each concentration of Triclosan.

Group E			
concentration of PCMX ($\mu\text{g}/\text{ml}$)	Peak area of PCMX		
	Run 1	Run 2	Average
100	800714	800846.8	800274.8
50	394603.9	395058.6	395610.2
20	160535.6	160486.5	160791.9
10	80568.8	80662.9	80680.9
5	40685.2	40797.7	40748.8
2	15982.8	16006.3	16153.6

This graph shows the linearity curve of group E



Appendix D

number of Run	High (80 µg/ml)	Medium (40 µg/ml)	Low (4 µg/ml)
	Peak area of PCMX	Peak area of PCMX	Peak area of PCMX
1	593852.1	298126.7	29462.7
2	593759.8	297765.6	29495.6
3	593891.8	297839.3	29480.1
4	593594.8	298251.8	29593.9
5	593805.5	297558.4	29566.4
Mean	593780.8	297908.36	29519.74
Standard Deviation	115.1648601	279.8415141	57.19373217
Relative standard Deviation (RSD)	0.019395181	0.093935435	0.193747412

This table shows the Relative standard Deviation (RSD) for intra-day precision

This table shows the Relative Standard Deviation (RSD) for inter-day precision for the first day.

First Day			
number of Run	High (80 µg)	Medium (40 µg)	Low (4 µg)
	Peak area of PCMX	Peak area of PCMX	Peak area of PCMX
1	589091.4	296194.2	29473.8
2	586285.8	296442.8	29672.2
3	588219	296554.3	29419.8
4	588674.7	296431.9	29254.6
5	587630.8	296833.5	29254.6
Mean	587980.34	296491.34	29415
Standard Deviation	1091.695098	231.9584295	173.9889652
Relative standard Deviation (RSD)	0.18566864	0.07823447	0.591497417

This table shows the Relative Standard Deviation (RSD) for inter-day precision for the second day.

Second Day			
number of Run	High (80 µg)	Medium (40 µg)	Low (4 µg)
	Peak area of PCMX	Peak area of PCMX	Peak area of PCMX
1	588791.4	296192	29473.8
2	585285.8	296217.4	29672.2
3	589218	295374.4	29419.8
4	588874.7	296404.7	29254.6
5	589430.8	295453.1	29254.6
Mean	588320.14	295928.32	29415
Standard Deviation	1715.849661	477.6750224	173.9889652
Relative standard Deviation (RSD)	0.291652375	0.161415786	0.591497417

This table shows the Relative Standard Deviation (RSD) for inter-day precision for the third day.

Third-Day			
number of Run	High (80 µg)	Medium (40 µg)	Low (4 µg)
	Peak area of PCMX	Peak area of PCMX	Peak area of PCMX
1	591999.7	297951.5	29473.8
2	591521.5	297187.3	29672.2
3	591015.6	297568.6	29419.8
4	590192	296814.2	29254.6
5	590477.5	297125.3	29254.6
Mean	591041.26	297329.38	29415
Standard Deviation	739.7573947	439.1768744	173.9889652
Relative standard Deviation (RSD)	0.125161718	0.147707191	0.591497417

This table shows the Relative Standard Deviation (RSD) for inter-day precision for the fourth day.

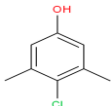
fourth Day			
number of Run	High (80 µg)	Medium (40 µg)	Low (4 µg)
	Peak area of PCMX	Peak area of PCMX	Peak area of PCMX
1	593852.1	298126.7	29462.7
2	593759.8	297765.6	29495.6
3	593891.8	297839.3	29480.1
4	593594.8	298251.8	29593.9
5	593805.5	297558.4	29566.4
Mean	593780.8	297908.36	29519.74
Standard Deviation	115.1648601	279.8415141	57.19373217
Relative standard Deviation (RSD)	0.019395181	0.093935435	0.193747412

This table shows the Relative Standard Deviation (RSD) for inter-day precision for the fifth day.

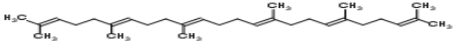
Fifth Day			
number of Run	High (80 µg)	Medium (40 µg)	Low (4 µg)
	Peak area of PCMX	Peak area of PCMX	Peak area of PCMX
1	595840.9	298858.9	29735.8
2	596057.6	299022	29468.5
3	595817	299029.3	29582.7
4	595879.8	299051.9	29655.7
5	595984.2	299230.3	29588.2
Mean	595915.9	299038.48	29606.18
Standard Deviation	101.8002947	131.8899617	98.84830297
Relative standard Deviation (RSD)	0.017082997	0.044104679	0.333877261

APPENDIX E

Chloroxylenol

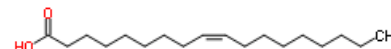
Structural group	Frequency	F_{di} ($J^{1/2} \cdot cm^{3/2} \cdot mol^{-1}$)	F_{pi}^2 ($J^{1/2} \cdot cm^{3/2} \cdot mol^{-1}$)	E_{hi} (J/mol)	V (cm^3/mol)	Molecular weight (g/mol)
-CH3	2	840	0	0	67	30.07
(o,m,p) phenylene	1	1270	12100	0	52.4	75.09
-Cl	1	450	302500	400	24	35.45
-OH	1	210	250000	20000	10	17.01
more planes of symmetry			calculated Molar Volume		153.4	
$\Sigma=$		2770	564600	20400		157.62
$\delta_D = \Sigma F_D / MV$	18.06					
$\delta_P = (\Sigma F_P^2)^{1/2} / MV$	4.90					
$\delta_H = (\Sigma F_H / MV)^{1/2}$	11.53					
$\delta = (\delta_D^2 + \delta_P^2 + \delta_H^2)^{1/2}$	21.98					

SQUALENE

Structural group	Frequency	F_{di} ($J^{1/2} \cdot cm^{3/2} \cdot mol^{-1}$)	F_{pi}^2 ($J^{1/2} \cdot cm^{3/2} \cdot mol^{-1}$)	E_{hi} (J/mol)	V (cm^3/mol)	Molecular weight (g/mol)
-CH3	8	3360	0	0	268	120.28
-CH2-	10	2700	0	0	161	140.27
=CH-	6	1200	0	0	81	78.11
=C<	6	420	0	0	-33	72.07
more planes of symmetry			calculated Molar Volume		477	
$\Sigma=$		7680	0	0		410.73
$\delta_D = \Sigma F_D / MV$	16.10					
$\delta_P = (\Sigma F_P^2)^{1/2} / MV$	0.00					
$\delta_H = (\Sigma F_H / MV)^{1/2}$	0.00					
$\delta = (\delta_D^2 + \delta_P^2 + \delta_H^2)^{1/2}$	16.10					

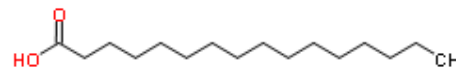
OLEIC ACID

Structural group	Frequency	F_{di} ($J^{1/2} \cdot cm^{3/2} \cdot mol^{-1}$)	F_{pi}^2 ($J^{1/2} \cdot cm^{3/2} \cdot mol^{-1}$)	E_{hi} (J/mol)	V (cm^3/mol)	Molecular weight (g/mol)
-CH ₃	1	420	0	0	33.5	15.04
-CH ₂ -	14	3780	0	0	225.4	196.38
=CH-	2	400	0	0	27	26.04
-COOH	1	530	176400	10000	28.5	45.02
more planes of symmetry			calculated Molar Volume		314.4	
$\Sigma =$		5130	176400	10000		282.47
$\delta_D = \Sigma F_D / MV$	16.32					
$\delta_P = (\Sigma F_P^2)^{1/2} / MV$	1.34					
$\delta_H = (\Sigma F_H / MV)^{1/2}$	5.64					
$\delta = (\delta_D^2 + \delta_P^2 + \delta_H^2)^{1/2}$	17.32					



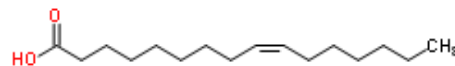
PALMITIC ACID

Structural group	Frequency	F_{di} ($J^{1/2} \cdot cm^{3/2} \cdot mol^{-1}$)	F_{pi}^2 ($J^{1/2} \cdot cm^{3/2} \cdot mol^{-1}$)	E_{hi} (J/mol)	V (cm^3/mol)	Molecular weight (g/mol)
-CH ₃	1	420	0	0	33.5	15.04
-CH ₂ -	14	3780	0	0	225.4	196.38
-COOH	1	530	176400	10000	28.5	45.02
more planes of symmetry			calculated Molar Volume		287.4	
$\Sigma =$		4730	176400	10000		256.43
$\delta_D = \Sigma F_D / MV$	16.46					
$\delta_P = (\Sigma F_P^2)^{1/2} / MV$	1.46					
$\delta_H = (\Sigma F_H / MV)^{1/2}$	5.90					
$\delta = (\delta_D^2 + \delta_P^2 + \delta_H^2)^{1/2}$	17.54					

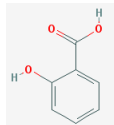


PALMITOLEIC ACID

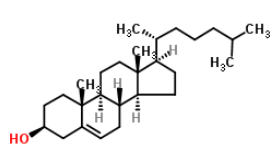
Structural group	Frequency	F_{di} ($J^{1/2} \cdot cm^{3/2} \cdot mol^{-1}$)	F_{pi}^2 ($J^{1/2} \cdot cm^{3/2} \cdot mol^{-1}$)	E_{hi} (J/mol)	V (cm^3/mol)	Molecular weight (g/mol)
-CH ₃	1	420	0	0	33.5	15.04
-CH ₂ -	12	3240	0	0	193.2	168.33
=CH-	2	400	0	0	27	26.04
-COOH	1	530	176400	10000	28.5	45.02
more planes of symmetry			calculated Molar Volume		282.2	
$\Sigma =$		4590	176400	10000		254.42
$\delta_D = \Sigma F_D / MV$	16.27					
$\delta_P = (\Sigma F_P^2)^{1/2} / MV$	1.49					
$\delta_H = (\Sigma F_H / MV)^{1/2}$	5.95					
$\delta = (\delta_D^2 + \delta_P^2 + \delta_H^2)^{1/2}$	17.38					



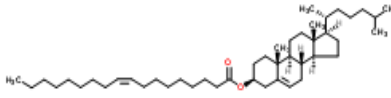
SALICYLIC ACID

Structural group	Frequency	F_{di} ($J^{1/2} \cdot cm^{3/2} \cdot mol^{-1}$)	F_{pi}^2 ($J^{1/2} \cdot cm^{3/2} \cdot mol^{-1}$)	E_{hi} (J/mol)	V (cm^3/mol)	Molecular weight (g/mol)
(o,m,p) phenylene	1	1270	12100	0	52.4	76.10
-OH	1	210	250000	20000	10	17.01
-COOH	1	530	176400	10000	28.5	45.02
ring	1	190	0	0	16	0.00
more planes of symmetry			calculated Molar Volume		106.9	
$\Sigma=$		2200	438500	30000		138.12
$\delta_D = \Sigma F_D / MV$	20.58					
$\delta_P = (\Sigma F_P^2)^{1/2} / MV$	6.19					
$\delta_H = (\Sigma F_H / MV)^{1/2}$	16.75					
$\delta = (\delta_D^2 + \delta_P^2 + \delta_H^2)^{1/2}$	27.25					

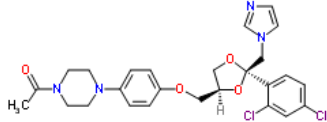
CHOLESTEROL

Structural group	Frequency	F_{di} ($J^{1/2} \cdot cm^{3/2} \cdot mol^{-1}$)	F_{pi}^2 ($J^{1/2} \cdot cm^{3/2} \cdot mol^{-1}$)	E_{hi} (J/mol)	V (cm^3/mol)	Molecular weight (g/mol)
-CH ₃	5	2100	0	0	167.5	75.18
-CH ₂ -	11	2970	0	0	177.1	154.30
>CH-	7	560	0	0	-7	91.13
>C<	2	-140	0	0	-38.4	24.02
=CH-	1	200	0	0	13.5	13.02
=C<	1	70	0	0	-5.5	12.01
-OH	1	210	250000	20000	10	17.01
ring	4	760	0	0	64	0.00
more planes of symmetry			calculated Molar Volume		381.2	
$\Sigma =$		6730	250000	20000		386.67
$\delta_D = \Sigma F_D / MV$	17.65					
$\delta_P = (\Sigma F_P^2)^{1/2} / MV$	1.31					
$\delta_H = (\Sigma F_H / MV)^{1/2}$	7.24					
$\delta = (\delta_D^2 + \delta_P^2 + \delta_H^2)^{1/2}$	19.13					

CHOLESTERYL OLEATE

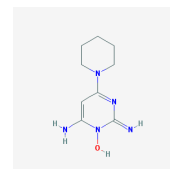
Structural group	Frequency	F_{ai} ($J^{1/2} \cdot cm^{3/2} \cdot mol^{-1}$)	F_{pi}^2 ($J^{1/2} \cdot cm^{3/2} \cdot mol^{-1}$)	E_{hi} (J/mol)	V (cm^3/mol)	Molecular weight (g/mol)
-CH3	6	2520	0	0	201	90.21
-CH2-	25	6750	0	0	402.5	350.68
>CH-	7	560	0	0	-7	91.13
>C<	2	-140	0	0	-38.4	24.02
=CH-	3	600	0	0	40.5	39.06
=C<	1	70	0	0	-5.5	12.01
-COO-	1	390	240100	7000	18	44.01
ring	4	760	0	0	64	0.00
more planes of symmetry			calculated Molar Volume		675.1	
$\Sigma=$		11510	240100	7000		651.12
$\delta_D = \Sigma F_D / MV$	17.05					
$\delta_P = (\Sigma F_P^2)^{1/2} / MV$	0.73					
$\delta_H = (\Sigma F_H / MV)^{1/2}$	3.22					
$\delta = (\delta_D^2 + \delta_P^2 + \delta_H^2)^{1/2}$	17.37					

KETOCONAZOLE

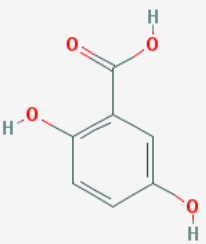
Structural group	Frequency	F_{di} ($J^{1/2} \cdot cm^{3/2} \cdot mol^{-1}$)	F_{pi}^2 ($J^{1/2} \cdot cm^{3/2} \cdot mol^{-1}$)	E_{hi} (J/mol)	V (cm^3/mol)	Molecular weight (g/mol)
-CH3	1	420	0	0	33.5	15.04
-CH ₂ -	7	1890	0	0	112.7	98.19
>CH-	1	80	0	0	-1	13.02
>C<	1	-70	0	0	-19.2	12.01
=CH-	10	2000	0	0	135	130.19
=C<	5	350	0	0	-27.5	60.06
-Cl	2	900	605000	800	48	70.91
-O-	3	300	480000	9000	11.4	48.00
-CO-	1	290	592900	2000	10.8	28.01
-N<	4	80	2560000	20000	-36	56.03
ring	5	950	0	0	80	0.00
more planes of symmetry			calculated Molar Volume		347.7	
$\Sigma=$		7190	4237900	31800		531.44
$\delta_D = \Sigma F_D / MV$	20.68					
$\delta_P = (\Sigma F_P^2)^{1/2} / MV$	5.92					
$\delta_H = (\Sigma F_H / MV)^{1/2}$	9.56					
$\delta = (\delta_D^2 + \delta_P^2 + \delta_H^2)^{1/2}$	23.54					

Minoxidil

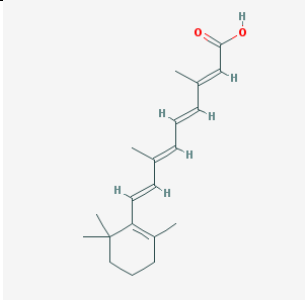
Structural group	Frequency	F_{di} ($J^{1/2} \cdot cm^{3/2} \cdot mol^{-1}$)	F_{pi}^2 ($J^{1/2} \cdot cm^{3/2} \cdot mol^{-1}$)	E_{hi} (J/mol)	V (cm^3/mol)	Molecular weight (g/mol)
-CH ₂ -	5	1350	0	0	80.5	70.14
=CH-	1	200	0	0	13.5	13.02
=C<	3	210	0	0	-16.5	36.03
-OH	1	210	250000	20000	10	17.01
-NH ₂	1	280	0	8400	19.2	16.02
-NH-	1	160	44100	3100	4.5	15.01
-N<	3	60	1920000	15000	-27	42.02
ring	2	380	0	0	32	0.00
one plane of symmetry						
two planes of symmetry						
more planes of symmetry						
$\Sigma=$		2850	2214100	46500	116.2	209.25
$\delta_D = \Sigma F_D / MV$	24.53					
$\delta_P = (\Sigma F_P^2)^{1/2} / MV$	12.81					
$\delta_H = (\Sigma F_H / MV)^{1/2}$	20.00					
$\delta = (\delta_D^2 + \delta_P^2 + \delta_H^2)^{1/2}$	34.14					



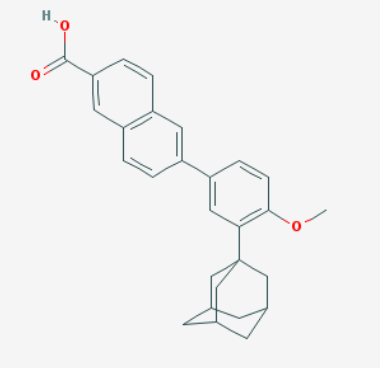
2,5-Dihydroxybenzoic acid

Structural group	Frequency	F_{di} ($J^{1/2} \cdot cm^{3/2} \cdot mol^{-1}$)	F_{pi}^2 ($J^{1/2} \cdot cm^{3/2} \cdot mol^{-1}$)	E_{hi} (J/mol)	V (cm^3/mol)	Molecular weight (g/mol)
(o,m,p) phenylene	1	1270	12100	0	52.4	75.09
-OH	2	420	500000	40000	20	34.01
-COOH	1	530	176400	10000	28.5	45.02
ring	1	190	0	0	16	0.00
more planes of symmetry			calculated Molar Volume		116.9	
$\Sigma=$		2410	688500	50000		154.12
$\delta_D = \Sigma F_D / MV$	20.62					
$\delta_P = (\Sigma F_P^2)^{1/2} / MV$	7.10					
$\delta_H = (\Sigma F_H / MV)^{1/2}$	20.68					
$\delta = (\delta_D^2 + \delta_P^2 + \delta_H^2)^{1/2}$	30.05					

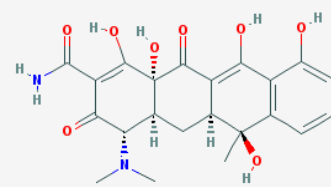
TRITINOIN

Structural group	Frequency	F_{di} ($J^{1/2} \cdot cm^{3/2} \cdot mol^{-1}$)	F_{pi}^2 ($J^{1/2} \cdot cm^{3/2} \cdot mol^{-1}$)	E_{hi} (J/mol)	V (cm^3/mol)	Molecular weight (g/mol)
-CH ₃	5	2100	0	0	167.5	75.18
-CH ₂ -	3	810	0	0	48.3	42.08
>C<	1	-70	0	0	-19.2	12.01
=CH-	6	1200	0	0	81	78.11
=C<	4	280	0	0	-22	48.04
-COOH	1	530	176400	10000	28.5	45.02
ring	1	190	0	0	16	0.00
more planes of symmetry			calculated Molar Volume		300.1	
$\Sigma=$		5040	176400	10000		300.44
$\delta_D = \Sigma F_D / MV$	16.79					
$\delta_P = (\Sigma F_P^2)^{1/2} / MV$	1.40					
$\delta_H = (\Sigma F_H / MV)^{1/2}$	5.77					
$\delta = (\delta_D^2 + \delta_P^2 + \delta_H^2)^{1/2}$	17.81					

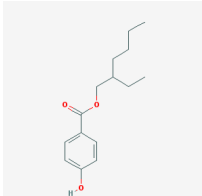
ADAPALENE

Structural group	Frequency	F_{di} ($J^{1/2} \cdot cm^{3/2} \cdot mol^{-1}$)	F_{pi}^2 ($J^{1/2} \cdot cm^{3/2} \cdot mol^{-1}$)	E_{hi} (J/mol)	V (cm^3/mol)	Molecular weight (g/mol)
-CH ₃	1	420	0	0	33.5	15.04
-CH ₂ -	6	1620	0	0	96.6	84.16
>CH-	3	240	0	0	-3	39.06
>C<	1	-70	0	0	-19.2	12.01
=CH-	9	1800	0	0	121.5	117.17
=C<	7	490	0	0	-38.5	84.08
-O-	1	100	160000	3000	3.8	16.00
-COOH	1	530	176400	10000	28.5	45.02
ring	6	1140	0	0	96	0.00
more planes of symmetry			calculated Molar Volume		319.2	
$\Sigma=$		6270	336400	13000		412.53
$\delta_D = \Sigma F_D / MV$	19.64					
$\delta_P = (\Sigma F_P^2)^{1/2} / MV$	1.82					
$\delta_H = (\Sigma F_H / MV)^{1/2}$	6.38					
$\delta = (\delta_D^2 + \delta_P^2 + \delta_H^2)^{1/2}$	20.73					

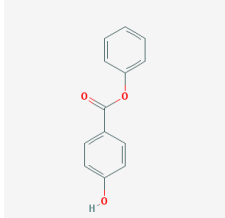
TETRACYCLINE

Structural group	Frequency	F_{di} ($J^{1/2} \cdot cm^{3/2} \cdot mol^{-1}$)	F_{pi}^2 ($J^{1/2} \cdot cm^{3/2} \cdot mol^{-1}$)	E_{hi} (J/mol)	V (cm^3/mol)	Molecular weight (g/mol)
-CH3	3	1260	0	0	100.5	45.11
-CH ₂ -	1	270	0	0	16.1	14.03
>CH-	3	240	0	0	-3	39.06
>C<	2	-140	0	0	-38.4	24.02
=CH-	3	600	0	0	40.5	39.06
=C<	7	490	0	0	-38.5	84.08
-OH	5	1050	1250000	100000	50	85.04
-CO-	3	870	1778700	6000	32.4	84.03
-NH ₂	1	280	0	8400	19.2	16.02
-N<	1	20	640000	5000	-9	14.01
ring	4	760	0	0	64	0.00
more planes of symmetry			calculated Molar Volume		233.8	
$\Sigma=$		5700	3668700	119400		444.45
$\delta_D = \Sigma F_D / MV$	24.38					
$\delta_P = (\Sigma F_P^2)^{1/2} / MV$	8.19					
$\delta_H = (\Sigma F_H / MV)^{1/2}$	22.60					
$\delta = (\delta_D^2 + \delta_P^2 + \delta_H^2)^{1/2}$	34.24					

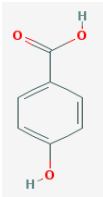
ETHYL HEXYL 4 HYDROXY BENZOATE

Structural group	Frequency	F_{di} ($J^{1/2} \cdot cm^{3/2} \cdot mol^{-1}$)	F_{pi}^2 ($J^{1/2} \cdot cm^{3/2} \cdot mol^{-1}$)	E_{hi} (J/mol)	V (cm^3/mol)	Molecular weight (g/mol)
-CH3	2	840	0	0	67	30.07
-CH ₂ -	5	1350	0	0	80.5	70.14
>CH-	1	80	0	0	-1	13.02
(o,m,p) phenylene	1	1270	12100	0	52.4	76.10
-OH	1	210	250000	20000	10	17.01
-COO-	1	390	240100	7000	18	44.01
ring	1	190	0	0	16	0.00
more planes of symmetry			calculated Molar Volume		242.9	
$\Sigma=$		4330	502200	27000		250.34
$\delta_D = \Sigma F_D / MV$	17.83					
$\delta_P = (\Sigma F_P^2)^{1/2} / MV$	2.92					
$\delta_H = (\Sigma F_H / MV)^{1/2}$	10.54					
$\delta = (\delta_D^2 + \delta_P^2 + \delta_H^2)^{1/2}$	20.92					

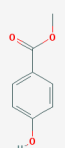
PHENYL 4 HYDROXY BENZOATE

Structural group	Frequency	F_{di} ($J^{1/2}.cm^{3/2}.mol^{-1}$)	F_{pi}^2 ($J^{1/2}.cm^{3/2}.mol^{-1}$)	E_{hi} (J/mol)	V (cm^3/mol)	Molecular weight (g/mol)
=CH-	5	1000	0	0	67.5	65.10
=C<	1	70	0	0	-5.5	12.01
(o,m,p) phenylene	1	1270	12100	0	52.4	76.10
-OH	1	210	250000	20000	10	17.01
-COO-	1	390	240100	7000	18	44.01
ring	2	380	0	0	32	0.00
more planes of symmetry			calculated Molar Volume		174.4	
$\Sigma=$		3320	502200	27000		214.22
$\delta_D = \Sigma F_D / MV$	19.04					
$\delta_P = (\Sigma F_P^2)^{1/2} / MV$	4.06					
$\delta_H = (\Sigma F_H / MV)^{1/2}$	12.44					
$\delta = (\delta_D^2 + \delta_P^2 + \delta_H^2)^{1/2}$	23.10					

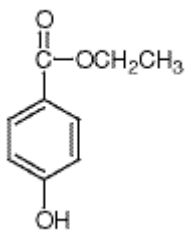
4 HYDROXY BENZOIC ACID

Structural group	Frequency	F_{ai} ($J^{1/2}.cm^{3/2}.mol^{-1}$)	F_{pi}^2 ($J^{1/2}.cm^{3/2}.mol^{-1}$)	E_{hi} (J/mol)	V (cm^3/mol)	Molecular weight (g/mol)
(o,m,p) phenylene	1	1270	12100	0	52.4	76.10
-OH	1	210	250000	20000	10	17.01
-COOH	1	530	176400	10000	28.5	45.02
ring	1	190	0	0	16	0.00
more planes of symmetry			calculated Molar Volume		106.9	
$\Sigma=$		2200	438500	30000		138.12
$\delta_D = \Sigma F_D / MV$	20.58					
$\delta_P = (\Sigma F_P^2)^{1/2} / MV$	6.19					
$\delta_H = (\Sigma F_H / MV)^{1/2}$	16.75					
$\delta = (\delta_D^2 + \delta_P^2 + \delta_H^2)^{1/2}$	27.25					

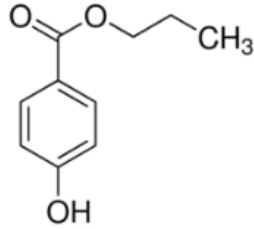
METHYL 4 HYDROXY BENZOATE

Structural group	Frequency	F_{di} ($J^{1/2}.cm^{3/2}.mol^{-1}$)	F_{pi}^2 ($J^{1/2}.cm^{3/2}.mol^{-1}$)	E_{hi} (J/mol)	V (cm^3/mol)	Molecular weight (g/mol)
-CH3	1	420	0	0	33.5	15.04
(o,m,p) phenylene	1	1270	12100	0	52.4	76.10
-OH	1	210	250000	20000	10	17.01
-COO-	1	390	240100	7000	18	44.01
ring	1	190	0	0	16	0.00
more planes of symmetry			calculated Molar Volume		129.9	
$\Sigma=$		2480	502200	27000		152.15
$\delta_D = \Sigma F_D / MV$	19.09					
$\delta_P = (\Sigma F_P^2)^{1/2} / MV$	5.46					
$\delta_H = (\Sigma F_H / MV)^{1/2}$	14.42					
$\delta = (\delta_D^2 + \delta_P^2 + \delta_H^2)^{1/2}$	24.54					

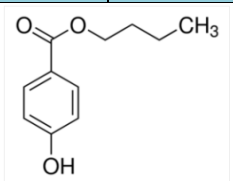
ETHYL 4 HYDROXY BENZOATE

Structural group	Frequency	F_{di} ($J^{1/2}.cm^{3/2}.mol^{-1}$)	F_{pi}^2 ($J^{1/2}.cm^{3/2}.mol^{-1}$)	E_{hi} (J/mol)	V (cm^3/mol)	Molecular weight (g/mol)
-CH3	1	420	0	0	33.5	15.04
-CH2-	1	270	0	0	16.1	14.03
(o,m,p) phenylene	1	1270	12100	0	52.4	76.10
-OH	1	210	250000	20000	10	17.01
-COO-	1	390	240100	7000	18	44.01
ring	1	190	0	0	16	0.00
more planes of symmetry			calculated Molar Volume		146	
$\Sigma=$		2750	502200	27000		166.18
$\delta_D = \Sigma F_D / MV$	18.84					
$\delta_P = (\Sigma F_P^2)^{1/2} / MV$	4.85					
$\delta_H = (\Sigma F_H / MV)^{1/2}$	13.60					
$\delta = (\delta_D^2 + \delta_P^2 + \delta_H^2)^{1/2}$	23.73					

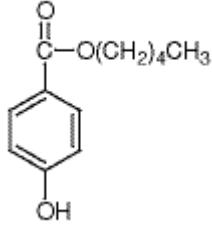
PROPYL 4 HYDROXY BENZOATE

Structural group	Frequency	F_{di} ($J^{1/2} \cdot cm^{3/2} \cdot mol^{-1}$)	F_{pi}^2 ($J^{1/2} \cdot cm^{3/2} \cdot mol^{-1}$)	E_{hi} (J/mol)	V (cm^3/mol)	Molecular weight (g/mol)
-CH ₃	1	420	0	0	33.5	15.04
-CH ₂ -	2	540	0	0	32.2	28.05
(o,m,p) phenylene	1	1270	12100	0	52.4	76.10
-OH	1	210	250000	20000	10	17.01
-COO-	1	390	240100	7000	18	44.01
ring	1	190	0	0	16	0.00
more planes of symmetry			calculated Molar Volume		162.1	
$\Sigma=$		3020	502200	27000		180.21
$\delta_D = \Sigma F_D / MV$	18.63					
$\delta_P = (\Sigma F_P^2)^{1/2} / MV$	4.37					
$\delta_H = (\Sigma F_H / MV)^{1/2}$	12.91					
$\delta = (\delta_D^2 + \delta_P^2 + \delta_H^2)^{1/2}$	23.08					

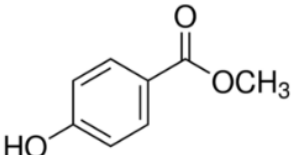
BUTYL 4 HYDROXY BENZOATE

Structural group	Frequency	F_{di} ($J^{1/2} \cdot cm^{3/2} \cdot mol^{-1}$)	F_{pi}^2 ($J^{1/2} \cdot cm^{3/2} \cdot mol^{-1}$)	E_{hi} (J/mol)	V (cm^3/mol)	Molecular weight (g/mol)
-CH3	1	420	0	0	33.5	15.04
-CH ₂ -	3	810	0	0	48.3	42.08
(o,m,p) phenylene	1	1270	12100	0	52.4	76.10
-OH	1	210	250000	20000	10	17.01
-COO-	1	390	240100	7000	18	44.01
ring	1	190	0	0	16	0.00
more planes of symmetry			calculated Molar Volume		178.2	
$\Sigma=$		3290	502200	27000		194.23
$\delta_D = \Sigma F_D / MV$	18.46					
$\delta_P = (\Sigma F_P^2)^{1/2} / MV$	3.98					
$\delta_H = (\Sigma F_H / MV)^{1/2}$	12.31					
$\delta = (\delta_D^2 + \delta_P^2 + \delta_H^2)^{1/2}$	22.54					

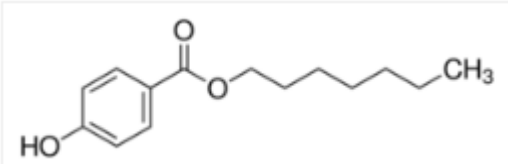
AMYL 4 HYDROXY BENZOATE

Structural group	Frequency	F_{di} ($J^{1/2} \cdot cm^{3/2} \cdot mol^{-1}$)	F_{pi}^2 ($J^{1/2} \cdot cm^{3/2} \cdot mol^{-1}$)	E_{hi} (J/mol)	V (cm^3/mol)	Molecular weight (g/mol)
-CH3	1	420	0	0	33.5	15.04
-CH ₂ -	4	1080	0	0	64.4	56.11
(o,m,p) phenylene	1	1270	12100	0	52.4	76.10
-OH	1	210	250000	20000	10	17.01
-COO-	1	390	240100	7000	18	44.01
ring	1	190	0	0	16	0.00
more planes of symmetry			calculated Molar Volume		194.3	
Σ=		3560	502200	27000		208.26
$\delta_D = \Sigma F_D / MV$	18.32					
$\delta_P = (\Sigma F_P^2)^{1/2} / MV$	3.65					
$\delta_H = (\Sigma F_H / MV)^{1/2}$	11.79					
$\delta = (\delta_D^2 + \delta_P^2 + \delta_H^2)^{1/2}$	22.09					

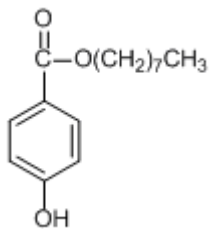
METHYL 4 HYDROXY BENZOATE

Structural group	Frequency	F_{ai} ($J^{1/2} \cdot cm^{3/2} \cdot mol^{-1}$)	F_{pi}^2 ($J^{1/2} \cdot cm^{3/2} \cdot mol^{-1}$)	E_{hi} (J/mol)	V (cm^3/mol)	Molecular weight (g/mol)
-CH3	1	420	0	0	33.5	15.04
-CH ₂ -	5	1350	0	0	80.5	70.14
(o,m,p) phenylene	1	1270	12100	0	52.4	76.10
-OH	1	210	250000	20000	10	17.01
-COO-	1	390	240100	7000	18	44.01
ring	1	190	0	0	16	0.00
more planes of symmetry			calculated Molar Volume		210.4	
$\Sigma =$		3830	502200	27000		222.29
$\delta_D = \Sigma F_D / MV$	18.20					
$\delta_P = (\Sigma F_P^2)^{1/2} / MV$	3.37					
$\delta_H = (\Sigma F_H / MV)^{1/2}$	11.33					
$\delta = (\delta_D^2 + \delta_P^2 + \delta_H^2)^{1/2}$	21.70					

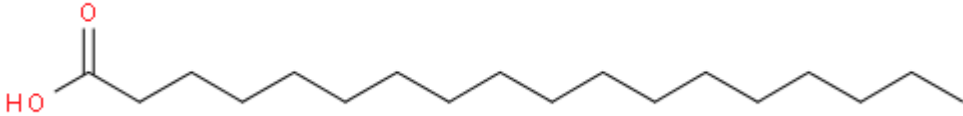
HEPTYL 4 HYDROXY BENZOATE

Structural group	Frequency	F_{di} ($J^{1/2}.cm^{3/2}.mol^{-1}$)	F_{pi}^2 ($J^{1/2}.cm^{3/2}.mol^{-1}$)	E_{hi} (J/mol)	V (cm^3/mol)	Molecular weight (g/mol)
-CH3	1	420	0	0	33.5	15.04
-CH2-	6	1620	0	0	96.6	84.16
(o,m,p) phenylene	1	1270	12100	0	52.4	76.10
-OH	1	210	250000	20000	10	17.01
-COO-	1	390	240100	7000	18	44.01
ring	1	190	0	0	16	0.00
more planes of symmetry			calculated Molar Volume		226.5	
$\Sigma=$		4100	502200	27000		236.31
$\delta_D = \Sigma F_D / MV$	18.10					
$\delta_P = (\Sigma F_P^2)^{1/2} / MV$	3.13					
$\delta_H = (\Sigma F_H / MV)^{1/2}$	10.92					
$\delta = (\delta_D^2 + \delta_P^2 + \delta_H^2)^{1/2}$	21.37					

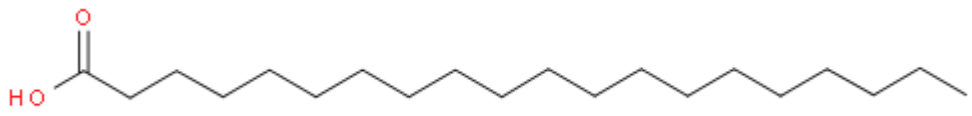
OCTYL 4 HYDROXY BENZOATE

Structural group	Frequency	F_{di} ($J^{1/2}.cm^{3/2}.mol^{-1}$)	F_{pi}^2 ($J^{1/2}.cm^{3/2}.mol^{-1}$)	E_{hi} (J/mol)	V (cm^3/mol)	Molecular weight (g/mol)
-CH3	1	420	0	0	33.5	15.04
-CH2-	7	1890	0	0	112.7	98.19
(o,m,p) phenylene	1	1270	12100	0	52.4	76.10
-OH	1	210	250000	20000	10	17.01
-COO-	1	390	240100	7000	18	44.01
ring	1	190	0	0	16	0.00
more planes of symmetry			calculated Molar Volume		242.6	
$\Sigma=$		4370	502200	27000		250.34
$\delta_D = \Sigma F_D / MV$	18.01					
$\delta_P = (\Sigma F_P^2)^{1/2} / MV$	2.92					
$\delta_H = (\Sigma F_H / MV)^{1/2}$	10.55					
$\delta = (\delta_D^2 + \delta_P^2 + \delta_H^2)^{1/2}$	21.08					

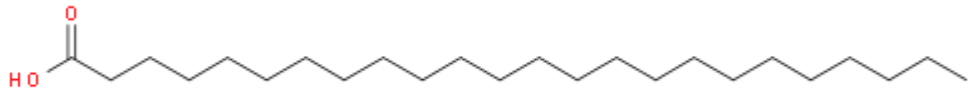
Stearic acid

Structural group	Frequency	F_{di} ($J^{1/2}.cm^{3/2}.mol^{-1}$)	F_{pi^2} ($J^{1/2}.cm^{3/2}.mol^{-1}$)	E_{hi} (J/mol)	V (cm^3/mol)	Molecular weight (g/mol)
-CH ₃	1	420	0	0	33.5	15.04
-CH ₂ -	16	4320	0	0	257.6	224.43
-COOH	1	530	176400	10000	28.5	45.02
more planes of symmetry			calculated Molar Volume		319.6	
$\Sigma=$		5270	176400	10000		284.49
$\delta_D = \Sigma F_D / MV$	16.49					
$\delta_P = (\Sigma F_P^2)^{1/2} / MV$	1.31					
$\delta_H = (\Sigma F_H / MV)^{1/2}$	5.59					
$\delta = (\delta_D^2 + \delta_P^2 + \delta_H^2)^{1/2}$	17.46					

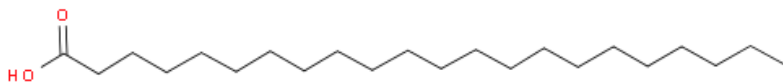
Arachidic acid

Structural group	Frequency	F_{di} ($J^{1/2} \cdot cm^{3/2} \cdot mol^{-1}$)	F_{pi}^2 ($J^{1/2} \cdot cm^{3/2} \cdot mol^{-1}$)	E_{hi} (J/mol)	V (cm^3/mol)	Molecular weight (g/mol)
-CH3	1	420	0	0	33.5	15.04
-CH ₂ -	18	4860	0	0	289.8	252.49
-COOH	1	530	176400	10000	28.5	45.02
more planes of symmetry			calculated Molar Volume		351.8	
$\Sigma=$		5810	176400	10000		312.54
$\delta_D = \Sigma F_D / MV$	16.52					
$\delta_P = (\Sigma F_P^2)^{1/2} / MV$	1.19					
$\delta_H = (\Sigma F_H / MV)^{1/2}$	5.33					
$\delta = (\delta_D^2 + \delta_P^2 + \delta_H^2)^{1/2}$	17.40					

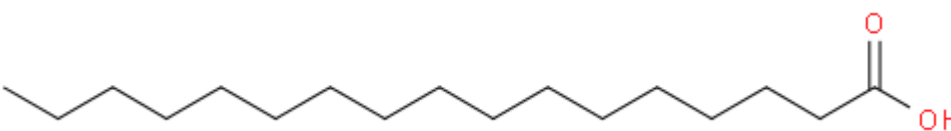
Lignoceric acid

Structural group	Frequency	F_{di} ($J^{1/2} \cdot cm^{3/2} \cdot mol^{-1}$)	F_{pi}^2 ($J^{1/2} \cdot cm^{3/2} \cdot mol^{-1}$)	E_{hi} (J/mol)	V (cm^3/mol)	Molecular weight (g/mol)
-CH3	1	420	0	0	33.5	15.04
-CH ₂ -	22	5940	0	0	354.2	308.60
-COOH	1	530	176400	10000	28.5	45.02
more planes of symmetry			calculated Molar Volume		416.2	
$\Sigma=$		6890	176400	10000		368.65
$\delta_D = \Sigma F_D / MV$	16.55					
$\delta_P = (\Sigma F_P^2)^{1/2} / MV$	1.01					
$\delta_H = (\Sigma F_H / MV)^{1/2}$	4.90					
$\delta = (\delta_D^2 + \delta_P^2 + \delta_H^2)^{1/2}$	17.29					

Behenic acid

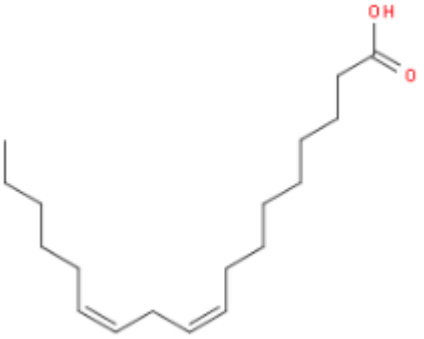
Structural group	Frequency	F_{di} ($J^{1/2} \cdot cm^{3/2} \cdot mol^{-1}$)	F_{pi}^2 ($J^{1/2} \cdot cm^{3/2} \cdot mol^{-1}$)	E_{hi} (J/mol)	V (cm^3/mol)	Molecular weight (g/mol)
-CH ₃	1	420	0	0	33.5	15.04
-CH ₂ -	20	5400	0	0	322	280.54
-COOH	1	530	176400	10000	28.5	45.02
more planes of symmetry			calculated Molar Volume		384	
$\Sigma =$		6350	176400	10000		340.59
$\delta_D = \Sigma F_D / MV$	16.54					
$\delta_P = (\Sigma F_P^2)^{1/2} / MV$	1.09					
$\delta_H = (\Sigma F_H / MV)^{1/2}$	5.10					
$\delta = (\delta_D^2 + \delta_P^2 + \delta_H^2)^{1/2}$	17.34					

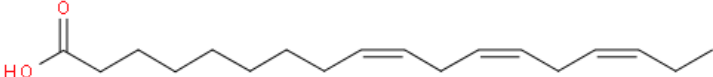
Margaric acid

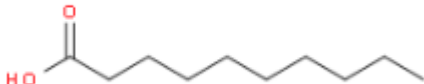
Structural group	Frequency	F_{di} ($J^{1/2} \cdot cm^{3/2} \cdot mol^{-1}$)	F_{pi}^2 ($J^{1/2} \cdot cm^{3/2} \cdot mol^{-1}$)	E_{hi} (J/mol)	V (cm^3/mol)	Molecular weight (g/mol)
-CH ₃	1	420	0	0	33.5	15.04
-CH ₂ -	15	4050	0	0	241.5	210.41
-COOH	1	530	176400	10000	28.5	45.02
more planes of symmetry			calculated Molar Volume		303.5	
$\Sigma =$		5000	176400	10000		270.46
$\delta_D = \Sigma F_D / MV$	16.47					
$\delta_P = (\Sigma F_P^2)^{1/2} / MV$	1.38					
$\delta_H = (\Sigma F_H / MV)^{1/2}$	5.74					
$\delta = (\delta_D^2 + \delta_P^2 + \delta_H^2)^{1/2}$	17.50					

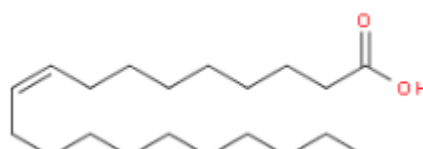
Linoleic acid

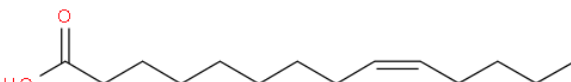
Structural group	Frequency	F_{di} ($J^{1/2}.cm^{3/2}.mol^{-1}$)	F_{pi}^2 ($J^{1/2}.cm^{3/2}.mol^{-1}$)	E_{hi} (J/mol)	V (cm^3/mol)	Molecular weight (g/mol)
-CH3	1	420	0	0	33.5	15.04
-CH ₂ -	12	3240	0	0	193.2	168.33

=CH-	4	800	0	0	54	52.08
-COOH	1	530	176400	10000	28.5	45.02
more planes of symmetry			calculated Molar Volume		309.2	
$\Sigma=$		4990	176400	10000		280.45
$\delta_D = \Sigma F_D / MV$	16.14					
$\delta_P = (\Sigma F_P^2)^{1/2} / MV$	1.36					
$\delta_H = (\Sigma F_H / MV)^{1/2}$	5.69					
$\delta = (\delta_D^2 + \delta_P^2 + \delta_H^2)^{1/2}$	17.16					

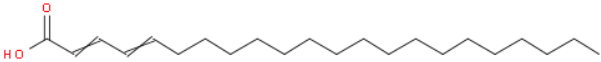
Linolenic acid						
Structural group	Frequency	F_{di} ($J^{1/2} \cdot cm^{3/2} \cdot mol^{-1}$)	F_{pi}^2 ($J^{1/2} \cdot cm^{3/2} \cdot mol^{-1}$)	E_{hi} (J/mol)	V (cm^3/mol)	Molecular weight (g/mol)
-CH ₃	1	420	0	0	33.5	15.04
-CH ₂ -	10	2700	0	0	161	140.27
=CH-	6	1200	0	0	81	78.11
-COOH	1	530	176400	10000	28.5	45.02
more planes of symmetry			calculated Molar Volume		304	
$\Sigma=$		4850	176400	10000		278.44
$\delta_D = \Sigma F_D / MV$	15.95					
$\delta_P = (\Sigma F_P^2)^{1/2} / MV$	1.38					
$\delta_H = (\Sigma F_H / MV)^{1/2}$	5.74					
$\delta = (\delta_D^2 + \delta_P^2 + \delta_H^2)^{1/2}$	17.01					

Capric Acid						
Structural group	Frequency	F_{di} ($J^{1/2} \cdot cm^{3/2} \cdot mol^{-1}$)	F_{pi}^2 ($J^{1/2} \cdot cm^{3/2} \cdot mol^{-1}$)	E_{hi} (J/mol)	V (cm^3/mol)	Molecular weight (g/mol)
-CH ₃	1	420	0	0	33.5	15.04
-CH ₂ -	8	2160	0	0	128.8	112.22
-COOH	1	530	176400	10000	28.5	45.02
more planes of symmetry			calculated Molar Volume		190.8	
$\Sigma=$		3110	176400	10000		172.27
$\delta_D = \Sigma F_D / MV$	16.30					
$\delta_P = (\Sigma F_P^2)^{1/2} / MV$	2.20					
$\delta_H = (\Sigma F_H / MV)^{1/2}$	7.24					
$\delta = (\delta_D^2 + \delta_P^2 + \delta_H^2)^{1/2}$	17.97					

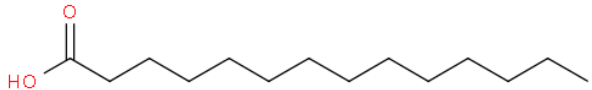
Gadoleic acid						
Structural group	Frequency	F_{di} ($J^{1/2} \cdot cm^{3/2} \cdot mol^{-1}$)	F_{pi}^2 ($J^{1/2} \cdot cm^{3/2} \cdot mol^{-1}$)	E_{hi} (J/mol)	V (cm^3/mol)	Molecular weight (g/mol)
-CH3	1	420	0	0	33.5	15.04
-CH ₂ -	16	4320	0	0	257.6	224.43
=CH-	2	400	0	0	27	26.04
-COOH	1	530	176400	10000	28.5	45.02
more planes of symmetry			calculated Molar Volume		346.6	
$\Sigma=$		5670	176400	10000		310.52
$\delta_D = \Sigma F_D / MV$	16.36					
$\delta_P = (\Sigma F_P^2)^{1/2} / MV$	1.21					
$\delta_H = (\Sigma F_H / MV)^{1/2}$	5.37					
$\delta = (\delta_D^2 + \delta_P^2 + \delta_H^2)^{1/2}$	17.26					

Myristoleic acid						
Structural group	Frequency	F_{di} ($J^{1/2} \cdot cm^{3/2} \cdot mol^{-1}$)	F_{pi}^2 ($J^{1/2} \cdot cm^{3/2} \cdot mol^{-1}$)	E_{hi} (J/mol)	V (cm^3/mol)	Molecular weight (g/mol)
-CH3	1	420	0	0	33.5	15.04
-CH ₂ -	10	2700	0	0	161	140.27
=CH-	2	400	0	0	27	26.04
-COOH	1	530	176400	10000	28.5	45.02
more planes of symmetry			calculated Molar Volume		250	
$\Sigma=$		4050	176400	10000		226.36
$\delta_D = \Sigma F_D / MV$	16.20					
$\delta_P = (\Sigma F_P^2)^{1/2} / MV$	1.68					
$\delta_H = (\Sigma F_H / MV)^{1/2}$	6.32					
$\delta = (\delta_D^2 + \delta_P^2 + \delta_H^2)^{1/2}$	17.47					

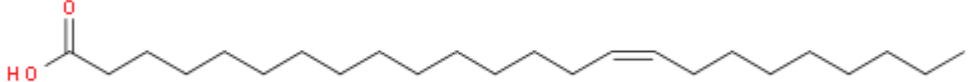
Docosadienoic acid

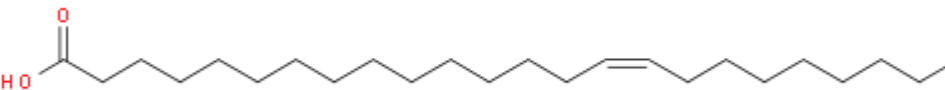
Structural group	Frequency	F_{di} ($J^{1/2} \cdot cm^{3/2} \cdot mol^{-1}$)	F_{pi}^2 ($J^{1/2} \cdot cm^{3/2} \cdot mol^{-1}$)	E_{hi} (J/mol)	V (cm^3/mol)	Molecular weight (g/mol)
-CH ₃	1	420	0	0	33.5	15.04
-CH ₂ -	16	4320	0	0	257.6	224.43
=CH-	4	800	0	0	54	52.08
-COOH	1	530	176400	10000	28.5	45.02
more planes of symmetry			calculated Molar Volume		373.6	
Σ=		6070	176400	10000		336.56
$\delta_D = \Sigma F_D / MV$	16.25					
$\delta_P = (\Sigma F_P^2)^{1/2} / MV$	1.12					
$\delta_H = (\Sigma F_H / MV)^{1/2}$	5.17					
$\delta = (\delta_D^2 + \delta_P^2 + \delta_H^2)^{1/2}$	17.09					

Myristic acid

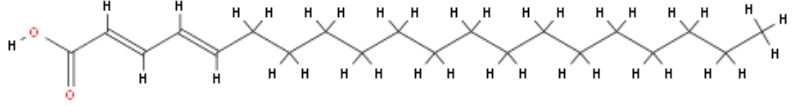
Structural group	Frequency	F_{di} ($J^{1/2} \cdot cm^{3/2} \cdot mol^{-1}$)	F_{pi}^2 ($J^{1/2} \cdot cm^{3/2} \cdot mol^{-1}$)	E_{hi} (J/mol)	V (cm^3/mol)	Molecular weight (g/mol)
-CH ₃	1	420	0	0	33.5	15.04
-CH ₂ -	12	3240	0	0	193.2	168.33
-COOH	1	530	176400	10000	28.5	45.02
more planes of symmetry			calculated Molar Volume		255.2	
$\Sigma =$		4190	176400	10000		228.38
$\delta_D = \Sigma F_D / MV$	16.42					
$\delta_P = (\Sigma F_P^2)^{1/2} / MV$	1.65					
$\delta_H = (\Sigma F_H / MV)^{1/2}$	6.26					
$\delta = (\delta_D^2 + \delta_P^2 + \delta_H^2)^{1/2}$	17.65					

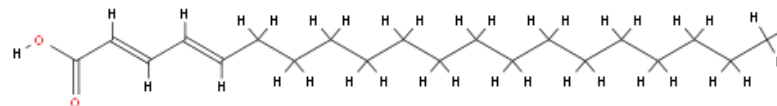
Nervonic acid

Structural group	Frequency	F_{di} ($J^{1/2} \cdot cm^{3/2} \cdot mol^{-1}$)	F_{pi}^2 ($J^{1/2} \cdot cm^{3/2} \cdot mol^{-1}$)	E_{hi} (J/mol)	V (cm^3/mol)	Molecular weight (g/mol)
-CH ₃	1	420	0	0	33.5	15.04
-CH ₂ -	20	5400	0	0	322	280.54
=CH-	2	400	0	0	27	26.04
-COOH	1	530	176400	10000	28.5	45.02
more planes of symmetry			calculated Molar Volume		411	
$\Sigma =$		6750	176400	10000		366.63
$\delta_D = \Sigma F_D / MV$	16.42					
$\delta_P = (\Sigma F_P^2)^{1/2} / MV$	1.02					
$\delta_H = (\Sigma F_H / MV)^{1/2}$	4.93					
$\delta = (\delta_D^2 + \delta_P^2 + \delta_H^2)^{1/2}$	17.18					

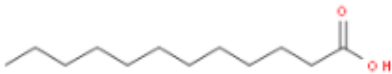


Eicosadienoic acid

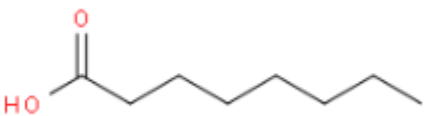
Structural group	Frequency	F_{di} ($J^{1/2} \cdot cm^{3/2} \cdot mol^{-1}$)	F_{pi}^2 ($J^{1/2} \cdot cm^{3/2} \cdot mol^{-1}$)	E_{hi} (J/mol)	V (cm^3/mol)	Molecular weight (g/mol)
-CH ₃	1	420	0	0	33.5	15.04
-CH ₂ -	14	3780	0	0	225.4	196.38
=CH-	4	800	0	0	54	52.08
-COOH	1	530	176400	10000	28.5	45.02
more planes of symmetry			calculated Molar Volume		341.4	
$\Sigma =$		5530	176400	10000		308.51
$\delta_D = \Sigma F_D / MV$	16.20					
$\delta_P = (\Sigma F_P^2)^{1/2} / MV$	1.23					
$\delta_H = (\Sigma F_H / MV)^{1/2}$	5.41					
$\delta = (\delta_D^2 + \delta_P^2 + \delta_H^2)^{1/2}$	17.12					



Lauric acid

Structural group	Frequency	F_{di} ($J^{1/2} \cdot cm^{3/2} \cdot mol^{-1}$)	F_{pi}^2 ($J^{1/2} \cdot cm^{3/2} \cdot mol^{-1}$)	E_{hi} (J/mol)	V (cm^3/mol)	Molecular weight (g/mol)
-CH ₃	1	420	0	0	33.5	15.04
-CH ₂ -	10	2700	0	0	161	140.27
-COOH	1	530	176400	10000	28.5	45.02
more planes of symmetry			calculated Molar Volume		223	
$\Sigma=$		3650	176400	10000		200.32
$\delta_D = \Sigma F_D / MV$	16.37					
$\delta_P = (\Sigma F_P^2)^{1/2} / MV$	1.88					
$\delta_H = (\Sigma F_H / MV)^{1/2}$	6.70					
$\delta = (\delta_D^2 + \delta_P^2 + \delta_H^2)^{1/2}$	17.78					

Caprylic acid

Structural group	Frequency	F_{di} ($J^{1/2} \cdot cm^{3/2} \cdot mol^{-1}$)	F_{pi}^2 ($J^{1/2} \cdot cm^{3/2} \cdot mol^{-1}$)	E_{hi} (J/mol)	V (cm^3/mol)	Molecular weight (g/mol)
-CH ₃	1	420	0	0	33.5	15.04
-CH ₂ -	6	1620	0	0	96.6	84.16
-COOH	1	530	176400	10000	28.5	45.02
more planes of symmetry			calculated Molar Volume		158.6	
$\Sigma=$		2570	176400	10000		144.22
$\delta_D = \Sigma F_D / MV$	16.20					
$\delta_P = (\Sigma F_P^2)^{1/2} / MV$	2.65					
$\delta_H = (\Sigma F_H / MV)^{1/2}$	7.94					
$\delta = (\delta_D^2 + \delta_P^2 + \delta_H^2)^{1/2}$	18.24					

